Lanthanide Nanoparticles for Improving the Sensitivity of Mass Cytometry at the Single-Cell Level

By Mahnaz Maddahfar

Thesis submitted in fulfilment of the requirements for
the degree of **Doctor of Philosophy**

Under the supervision of Prof. Dayong Jin, Prof. Barbara Fazekas
de St Groth, Prof. Martina Stenzel, Dr. Shihui Wen.

University of Technology Sydney
Faculty of Science, School of Mathematical and Physical
Sciences, Institute for Biomedical Materials and Devices.

November 2022

CERTIFICATE OF ORIGINAL AUTHORSHIP

I, *Mahnaz Maddahfar,* declare that this thesis is submitted in fulfilment of the requirements for the award of *Doctor of Philosophy*, in the *School of Mathematics and Physical Science, Faculty of Science* at the University of Technology Sydney.

This thesis is wholly my own work unless otherwise referenced or acknowledged. In addition, I certify that all information sources and literature used are indicated in the thesis.

This document has not been submitted for qualifications at any other academic institution.

This research is supported by the Australian Government Research Training Program.

Signature: Production Note:
Signature removed prior to publication.

Date: 20/11/2022

Acknowledgments

Completing my PhD in nanobiotechnology is undoubtedly the biggest achievement in my whole life. PhD, Doctor of Philosophy, means the study of the fundamental nature of knowledge, reality, and existence. From my point of view, PhD, as the name implies, includes not only deep learning and deep passion for problem-solving but also how to communicate with a multidisciplinary team (enhancing the spirit of collaboration), how to be patient and resilient during the ups and downs of life, and how to strengthen the spirit of persistence to achieve an ultimate goal. After migrating to Australia with my husband in 2018 and starting my PhD journey, never even one percent did I picture myself obtaining a PhD in nanobiotechnology overseas because of language problem, lack of knowledge, having different background etc. Every single moment I look back, I sincerely realise that I would not have completed my journey without all the people in my life, including my husband, my family, my supervisors, my colleagues, my friends, who have supported me in one way or another. I would like to thank everyone who paved the hard way of my PhD.

First of all, I would like to express thanks to my principal supervisor, **Professor Dayong Jin**, ARC Laureate Fellow, the director of the Institute for Biomedical Materials & Devices (IBMD), who helped me to do a PhD in Australia and familiarised me with physics and fluorescent materials that are applicable in the biomedical field. Under his supervision and leadership, I learned how strengthening my positive attitude towards life and being consistent and hardworking can affect reaching our ultimate goal. He taught me how to communicate with other people to expand the angles of the PhD project. I appreciate him teaching me how to become an independent researcher and an expert in my field. I appreciate his endeavour in English proofreading my thesis.

I would like to express my gratitude to our collaborator, my co-supervisor, **Professor Barbara Fazekas**, the director of Ramaciotti Facility for Human Systems Biology, University of Sydney, for introducing me to the world of biology especially highly multi-parametric analysis of immune cells through flow cytometry and mass cytometry. Having not taken any biology classes prior to joining this project, Barbara taught me hand by hand how to do a biology experiment for my PhD project. Under her supervision and leadership, I learned how to think critically and scientifically, how to design experiments, how to be more organised, how to be more accurate during conducting experiments and analysing the data. I appreciate her effort and advice regarding my paper and my thesis. I

want to thank the Sydney Cytometry staff, my colleagues, **Dr. Helen McGuire, Dr. Lucinda Beutler, Mrs. Bavani Gunasegaran**, for their tremendous help in providing the additional reagents and running the samples in conventional flow and mass cytometry.

I would like to thank another collaborator, my co-supervisor, **Professor Martina Stenzel**, ARC Laureate Fellow, a world-leading researcher in polymer chemistry and its applications, at the University of New South Wales (UNSW), for providing me GPC (Gel Permeation Chromatography) to characterise the polymers for surface functionalisation of nanoparticles. I also appreciate her supervision regarding polymer synthesis and characterisation in my project. Many thanks for her endeavours in revising my paper. I would like to thank **Dr. Lin Zhang** for her tremendous help in teaching polymer preparation and running GPC of my samples.

I would like to express my warm thank to **Dr. Shihui Wen**, my co-supervisor, for his significant contribution to my PhD journey. He provided me with the lanthanide nanoparticles for my research project. He taught me how to write my annual PhD report, how to write my paper, and how to organise my data. His patience and kindness inspired me to ask questions from him during my PhD. I appreciate his effort to polish my thesis.

I would like to express my gratitude to **Associate Professor Olga Shimoni** for her efforts to provide lab facilities during my PhD. During the first year of my PhD, she spent significant time comforting me and inspiring me to keep a positive attitude towards the PhD. I appreciate her keeping her office door open to answer the student's questions. She provided me with some advice to write my paper as well.

I would like to express my warm thank to my colleagues, **Dr. Hao He**, who gave me some valuable suggestions that how I could increase my knowledge in biology, bioanalytical chemistry, material science, polymers, etc, **Dr. Jiayan Liao**, **Dr. JiaJia Zhou, Mr. Tesfaye Asrat, Dr. Guochen Bao, Dr. Guocheng Fang, Mrs. Guan Huang, Mr. Lei Ding, Mrs. Xiangjun Di, Mrs. Nabila Morshed,** who helped me to conduct the laboratory work. They provided me with laughter and fun during my PhD.

I would like to thank **Dr. Maryam Parviz**, who provided me with some friendly advice in the Australian academic environment. She and her husband **Dr. Iman Manavi Tehrani** beautifully and kindly shared their experiences about their PhD journey and treated me as their sister.

Finally, I would like to thank the **YouTube channel** for its online video platform. Its contributors provided me with videos related to chemistry, biology, bioanalytical chemistry, physics, history, economics, etc., which were very helpful in increasing my knowledge. I also learned how to use different software associated with my PhD project.

Format of thesis

This is a thesis by a compilation with five chapters.

Chapter 1 includes a comprehensive study of a PhD project called a literature review.

Chapter 2 includes Materials and methods.

Chapters 3 and 4 are experimental, results, and discussion sections, including 1 published paper and 1 unpublished work.

Chapter 5 includes the conclusions, and future perspectives.

Chapter 1

Significance of biomarker research

↓

Pros and cons of current detection techniques

↓

Significance of mass cytometry assay

Challenges

↓

❖ Sensitivity

↓

Lanthanide nanoparticles in enhancing the sensitivity

↓

| Preparation | Surface modification | Antibody bio-conjugation |
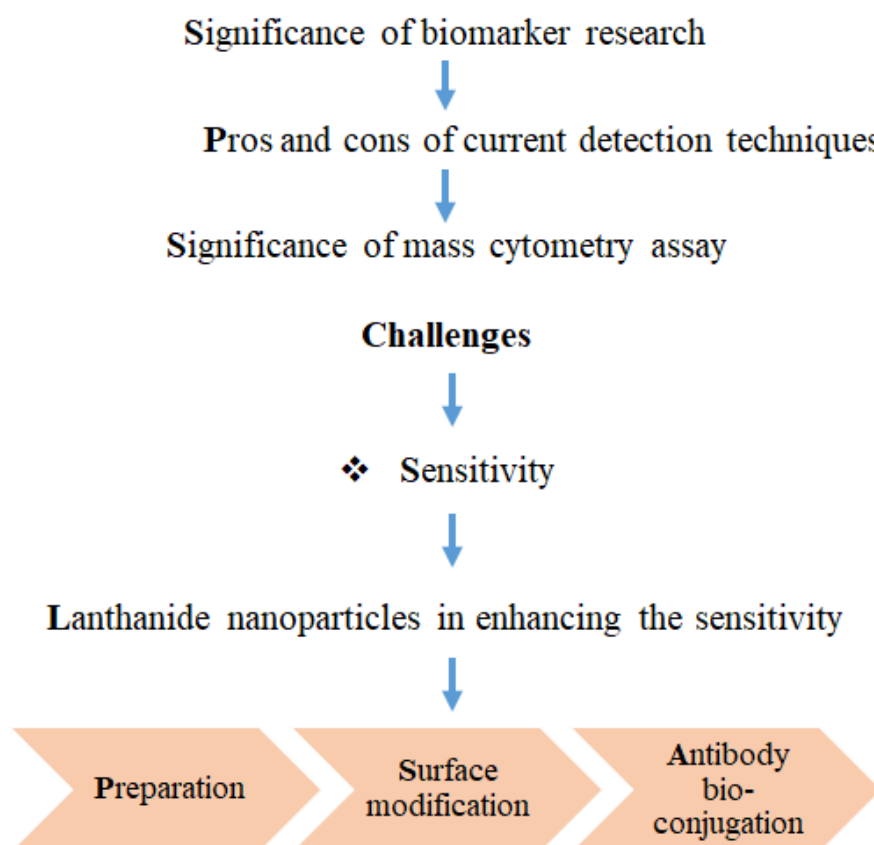
Chapter 2

Materials and Methods

Chapter 3

Surface chemistry and polymers

Chapter 4

Site-specific labelling of antibody (IgG) by LnNPs

Chapter 5

Conclusions and Future perspectives

List of publications, conferences, and awards

Research papers

[1] **Mahnaz Maddahfar**, Shihui Wen, Seyed Mostafa Hosseinpour Mashkani, Lin Zhang, Olga Shimoni, Martina Stenzel, Jiajia Zhou, Barbara Fazekas de St Groth*, Dayong Jin*. Stable and high-efficient antibody-nanoparticles conjugation. Bioconjugate Chemistry (published). https://doi.org/10.1021/acs.bioconjchem.1c00192

[2] **Mahnaz Maddahfar**, Barbara Fazekas de St Groth*, Seyed Mostafa Hosseinpour Mashkani, Shihui Wen , Helen McGuire, Nima Sayyadi, , Martina Stenzel, Dayong Jin*. Functionalising lanthanide nanoparticles in flow cytometry and mass cytometry application: A comparison of strategies. (in preparation)

[3] Zayakhuu Gerelkhuu, Haribalan Perumalsamy, **Mahnaz Maddahfar**, Dayong Jin, Jaewoo Song, and Tae Hyun Yoon*. A study on peripheral blood mononuclear cell and upconversion nanoparticles using single-cell mass cytometry. (Submitted to Environmental Science: Nano).

[4] Yinghui Chen, Olga Shimoni, Guan Huang, Shihui Wen, Jiayan Liao, Hien Duong, **Mahnaz Maddahfar,** Qian Su, David Ortega, Yanling Lu, Douglas Campbell, Bradley Walsh, Dayong Jin*. Upconversion nanoparticle-assisted single-molecule assay for detecting circulating antigens of aggressive prostate cancer https://doi.org/10.1002/cyto.a.24504

[5] Guan Huang, Ying Zhu, Shihui Wen, Haoqi Mei, Yongtao Liu, Dejiang Wang, **Mahnaz Maddahfar**, Qian Peter Su, Gungun Lin*, Yinghui Chen*, Dayong Jin*. Single small extracellular vesicle (sEV) quantification by upconversion nanoparticles. https://doi.org/10.1021/acs.nanolett.2c00724

[6] Xiangjun Di, Qian Peter Su*, Dejiang Wang, Yongtao Liu, **Mahnaz Maddahfar**, Jiajia Zhou, Dayong Jin. Spatiotemporally mapping temperature dynamics of lysosomes and mitochondria using cascade organelle-targeting upconversion nanoparticles. https://doi.org/10.1073/pnas.2207402119

[7] Lei Ding, Xuchen Shan, Dejiang Wang, Baolei Liu*, Ziqing Du, Xiangjun Di, Chaohao Chen*, **Mahnaz Maddahfar**, Ling Zhang, Yuzhi Shi, Peter Reece, Benjamin Halkon, Igor Aharonovich, Xiaoxue Xu*, Fan Wang*. Lanthanide Ion Resonance-Driven Rayleigh Scattering of Nanoparticles for Dual-Modality Interferometric Scattering Microscopy. https://doi.org/10.1002/advs.202203354

Conferences:

[1] **Mahnaz Maddahfar*** Dayong Jin, Barbara Fazekas de St Groth, Shihui wen. Lanthanide Nanoparticles for improving the sensitivity of Mass Cytometry at the Single-cell level. International Conference on Nanoscience and Nanotechnology (ICONN 2020) and International Conference on BioNano Innovation (ICBNI- Poster presentation). February 2020 at Brisbane, Australia.

[2] **Mahnaz Maddahfar*** Dayong Jin, Barbara Fazekas de St Groth, Shihui wen. Lanthanide Nanoparticles for improving the sensitivity of Mass Cytometry at the Single-cell level. International Society of Advanced Cytometry (ISAC- Poster presentation). September 2020 at Philadelphia, USA.

[3] **Mahnaz Maddahfar***. Lanthanide Nanoparticles for improving the sensitivity of Mass Cytometry at the Single-cell level. Biomedical Shark Tank, Institute for Biomedical Materials and Devices (IBMD- Oral presentation). 17 February 2020 at Sydney, Australia.

[4] **Mahnaz Maddahfar*** Dayong Jin, Barbara Fazekas de St Groth. Nanotechnology in mass cytometry assays. Australian Cytometry Society (ACS- Oral presentation). 7th-10th November 2021 at Sydney, Australia.

[5] **Mahnaz Maddahfar*** Dayong Jin, Barbara Fazekas de St Groth. Lanthanide Nanoparticles for improving the sensitivity of mass cytometry at the single-cell level. 4th World Congress on Materials Science and Engineering (WCMSE- Oral presentation). November 16th -17th, 2021 at Miami, USA

[6] **Mahnaz Maddahfar*** Dayong Jin, Barbara Fazekas de St Groth. Lanthanide nanoparticles in Mass cytometry. 3rd International Conference on Advanced Materials Science and Nanotechnology. (Oral presentation). August 18th-19th, 2022, Singapore.

Awards:

TCRN PhD Scholarship Top-up Awards. Translational Cancer Research Network

Best Student Award. Biomedical Shark Tank: Tomorrows Technology for Today's Biomedical Frontiers

International Conference Fund on Bio-Nano Innovation (ICBNI). Australian Nanotechnology Network (ANN)

Vice-Chancellor's Graduate Research Student Conference Fund. UTS, Australia.

IBMD Top-up PhD Scholarship Award. (UTS), Australia

Statement of Contribution of Authors

Mahnaz Maddahfar, Shihui Wen, Seyed Mostafa Hosseinpour Mashkani, Lin Zhang, Olga Shimoni, Martina Stenzel, Jiajia Zhou, Barbara Fazekas de St Groth*, Dayong Jin*. Stable and high-efficient antibody-nanoparticles conjugation. Bioconjugate Chemistry (published). https://doi.org/10.1021/acs.bioconjchem.1c00192

	M.M	S.W	S.M.H.M	L.Z	O.S	M.S	J.Z	B.F	D.J
Experimental Design	X		X					X	X
Sample Preparation	X	X	X					X	
Data Collection	X			X				X	
Analysis Data	X	X		X	X	X		X	
Writing Manuscript	X		X						
Drawing Graphs	X			X			X	X	
Review &Editing	X	X	X	X		X	X	X	X

Mahnaz Maddahfar, Barbara Fazekas de St Groth*, Seyed Mostafa Hosseinpour Mashkani, Shihui Wen, Helen McGuire, Nima Sayyadi, Martina Stenzel, Dayong Jin*. Functionalising lanthanide nanoparticles in flow cytometry and mass cytometry application: A comparison of strategies. Cytometry part A (in preparation)

	M.M	B.F	S.M.H.M	S.W	H.M	N.S	M.S	D.J
Experimental Design	X	X				X		
Sample Preparation	X	X	X	X	X			
Data Collection	X	X						
Analysis Data	X	X						
Writing Manuscript	X	X						
Drawing Graphs	X	X	X					
Review &Editing	X	X	X	X	X		X	X

List of Acronyms (in alphabetic order)

ADH	Adipic acid dihydrazide
AIBN	2,20-azobisisobutyronitrile
AuNPs	Gold nanoparticles
BTPA	2-(n-butyltrithiocarbonate)-propionic acid
CT	Computed tomography
CIT	Citrate
CYTOF	Cytometry time of flight
DDA	1,10-decanedicarbocylic
DLS	Dynamic light scattering
DNA	Deoxyribonucleic acid
DNP	Diameter of nanoparticles
DMSA	3-dimercaptosuccinic acid
DOTA	1,4,7,10-tetraazacyclododecane-1,4,7,10-tetraacetic acid
DTPA	Diethylenetriaminepentaacetic acid
EDC	1-ethyl-3-(3-dimethylaminopropyl) carbodiimide hydrochloride
ELISA	Enzyme-linked immunosorbent assay
FA	Folic acid
FT-IR	Fourier-transform infrared spectroscopy
FSC	Forward scattering channel
GPC	Gel permeation chromatography
HEPES	(4-(2-hydroxyethyl)-1-piperazineethanesulfonic acid)
HRTEM	High-resolution transmission electron microscope
HFS	HEPES fetal serum

ICP-MS	Inductively coupled plasma-mass spectrometry
LnNPs	Lanthanide nanoparticles
mAbs	Monocolonal antibody
MAEP	Monoacryloxyethyl phosphate
MCPs	Metal-chelating polymers
MC	Mass cytometry
MES	2-(N-morpholino)ethanesulfonic acid
MF	Melamine formaldehyde
MPA	Mercaptopropionic acid
MFI	Mean fluorescent intensity
MRI	Magnetic resonance imaging
MSA	Mercaptosuccinic acid
MWCO	Molecular weight cut-off
MUA	Mercaptoundecanoic
NHS	N-hydroxysuccinimide
NIH	National institutes of health
NIR	Near infrared
NMR	Nuclear magnetic resonance
NPs	Nanoparticles
OA	Oleic acid
ODE	1-octadecene
OEGMEA	Oligo (ethylene glycol) methylether acrylate
OM	Oleyl amine
PAA	Poly (acrylic acid)

PAH	Poly (allylamine hydrochloride)
PAMAM	Poly (amido amine)
PBMC	Peripheral blood mononuclear cell
PDI	Poly dispersity index
PE	Phycierythrin
PEG	Polyethylene glycol
PFA	Paraformaldehyde
PSA	Prostate specific antigen
PVP	Poly(vinylpyrrolidone)
PG	Bis-phosphono glycine
QDs	Quantum dots
RAFT	Reversible addition-fragmental chain-transfer polymerization
RIA	Radioimmunoassay
RNA	Ribonucleic acid
ScFv	Single-chain variable fragment
SEC	Size exclusion chromatography
SERS	Surface-enhanced raman scattering
SSC	Side scattering channel
SNP	Specific surface area
Sulfo-NHS	N-hydroxysulfosuccinimide
TCEP	Tris(2-carboxyethyl)phosphine
THF	Tetrahydrofuran
TEOS	Tetraethyl silicate
TEM	Transmission electron microscopy

TGA Thermal gravimetric analysis

UCNPs Up-conversion nanoparticles

UV Ultraviolent

XEDS X-ray energy dispersive spectroscopy

Contents

List of Figures

List of Tables

Abstract

Early detection of cancer increases the possibility of successful treatment which often requires the multiplexed detection of a panel of biomarkers of molecules and single cells. Mass cytometry (CyTOF), combining the powers of flow cytometry and mass spectrometry provides simultaneous measurement of over 40 cellular parameters at single-cell resolution, significantly augmenting the ability of cytometry to evaluate complex cellular systems and processes. This technology is based on isotopically-labelled antibodies as tags and mass spectrometry time-of-flight to distinguish the individual isotope labels on single cells. However, metal chelating polymers, currently used in CyTOF, have been found insufficient in detecting low abundance biomarkers, as the number of metal atoms per tag is too low to detect biomarker expression at levels of 10^2 to 10^4 per cell.

This thesis aims to address the issue of the low sensitivity of mass cytometry by developing lanthanide nanoparticles as cellular barcoding mass-tags, as individual nanoparticles can be doped with a considerable number of elemental atoms, typically in the range of 10^4-10^6 lanthanide ions per nanoparticle. As the key to producing bio-specific nanoparticles lies in the surface functionalisation of LnNPs and their subsequent conjugation to antibodies, the first focus of this thesis is on the design and synthesis of a well-defined diblock copolymer with tuneable size composed of monoacryloxyethyl phosphate block and oligo(ethylene glycol) methyl ether acrylate block through the RAFT polymerisation technique. Systematic insight into the effect of the chain length of POEGMEA on the long-term colloidal stability and antibody-conjugation efficiency of nanoparticles has been provided.

Next, I explored two novel bioconjugation strategies to couple anti-B220 antibody to LnNPs: a) Carbodiimide chemistry in which carboxylate groups of polymer capped LnNPs target lysine sidechains of the antibody, b) Schiff-base interaction in which hydrazide functionalised LnNPs target aldehyde groups in the Fc region of oxidised IgG antibody. Both conjugation strategies were applied to assess the sensitivity and specificity of the LnNP-coupled antibody as a ligand-specific probe for mass cytometry assays. Random orientation of antibodies on the surface of polymer-LnNP and failure to exclude free LnNPs from the coupled ones caused the carbodiimide strategy to generate significant background in CyTOF, making it difficult to distinguish signal. However, the

combination of Schiff-based chemistry to orient coupling of IgG antibodies to LnNPs and the use of a blocking reagent to allow separation of free versus conjugated nanoparticles increased conjugation efficacy and significantly improved signal to noise ratio in mass cytometry assays.

Chapter 1: Literature review

1.1.   Introduction

Cancer, the second most common cause of death and disability in the third millennium, occurs when malformed cells grow in an uncontrolled way. They have the potential to invade surrounding tissues and propagate throughout the body, causing more damage. According to the Australian Institute of Health and Welfare, the estimated number of cancer cases diagnosed in 2020 was 145,483, which included 76,729 males and 68,754 females. The number of deaths from cancer in 2020 was estimated to be 48,099.[1] Despite these sombre statistics, human understanding of cancer has increased over the years, leading to a decrease in mortality rates; therefore, in the current era, attention has turned towards improving the diagnosis of cancer, especially at the early stages when treatment is more effective. There are various types of cancer screening techniques including (1) Papanicolau test for diagnosis of cervical cancer and mammography for the detection of breast cancer in women,[2] (2) prostate-specific antigen (PSA) blood test for identification of prostate cancer in men,[3] (3) colon cancer detection by a stool occult blood test,[4] and (4) other cancer detection methods including endoscopy,[5] CT scan,[6] X-ray,[7] ultrasound imaging,[8] and MRI.[9] Although an early cancer diagnosis is essential for effective treatment, the standard diagnostic methods mentioned above are not fully effective for the early detection of all cancer. Also, some of the above methods are very expensive and unavailable to many people. Therefore, it is important to develop a technology that is specific, trustworthy, and easy to perform as the first-line methodology for early detection of cancers. Combinations of cancer biomarkers and nanotechnology represent a powerful technique to expand effective diagnostic methods for earlier detection of cancer.

1.2.   Biomarkers

A biomarker is a measurable indicator of a normal or abnormal process, a biological condition associated with disease, or a molecular signature of disease. Biomarkers are also powerful tools for studying disruption or alteration in cellular processes, providing information regarding cancer cells.[10, 11] This information allows researchers to understand the mechanisms underlying the initiation and progression of a disease to design an effective method to diagnose and treat that disease. There are several types of biomarkers including proteins, DNA, and RNA.[12] As a result of developing proteomic technologies, various biomarkers for different kinds of cancers have been discovered. For example,

DNA biomarkers of well-known cancers were detected by DNA methylation analysis.[13] Also, in recent decades, scientific researchers have been using nanotechnology to detect biomarkers more sensitively and specifically.[14] To provide a precise picture of the stage of cancer during diagnosis, analysing one biomarker is rarely enough, as cancer displays enormous cellular diversity. Therefore, a high-throughput bioassay is preferred, which examines an extensive panel of biomarkers simultaneously.[15,16] For instance, measurement of 30 different biomarkers is required to diagnose and classify leukemia to make a confident decision on treatment.[17]

1.3. Biomarker research

Biomarker research includes three stages: detection, confirmation, and validation.[18] The aim of the detection stage is to extensively examine the protein content from a sample and detect biomarkers related to the disease. Mass spectrometry provides a great opportunity for scientists worldwide to comprehensively study proteins via a technique called proteomics.[19,20] After the confirmation stage, each biomarker candidate is prioritised and pre-screened and is then ready to move on to clinical biomarker confirmation test. Also, during the confirmation stage, antibody-based protocols may be developed to quantitatively measure proteins related to the disease in clinically accessible bodily fluids.[21] The advent of antibody-antigen based immunoassays has had a great impact on the development of many biomarker mapping techniques using antibodies labelled with radioactive, enzyme, fluorescent, or luminescent components in competitive or sandwich immunoassays.[12,22] The enzyme-linked immunosorbent assay (ELISA), invented by Engvall, has been used as the gold standard of high sensitivity protein quantification measurement.[23,24] ELISA is a cheap assay for analysis of a preclinical/clinical sample, usually less than 50 USD per analyte.[25] However, the main challenge of ELISA is developing antibodies to detect biomarkers. In other words, it is hard to generate antibodies for recently discovered biomarkers. Biomarker purification processes are also costly and time-consuming, and ELISA is not a high throughput assay.[26] Another method for biomarker detection is radioimmunoassay (RIA), which is also employed in clinical practice.[27] This method is based on competition for antibody binding between an antigen labelled with gamma radioactive isotopes, such as ^{125}I, and the unlabelled antigen in the sample. The amount of unlabelled antigen in the samples can be calculated by measuring the amount of antibody-bound versus free radio-labelled antigen. Despite the sensitivity of RIA, it has the same disadvantage as ELISA, namely a

requirement for a specific, high affinity antibody against the antigen.[28] Each new biomarker requires the development and testing of a new RIA, so this method is time and labour-consuming with low level of yield. Most importantly, the main disadvantage of RIAs is related to the use of radioactive materials that impact the safety of the operator, the management of the radioactive waste, and the need for special facilities to process radioactive precursors.

1.3.1 ICP-MS for Biomarker Detection

To detect several biomarkers simultaneously for a quick diagnostic statement, some multi-analyte assays have been proposed, including quantum dots fluorescence immune-assay, up-converting phosphor-based immunoassay, and so on.[29-32] In comparison with other immunoassays, inductively coupled plasma mass spectrometry (ICP-MS) combined with element-tagged based immunoassay is a powerful technique for the simultaneous determination of multiple biomolecules since they avoid the drawback of spectral overlap inherent in fluorochrome-based assays.[33, 34] The combination of immunoassays and ICP-MS (**Figure 1.1**)[35] generates a powerful bioanalytical tool to simultaneously measure multiple parameters detected using elemental tags.[36, 37] Antibodies labelled with isotopes are applied to target various biomarkers. Isotopic tags, with low biological background, can be measured through the ICP-MS when immune complexes are dissolved in acidic media.

In these assays, the presence of the labelling isotope indicates the presence of the relevant biomarker. Multiple studies have demonstrated the high level of sensitivity and selectivity of ICP-MS to identify and quantify biomarkers.[38] Tanner and co-workers at Toronto University coupled ICP-MS with four immunoassay techniques, including centrifugal filtration, protein affinity, size exclusion gel filtration, and enzyme-linked immunosorbent assay. Trace amounts of the targeted protein, as low as 0.1-0.5 ng/mL, were detected using commercially available immune conjugates of nanogold goat anti-human Fabs.[39, 40] Although ICP-MS has a great ability to detect biomarkers, it is not a useful bioanalytical tool for individual cells, in contrast, its application as a bulk analytical tool. The information obtained from the bulk analysis is related to the average response of what may be a highly heterogeneous population of the cells, rather than to the individual cells within the population.[41] To avoid missing the information derived from every single cell, it is necessary to focus on individual-cell analysis.
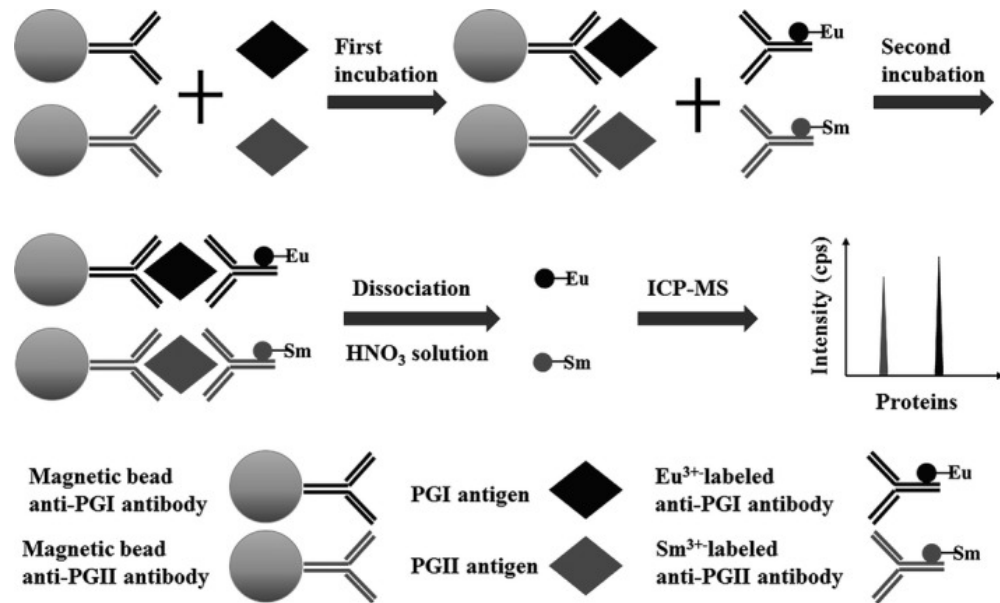
Figure 1.1 Combination of sandwich and ICP-MS assays.[35]

1.3.2 Flow cytometry for biomarker detection

Flow cytometry is a widely used for single cell assay and has well-established commercially available reagents and instruments. The basic principle of flow cytometry is the passage of cells past a laser in a single stream, so they can be detected, counted, and sorted (**Figure 1.2**). Cell components are fluorescently labelled and then excited by the laser to emit light at varying wavelengths.[42] The fluorescence can then be measured to determine the amount and type of cells present in a sample. Up to thousands of cells per second can be analysed as they pass through the liquid stream. In modern flow cytometers, a beam of laser light is directed at a hydrodynamically focused stream of fluid that carries the cells. Several detectors are carefully placed around the stream, at the point where the fluid passes through the light beam. One of these detectors is in line with the light beam and is used to measure Forward Scatter or FSC. Another detector is placed perpendicular to the stream and is used to measure Side Scatter (SSC). Since fluorescent labels are used to detect the different cells or components, fluorescent detectors are also in place.[43] The suspended particles or cells, which may range in size from 0.2 to 150 μm, pass through the light beam and scatter the light rays. The fluorescently labelled antibodies that bind to cell components are excited by the laser and emit light at a longer wavelength than the light source. This is then detected by the detectors. The detectors, therefore, pick up a combination of scattered and fluorescent light. This data is then analysed by a computer attached to the flow cytometer using special software. The

relative gain of each detector (one for each fluorescent emission peak) is adjusted for this detection. Using light measurements, different information can be gathered about the physical and chemical structure of the cells. Generally, FSC can detect the cell volume whereas SSC reflects the inner complexity of the cell such as its cytoplasmic granule content or nuclear structure. Thus different types of information can be generated by analysing scattering patterns like size, complexity, phenotype, and the expression of targeted proteins.[44] Growing knowledge about chemistry, instrumentation, and software make it possible to increase the number of biomarkers that can be measured simultaneously by flow cytometry.[45, 46] The Roederer lab at the National Institutes of Health (NIH) reported a pioneering study of using 17 fluorescent colours and 2 physical parameters for immune-phenotyping T cell populations.[47] However, using up to 17 colours is technically challenging to set up and leaves a little room to add more parameters. The major problem in flow cytometry is the overlapping of fluorescence emissions of fluorochromes, which restricts the number of biomarkers that can be measured simultaneously. Also, biological background signals, termed auto-fluorescence, have a negative effect on the preparation and storage of samples for fluorescent flow cytometry.
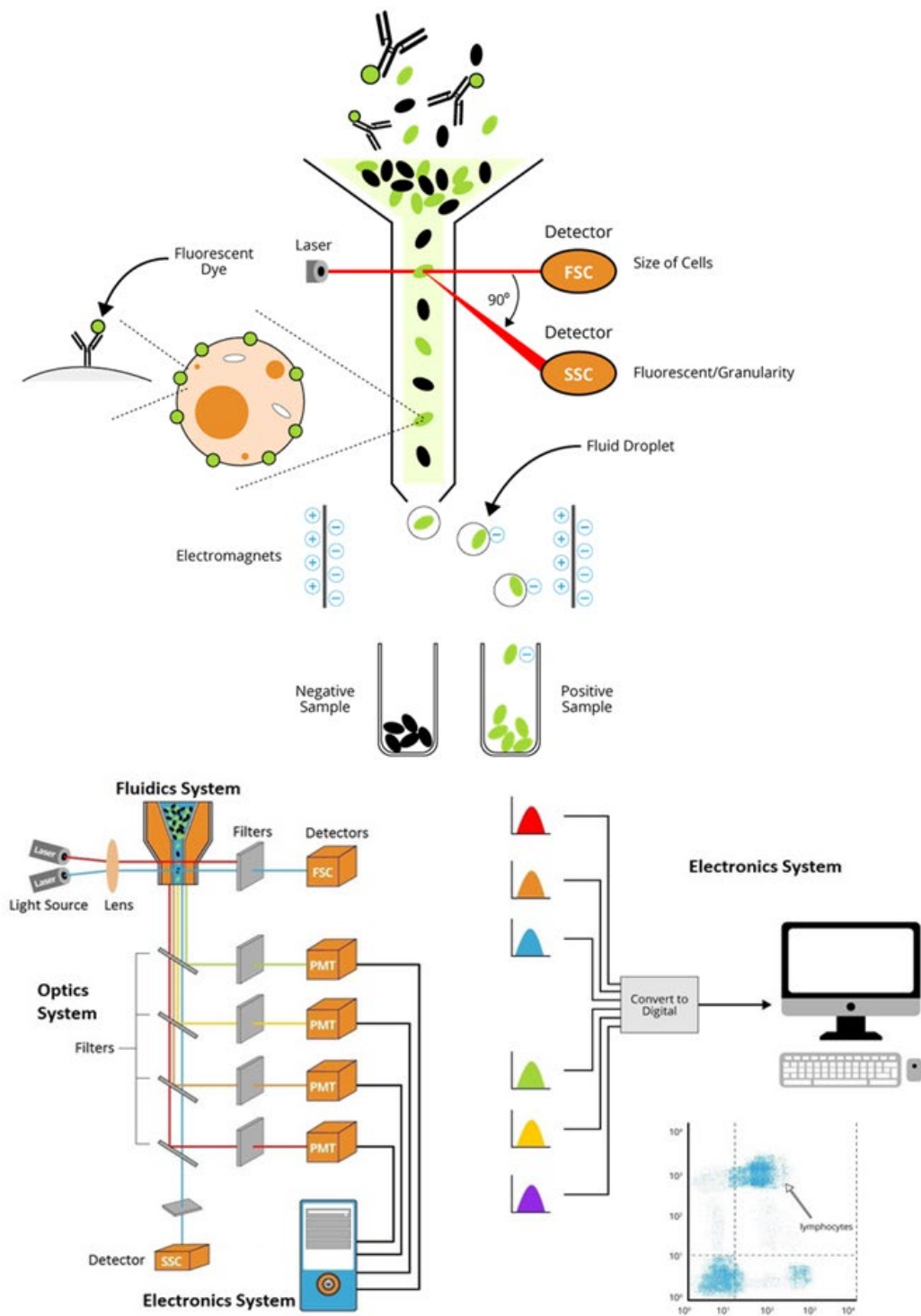
Figure 1.2. Schematic of a flow cytometer. Adapted from website https://www.bosterbio.com/protocol-and troubleshooting/flow-cytometry-principle

1.3.3 Mass Cytometry (CyTOF): a novel technique to detect biomarkers at the single-cell level

Mass cytometry is an innovative technique designed to overcome the multiplexing limitation of conventional flow cytometry which were generated by overlapping emission spectra of fluorochromes. It employs heavy metal isotope as tag in place of fluorescent tags, which resulted in no background signal and also help removing the intrinsic auto-fluorescence of biological samples. Mass cytometry technically can accomplish the simultaneous detection of dozens of biomarkers, which is useful for multi-parameter, single-cell analyses in heterogeneous small samples, such as immune and cancer cells without requiring compensation between mass signals.[48,49] In mass cytometry cells can be stained by antibodies labelled with metal isotope in a way similar to what is done for flow cytometry. They are delivered to the nebulizer from the sample loader. The samples are aerosolised in the nebulizer and directed through the spray chamber to the ICP torch. The cells are vaporized, atomized, and ionized in the plasma. The cells undergo a multistep process within the instrument, resulting in the generation of a file that records the identity and amount of each probe for each cell (**Figure 1.3**).[50] The inventor of the mass cytometer, Professor Scott Tanner from Toronto University, once called it "a flow cytometer with a mass spectrometer detector".[51] Currently the commercially available mass cytometry tag are mainly based on lanthanide isotopes. Lanthanides (Ln), a series of chemical elements consisting of 15 metallic elements with similar chemistry, stability, and significantly low natural abundance in biological systems. The reporter probe is a metal-chelating polymer (MCP) consisting of two parts: multiple metal-chelating sites along the polymer backbone and a functional group that can facilitate conjugation of MCPs to antibodies.[52] For instance, DTPA and DOTA, polydentate chelators, have high binding affinity and low exchange rate to yttrium (Y) and 15 Ln metals.[53] The initial Ln-doped MCPs for mass cytometry applications were synthesised by Lou and co-workers in 2007 using DOTA as the chelating group.[54] The synthesis procedure of MCPs begins with combining an acrylic acid-based polymer with Ln chelating groups (i.e. DOTA or DTPA) via amide bond formation. The bis-maleimide cross-linker is used to functionalise the thiol group of polymer synthesised through the reversible addition-fragmental chain-transfer polymerisation, (RAFT) technique. Antibodies can be conjugated to Ln-doped MCPs through the covalent bond of their free thiols groups with the free maleimide on the cross-linker. The commercial MCPs, MaxPar reagents, are efficient for multiplexed

mass cytometry if the biomarker expression level is greater than 10^4-10^7molecules per cell and an antibody with high affinity for the biomarker is available.[55, 56] In 2011, mass cytometry was brought to the attention of the scientific world by a publication from Stanford University that reported the analysis of more than 30 biomarkers using a mass cytometer.[57] In another experiment, Bodenmiller et al. investigated the application of 7 tags to barcode an entire 96-well plate of samples.[58] In addition, the Davis group investigated the combination of mass cytometry with combinatorial peptide-MHC tetramer binding to multiplex identify and characterise the epitopes on the T cells.[59]
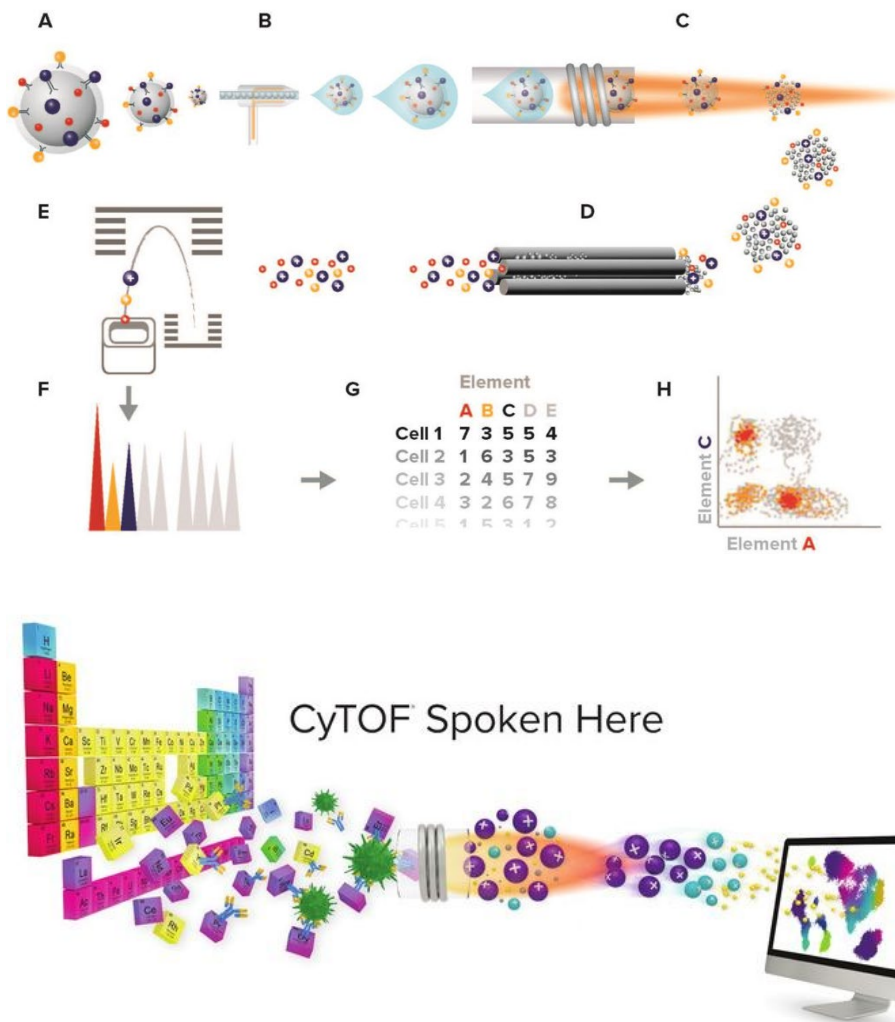
Figure 1.3. Mass cytometry workflow. Cells labelled with metal-conjugated antibodies in solution (A) are injected into the nebulizer (B). They are aerosolised and reduced to single cell-containing droplets. The cells are directed to the ICP torch, where they are vaporized, atomized, and ionized in the plasma (C). The high pass optic removes the low-mass ions (D), resulting in an ion cloud that enters the TOF mass analyser. The ions are separated based on their mass and are accelerated to the detector (E). The detector

measures the quantity of each isotope for each cell in the sample; data is generated in an FCS format (G) and analysed (H). [60]

Despite the advantages of MCPs, they do not provide enough sensitivity to identify low expression of biomarkers on the cell surface as they carry only 100-250 metal atoms per antibody.[48, 59] Since the ion transmission efficiency of the instrument is low, with a limit of detection of 3 to 10×10^5 lanthanide ions, increasing the number of lanthanide ions on each antibody would improve the sensitivity of the mass cytometer, given the linear relationship between number of metal atoms on each antibody and the sensitivity of mass cytometry.[61] There have been two approaches so far to increase the number of metal atoms per tag. One strategy is to coordinate lanthanide elements to semiconducting polymer-micelle dots that can carry 1000-2000 lanthanide ions, and then conjugate to antibodies. With this technique, the researchers observed an increase in sensitivity by a factor of 4 to 6 over a commercial MCP reagent, depending on the marker studied.[62] Another example is polystyrene nanoparticles containing approximately 2000 lanthanide ions, which have been used to label cell populations to study endocytosis.[63] The second approach to increase the amount of elements per tag is to use inorganic nanoparticles, which can carry thousands of ions depending on their size. For example, Schultz and co-workers used commercially available streptavidin coated silver nanoparticles with two different diameters, 10 and 40 nm, to identify CD25 in peripheral blood mononuclear cells (PBMCs).[61] However 40 nm diameter silver nanoparticles enhanced the sensitivity of CD25 detection only 2 to 3 fold over the MCP reagent, a surprisingly small increase as 40 nm silver nanoparticles contain about 2 million silver atoms, which should have generated at least a 20 to 30-fold increase in signal. Therefore, these mass tags did not seem to fulfil the theoretical potential of nanoparticles reagents. Zhang and co-workers fabricated and tested azide functionalised TaO_2 nanoparticles as a mass tag in mass cytometry assays.[64] They showed that TaO_2NP-antibody conjugates could detect CD25 abundance in PBMCs roughly 9 times more than Maxpar-CD25-conjugated antibody. However, the sensitivity of their mass reporter was limited by high nonspecific binding signals observed at higher NP doses.[64] Lanthanide nanoparticles of the general form $NaLnF_4$ are particularly attractive as potential high sensitivity reagents for mass cytometry-based single cell assays. Winnik and co-workers at Toronto University produced different LnNPs containing different numbers of Ln atoms, e.g $NaNdF_4$ nanosheets (9 nm diameter and 3 nm thickness) containing ~6000 Nd atoms per

nanocrystal, $NaTbF_4$ nanoparticles (10 nm diameter) containing 8000 Tb atoms, and $NaTbF_4$ nanoparticles (15 nm diameter) containing 25,000 Tb atoms, to increase the sensitivity of mass cytometry.[65, 66] However, to serve as high sensitive mass tag, lanthanide nanoparticles are required to meet four essential criteria: 1) uniform size with diameter 5-30 nm and C_v are less than 5%, 2) colloidal stability in physiological buffers and in the presence of biomolecules, 3) minimal nonspecific binding to cells, and 4) functional groups for attachment to Abs or other biomolecules. Since LnNPs are not intrinsically biocompatible due to coating by hydrophobic ligand such as oleic acid (OA), surface functionalisation of them is critical to satisfy the current requirements for their application in mass cytometry. For example, Pichaandi and coworkers employed 30 nm diameter $NaYF_4$;Yb, Er NPs (LnNPs) which were functionalised by lipid bilayer containing DOPC, egg sphingomyelin (ESM), and cholesterol, as well as varying concentrations of a PEG-lipid conjugate, 1,2-distearoyl-sn-glycero-3-phosphoethanolamine-N-[methoxyPEG2000] (DSPE-PEG2k-OMe).[67] They demonstrated that the lipid coated LnNPs were stable up to 1 month with minimal nonspecific binding to cells as determined by mass cytometry. However, the lipid bilayer coated LnNPs were unsuitable for use as a mass reporter due to their lack of reactive functional groups. In another experiment, the group functionalised $NaHoF_4$ NPs (12 nm) with a silica layer to produce a mass tag. They observed 450-fold signal enhancement compared to a MCP-antibody conjugate in the detection of the CD14 molecule, both in individual cell lines and in PBMC samples. However, they noted that the ratio of specific to NSB for these NPs varied both with the target antigen and with the cell line, and the nanoparticles were not stable.[66] Cao and et al reported a series of mono-, di-, and tetraphosphonate PEG ligands as surface coating to functionalise different lanthanide nanoparticles for use as mass tags.[68, 69] They tested long term colloidal stability of nanoparticles in different physiological buffers such as PBS buffer. They observed that only tetraphosphonate PEG ligand coated LnNPs offered stability in PBS. However, this ligand was not applicable for generating mass tags due to the onerous synthesis procedure and lack of a reactive functional group for coupling to antibodies. Despite substantial recent progress in generating functionalised LnNPs as potential high sensitivity reagents for mass cytometry,[70, 71] to best of our knowledge, there have been no reports describing the design and fabrication of surface coated LnNPs that satisfy all the essential criteria listed above.

This thesis mainly focuses on preparing functionalised LnNPs with the size of 23 nm in diameter as a tagging reagent to enhance the sensitivity of mass cytometry at the single-cell level. Therefore, it covers 1) LnNPs preparation and characterisation 2) designing and synthesising the polymers with tuneable size to yield well-dispersed and target-specific bio-nano-conjugates, and 3) exploring two different conjugation strategies for coupling LnNPs to monoclonal anti-B220 antibodies.

In the following sections, we will describe the lanthanide nanoparticles, their synthesis procedures, their surface functionalisation approaches, and bioconjugation strategies in detail.

1.4. Lanthanide Nanoparticles

Lanthanide-doped nanoparticles (LnNPs) in a typical host matrix of $NaLnF_4$ have been developed for converting multiple low-energy near-infrared (NIR) photons into high-energy visible and ultraviolet (UV) light.[72,73] The unique anti-Stokes emission of LnNPs provides opportunities for a range of biomedical applications, including ultrasensitive bioassays,[74] deep-tissue super-resolution imaging,[75,76] multimodal biomedical imaging,[77,78] photodynamic therapy[79,80] and NIR-triggered release of genes and drugs.[81,82] LnNPs with spectral down-shifting properties have further led to recent progress in the development of NIR deep-tissue imaging applications.[83, 84] In addition, the high elemental lanthanide content of LnNPs renders them suitable as labels for mass flow cytometry and mass spectroscopy imaging applications, potentially increasing the sensitivity of these assays.[65,67, 85-87] Many synthesis procedures have been studied to synthesise LnNPs with uniform size distribution.[88,89] Since the size and morphology of LnNPs is highly dependent on the reaction conditions such as reaction time, temperature, the concentration of precursors, and type of reaction procedure,[72] various synthetic strategies of LnNPs will be discussed in the following section.

1.5. Typical synthetic procedures for lanthanide nanoparticles

Monodispersed Ln^{3+} based nanoparticles are required for biomedical application; so, soft chemical routs (solution-based) have been explored to prepare different lanthanide nanoparticles. One of the advantages of the wet chemical strategy is that the synthetic parameters including, reaction temperature and time, pH, the concentration of precursors, and surfactants during the chemical reaction can be controlled, which will affect phase structure, size distribution, and morphology of lanthanide nanoparticles. Moreover,

synthesis by the soft chemical technique is well suited for producing functionalised lanthanide nanoparticles as the functional group can be easily modified and then conjugated with biological molecules.

1.5.1 Thermal decomposition

Thermal decomposition is a process in which organometallic precursors are decomposed with the assistance of high-boiling point organic solvents under vacuum conditions.[90] In the thermal decomposition method, organic salts such as trifluoroacetates are typically used for Ln^{3+}-based organometallic precursors, 1-Octadecene (ODE) is commonly used as a high boiling-point organic solvent, and oleic acid (OA) and oleyl amine (OM) are used as coordinator solvents/surfactants to enhance crystallisation by absorption on the surface of nanoparticles, preventing aggregation. In this technique, high temperature is required to break the bond between C-F to assist crystal nucleation and growth processes which are essential for generating uniform nanoparticles.[91] **Figure 1.4** shows the TEM of different lanthanide nanoparticles synthesised by thermal decomposition technique.
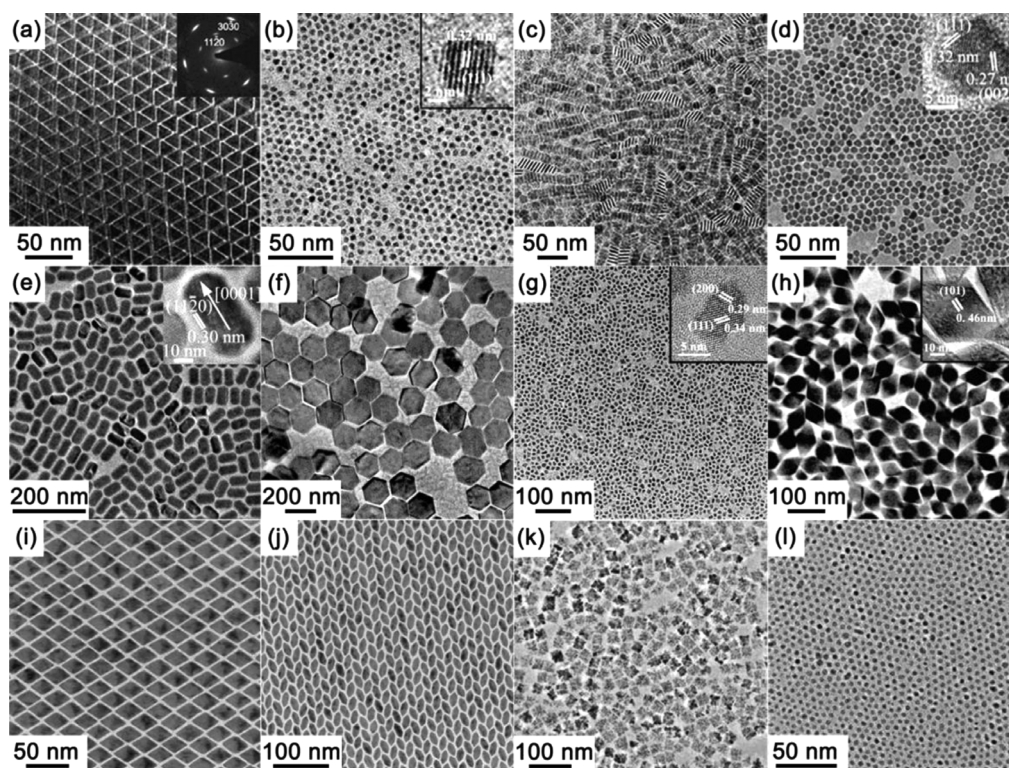
Figure 1.4. Transmission electron microscopy (TEM) images of LaF$_3$ (a), LaOF:Eu (b), LaOCl (c), cubic phased NaYF$_4$ (d), hexagonal phased NaYF$_4$ (e), hexagonal phased NaYF$_4$:Yb,Er (f), KPrF$_4$ (g), LiErF$_4$ (h), DyF$_3$ (i), TbF$_3$ (j), CeO$_2$ (k), and CeO$_2$ (l) nanoparticles synthesised from thermal decomposition.[91, 92]

However, this method has not been widely adopted as it requires an expensive and air-sensitive metal precursor, as well as generating a highly toxic by-product.[93]

1.5.2 Hydrothermal/Solvothermal synthesis

The hydrothermal/solvothermal methods for synthesising nanoparticles are highly dependent on superheated solvents, requiring relatively high-pressure autoclaves.[94] Good crystallinity is one of the features of nanoparticles produced by this method as the high pressure leads to high solvability and reactivity of precursors. In these methods, nanoparticle size and morphology are easily tuneable due to the high flexibility of reaction parameters. In summary, these methods are effective for synthesising high-quality of LnNPs. Moreover, various types of Ln^{3+} precursors such as oxides, chlorides, nitrates, and acetylacetonates can be used in these methods. Liang and co-workers synthesised $GdVO_4$:Yb, Er up-conversion nanoparticles through the hydrothermal method (**Figure1.5**). They used SiO_2 to prevent particle aggregation and growth during the thermal treatment.[95]
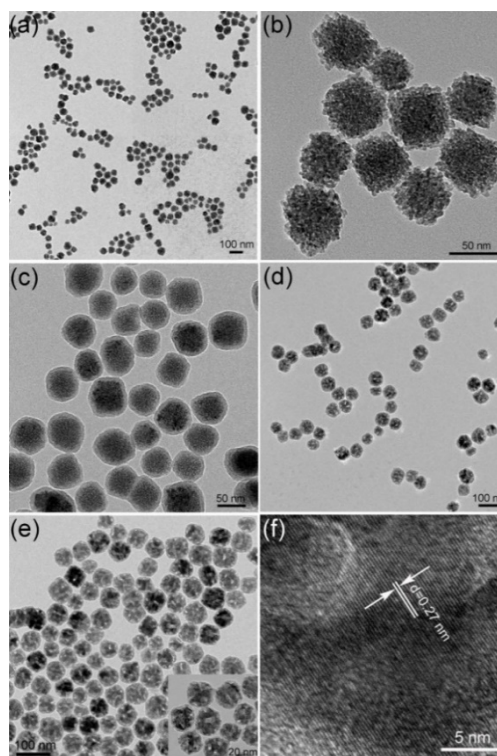
Figure 1.5. TEM images showing the preparation process of high-quality $GdVO_4$:Yb, Er nanoparticles. (a) $GdVO_4$:Yb, Er nanoparticles prepared by hydrothermal method. (b) High magnification image of the crude $GdVO_4$:Yb, Er nanoparticles. (c) SiO_2 coated $GdVO_4$:Yb, Er nanoparticles. (d) Calcination of (c) at 750 $^{\circ}$C for 2 h. (e) Removal of SiO_2 shell of (d) in aqueous NaOH solution. The bottom inset shows a TEM image at high magnification. (f) HRTEM of high-quality $GdVO_4$:Yb, Er nanoparticles.[95]

However, this method has its drawbacks, which restrict its use in the preparation of LnNPs. First, rigorous and harsh synthesis conditions such as an anhydrous and oxygen-free environment as well as high reaction temperature, require careful handling. Second, the high-boiling solvents used in this method are expensive, and the by-products of trifluoroacetate precursors are highly toxic. Third, it is impossible to observe the nanocrystal growth processes in real-time. Fourth, in some cases, to improve the quality of nanoparticles, they are required the further heat treatment and calcination.[96]

1.5.3 Precipitation/Coprecipitation

The coprecipitation method is one of the earliest and most convenient techniques for synthesising Ln^{3+}-doped nanoparticles due to the mild operating conditions, simple protocols, and low-cost equipment.[97] This method involves the concurrent precipitation of several ions to form nanoparticles. It can take place in both aqueous and organic solutions.

1.5.3.1. Precipitation/Co-precipitation in aqueous solution

Ln^{3+}-based chlorides, nitrates, NaF, and NH_4F are used to provide Ln^{3+} and F^- ions, respectively, in the precipitation reaction. Hydrolysis of Ln^{3+} is the major process involved in synthesising Ln^{3+}-based oxide nanoparticles. Shen and his co-workers reported (**Figure 1.6**) the synthesis of LaF_3: Yb^{3+}, Ln^{3+} salt nanoparticles using the co-precipitation method followed by heat treatment at different temperatures in the range of 180 °C to 600 °C.[98]
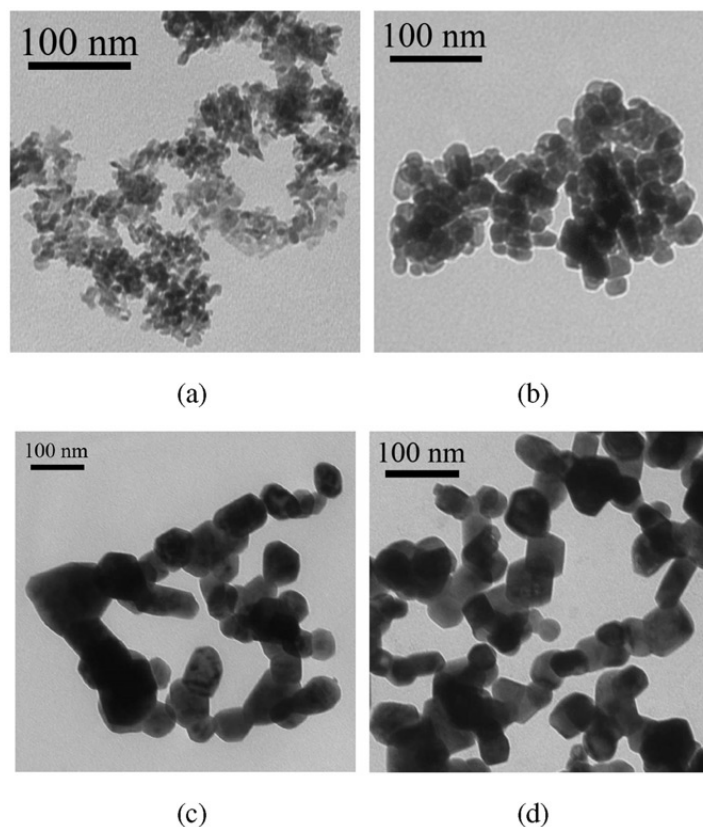
Figure 1.6. TEM images of 20 % mole Yb^{3+} and 2 % mole Er^{3+} co-doped LaF$_3$ nanoparticles (a) as-prepared and after heat treatment at (b) 180 $^\circ$C, (c) 400 $^\circ$C, and (d) 600 $^\circ$C.[98]

Due to the low reaction temperature used in an aqueous solution, the crystallinity of nanoparticles is low and further heat treatment is frequently necessary to improve the quality of the nanoparticles. As a result, precipitation in an organic solution was suggested as an alternative more suitable for preparing high-quality and crystallised nanoparticles.

1.5.3.2. Precipitation/Coprecipitation in organic solution

In this method, lanthanide precursors including (OA$^-$), (CH3COO$^-$), (Cl$^-$), (NO$_3$$^-$) are used to generate Ln^{3+} cations. Meanwhile, anions can be supplied from sodium fluoride, sodium hydroxide, or ammonium fluoride. 1-octadecene (ODE) is used as a solvent and oleic acid (OA) and oleylamine (OM) can be used not only to adjust the particle size and morphology of the final nanoparticles to prevent aggregations but can also be used as the solvent. Ye and his co-workers reported (**Figure 1.7**) the synthesis of β-NaYF$_4$-based lanthanide nanoparticles with various morphologies such as spheres, rods, hexagonal prisms, and plates, with the aid of the coprecipitation method in an organic solution. They used OA and ODE as the capping agent and solvent, respectively.[99]

It is noteworthy that the coprecipitation method is a suitable method to synthesise hollow nano/microspheres with the aid of some materials such as silica, carbon, polystyrene, or melamine-formaldehyde (MF) spheres. As an illustration, Ln^{3+}-doped LaF_3, YVO_4, and RE_2O_3 (RE = La, Gd, Lu, Y) have been synthesised through the coprecipitation method.[100-102] Therefore, this method inspired us to prepare LnNPs as the basis for labelled reagents for biomedical application, especially as mass tags to improve the sensitivity of mass cytometry at the single-cell level. Lanthanide nanoparticle preparation and characterisation will be discussed in chapter 3.
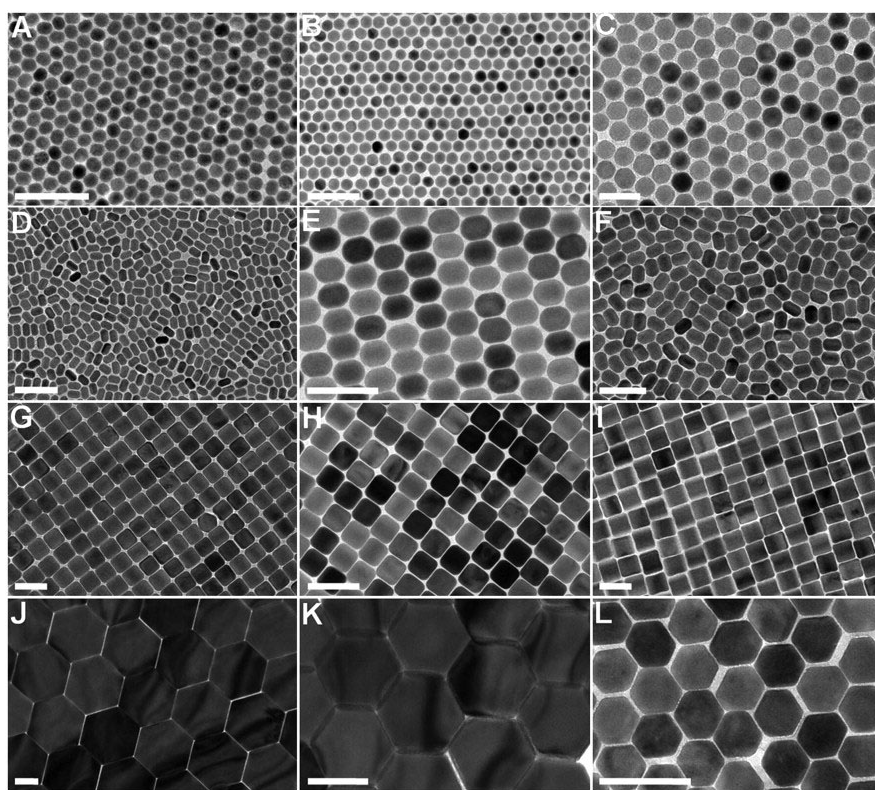
Figure 1.7. TEM images of the β-$NaYF_4$-based LnNPs. (A, D, G, J) $NaYF_4$:Yb/Er (20/2 % mole) LnNPs. (B, E, H, K) $NaYF_4$: Yb/Tm (22/0.2 % mole) LnNPs. (F, I) $NaYF_4$: Yb/Ho (20/2 % mole) LnNPs. (C, L) $NaYF_4$: Yb/Ce/Ho (20/11/2 % mole) LnNPs. All scale bars represent 100 nm.[99]

1.6.   Surface modification of lanthanide nanoparticles

The key to modifying lanthanide nanoparticles to produce bio-specific nanoparticles that are stable in biological and physiological environments lies in their surface functionalisation and conjugation to a bio-active molecule or ligand. As mentioned in the previous section, high-quality LnNPs with tuneable size, shape, and composition are

synthesised at high temperatures with a cap of oleic acids.[65] A variety of surface modification methods have been developed to improve biocompatibility, including chemical modification of the hydrophobic ligand on the surface,[103] bilayer coating with amphiphilic molecules or polymer,[104] addition of an outer silica coating,[86,105] and complete replacement of the original oleic acid moieties. **Figure 1.8** demonstrates these surface modification methods, which are discussed in the following sections.[106]
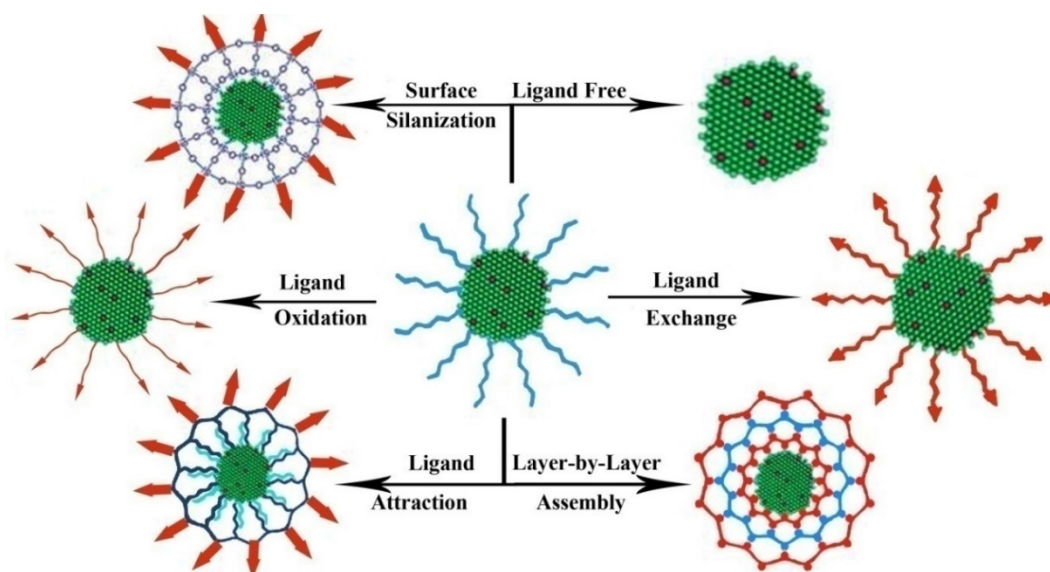
Figure 1.8. Schematic illustration of LnNPs surface modification strategies.[106]

1.6.1 Bilayer Coating with Polymers or Amphiphilic Molecules

In this technique, Van der Waals interaction and electrostatic attraction between OA (hydrophobic capping ligands) on the surface of the LnNPs and new amphiphilic molecules drives LnNPs to transfer from the oil to the water phase. This method provides bilayer coating on the surface of LnNPs in which the hydrophobic tail of amphiphilic molecules (ligand) can intercalate with long-tail Oleate-capped LnNPs, while hydrophilic head groups are directed outward. As a result of the formation of the bilayer around the LnNPs as shown in **Figure 1.9**,[103] the hydrophilic head groups render the particles well dispersible in water. In addition, the hydrophilic (outer side) portion of the amphiphilic ligand can provide different functional groups to facilitate bioconjugation of LnNPs with biological molecules such as proteins, antibodies, DNA. [107] Mitchell A. Winnik and his team used phospholipid bilayer vesicles (liposomes) to encapsulate LnNPs to reduce non-specific binding in mass cytometry assays.[67] However, the size, shape, and layer thickness of lanthanide nanoparticles cannot be controlled by bilayer coating with an amphiphilic

molecule. In addition, this method is not only time-consuming but also increases the hydrodynamic diameter of coated LnNPs which restricts their biological applications.[108]
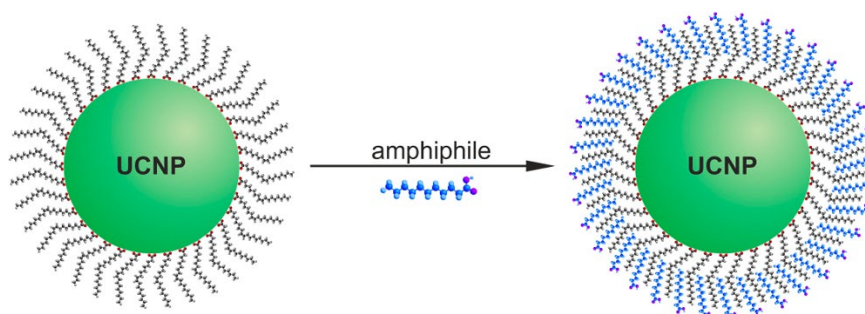
Figure 1.9. Principle of bilayer formation by coating the oleate-capped UCNP with an amphiphilic possessing a hydrophilic or ionic end group, thus converting the hydrophobic particles to hydrophilic ones.[103]

1.6.2 Direct modification of the original ligand

In the direct modification technique, the oxidation of alkene of surfactant on the surface of OA-LnNPs is required to produce a COOH functional group to make LnNPs disperse in an aqueous solution. In this method, strong oxidising agents like Lemieux-von Rudloff reagent and ozone[109-111] are used to reduce the OA or OM on the surface of LnNPs. As a vivid illustration, Li and his team[109] for the first time, oxidised OA successfully to produce two new carboxyl groups in the presence of Lemieux-von Rudloff reagent. The schematic illustration can be seen in **Figure 1.10**.
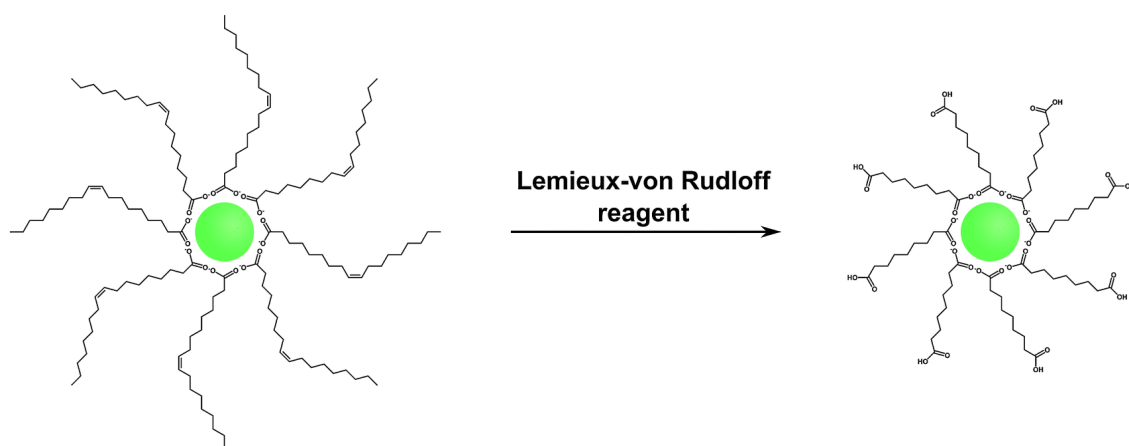
Figure 1.10 Schematic illustration of ligand oxidation of OA-capped LnNPs via Lemieux-von Rudloff reagent.[109]

However, some drawbacks restrict the use of direct modification methods in biological applications. First, the method is time-consuming and generates a low level of yield. Second, the only functional group that can be obtained from this technique is a carboxylic functional group, which limits their coupling to different biomolecules in biomedical applications. Third, direct oxidation of OA-capped LnNPs provides only short-term stability of LnNPs in aqueous environments.[112] Another simple surface modification through the direct modification method is ligand removal in which the OA can be removed with the assistance of direct acid wash (i.e. HCl) or washed with an excess of ethanol during the sonication process. As an illustration, Kumar, et al. reported removal of OA through the sonication of LnNPs with an excess of ethanol.[113] Moreover, Capobianco's group, demonstrated removal of OA from LnNPs surface through the acid treatment (**Figure 1.11**).[114] Under an acidic environment (pH= 2-4) and ultrasonic treatment, the ended-carboxylate of OA on the surface of LnNPs can be protonated to generate oleic acid, and then the free oleic acid can be extracted and removed with diethyl ether. Nevertheless, the use of ligand removal restricts bioanalytical applications due to the absence of any functional groups and the flocculation of LnNPs.[115]
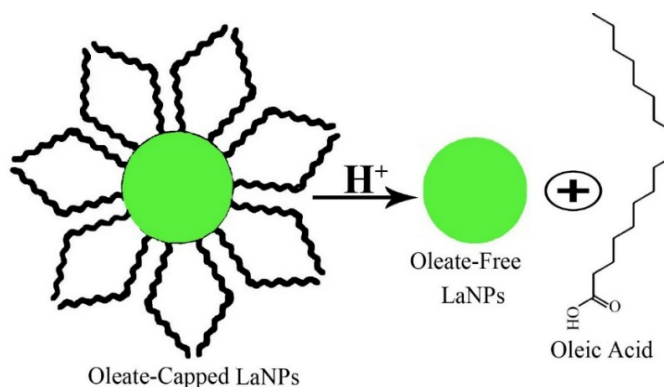
Figure 1.11 Schematic illustration of removal of originally capped surface ligands on LnNPs.[114]

1.6.3 Growing a silica shell and silanisation

Adding silica shells around the LnNPs can be another strategy to give biocompatibility, water solubility, and functionality to LnNPs (**Figure 1.12**). Based on the polar character of surfactant on the LnNPs surface, two surface silanization strategies can be applied: the Stober method,[116,117] and the reverse micro-emulsion method.[118] Stober technique is helpful to functionalise hydrophilic LnNPs with the aid of tetraethyl silicate (TEOS) in

the presence of ethanol and ammonia.[119] The reverse microemulsion method involves surface salinising the LnNPs with hydrophobic capping ligands. In this method, Igepal CO-520 (nonylphenol ethoxylate) is used in reverse micro-emulsion to polymerise precursors.[120] Although surface silanisation provides water solubility for LnNPs@SiO$_2$, it suffers from severe drawbacks compared to other surface modification strategies.[121-123] First, LnNPs functionalised with surface salinisation will aggregate and precipitate after several hours of functionalisation, resulting in LnNPs with poor colloidal stability in aqueous environments. Second, this method drastically changes the shape and hydrodynamic diameter of LnNPs, which can restrict their use in biomedical applications. The third disadvantage is related to the luminescence properties of LnNPs. The emission intensity of the LnNPs has been reported to be reduced after adding a layer of silica to the surface.[124]
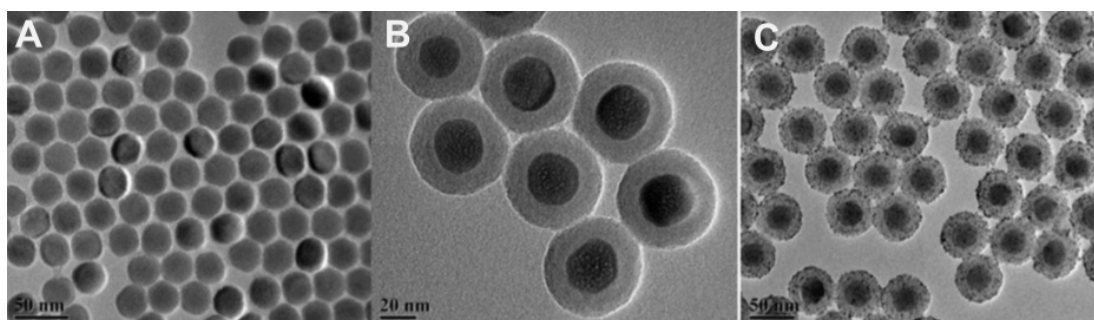
Figure 1.12 TEM images of UCNPs (A), UCNP@SiO$_2$ (C, D).[118]

1.6.4 Ligand exchange

Ligand exchange is not only an efficient and versatile method for surface modification of LnNPs, but also preserves the shape, size, and optical properties of LnNPs while allowing exchange with a wide variety of hydrophilic ligands. There are two types of ligand exchange: (1) direct ligand exchange through replacing OA or OM ligand (primary ligand) with hydrophilic ligand (secondary ligand) and (2) two-step ligand exchange by strong acid NOBF$_4$ (such as nitrosyl tetrafluoroborate) to remove the primary ligand followed by coating with the secondary ligand. In the direct ligand exchange technique, a primary ligand can be completely replaced by a secondary ligand that has a higher affinity towards lanthanide ions (Ln^{+3}) and also a high degree of polarity to achieve water solubility. The affinity of secondary ligands for positively charged ions increases with the

availability of unpaired electrons: -SH＜-NH$_2$＜-COOH＜-PO$_4$.[125] For direct ligand exchange, secondary ligands or polymers that have been used to functionalise lanthanide nanoparticles have included citrate,[126] poly(ethylene glycol) PEGylate-phosphate (PEGP),[127] poly (amidoamine) (PAMAM),[128] poly (allylamine hydrochloride) (PAH),[129] mercaptopropionic acid (MPA),[130] poly(acrylic acid) (PAA),[131] poly (vinylpyrrolidone) (PVP) ,[132] monothiolated hetero bifunctional PEGs ,[133] 3-dimercaptosuccinic acid (DMSA),[134] mercaptosuccinic acid (MSA),[135] 1,10-decanedicarbocylic (DDA), and mercaptonudecanoic (MUA).[136] Secondary ligands on the surface of LnNPs not only transfer them to the water phase but also provide the functional groups for further bio-conjugation. As an example, PAA provides carboxyl functional groups which can be covalently bound to primary amine groups of the protein target. In terms of long term colloidal stability of LnNPs via ligand exchange, Hou and et al coated NaGdF$_4$ with PEG bearing two phosphate groups which exhibited excellent colloidal stability in water and PBS buffer, and demonstrated that this produced a probe suitable for tumour-specific targeting and strong magnetic resonance (MR) contrast enhancement. They observed that the nanoparticles were stable for 1 year.[137,138] Our group functionalised UCNPs with PEG-like ligands containing different anchoring groups including, phosphate, carboxylic and sulfonic acids via ligand exchange. We observed that the LnNPs@POEGA-*b*-PMAEP remained monodispersed with an unchanged average size for 1 week even in physiological buffers such as MES (pH 4.5) and PBS (pH 7.4), while the other two only maintained clarity for the first few hours before aggregation. This finding provides an important reference for selecting suitable ligands.[125]

Two-step ligand exchange is based on removing the primary organic ligand by a powerful acid (such as NOBF$_4$) and replacing it with secondary ligand to provide LnNPs that are soluble in aqueous solution and biocompatible for biological application. For example, Hirsch and his team investigated the long-term colloidal and chemical stability in an aqueous solution of functionalised lanthanide nanoparticles that had been modified by a two-step ligand exchange method. They used NOBF$_4$ to remove the OA capping agent of nanoparticles and covered the surface with small ligands and polymers.[139] **Figure 1.13** shows a schematic illustration of two-step ligand exchange for the surface modification of lanthanide nanoparticles. However, two-step ligand exchange is time consuming and prone to generate aggregates. For example, Hirsch reported that, by adding small ligands such as PAH and PAA, the LnNPs tend to aggregate. **Figure 1.14** illustrates the TEM

images of LnNPs modified by different ligands through a two-step ligand exchange strategy.

In this project, direct ligand exchange was carried out to replace oleic acid on the surface of LnNPs. We designed and synthesised diblock copolymers composed of poly(oligo (ethylene glycol) methyl ether acrylate) (POEGMEA) containing polyethylene glycol and monoacryloxyethyl phosphate (MAEP) units through Reversible Addition Fragmentation Chain Transfer RAFT polymerisation. The phosphate group drives the replacement reaction due to the high affinity of the phosphate functional group (PO_4^{3-}) towards lanthanide ions (Ln^{3+}), thereby acting as an inner shell on the surface of lanthanide nanoparticles. POEGMEA block can act as an outer shell to improve colloidal stability, biocompatibility, and immunogenicity of lanthanide nanoparticles in biological application especially flow cytometry and mass cytometry assays. The synthesis details and characterisation of POEGMEA-*b*-PMAEP and surface modification of LnNPs will be described in chapter 3.
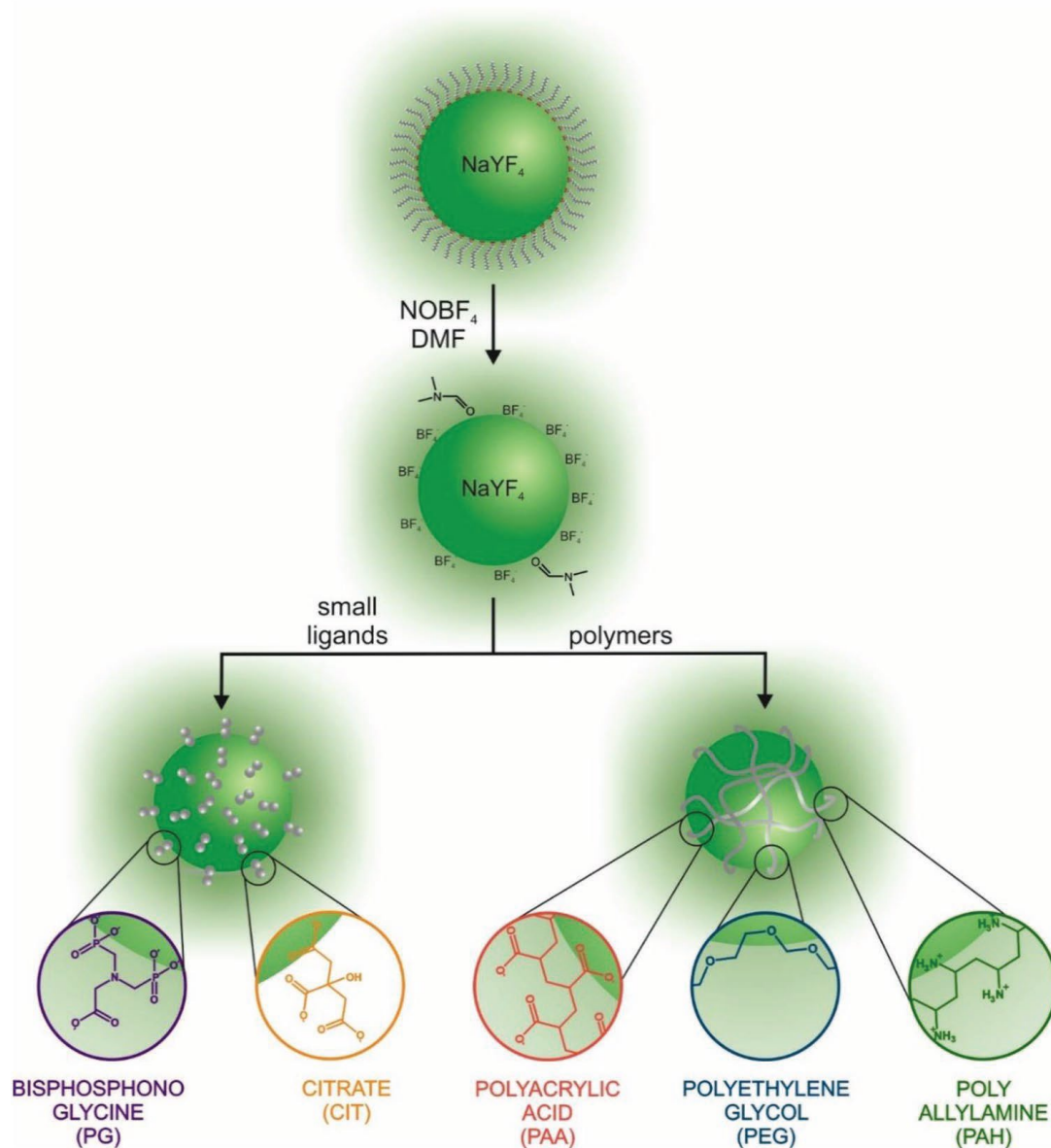
Figure 1.13. Scheme of the two-step ligand exchange for the surface modification of LnNPs. In the first step, the oleate is removed via the addition of NOBF4. The bare LnNPs are stabilised via BF^{-4} ions. In the next step, the particles are modified with the desired ligand (here PG, CIT, PAA, PEG, and PAH).[139]
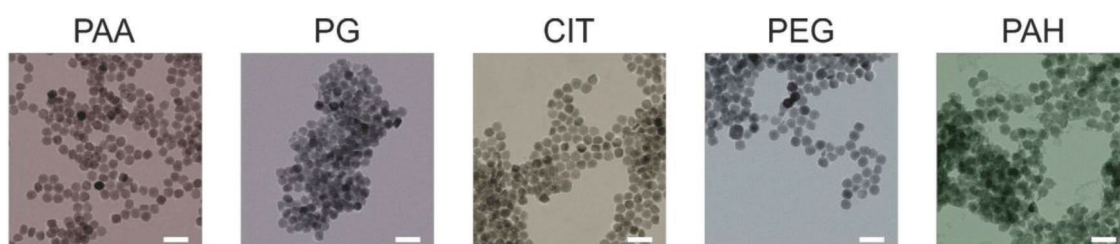
Figure 1.14. TEM images of LnNPs with different surface capping (red = PAA, purple = PG, orange = CIT, blue = PEG, and green = PAH). In the case of capping with small molecules, aggregation and strong dissolution can be observed.[139]

1.7. Bioconjugation

After surface modification of lanthanide nanoparticles, further conjugation to biomolecules such as folic acid, biotin, peptide, antibody, protein, avidin, and DNA, can be obtained by linking to functional groups (e.g. -COOH, -NH$_2$, -SH) on the surface of LnNPs. This biofunctionalisation of LnNPs paves the way for potential bioapplications ranging from ultrasensitive molecular assays, multi-modal bio-imaging and targeted delivery to activation of drugs.[140] **Figure 1.15** illustrates a schematic of biofunctionalised nanoparticles with different biomolecules. There are two types of bioconjugation of LnNPs: 1) physisorption or electrostatic absorption and 2) chemical covalent linkage.

The physisorption strategy is based on non-covalent forces such as electrostatic attraction and is a convenient and straightforward technique. The physisorption method preserves the biological activities of biomolecules due to the absence of chemical linkage. However, it results in a poor yield. The second disadvantage of the physisorption method is decreasing the binding capability of LnNPs to target biomolecules due to the disordered orientation of biomolecules in relation to LnNPs. Last but not least, when the electrostatic force between the nanoparticles and biomolecules is weak, nanoparticles and/or biomolecules released from the unstable biofunctionalised nanoparticles can lead to non-specific binding.[141]

The second bioconjugation technique, chemical covalent linkage, solves the problem of non-specific binding employing chemical linkage, increasing the yield of the desired complex.[141] Chemical covalent linkage takes place between the functional group of LnNPs and the reactive group of the biomolecules.[142] In this technique, biomolecules couple to the surface of LnNPs directly through the pairing of functional groups. For example, biomolecules such as nucleic acid, aptamers, and folic acid can be conjugated to the LnNPs surface through mercapto and amine groups. Multifunctional PEG polymers can also be used as the cross-linkers facilitating chemical covalent linkage to biomolecules, with the additional benefit of improving water solubility. The cross-linkers can be attached to the surface of LnNPs and biomolecules through chemical or physical absorption. In some cases, biomolecules such as antibodies, streptavidin, and some toxins have been used as the cross-linkers to improve the bioactivity and water solubility of LnNPs.[143,144]
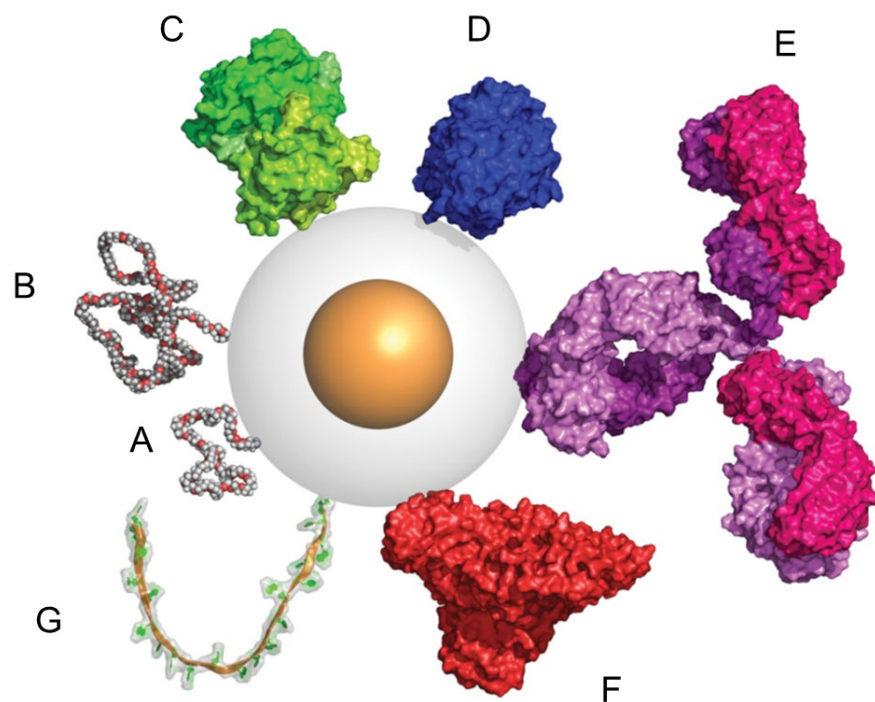
Figure 1.15. Relative size of nanoparticles and biomolecules, drawn to scale. Schematic representation of a nanoparticle with 5nm core diameter, 10 nm shell diameter, with PEG molecules of 2000 (A) and 5000 g mol^{-1} (B), streptavidin (C), transferrin (D), antibody (IgG, E), albumin (F), single-stranded DNA (20 mer, cartoon and space filling) (G) . Proteins are crystal structures taken from the Protein Data Bank (http://www.rcsb.org) and displayed as surfaces; PEG and DNA have been modelled from their chemical structure and space filling.[145]

In the chemical covalent linkage method, carboxyl (-COOH) and primary amine groups (NH$_2$) are useful for modifying the surface of LnNPs. In addition, 1-ethyl-3-(3-dimethylaminopropyl) carbodiimide hydrochloride (EDC) and N-hydroxysuccinimide (NHS) are usually used as the activators in bio-conjugation. For example, poly(acrylic acid) (PAA) and 3-dimercaptosuccinic acid (DMSA) can be applied to create carboxylic acid on the surface of LnNPs, to conjugate with biomolecules containing primary amine groups. **Figure 1.16** shows how EDC can activate the carboxyl group, which is then stabilised by Sulfo-NHS to react with a primary amine, to create a strong amide bond.
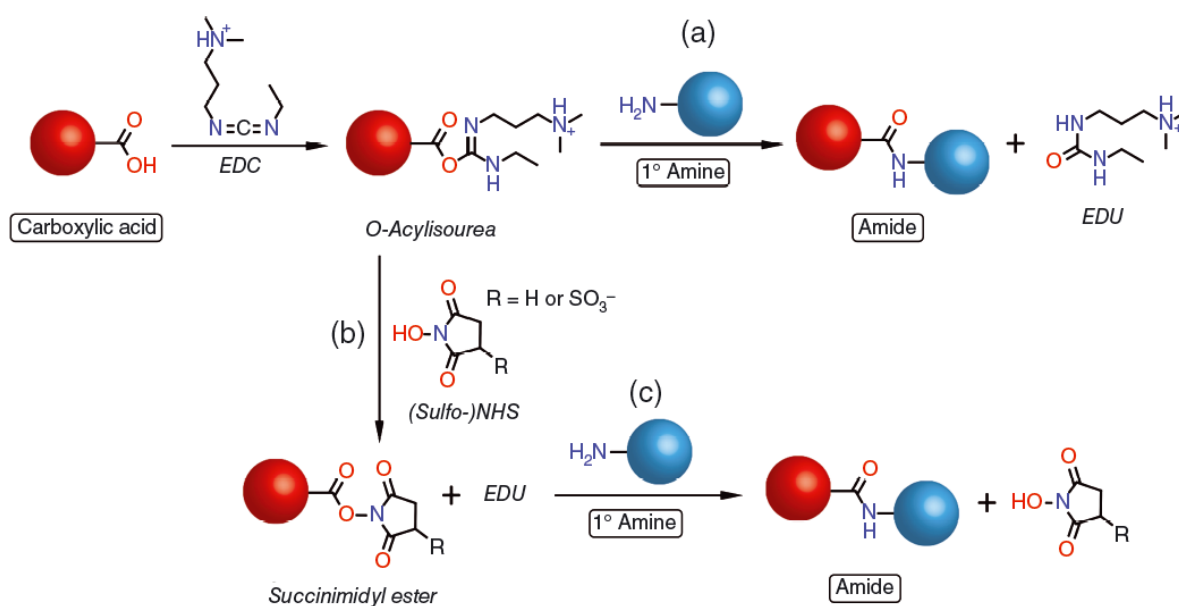
Figure1.16. Schematic illustration of EDC/NHS chemistry. N-(3-Dimethylaminopropyl)-N′-ethylcarbodiimide (EDC) activates a carboxylic acid to an O-acylisourea intermediate that can react with (a) a primary amine to yield an amide or (b) N-hydroxysuccinimide (NHS) or sulfo-NHS to yield a more stable but still reactive succinimidyl ester. (c) The succinimidyl ester reacts with an amine to yield an amide.[146]

In addition, maleimide groups in maleimide functionalised LnNPs can be used for bio-conjugating of LnNPs with biomolecules containing -SH groups through the formation of a thio-ether bond under physiological conditions. **Figure 1.17** shows a schematic illustration of conjugation of SH-maleimide.
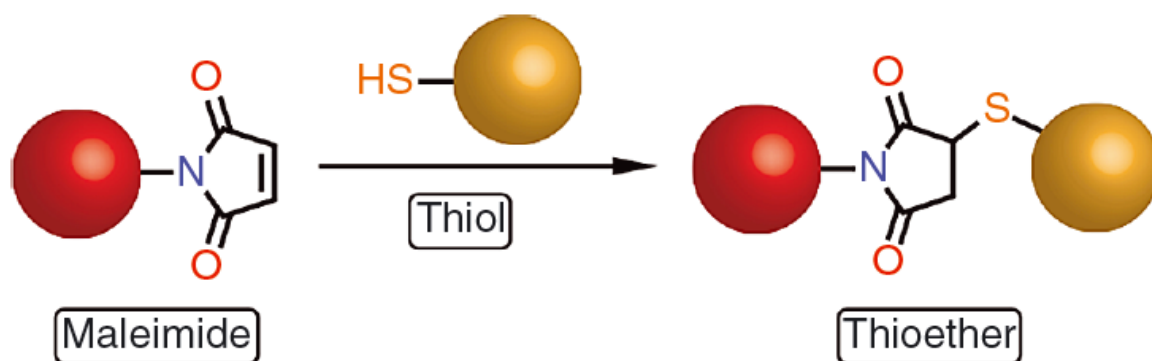
Figure 1.17. Michael addition between a maleimide and a thiol to form a stable thio-ether linkage.[146]

Another surface biofunctionalisation of LnNPs is, the addition of avidin or streptavidin, which has a high affinity for biotin and thereby allows conjugation of LnNPs to biotinylated molecules or proteins (**Figure 1.18**).[146]
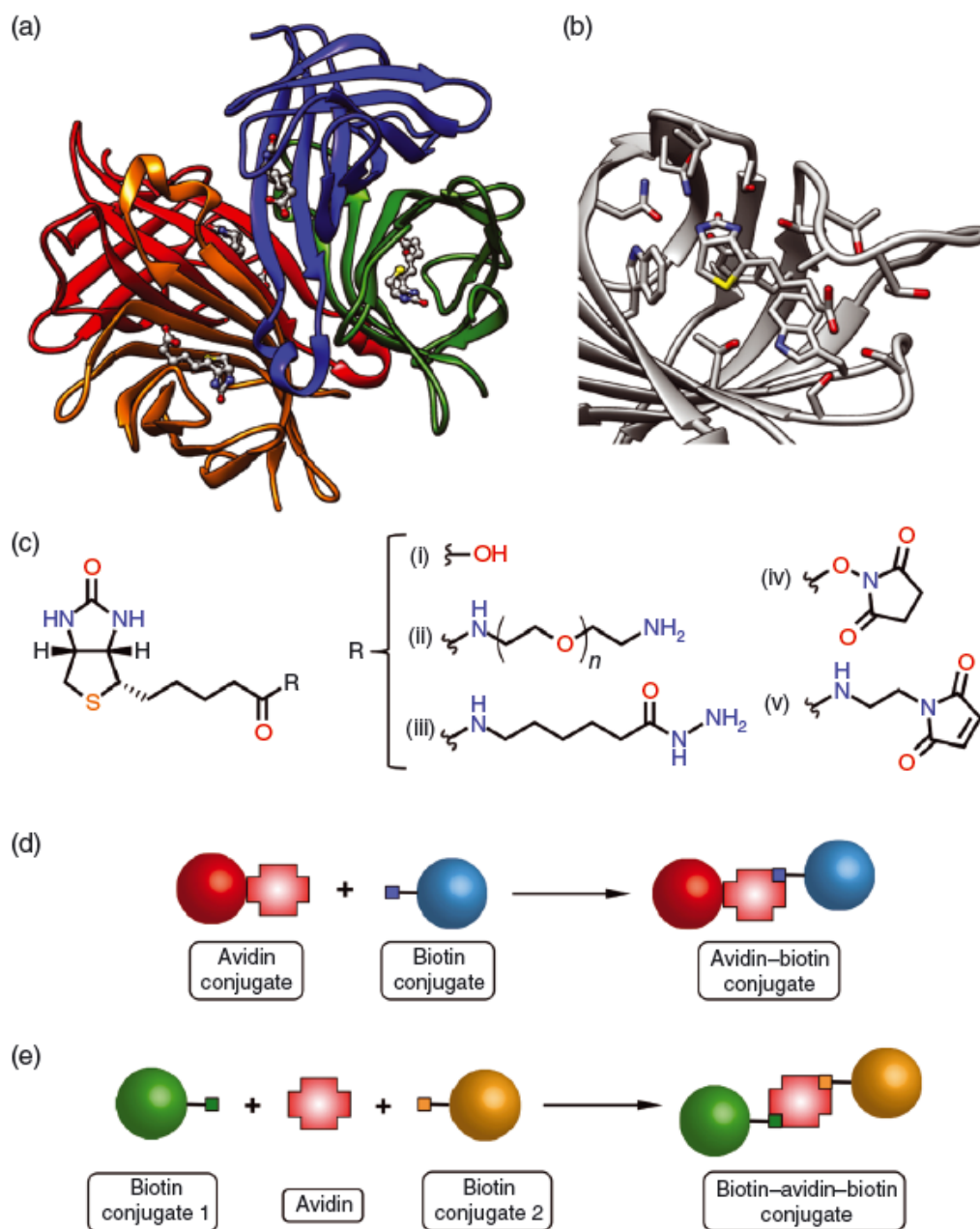
Figure 1.18. (a) Tetrameric ribbon structure of streptavidin bound to four biotin ligands. (b) Close-up view of the biotin-binding pocket of avidin. (c) Structure of (i) biotin and its derivatives: (ii) amine, (iii) hydrazide, (iv) succinimidyl ester, and (v) maleimide. (d) Direct conjugation between biotin and (strept) avidin-modified biomolecules. (e) Indirect conjugation between two biotinylated biomolecules using (strept) avidin.[146]

Chapter 1

Primary amines or hydrazides can spontaneously react with aldehydes and ketones to form imines under Schiff-bases interaction, as shown in **Figure 1.19**. IgG is a glycoprotein with a conserved carbohydrate moiety that can be oxidised by reagents such as sodium periodate (NaIO$_4$) (**Figure 1.20**). This allows hydrazide/amine-functionalised lanthanide nanoparticles to be coupled to antibodies through Schiff-base reaction. Although these reactions will proceed in an aqueous media, the reaction is reversible, and the imines are ultimately unstable as the equilibrium shifts to the unconjugated amine and carbonyl groups. To address this shortcoming, reductive amination is usually carried out either as a one-pot or two-step reaction with sodium cyanoborohydride, yielding a stable secondary amine, as shown in **Figure 1.19**.[146] The major advantage of this strategy is that it targets the same site on each antibody, orienting it with the antigen-binding site facing away from the nanoparticle and allowing for efficient antigen binding of the LnNP-antibody complex.
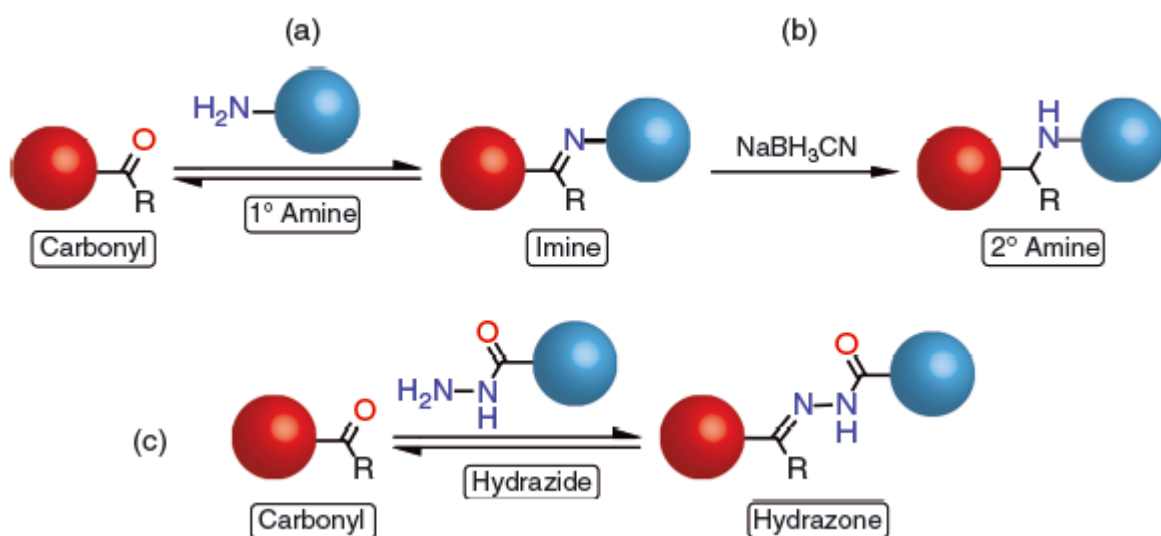
Figure 1.19. Schematic illustration of Schiff-base reaction. (a) The reaction between a carbonyl (aldehyde or ketone) and a primary amine to form an unstable imine, followed by (b) reduction to a stable secondary amine with sodium cyanoborohydride. (c) The reaction between a carbonyl and a hydrazide form a hydrazone bond.[146]
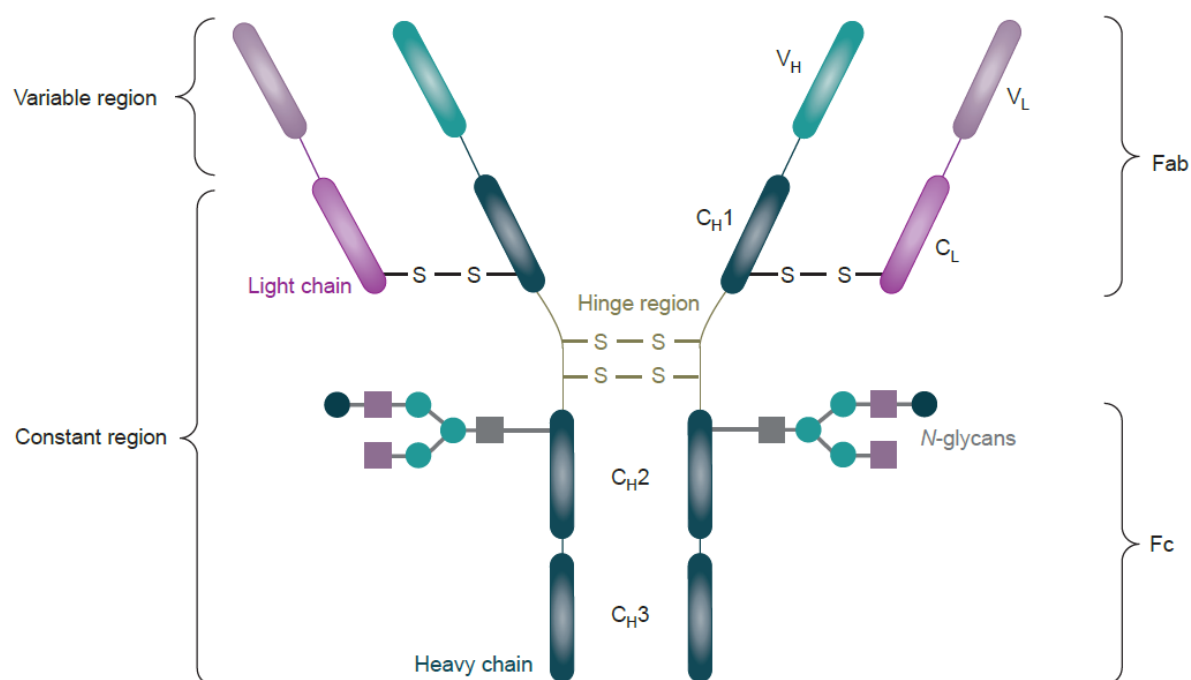
Figure 1.20. The general structure of an immunoglobulin G1 (IgG1) highlighting key components. Fab arms comprise the variable antigen-binding region whereas Fc fragments have a conserved sequence that binds to various cell receptors. N-glycosylation site is at the conserved N297 residue of the Fc region.[147]

1.8. Thesis outline

Our primary goal is to develop effective lanthanide nanoparticles as mass tag reagents that are able to detect low abundance cellular markers in mass cytometry applications. Lanthanide nanoparticle-based mass tags for mass cytometry assays should be stable under physiological conditions, have uniform size with narrow size distribution, show minimal nonspecific bindings to cells, and possess functional groups suitable for conjugation to antibodies or other bio-reagents. Therefore, we focused on designing and fabricating a hydrophilic polymer as a surface coating for LnNPs to meet all the above-mentioned requirements. We developed two conjugation strategies to couple LnNPs with anti-B220 antibody to detect the B220 molecule on mouse spleen B cells and human B cells within PBMCs. Finally we tested conjugation efficiency of LnNP-antibody by flow and mass cytometry assays.

The following chapter (chapter 2) explains the materials and methods, equipment, and instruments used to synthesise and characterisation of LnNPs, biocompatible polymers, surface functionalisation, and bioconjugation of LnNPs.

Chapter 3 explores synthesis and characterisation of LnNPs and hydrophilic polymer with tuneable size. It evaluates long-term colloidal stability and antibody conjugation efficiency of LnNPs with different size of hydrophilic polymers which are the main challenges of LnNPs for biological applications, especially in flow and mass cytometry assays. Carbodiimide chemistry was employed for LnNP-antibody conjugation in which about 0.9% of the coupled antibody retained its activity to recognize B220 biomarkers on the B cells. The low proportion of antibody that retained B220-binding activity was likely due to random orientation coupling of the antibody on the surface of LnNPs. The use of EDC/Sulfo-NHS chemistry also resulted in residual unoccupied carboxylate moieties that produce nonspecific binding, and was unable to exclude free LnNPs. Both factors contributed to a high level of background in mass cytometry. To address these shortcomings, directional antibody conjugation to the LnNPs surface was introduced.

Chapter 4 covers another bioconjugation strategy using Schiff-base chemistry. This method was chosen to ensure directional conjugation of LnNPs and anti-B220 antibody, reducing the likelihood that the antibody orientation would be incompatible with binding to B220 on the surface of cells. New surface modification of LnNPs was carried out by adding a homogeneous functional linker that contained hydrazide. The hydrazide functionalised LnNPs target aldehyde groups that can be generated by oxidising of the conserved glycan in the Fc portion of IgG. This provided a potentially simple and effective method for site-specific and self-oriented immobilization of antibodies on LnNPs in which 13 % of the coupled antibody retained its activity to recognize the B220 molecule. In addition, it required a smaller amount of antibodies during covalent binding as compared to carbodiimide chemistry. Also, the background was significantly reduced in mass cytometry single cell assays.

Finally, chapter 5 summarises the key points of research, research accomplishment, and future perspectives for the development of lanthanide nanoparticles as mass tag reagents for signal enhancement in mass cytometer for identifying of low abundance cellular markers.

References

1.   Health, A. I. o.; Welfare *Cancer data in Australia*; AIHW: Canberra, 2020.

2.   Mitteldorf, C. A. T. S., Cervical cancer screening: from Pap smear to future strategies %J Jornal Brasileiro de Patologia e Medicina Laboratorial. **2016,** *52*, 238-245.

3.   Brett, T., Prostate specific antigen. *Australian family physician* **2011,** *40*, 497-500.

4.   Kościelniak-Merak, B.; Radosavljevic, B.; Zając, A.; Tomasik, P., Faecal Occult Blood Point-of-Care Tests. *Journal of Gastrointestinal Cancer* **2018,** *49*, 1-4.

5.   Dam, J.; Brugge, W., Endoscopy of the Upper Gastrointestinal Tract. *The New England journal of medicine* **2000,** *341*, 1738-48.

6.   Subburaj, K., *CT Scanning – Techniques and Applications*. 2011.

7.   Bradley, S. H.; Abraham, S.; Callister, M. E. J.; Grice, A.; Hamilton, W. T.; Lopez, R. R.; Shinkins, B.; Neal, R. D., Sensitivity of chest X-ray for detecting lung cancer in people presenting with symptoms: a systematic review. *British Journal of General Practice* **2019,** *69* (689), e827.

8.   Guo, R.; Lu, G.; Qin, B.; Fei, B., Ultrasound Imaging Technologies for Breast Cancer Detection and Management: A Review. *Ultrasound in Medicine & Biology* **2017,** *44*.

9.   ojeda-fournier, H.; Comstock, C., MRI for breast cancer: Current indications. *The Indian journal of radiology & imaging* **2009,** *19*, 161-9.

10.   Kumar, S.; Mohan, A.; Guleria, R., Biomarkers in cancer screening, research and detection: present and future: a review. *Biomarkers : biochemical indicators of exposure, response, and susceptibility to chemicals* **2006,** *11*, 385-405.

11.   De Matteis, S.; Bonafè, M.; Giudetti, A. M., Urinary Metabolic Biomarkers in Cancer Patients: An Overview. *Methods in molecular biology (Clifton, N.J.)* **2021,** *2292*, 203-212.

12.   Hanash, S. M.; Pitteri, S. J.; Faca, V. M., Mining the plasma proteome for cancer biomarkers. *Nature* **2008,** *452* (7187), 571-9.

13.   Saerens, D.; Huang, L.; Kristien, B.; Muyldermans, S., Antibody Fragments as Probe in Biosensor Development. *Sensors* **2008,** *8*.

14.   D'Haeseleer, P., How does DNA sequence motif discovery work? *Nature biotechnology* **2006,** *24*, 959-61.

15.   Atkuri, K. R.; Stevens, J. C.; Neubert, H., Mass cytometry: a highly multiplexed single-cell technology for advancing drug development. *Drug metabolism and disposition: the biological fate of chemicals* **2015,** *43* (2), 227-33.

16.   Gérard, A.; Woolfe, A.; Mottet, G.; Reichen, M.; Castrillon, C.; Menrath, V.; Ellouze, S.; Poitou, A.; Doineau, R.; Briseno-Roa, L.; Canales-Herrerias, P.; Mary, P.; Rose, G.; Ortega, C.; Delincé, M.; Essono, S.; Jia, B.; Iannascoli, B.; Richard-Le Goff, O.; Kumar, R.; Stewart, S. N.; Pousse, Y.; Shen, B.; Grosselin, K.; Saudemont, B.; Sautel-Caillé, A.; Godina, A.; McNamara, S.; Eyer, K.; Millot, G. A.; Baudry, J.; England, P.; Nizak, C.; Jensen, A.; Griffiths, A. D.; Bruhns, P.; Brenan, C., High-throughput single-cell activity-based screening and sequencing of antibodies using droplet microfluidics. *Nature biotechnology* **2020,** *38* (6), 715-721.

17.   Kaleem, Z.; Crawford, E.; Pathan, M. H.; Jasper, L.; Covinsky, M. A.; Johnson, L. R.; White, G., Flow cytometric analysis of acute leukemias. Diagnostic utility and critical analysis of data. *Archives of pathology & laboratory medicine* **2003,** *127* (1), 42-8.

18.   Kinsinger, C. R.; Apffel, J.; Baker, M.; Bian, X.; Borchers, C. H.; Bradshaw, R.; Brusniak, M.-Y.; Chan, D. W.; Deutsch, E. W.; Domon, B.; Gorman, J.; Grimm, R.; Hancock, W.; Hermjakob, H.; Horn, D.; Hunter, C.; Kolar, P.; Kraus, H.-J.; Langen, H.; Linding, R.; Moritz, R. L.; Omenn, G. S.; Orlando, R.; Pandey, A.; Ping, P.; Rahbar, A.; Rivers, R.; Seymour, S. L.; Simpson, R. J.; Slotta, D.; Smith, R. D.; Stein, S. E.; Tabb, D. L.; Tagle, D.; Yates, J. R.; Rodriguez, H., Recommendations for mass spectrometry data quality metrics for open access data (corollary to the Amsterdam Principles). *J Proteome Res* **2012,** *11* (2), 1412-1419.

19.   Wang, P.; Whiteaker, J. R.; Paulovich, A. G., The evolving role of mass spectrometry in cancer biomarker discovery. *Cancer Biol Ther* **2009,** *8* (12), 1083-1094.

References

20.   Manzi, M.; Riquelme, G.; Zabalegui, N.; Monge, M. E., Improving diagnosis of genitourinary cancers: Biomarker discovery strategies through mass spectrometry-based metabolomics. *Journal of Pharmaceutical and Biomedical Analysis* **2020,** *178*, 112905.

21.   Danna, E. A.; Nolan, G. P., Transcending the biomarker mindset: deciphering disease mechanisms at the single cell level. *Current opinion in chemical biology* **2006,** *10* (1), 20-27.

22.   Xiao, L.; Zhu, A.; Xu, Q.; Chen, Y.; Xu, J.; Weng, J., Colorimetric Biosensor for Detection of Cancer Biomarker by Au Nanoparticle-Decorated Bi2Se3 Nanosheets. *ACS Applied Materials & Interfaces* **2017,** *9* (8), 6931-6940.

23.   Engvall, E.; Perlmann, P., Enzyme-linked immunosorbent assay (ELISA) quantitative assay of immunoglobulin G. *Immunochemistry* **1971,** *8* (9), 871-874.

24.   Arya, S. K.; Estrela, P., Recent Advances in Enhancement Strategies for Electrochemical ELISA-Based Immunoassays for Cancer Biomarker Detection. *Sensors* **2018,** *18* (7).

25.   Lee, J. W.; Figeys, D.; Vasilescu, J., Biomarker assay translation from discovery to clinical studies in cancer drug development: quantification of emerging protein biomarkers. *Adv Cancer Res* **2007,** *96*, 269-298.

26.   Cummings, J.; Ward, T. H.; Greystoke, A.; Ranson, M.; Dive, C., Biomarker method validation in anticancer drug development. *Br J Pharmacol* **2008,** *153* (4), 646-656.

27.   Schall, R. F., Jr.; Tenoso, H. J., Alternatives to radioimmunoassay: labels and methods. *Clinical Chemistry* **1981,** *27* (7), 1157-1164.

28.   Wu, A. M.; Senter, P. D., Arming antibodies: prospects and challenges for immunoconjugates. *Nature biotechnology* **2005,** *23* (9), 1137-46.

29.   Xue, T.-Y.; Mei, L.-P.; Xu, Y.-T.; Liu, Y.-L.; Fan, G.-C.; Li, H.-Y.; Ye, D.; Zhao, W.-W., Nanoporous Semiconductor Electrode Captures the Quantum Dots: Toward Ultrasensitive Signal-On Liposomal Photoelectrochemical Immunoassay. *Analytical Chemistry* **2019,** *91* (6), 3795-3799.

30.   Hu, Q.; Wei, Q.; Zhang, P.; Li, S.; Xue, L.; Yang, R.; Wang, C.; Zhou, L., An up-converting phosphor technology-based lateral flow assay for point-of-collection detection of morphine and methamphetamine in saliva. *Analyst* **2018,** *143* (19), 4646-4654.

31.   Farka, Z.; Jurik, T.; Kovar, D.; Trnkova, L.; Skladal, P., Nanoparticle-Based Immunochemical Biosensors and Assays: Recent Advances and Challenges. *Chem Rev* **2017,** *117* (15), 9973-10042.

32.   Lee, S. Y.; Lin, M.; Lee, A.; Park, Y. I., Lanthanide-Doped Nanoparticles for Diagnostic Sensing. *Nanomaterials (Basel)* **2017,** *7* (12).

33.   Wang, X.; Wang, X.; Qin, W.; Lin, H.; Wang, J.; Wei, J.; Zhang, Y.; Qian, X., Metal–tag labeling coupled with multiple reaction monitoring-mass spectrometry for absolute quantitation of proteins. *Analyst* **2013,** *138* (18), 5309-5317.

34.   Yang, B.; Zhang, Y.; Chen, B.; He, M.; Yin, X.; Wang, H.; Li, X.; Hu, B., A multifunctional probe for ICP-MS determination and multimodal imaging of cancer cells. *Biosensors & bioelectronics* **2017,** *96*, 77-83.

35.   Jiang, W.; Sun, G.; Zhang, Y.; Hu, Z.; Wen, X.; Men, S.; Xing, Z.; Zhang, S.; Huang, B.; Wang, C., Simultaneous determination of gastric cancer biomarkers pepsinogen PGI/PGII using element tagged immunoassay coupled with inductively coupled plasma mass spectrometry detection. *Journal of Clinical Laboratory Analysis* **2020,** *34* (7), e23287.

36.   Sanz-Medel, A., ICP-MS for multiplex absolute determinations of proteins. *Analytical and Bioanalytical Chemistry* **2010,** *398* (5), 1853-1859.

37.   Alonso-García, F. J.; Blanco-González, E.; Montes-Bayón, M., An inductively coupled plasma-mass spectrometry (ICP-MS) linked immunoassay by means of iodinated antibodies for transferrin quantitative analysis in breast cancer cell lines. *Talanta* **2019,** *194*, 336-342.

38.   Sanz-Medel, A.; Montes-Bayón, M.; del Rosario Fernández de la Campa, M.; Encinar, J. R.; Bettmer, J., Elemental mass spectrometry for quantitative proteomics. *Analytical and bioanalytical chemistry* **2008,** *390* (1), 3-16.

References

39.   Baranov, V.; Quinn, Z.; Bandura, D.; Tanner, S., A Sensitive and Quantitative Element-Tagged Immunoassay with ICPMS Detection. *Analytical chemistry* **2002,** *74*, 1629-36.

40.   Quinn, Z. A.; Baranov, V. I.; Tanner, S. D.; Wrana, J. L., Simultaneous determination of proteins using an element-tagged immunoassay coupled with ICP-MS detection. *Journal of Analytical Atomic Spectrometry* **2002,** *17* (8), 892-896.

41.   Chattopadhyay, P. K.; Gierahn, T. M.; Roederer, M.; Love, J. C., Single-cell technologies for monitoring immune systems. *Nature immunology* **2014,** *15* (2), 128-35.

42.   McKinnon, K. M., Flow Cytometry: An Overview. *Curr Protoc Immunol* **2018,** *120*, 5.1.1-5.1.11.

43.   Bhaumik, A.; Das, S.; Roy Sarkar, S.; Chakraborty, P.; Chowdhury, B., Diagnosis of Acute Leukemia by Flowcytometry in Population of Tripura, North-east India. *Journal of Evidence Based Medicine & Healthcare.* **2014,** *1*, 1320-1328.

44.   Ferrer-Font, L.; Pellefigues, C.; Mayer, J. U.; Small, S. J.; Jaimes, M. C.; Price, K. M., Panel Design and Optimization for High-Dimensional Immunophenotyping Assays Using Spectral Flow Cytometry. *Current Protocols in Cytometry* **2020,** *92* (1), e70.

45.   Antal-Szalmás, P.; Nagy, B., Jr.; Debreceni, I. B.; Kappelmayer, J., Measurement of Soluble Biomarkers by Flow Cytometry. *EJIFCC* **2013,** *23* (4), 135-142.

46.   Yang, H. C.; Rhee, W. J., Single Step In Situ Detection of Surface Protein and MicroRNA in Clustered Extracellular Vesicles Using Flow Cytometry. *Journal of clinical medicine* **2021,** *10* (2).

47.   Chattopadhyay, P. K.; Price, D. A.; Harper, T. F.; Betts, M. R.; Yu, J.; Gostick, E.; Perfetto, S. P.; Goepfert, P.; Koup, R. A.; De Rosa, S. C.; Bruchez, M. P.; Roederer, M., Quantum dot semiconductor nanocrystals for immunophenotyping by polychromatic flow cytometry. *Nat Med* **2006,** *12* (8), 972-7.

48.   Bendall, S. C.; Nolan, G. P.; Roederer, M.; Chattopadhyay, P. K., A deep profiler's guide to cytometry. *Trends Immunol* **2012,** *33* (7), 323-32.

49.   Tanner, S. D.; Baranov, V. I.; Ornatsky, O. I.; Bandura, D. R.; George, T. C., An introduction to mass cytometry: fundamentals and applications. *Cancer Immunol Immunother* **2013,** *62* (5), 955-65.

50.   Spitzer, M. H.; Nolan, G. P., Mass Cytometry: Single Cells, Many Features. *Cell* **2016,** *165* (4), 780-91.

51.   Tanner, S.; Bandura, D.; Ornatsky, O.; Baranov, V.; Nitz, M.; Winnik, M., Flow cytometer with mass spectrometer detection for massively multiplexed single-cell biomarker assay. *Pure Appl. Chem* **2008,** *80*, 2627-2641.

52.   Bodenmiller, B.; Zunder, E. R.; Finck, R.; Chen, T. J.; Savig, E. S.; Bruggner, R. V.; Simonds, E. F.; Bendall, S. C.; Sachs, K.; Krutzik, P. O.; Nolan, G. P., Multiplexed mass cytometry profiling of cellular states perturbed by small-molecule regulators. *Nature biotechnology* **2012,** *30* (9), 858-867.

53.   Parker, D.; Dickins, R. S.; Puschmann, H.; Crossland, C.; Howard, J. A., Being excited by lanthanide coordination complexes: aqua species, chirality, excited-state chemistry, and exchange dynamics. *Chem Rev* **2002,** *102* (6), 1977-2010.

54.   Lou, X.; Zhang, G.; Herrera, I.; Kinach, R.; Ornatsky, O.; Baranov, V.; Nitz, M.; Winnik, M. A., Polymer-based elemental tags for sensitive bioassays. *Angew Chem Int Ed Engl* **2007,** *46* (32), 6111-4.

55.   Majonis, D.; Herrera, I.; Ornatsky, O.; Schulze, M.; Lou, X.; Soleimani, M.; Nitz, M.; Winnik, M. A., Synthesis of a Functional Metal-Chelating Polymer and Steps toward Quantitative Mass Cytometry Bioassays. *Analytical Chemistry* **2010,** *82* (21), 8961-8969.

56.   Illy, N.; Majonis, D.; Herrera, I.; Ornatsky, O.; Winnik, M. A., Metal-chelating polymers by anionic ring-opening polymerization and their use in quantitative mass cytometry. *Biomacromolecules* **2012,** *13* (8), 2359-2369.

57.   Leipold, M. D.; Obermoser, G.; Fenwick, C.; Kleinstuber, K.; Rashidi, N.; McNevin, J. P.; Nau, A. N.; Wagar, L. E.; Rozot, V.; Davis, M. M.; DeRosa, S.; Pantaleo, G.; Scriba, T. J.;

Walker, B. D.; Olsen, L. R.; Maecker, H. T., Comparison of CyTOF assays across sites: Results of a six-center pilot study. *Journal of immunological methods* **2018,** *453*, 37-43.

58.   Bodenmiller, B.; Zunder, E. R.; Finck, R.; Chen, T. J.; Savig, E. S.; Bruggner, R. V.; Simonds, E. F.; Bendall, S. C.; Sachs, K.; Krutzik, P. O.; Nolan, G. P., Multiplexed mass cytometry profiling of cellular states perturbed by small-molecule regulators. *Nature biotechnology* **2012,** *30* (9), 858-67.

59.   Newell, E. W.; Sigal, N.; Nair, N.; Kidd, B. A.; Greenberg, H. B.; Davis, M. M., Combinatorial tetramer staining and mass cytometry analysis facilitate T-cell epitope mapping and characterization. *Nature biotechnology* **2013,** *31* (7), 623-9.

60.   Bandura, D. R.; Baranov, V. I.; Ornatsky, O. I.; Antonov, A.; Kinach, R.; Lou, X.; Pavlov, S.; Vorobiev, S.; Dick, J. E.; Tanner, S. D., Mass Cytometry: Technique for Real Time Single Cell Multitarget Immunoassay Based on Inductively Coupled Plasma Time-of-Flight Mass Spectrometry. *Analytical Chemistry* **2009,** *81* (16), 6813-6822.

61.   Schulz, A. R.; Stanislawiak, S.; Baumgart, S.; Grutzkau, A.; Mei, H. E., Silver nanoparticles for the detection of cell surface antigens in mass cytometry. *Cytometry A* **2017,** *91* (1), 25-33.

62.   Wu, X.; DeGottardi, Q.; Wu, I. C.; Yu, J.; Wu, L.; Ye, F.; Kuo, C. T.; Kwok, W. W.; Chiu, D. T., Lanthanide-Coordinated Semiconducting Polymer Dots Used for Flow Cytometry and Mass Cytometry. *Angew Chem Int Ed Engl* **2017,** *56* (47), 14908-14912.

63.   Vancaeyzeele, C.; Ornatsky, O.; Baranov, V.; Shen, L.; Abdelrahman, A.; Winnik, M. A., Lanthanide-containing polymer nanoparticles for biological tagging applications: nonspecific endocytosis and cell adhesion. *J Am Chem Soc* **2007,** *129* (44), 13653-60.

64.   Zhang, Y.; Zabinyakov, N.; Majonis, D.; Bouzekri, A.; Ornatsky, O.; Baranov, V.; Winnik, M. A., Tantalum Oxide Nanoparticle-Based Mass Tag for Mass Cytometry. *Anal Chem* **2020**.

65.   Tong, L.; Lu, E.; Pichaandi, J.; Zhao, G.; Winnik, M. A., Synthesis of Uniform NaLnF4 (Ln: Sm to Ho) Nanoparticles for Mass Cytometry. *The Journal of Physical Chemistry C* **2016,** *120* (11), 6269-6280.

66.   Pichaandi, J.; Zhao, G.; Bouzekri, A.; Lu, E.; Ornatsky, O.; Baranov, V.; Nitz, M.; Winnik, M. A., Lanthanide nanoparticles for high sensitivity multiparameter single cell analysis. *Chem Sci* **2019,** *10* (10), 2965-2974.

67.   Pichaandi, J.; Tong, L.; Bouzekri, A.; Yu, Q.; Ornatsky, O.; Baranov, V.; Winnik, M. A., Liposome-Encapsulated NaLnF4 Nanoparticles for Mass Cytometry: Evaluating Nonspecific Binding to Cells. *Chemistry of Materials* **2017,** *29* (11), 4980-4990.

68.   Cao, P.; Tong, L.; Hou, Y.; Zhao, G.; Guerin, G.; Winnik, M. A.; Nitz, M., Improving lanthanide nanocrystal colloidal stability in competitive aqueous buffer solutions using multivalent PEG-phosphonate ligands. *Langmuir* **2012,** *28* (35), 12861-70.

69.   Zhao, G.; Tong, L.; Cao, P.; Nitz, M.; Winnik, M. A., Functional PEG-PAMAM-tetraphosphonate capped NaLnF(4) nanoparticles and their colloidal stability in phosphate buffer. *Langmuir* **2014,** *30* (23), 6980-9.

70.   Lu, E.; Pichaandi, J.; Rastogi, C. K.; Winnik, M. A., Effect of Excess Ligand on the Reverse Microemulsion Silica Coating of NaLnF4 Nanoparticles. *Langmuir* **2022,** *38* (10), 3316-3326.

71.   Arnett, L. P.; Liu, J.; Zhang, Y.; Cho, H.; Lu, E.; Closson, T.; Allo, B.; Winnik, M. A., Biotinylated Lipid-Coated NaLnF4 Nanoparticles: Demonstrating the Use of Lanthanide Nanoparticle-Based Reporters in Suspension and Imaging Mass Cytometry. *Langmuir* **2022,** *38* (8), 2525-2537.

72.   Chen, G.; Qiu, H.; Prasad, P. N.; Chen, X., Upconversion nanoparticles: design, nanochemistry, and applications in theranostics. *Chem Rev* **2014,** *114* (10), 5161-214.

73.   Wen, S.; Zhou, J.; Zheng, K.; Bednarkiewicz, A.; Liu, X.; Jin, D., Advances in highly doped upconversion nanoparticles. *Nature Communications* **2018,** *9* (1), 2415.

74.   He, H.; Liu, B.; Wen, S.; Liao, J.; Lin, G.; Zhou, J.; Jin, D., Quantitative Lateral Flow Strip Sensor Using Highly Doped Upconversion Nanoparticles. *Analytical Chemistry* **2018,** *90* (21), 12356-12360.

75.   Bednarkiewicz, A.; Chan, E. M.; Kotulska, A.; Marciniak, L.; Prorok, K., Photon avalanche in lanthanide doped nanoparticles for biomedical applications: super-resolution imaging. *Nanoscale Horizons* **2019,** *4* (4), 881-889.

76.   Wang, F.; Wen, S.; He, H.; Wang, B.; Zhou, Z.; Shimoni, O.; Jin, D., Microscopic inspection and tracking of single upconversion nanoparticles in living cells. *Light: Science & Applications* **2018,** *7* (4), 18007-18007.

77.   Du, Z.; Gupta, A.; Clarke, C.; Cappadona, M.; Clases, D.; Liu, D.; Yang, Z.; Karan, S.; Price, W. S.; Xu, X., Porous Upconversion Nanostructures as Bimodal Biomedical Imaging Contrast Agents. *The Journal of Physical Chemistry C* **2020,** *124* (22), 12168-12174.

78.   Li, M.; Fang, H.; Liu, Q.; Gai, Y.; Yuan, L.; Wang, S.; Li, H.; Hou, Y.; Gao, M.; Lan, X., Red blood cell membrane-coated upconversion nanoparticles for pretargeted multimodality imaging of triple-negative breast cancer. *Biomaterials Science* **2020,** *8* (7), 1802-1814.

79.   Xu, J.; Xu, L.; Wang, C.; Yang, R.; Zhuang, Q.; Han, X.; Dong, Z.; Zhu, W.; Peng, R.; Liu, Z., Near-Infrared-Triggered Photodynamic Therapy with Multitasking Upconversion Nanoparticles in Combination with Checkpoint Blockade for Immunotherapy of Colorectal Cancer. *ACS Nano* **2017,** *11* (5), 4463-4474.

80.   Zhang, Y.; Huang, P.; Wang, D.; Chen, J.; Liu, W.; Hu, P.; Huang, M.; Chen, X.; Chen, Z., Near-infrared-triggered antibacterial and antifungal photodynamic therapy based on lanthanide-doped upconversion nanoparticles. *Nanoscale* **2018,** *10* (33), 15485-15495.

81.   Han, S.; Sung, W.; Kim, T. Y.; Yang, S. J.; Kim, S.; Lee, G.; Cho, K.; Hahn, S. K., Upconversion nanoparticles coated organic photovoltaics for near infrared light controlled drug delivery systems. *Nano Energy* **2021,** *81*, 105650.

82.   Ling, D.; Li, H.; Xi, W.; Wang, Z.; Bednarkiewicz, A.; Dibaba, S. T.; Shi, L.; Sun, L., Heterodimers made of metal–organic frameworks and upconversion nanoparticles for bioimaging and pH-responsive dual-drug delivery. *Journal of Materials Chemistry B* **2020,** *8* (6), 1316-1325.

83.   I, Y. L.; Jiang, M.; Xue, Z.; Zeng, S., 808 nm light triggered lanthanide nanoprobes with enhanced down-shifting emission beyond 1500 nm for imaging-guided resection surgery of tumor and vascular visualization. *Theranostics* **2020,** *10* (15), 6875-6885.

84.   Zhong, Y.; Dai, H., A mini-review on rare-earth down-conversion nanoparticles for NIR-II imaging of biological systems. *Nano Research* **2020,** *13*.

85.   Lin, W.; Hou, Y.; Lu, Y.; Abdelrahman, A. I.; Cao, P.; Zhao, G.; Tong, L.; Qian, J.; Baranov, V.; Nitz, M.; Winnik, M. A., A High-Sensitivity Lanthanide Nanoparticle Reporter for Mass Cytometry: Tests on Microgels as a Proxy for Cells. *Langmuir* **2014,** *30* (11), 3142-3153.

86.   Pichaandi, J.; Zhao, G.; Bouzekri, A.; Lu, E.; Ornatsky, O.; Baranov, V.; Nitz, M.; Winnik, M. A., Lanthanide nanoparticles for high sensitivity multiparameter single cell analysis. *Chemical Science* **2019,** *10* (10), 2965-2974.

87.   Ornatsky, O.; Bandura, D.; Baranov, V.; Nitz, M.; Winnik, M. A.; Tanner, S., Highly multiparametric analysis by mass cytometry. *J Immunol Methods* **2010,** *361* (1-2), 1-20.

88.   Qiu, P.; Zhou, N.; Chen, H.; Zhang, C.; Gao, G.; Cui, D., Recent advances in lanthanide-doped upconversion nanomaterials: synthesis, nanostructures and surface modification. *Nanoscale* **2013,** *5* (23), 11512-25.

89.   Li, H.; Xu, L.; Chen, G., Controlled Synthesis of Monodisperse Hexagonal NaYF(4):Yb/Er Nanocrystals with Ultrasmall Size and Enhanced Upconversion Luminescence. *Molecules* **2017,** *22* (12).

90.   Gainer, C. F.; Romanowski, M., A review of synthetic methods for the production of upconverting lanthanide nanoparticles. *Journal of Innovative Optical Health Sciences* **2013,** *07* (02), 1330007.

91.   Dong, H.; Du, S. R.; Zheng, X. Y.; Lyu, G. M.; Sun, L. D.; Li, L. D.; Zhang, P. Z.; Zhang, C.; Yan, C. H., Lanthanide Nanoparticles: From Design toward Bioimaging and Therapy. *Chem Rev* **2015,** *115* (19), 10725-815.

92. Zhang, Y.-W.; Sun, X.; Si, R.; You, L.-P.; Yan, C.-H., Single-Crystalline and Monodisperse LaF3 Triangular Nanoplates from a Single-Source Precursor. *Journal of the American Chemical Society* **2005,** *127* (10), 3260-3261.

93. Mader, H. S.; Kele, P.; Saleh, S. M.; Wolfbeis, O. S., Upconverting luminescent nanoparticles for use in bioconjugation and bioimaging. *Curr Opin Chem Biol* **2010,** *14* (5), 582-96.

94. Li, F.; Li, J.; Chen, L.; Huang, Y.; Peng, Y.; Luo, Y.; Zhang, L.; Mu, J., Hydrothermal Synthesis and Upconversion Properties of About 19 nm Sc2O3: Er3+, Yb3+ Nanoparticles with Detailed Investigation of the Energy Transfer Mechanism. *Nanoscale Research Letters* **2018,** *13* (1), 372.

95. Liang, Y.; Noh, H. M.; Xue, J.; Choi, H.; Park, S. H.; Choi, B. C.; Kim, J. H.; Jeong, J. H., High quality colloidal GdVO4:Yb,Er upconversion nanoparticles synthesized via a protected calcination process for versatile applications. *Materials & Design* **2017,** *130*, 190-196.

96. Gai, S.; Li, C.; Yang, P.; Lin, J., Recent progress in rare earth micro/nanocrystals: soft chemical synthesis, luminescent properties, and biomedical applications. *Chem Rev* **2014,** *114* (4), 2343-89.

97. Tinwala, H.; Shah, D.; Menghani, J.; Pati, R., Synthesis of La2Ce2O7 Nanoparticles by Co-Precipitation Method and Its Characterization. *Journal of Nanoscience and Nanotechnology* **2014,** *14*, 6072-6076.

98. Shen, H.; Wang, F.; Fan, X.; Wang, M., Synthesis of LaF3: Yb3+ ,Ln3+ nanoparticles with improved upconversion luminescence. *Journal of Experimental Nanoscience* **2007,** *2* (4), 303-311.

99. Ye, X.; Collins, J. E.; Kang, Y.; Chen, J.; Chen, D. T.; Yodh, A. G.; Murray, C. B., Morphologically controlled synthesis of colloidal upconversion nanophosphors and their shape-directed self-assembly. *Proc Natl Acad Sci U S A* **2010,** *107* (52), 22430-5.

100. Jia, G.; Lu, Y.; Zheng, Y.; Song, Y.; You, H., Facile Synthesis and Luminescence Properties of Highly Uniform MF/YVO 4 :Ln 3+ (Ln = Eu, Dy, and Sm) Composite Microspheres. *Crystal Growth & Design - CRYST GROWTH DES* **2009,** *9*, 3702-3706.

101. Xu, Z.; Gao, Y.; Liu, T.; Wang, L.; Bian, S.; Lin, J., General and facile method to fabricate uniform Y2O3:Ln3+ (Ln3+ = Eu3+, Tb3+) hollow microspheres using polystyrene spheres as templates. *Journal of Materials Chemistry* **2012,** *22* (40), 21695-21703.

102. Chen, M.; Xie, L.; Li, F.; Zhou, S.; Wu, L., Capillary-force-induced formation of luminescent polystyrene/(rare-earth-doped nanoparticle) hybrid hollow spheres. *ACS applied materials & interfaces* **2010,** *2* (10), 2733-2737.

103. Muhr, V.; Wilhelm, S.; Hirsch, T.; Wolfbeis, O. S., Upconversion nanoparticles: from hydrophobic to hydrophilic surfaces. *Acc Chem Res* **2014,** *47* (12), 3481-93.

104. Boyer, J.-C.; Manseau, M.-P.; Murray, J. I.; van Veggel, F. C. J. M., Surface modification of upconverting NaYF4 nanoparticles with PEG-phosphate ligands for NIR (800 nm) biolabeling within the biological window. *Langmuir : the ACS journal of surfaces and colloids* **2010,** *26* (2), 1157-1164.

105. Sedlmeier, A.; Gorris, H. H., Surface modification and characterization of photon-upconverting nanoparticles for bioanalytical applications. *Chem Soc Rev* **2015,** *44* (6), 1526-60.

106. Liu, Y.; Tu, D.; Zhu, H.; Ma, E.; Chen, X., Lanthanide-doped luminescent nano-bioprobes: from fundamentals to biodetection. *Nanoscale* **2013,** *5* (4), 1369-1384.

107. Du, Q.; Wu, X.; Bi, W.; Xing, B.; Yeow, E. K. L., Increasing antibiotic activity by rapid bioorthogonal conjugation of drug to resistant bacteria using an upconverted light-activated photocatalyst. *Journal of Materials Chemistry B* **2021**.

108. Bao, Y.; Luu, Q. A. N.; Lin, C.; Schloss, J. M.; May, P. S.; Jiang, C., Layer-by-layer assembly of freestanding thin films with homogeneously distributed upconversion nanocrystals. *Journal of Materials Chemistry* **2010,** *20* (38), 8356-8361.

109.   Chen, Z.; Chen, H.; Hu, H.; Yu, M.; Li, F.; Zhang, Q.; Zhou, Z.; Yi, T.; Huang, C., Versatile synthesis strategy for carboxylic acid-functionalized upconverting nanophosphors as biological labels. *J Am Chem Soc* **2008,** *130* (10), 3023-9.

110.   Hu, H.; Yu, M.; Li, F.; Chen, Z.; Gao, X.; Xiong, L.; Huang, C., Facile Epoxidation Strategy for Producing Amphiphilic Up-Converting Rare-Earth Nanophosphors as Biological Labels. *Chemistry of Materials* **2008,** *20* (22), 7003-7009.

111.   Zhou, H.-P.; Xu, C.-H.; Sun, W.; Yan, C.-H., Clean and Flexible Modification Strategy for Carboxyl/Aldehyde-Functionalized Upconversion Nanoparticles and Their Optical Applications. *Advanced Functional Materials* **2009,** *19* (24), 3892-3900.

112.   Dai, Y.; Yang, D.; Ma, P.; Kang, X.; Zhang, X.; Li, C.; Hou, Z.; Cheng, Z.; Lin, J., Doxorubicin conjugated NaYF(4):Yb(3+)/Tm(3+) nanoparticles for therapy and sensing of drug delivery by luminescence resonance energy transfer. *Biomaterials* **2012,** *33* (33), 8704-13.

113.   Kumar, R.; Nyk, M.; Ohulchanskyy, T. Y.; Flask, C. A.; Prasad, P. N., Combined Optical and MR Bioimaging Using Rare Earth Ion Doped NaYF4 Nanocrystals. *Advanced Functional Materials* **2009,** *19* (6), 853-859.

114.   Bogdan, N.; Vetrone, F.; Ozin, G. A.; Capobianco, J. A., Synthesis of ligand-free colloidally stable water dispersible brightly luminescent lanthanide-doped upconverting nanoparticles. *Nano letters* **2011,** *11* (2), 835-40.

115.   Bogdan, N.; Rodríguez, E. M.; Sanz-Rodríguez, F.; Iglesias de la Cruz, M. a. C.; Juarranz, Á.; Jaque, D.; Solé, J. G.; Capobianco, J. A., Bio-functionalization of ligand-free upconverting lanthanide doped nanoparticles for bio-imaging and cell targeting. *Nanoscale* **2012,** *4* (12), 3647-3650.

116.   Kong, L.; Kong, K.; Zhao, Y.; Chu, H., Tuning the luminescence properties of lanthanide coordination polymers with Ag@SiO2 nanoparticles. *Dalton Transactions* **2017,** *46* (19), 6447-6455.

117.   Mi, C.; Zhang, J.; Gao, H.; Wu, X.; Wang, M.; Wu, Y.; Di, Y.; Xu, Z.; Mao, C.; Xu, S., Multifunctional nanocomposites of superparamagnetic (Fe3O4) and NIR-responsive rare earth-doped up-conversion fluorescent (NaYF4 : Yb,Er) nanoparticles and their applications in biolabeling and fluorescent imaging of cancer cells. *Nanoscale* **2010,** *2* (7), 1141-1148.

118.   Xing, H.; Bu, W.; Zhang, S.; Zheng, X.; Li, M.; Chen, F.; He, Q.; Zhou, L.; Peng, W.; Hua, Y.; Shi, J., Multifunctional nanoprobes for upconversion fluorescence, MR and CT trimodal imaging. *Biomaterials* **2012,** *33* (4), 1079-1089.

119.   Sivakumar, S.; Diamente, P. R.; van Veggel, F. C., Silica-coated Ln3+-Doped LaF3 nanoparticles as robust down- and upconverting biolabels. *Chemistry (Weinheim an der Bergstrasse, Germany)* **2006,** *12* (22), 5878-84.

120.   Li, Z.; Guo, H.; Qian, H.; Hu, Y., Facile microemulsion route to coat carbonized glucose on upconversion nanocrystals as high luminescence and biocompatible cell-imaging probes. *Nanotechnology* **2010,** *21* (31), 315105.

121.   Wang, F.; Yang, X.; Ma, L.; Huang, B.; Na, N.; E, Y.; He, D.; Ouyang, J., Multifunctional up-converting nanocomposites with multimodal imaging and photosensitization at near-infrared excitation. *Journal of Materials Chemistry* **2012,** *22* (47), 24597-24604.

122.   Back, M.; Casagrande, E.; Brondin, C. A.; Ambrosi, E.; Cristofori, D.; Ueda, J.; Tanabe, S.; Trave, E.; Riello, P., Lanthanide-Doped Bi2SiO5@SiO2 Core–Shell Upconverting Nanoparticles for Stable Ratiometric Optical Thermometry. *ACS Applied Nano Materials* **2020,** *3* (3), 2594-2604.

123.   Zhou, M.; Ge, X.; Ke, D.-M.; Tang, H.; Zhang, J.-Z.; Calvaresi, M.; Gao, B.; Sun, L.; Su, Q.; Wang, H., The Bioavailability, Biodistribution, and Toxic Effects of Silica-Coated Upconversion Nanoparticles in vivo. **2019,** *7* (218).

124.   Rantanen, T.; Järvenpää, M.-L.; Vuojola, J.; Arppe, R.; Kuningas, K.; Soukka, T., Upconverting phosphors in a dual-parameter LRET-based hybridization assay. *Analyst* **2009,** *134* (8), 1713-1716.

125. Duong, H. T. T.; Chen, Y.; Tawfik, S. A.; Wen, S.; Parviz, M.; Shimoni, O.; Jin, D., Systematic investigation of functional ligands for colloidal stable upconversion nanoparticles. *RSC Advances* **2018,** *8* (9), 4842-4849.

126. Liu, B.; Shen, H.; Liu, D.; Hao, Y.; Zhu, X.; Shen, Q.; Qu, P.; Xu, M., Citrate/Tb lanthanide coordination polymer nanoparticles: Preparation and sensing of guanosine-5-monophosphate. *Sensors and Actuators B: Chemical* **2019,** *300*, 126879.

127. Boyer, J. C.; Manseau, M. P.; Murray, J. I.; van Veggel, F. C., Surface modification of upconverting NaYF4 nanoparticles with PEG-phosphate ligands for NIR (800 nm) biolabeling within the biological window. *Langmuir* **2010,** *26* (2), 1157-64.

128. Bogdan, N.; Vetrone, F.; Roy, R.; Capobianco, J. A., Carbohydrate-coated lanthanide-doped upconverting nanoparticles for lectin recognition. *Journal of Materials Chemistry* **2010,** *20* (35), 7543-7550.

129. Juan, J.; Cheng, L.; Shi, M.; Liu, Z.; Mao, X., Poly-(allylamine hydrochloride)-coated but not poly(acrylic acid)-coated upconversion nanoparticles induce autophagy and apoptosis in human blood cancer cells. *Journal of Materials Chemistry B* **2015,** *3* (28), 5769-5776.

130. Nyk, M.; Kumar, R.; Ohulchanskyy, T. Y.; Bergey, E. J.; Prasad, P. N., High Contrast in Vitro and in Vivo Photoluminescence Bioimaging Using Near Infrared to Near Infrared Up-Conversion in Tm3+ and Yb3+ Doped Fluoride Nanophosphors. *Nano letters* **2008,** *8* (11), 3834-3838.

131. Chen, G.; Ohulchanskyy, T. Y.; Law, W. C.; Ågren, H.; Prasad, P. N., Monodisperse NaYbF4 : Tm3+/NaGdF4 core/shell nanocrystals with near-infrared to near-infrared upconversion photoluminescence and magnetic resonance properties. *Nanoscale* **2011,** *3* (5), 2003-2008.

132. Jiang, S.; Win, K. Y.; Liu, S.; Teng, C. P.; Zheng, Y.; Han, M. Y., Surface-functionalized nanoparticles for biosensing and imaging-guided therapeutics. *Nanoscale* **2013,** *5* (8), 3127-48.

133. Xiong, L.; Chen, Z.; Tian, Q.; Cao, T.; Xu, C.; Li, F., High contrast upconversion luminescence targeted imaging in vivo using peptide-labeled nanophosphors. *Anal Chem* **2009,** *81* (21), 8687-94.

134. Chen, Q.; Wang, X.; Chen, F.; Zhang, Q.; Dong, B.; Yang, H.; Liu, G.; Zhu, Y., Functionalization of upconverted luminescent NaYF4 : Yb/Er nanocrystals by folic acid–chitosan conjugates for targeted lung cancer cell imaging. *Journal of Materials Chemistry* **2011,** *21* (21), 7661-7667.

135. Zhan, Q.; Qian, J.; Liang, H.; Somesfalean, G.; Wang, D.; He, S.; Zhang, Z.; Andersson-Engels, S., Using 915 nm Laser Excited Tm3+/Er3+/Ho3+-Doped NaYbF4 Upconversion Nanoparticles for in Vitro and Deeper in Vivo Bioimaging without Overheating Irradiation. *ACS Nano* **2011,** *5* (5), 3744-3757.

136. Shen, J.; Sun, L.-D.; Zhang, Y.-W.; Yan, C.-H., Superparamagnetic and upconversion emitting Fe3O4/NaYF4 : Yb,Er hetero-nanoparticles via a crosslinker anchoring strategy. *Chemical Communications* **2010,** *46* (31), 5731-5733.

137. Hou, Y.; Qiao, R.; Fang, F.; Wang, X.; Dong, C.; Liu, K.; Liu, C.; Liu, Z.; Lei, H.; Wang, F.; Gao, M., NaGdF4 Nanoparticle-Based Molecular Probes for Magnetic Resonance Imaging of Intraperitoneal Tumor Xenografts in Vivo. *ACS Nano* **2013,** *7* (1), 330-338.

138. Liu, C.; Gao, Z.; Zeng, J.; Hou, Y.; Fang, F.; Li, Y.; Qiao, R.; Shen, L.; Lei, H.; Yang, W.; Gao, M., Magnetic/Upconversion Fluorescent NaGdF4:Yb,Er Nanoparticle-Based Dual-Modal Molecular Probes for Imaging Tiny Tumors in Vivo. *ACS Nano* **2013,** *7* (8), 7227-7240.

139. Himmelstoß, S. F.; Hirsch, T., Long-Term Colloidal and Chemical Stability in Aqueous Media of NaYF4-Type Upconversion Nanoparticles Modified by Ligand-Exchange. *Particle & Particle Systems Characterization* **2019,** *36* (10).

140. Yang, Y. S.; Atukorale, P. U.; Moynihan, K. D.; Bekdemir, A.; Rakhra, K.; Tang, L.; Stellacci, F.; Irvine, D. J., High-throughput quantitation of inorganic nanoparticle biodistribution at the single-cell level using mass cytometry. *Nat Commun* **2017,** *8*, 14069.

References

141.   Conde, J.; Dias, J. T.; Grazu, V.; Moros, M.; Baptista, P. V.; de la Fuente, J. M., Revisiting 30 years of biofunctionalization and surface chemistry of inorganic nanoparticles for nanomedicine. *Front Chem* **2014,** *2*, 48.

142.   Gnach, A.; Bednarkiewicz, A., Lanthanide-doped up-converting nanoparticles: Merits and challenges. *Nano Today* **2012,** *7* (6), 532-563.

143.   Hermanson, G. T., Chapter 1 - Introduction to Bioconjugation. In *Bioconjugate Techniques (Third Edition)*, Hermanson, G. T., Ed. Academic Press: Boston, 2013; pp 1-125.

144.   Hermanson, G. T., Chapter 2 - Functional Targets for Bioconjugation. In *Bioconjugate Techniques (Third Edition)*, Hermanson, G. T., Ed. Academic Press: Boston, 2013; pp 127-228.

145.   Sperling, R. A.; Parak, W. J., Surface modification, functionalization and bioconjugation of colloidal inorganic nanoparticles. *Philos Trans A Math Phys Eng Sci* **2010,** *368* (1915), 1333-83.

146.   Algar, W. R., A Brief Introduction to Traditional Bioconjugate Chemistry. In *Chemoselective and Bioorthogonal Ligation Reactions*, 2017; pp 1-36.

147.   Chudasama, V.; Maruani, A.; Caddick, S., Recent advances in the construction of antibody-drug conjugates. *Nat Chem* **2016,** *8* (2), 114-9.

Chapter 2: Materials and Methods

2.1.   Materials

Yttrium(III) chloride hexahydrate ($YCl_3 \cdot 6H_2O$), ytterbium(III) chloride hexahydrate ($YbCl_3 \cdot 6H_2O$), erbium(III) chloride hexahydrate ($ErCl_3 \cdot 6H_2O$), sodium hydroxide (NaOH), ammonium fluoride (NH_4F) with 99.99% trace metals basis, oleic acid (OA), 1-Octadecene (ODE) with technical grade 90%, ethanol 100% pure, methanol 100% pure, cyclohexane for HPLC, $\geq$99.9%, tetrahydrofuran (THF) anhydrous, $\geq$99.9% inhibitor-free. Sodium fluoride (NaF) 99.99% trace metals basis, were purchased from Sigma Aldrich (Australia). Sodium hydroxide solution (50% in H_2O), 1-Butanethiol 99% (CH_3 $(CH_2)_3SH$), Milli-Q® integral water, Acetone Laboratory Reagent, $\geq$99.5% (CH_3COCH_3), Carbon disulphide (CS_2) anhydrous, $\geq$99%, 2-Bromopropionic acid 99% ($CH_3CHBrCOOH$), Hydrochloric acid ACS reagent, 37% (HCl), n-Hexane anhydrous, 95% ($CH_3(CH_2)_4CH_3$), monomer oligo(ethylene glycol) methyl ether acrylate with average Mn of 480 g.mol^{-1} (OEGMEA), 2,2'-azobisisobutyronitrile (AIBN) 97%, purified by recrystallisation twice from methanol, petroleum spirit boiling range 40-60°C, toluene anhydrous, 99.8% ($C_6H_5CH_3$), dialysis membrane with various molecular weight cut-offs from 3000 Da to 14000 Da, were purchased from Sigma Aldrich, Monoacryloxyethyl phosphate (MAEP) was purchased from Polyscience, USA. HEPES buffer solution 1 M, MES hydrate $\geq$99.5% (titration), Tris Buffer, 1.0 M, pH 8.0, Molecular Biology Grade - CAS 77-86-1 – Calbiochem, were supplied from Sigma Aldrich. N-(3-dimethylaminopropyl)-N′ -ethylcarbodiimide hydrochloride (EDC), adipic acid dihydrazide (ADH) $\geq$98% (titration) sodium chloride, N-hydroxysulfosuccinimide (Sulfo-NHS), O-2-(6-Oxocaproylamino) ethyl-O′-methylpolyethylene glycol 2′000, Sodium cyanoborohydride solution ($NaBH_3CN$) 5.0 M in 1 M NaOH, sodium periodate ($NaIO_4$) ACS reagent, $\geq$99.8%, were purchased from Sigma Aldrich. Bovine Serum Albumin (BSA), heat shock fraction, protease-free, fatty acid-free, essentially globulin free, pH 7, $\geq$98% were supplied from Sigma Aldrich. Rat monoclonal Ab (mAb) RA3-6B2 specific for mouse and human B220/CD45R was purchased from Bio-Legend. Phycoerythrin (PE)-conjugated goat anti-rat IgG, Falcon®, glycerol for molecular biology, $\geq$99.0%, purpald® $\geq$99%, Fetal calf serum, were purchased from Sigma Aldrich. Synthetic HFS buffer at (150 mM NaCl, 1 mM NaF, 15 mM HEPES, 5% fetal calf serum). 10% Paraformaldehyde (PFA) ampules (wt/vol in

water). DNA intercalator: 1 mL HEPES buffer 20 mM, 100 μL of 10% PFA, and 0.25 μL of Ir-Intercalator chelating polymer (500 μM stock concentration, Fluidigm).

2.2.   Equipment

Magnetic stirrer (0-1800 rpm), heating mantle (Range: room temperature to 400 °C), temperature controller (Range: room temperature to 400 °C) were purchased from Labquip (Australia). Three-neck round-bottom flask (50 mL, 100 mL), Flow control adapter (19/22) were supplied from Synthware (China). Teflon-coated, Elliptical rare earth extra power stir bars (15 × 10 mm) were purchased from Sigma-Aldrich (Australia). Micropipettes ranges: 10–100 μL, 100–1,000 μL, and 500–5,000 μL; Centrifuge 5424 and Centrifuge 5804 were supplied from Eppendorf (Germany), Vortex mixer (LSE) was purchased from Corning (Australia), ultrasonic cleaner Commercial Benchtop Cleaners (FXP) 2.7 Liter was purchased from Unisonics (Australia), Laboratory balance SJF2104 (0.1 mg) was supplied from ProSciTech (Australia). 2-neck round-bottom flask (50 mL, 100 mL), 1-neck round-bottom flask (25 mL), rubber septum, thermometer, syringes and needles, Aldrich® Essentials beaker, Griffin low form, capacity (5 mL, 25 mL, 50 mL, 100 mL) were purchased from Sigma Aldrich, Hotplate Magnetic Stirrers was supplied from Labfriend (Australia), Electrothermal IA6304 Benchtop Melting Point Apparatus Needs Lamp Covers, NRTL Certified 53L 200C Vacuum Oven (16x14x15") with Digital Temperature Controller - DZF-6050-ETL were purchased from Unisonics (Australia), Laboratory freeze dryer VaCo 2 was supplied from Labfriend (Australia). Oil bath which contains silicone oil was purchased from chem supply. Eppendorf tubes, BRAND® microcentrifuge tube, (1.5 mL, 2 mL) with lid, PP transparent, pack of 500, PARAFILM® M roll size 2 in. × 250 ft, were purchased from Sigma Aldrich. LLG-Headspace-Vials ND20 (5 mL and 10 mL) was supplied from Labfriend (Australia). Round-Bottom Polypropylene Tubes, 5 mL sterile polypropylene round-bottom tube for cell separation and cell culture; with or without caps were purchased from BioLegend. Amicon® Ultra 0.5 mL Centrifugal Filters, 96-well round-bottom plates (Greiner), were supplied from Sigma Alderich. Laboratory freeze-dryer VaCo 2 was supplied from Labfriend (Australia)

2.3. Characterisation methods and instruments

2.3.1 Transmission Electron Microscope (TEM)

TEM is a microscopy technique in which a beam of electrons is transmitted through a sample to form an image. The sample thickness should be less than 100 nm. An image is formed from the interaction of the electrons with the sample as the beam is transmitted through the specimen. The image is then magnified and focused onto an imaging device, such as a fluorescent screen, a layer of photographic film, or a sensor such as a scintillator attached to a charge-coupled device.[1] For LnNPs samples, TEM measurements were carried out using FEI Tecnai G2 20 TEM with a beam voltage of 200 kV. The OA capped LnNPs were drop-cast on a carbon-coated copper grid. Since the polymer-coated LnNPs are hydrophilic, the grids were pre-treated by glow discharge to render the surfaces hydrophilicity by producing the film surface negatively charged. LnNPs samples were diluted in cyclohexane, miliQ water, and different buffers at the concentration of 1 mg/mL to avoid aggregation.

2.3.2 Dynamic Light Scattering (DLS)

DLS is a technique to determine the size distribution of small particles in suspension. DLS measurements were performed by Malvern Instruments Zetasizer Nano ZS instrument equipped with a 4 mV He–Ne laser operating at 633 nm with a 173° backscatter measurement angle.[2] Three runs of 30 cycles were performed to determine the reproducibility and standard deviation of the measured hydrodynamic size values of nanoparticles. LnNPs samples were suspended in solvent at the concentration of 1 mg/mL and kept in disposabale cuvette. Size histograms were plotted by using Origin 2019 64Bit software.

2.3.3 Zeta Potential

The surface charge of LnNP samples were determined by Malvern Instruments Zetasizer Nano ZS instrument equipped with a 4 mV He–Ne laser operating at 633 nm. All measurements were performed in triplicate. The samples were kept in a capillary cuvette. The surface charge of functionalised LnNPs were calculated with software embedded in the instrument.

2.3.4 Fourier Transform Infrared Spectroscopy (FTIR)

FTIR is a technique used to obtain an infrared spectrum of absorption or emission of organic compondes in different phases such as solid, liquid, or gas. An FTIR spectrometer

simultaneously collects high-resolution spectral data over a wide spectral range.[3] In our study, FTIR spectra of samples were obtained using a Nicolet 7650 system. The samples were dried at 60°C in a vaccume oven overnight and the range of all the data was obtained from 4000 to 500 cm^{-1} with 64 scans.

2.3.5   Nuclear Magnetic Resonance (^{1}HNMR, ^{13}CNMR, ^{31}PNMR):

NMR is unique, well-resolved, and highly predictable for organic molecules. Different functional groups are distinguishable, and identical functional groups with differing neighboring substituents, still give different signals.[4] ^{1}HNMR spectra of the polymer were characterised by a 500 MHz Agilent instrument at 25°C in d$_6$-DMSO and D$_2$O. ^{1}HNMR, ^{13}C NMR, and ^{31}PNMR were carried out in CDCl$_3$ and D$_2$O, respectively.

2.3.6   Gel Permeation Chromatography (GPC):

GPC is a type of size exclusion chromatography (SEC) that separates analysts based on hydrodynamic volume, typically in organic solvents. The technique is often used for the analysis of polymers by which one can estimate the molecular weight and Đ of polymers.[5] Experiments were run on a Shimadzu modular system with SIL-10AD autoinjector, LC-10AT pump, CTO-10A oven, 5.0 μm bead guard column (50 × 7.8 mm) followed by four 300 × 7.8 mm linear columns with 500, 103, 104, 105 Å pore size and 5 μm particle size. The solvent system was N,N-dimethylacetamide (HPLC grade) with 0.05% w/v 2,6-dibutyl-4-methylphenol and 0.03% w/v LiBr. The flow rate was 1 mL min^{-1} at 50 °C and a refractive index detector was used (Shimadzu RID-10A). The calibration was performed using narrow polydispersity PMMA standards (0.5–1000 kDa) purchased from Polymer Laboratories.

2.3.7   Thermal Gravimetric Analysis (TGA):

The thermal gravimetric analyser continuously measures the mass of the sample while the temperature of a sample is changed over time.[6] In our experiments, TGA was conducted on a SQ600. Freeze-dried samples were heated from room temperature to 700 °C with constant temperature heat of 10 °C/min using N$_2$ as furnace gas with a ramp of 100 mL/min. The weight loss of polymers was calculated from 100 °C as the weight loss from RT to 100 °C was related to extra moisture.

2.3.8   NanoDrop™ 2000/2000c Spectrophotometers

Nano-Drop is full-spectrum, UV-Vis spectrophotometers used to quantify and assess the purity of DNA, RNA, protein and more.[7] The Nano-Drop 2000 and 2000c are the only

micro-volume spectrophotometers with patented sample retention technology that measure sample volumes as small as 0.5 μL. In our experiments, the NanoDrop was carried out to measure the antibody concentrations by which 2 μL of each sample was dipped onto the lower measurement pedestal to obtain the spectrum profiles at 280 nm.

2.3.9 Flow Cytometry (LSRFortessa X-20 flow cytometer (Becton Dickinson)

In flow cytometry, a suspension of single cells is labelled with antibodies against various surface or intracellular targets. These antibodies are conjugated to fluorescent molecules (fluorophores) that emit light when excited by a laser. Emitted light is captured by a fluorescence detector. The use of multiple lasers and detectors allows us to label cells with up to 26 individual fluorophore-conjugated antibodies.[8] This is a 4-laser cell analyser (405 nm, 488 nm, 561 nm, 628 nm, 20 parameters: 18 colours, 2 scatter), sample acquisition of 10,000 events/sec. Cells were resuspended in (100 μL) HFS in a 5 mL tube before abalysis. Data were analysed using FlowJo software (Becton Dickinson) and the mean fluorescence intensity of labelled populations was calculated to measure specific Ab binding.

2.3.10 Mass Cytometry (CyTOF) (Helios platform, (Fluidigm)

Put simply, mass cytometry replaces the fluorescent reporters used in fluorescence flow cytometry with metal isotopes, which are detected using time-of-flight mass spectrometry. This has expanded the number of parameters that can be detected simultaneously on single cells to approximately 40 (with >100 theoretically achievable), due to the absence of signal overlap between metal isotopes. This allows an investigator to measure a large number of extracellular and intracellular targets simultaneously. The preparation of samples for mass cytometry assays, dead cells were identified by incubation with cis-platinum, then samples were fixed in paraformaldehyde, and ^{191,193}Iridium was added to identify DNA, allowing cells to be identified. Data were normalised with reference to signals from lanthanide-containing beads included in each sample. Data were analysed using FlowJo software (Becton Dickinson). The LnNPs used in this project contain a mixture of metal isotopes that are distributed over 10 distinct channels in data from the Helios (^{89}Y, 24%; ^{174}Yb, 21%; ^{172}Yb, 15%; ^{173}Yb, 11%; ^{171}Yb, 10%; ^{176}Yb, 8%; ^{170}Er, 4%; ^{168}Er, 3%; ^{166}Er, 3%; ^{167}Er, 2%). For analysis, the ^{89}Y signal representing ~25% of total signal was analysed. Future conjugates manufactured specifically for mass cytometric applications will be made with isotopically pure

nanoparticles, so the expected signal will be four-fold higher than those presented in this project.

References

1.   Kannan, M., Transmission Electron Microscope -Principle, Components and Applications Illumination system (Electron gun and condenser lenses) Electron gun. 2018; pp 93-101.
2.   Sandhu, R.; Singh, N.; Dhankhar, J.; Gandhi, K.; Sharma, R., Dynamic light scattering (DLS) technique, principle, theoretical considerations and applications. 2018; pp 135-137.
3.   Khan, S.; Khan, S.; Khan, L.; Farooq, A.; Akhtar, K.; Asiri, A. M., Fourier Transform Infrared Spectroscopy: Fundamentals and Application in Functional Groups and Nanomaterials Characterization. 2018; pp 317-344.
4.   Edwards, J., Principles of NMR. **2009**.
5.   Hussain, Z., *Gel permeation Chromatography*. 2021.
6.   Ng, H. M.; mohamad saidi, N.; Omar, F. S.; Kasi, R.; T subramaniam, R.; Baig, S., Thermogravimetric Analysis of Polymers. **2018**, 1-29.
7.   Desjardins, P.; Hansen, J.; Allen, M., Microvolume Protein Concentration Determination Using the NanoDrop 2000c Spectrophotometer. *Journal of visualized experiments : JoVE* **2009,** *33*.
8.   Shukla, J., *Flow cytometry: An introduction and application to cytology*. 2018.

Chapter 3: Stable and high-efficient antibody-nanoparticles conjugation

Mahnaz Maddahfar, Shihui Wen, Seyed Mostafa Hosseinpour Mashkani, Lin Zhang, Olga Shimoni, Martina Stenzel, Jiajia Zhou, Barbara Fazekas de St Groth*, Dayong Jin*. Bioconjugate Chemistry. https://doi.org/10.1021/acs.bioconjchem.1c00192

3.1   The aim of the chapter

The successful application of LnNPs to antibody-based applications, such as flow cytometry and mass cytometry, requires that the LnNP-coupled antibody retains its sensitivity and specificity as a ligand-specific probe. In this chapter, we provide a systematic insight into the effect of the chain length of poly(oligo (ethylene glycol) methyl ether acrylate) (POEGMEA) contains poly(ethylene glycol) on the long-term colloidal stability and antibody-conjugation efficiency of nanoparticles.

3.2   Abstract

Functional ligands and polymers have frequently been used to yield target-specific bio-nano-conjugates. Herein, we provide a systematic insight into the effect of the chain length of poly(oligo (ethylene glycol) methyl ether acrylate) (POEGMEA) contains poly(ethylene glycol) on the colloidal stability and antibody-conjugation efficiency of nanoparticles. We employed Reversible Addition Fragmentation Chain Transfer, RAFT polymerisation to design diblock copolymers composed of 7 monoacryloxyethyl phosphate (MAEP) units and 6, 13, 35, or 55 OEGMEA units. We find that when the POEGMEA chain is short, the polymer cannot effectively stabilise the nanoparticles, and when the POEGMEA chain is long, the nanoparticles cannot be efficiently conjugated to the antibody. In other words, the majority of the carboxylic groups in larger POEGMEA chains are inaccessible to further chemical modification. We demonstrate that the polymer containing 13 OEGMEA units can effectively bind up to 64% of the antibody molecules, while the binding efficiency drops to 50% and 0% for the polymer containing 35 and 50 OEGMEA units. Moreover, flow cytometry assay statistically shows that about 0.9% of the coupled antibody retained its activity to recognise B220 biomarkers on the B

cells. This chapter suggests a library of stabile, specific and bio-active lanthanide-doped nano-conjugates for flow cytometry and mass cytometry applications.

Keywords: inorganic nanoparticles, lanthanide nanoparticles, colloidal stability, diblocked copolymer, RAFT polymerisation, POEGMEA, bioconjugation, flow cytometry, mass cytometry.

3.3 Graphical abstract
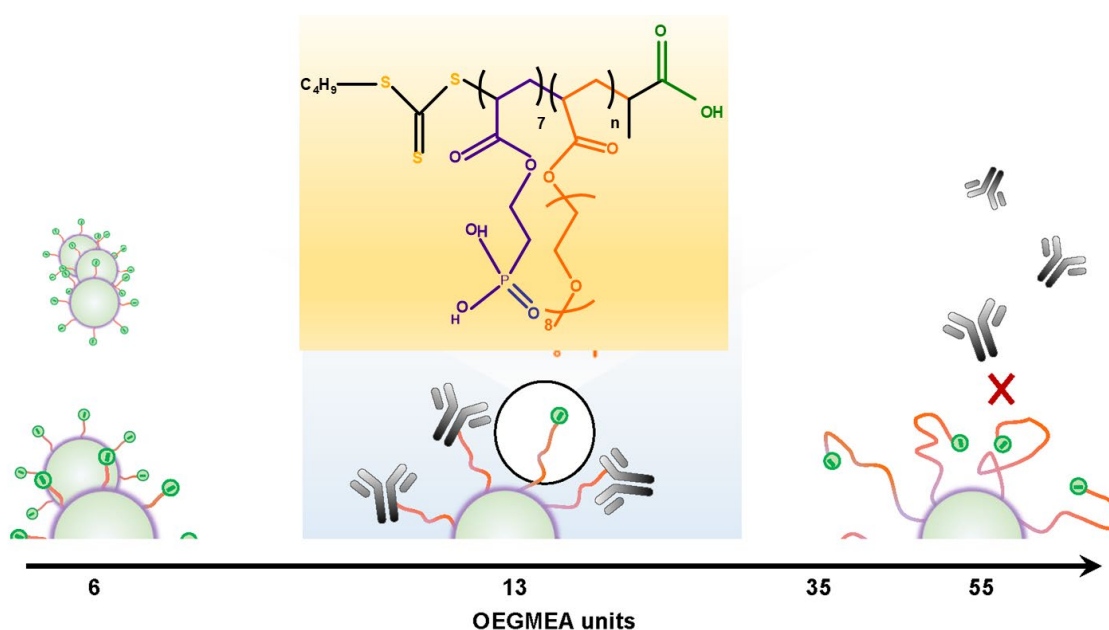
3.4 Introduction

Inorganic nanoparticles possess unique physical and chemical properties suitable for a broad range of biomedical applications, ranging from ultrasensitive molecular assays, multi-modal bio-imaging, and targeted delivery to activation of drugs.[1] Examples include iron oxide,[2] platinum,[3] and bismuth-based[4] nanoparticles being developed as contrast agents in MRI and X-ray imaging, gadolinium[5] and gold nanoparticles[6,7] employed in radio-sensitiser and drug delivery systems,[8] and semiconductor quantum dots (QDs) used as fluorescent labels.[9,10] In recent decades, lanthanide-doped nanoparticles (LnNPs) in a typical host matrix of NaLnF$_4$ have been developed for converting multiple low-energy near-infrared (NIR) photons into high-energy visible and ultraviolet (UV) light.[11,12] The unique anti-Stokes emission of LnNPs provides opportunities for a range of biomedical applications, including ultrasensitive bioassays,[13] deep-tissue super-resolution

Chapter 3

imaging,[14,15] multimodal biomedical imaging,[16,17] photodynamic therapy,[18,19] and NIR-triggered release of genes and drugs.[20,21] LnNPs with spectral down-shifting properties have further led to recent progress in the development of NIR deep-tissue imaging applications. [22,23] In addition, the high elemental lanthanide content of LnNPs renders them suitable as labels for mass flow cytometry and mass spectroscopy imaging applications, potentially increasing the sensitivity of these assays.[24-28] The key to modifying inorganic nanoparticles to produce bio-specific nanoparticles that are stable in biological and physiological environments lies in their surface functionalisation and conjugation to a bio-active molecule or ligand. High-quality LnNPs with tuneable size, shape, and composition have usually been synthesised at high temperatures with a cap of oleic acids.[28] A variety of surface modification methods have been developed to improve biocompatibility, including chemical modification of the hydrophobic ligand on the surface,[29] bilayer coating with amphiphilic molecules or polymers,[30] addition of an outer silica coating,[26, 31] and complete replacement of the original oleic acid moieties. For direct ligand exchange methods, polymers containing single or multiple anchoring ligands have been extensively used to modify the as-synthesised LnNPs by addition of a PEG-like block that forms an outer shell with improved colloidal stability, bio-compatibility, and immunogenicity.[32-34] Despite several studies reporting the development of polymers for surface functionalisation of LnNPs,[29] the effect of POEGMEA chain length on long-term colloidal stability and conjugation efficiency of LnNPs has not been examined.

In this chapter, we systematically investigated the effect of POEGMEA block length on colloidal stability and antibody conjugation efficiency of LnNPs. To this end, we used RAFT polymerisation technique to synthesise a well-defined diblock copolymer with a tuneable chain length of OEGMEA units ranging from 6 to 55. Our results indicate that a polymer containing 13 OEGMEA units retained long-term colloidal stability and achieved the highest efficiency of conjugation to antibodies (Abs). Polymers containing only 6 OEGMEA units failed to prevent aggregation of nanoparticles in an aqueous solution. Polymers with longer, more mobile chains comprising 35 or 55 OEGMEA units could effectively stabilise the nanoparticles in aqueous solution, but conjugation efficiency to Abs was reduced due to inaccessibility of the carboxylic end-functional group, which may have been wrapped inside of the coiled-structure of large polymers. Longer polymers also allowed increased interaction with the surface of adjacent nanoparticles. In addition, we found that polymers with OEGMEA lengths ranging from

13 to 55 units could be freeze-dried without any sign of aggregation, benefiting their long-term storage, especially when modified with antibodies.

3.5   Experimental

3.5.1   Synthesis of NaYF₄: Yb, Er nanocrystals

LnNPs used in our experiments were NaYF$_4$: 20%Yb, 2%Er. In a common synthesis procedure,[35] 1 mmol RECl$_3$·6H$_2$O (RE=Y, Yb, Er) with the mole ratio of (Y= 78%, Yb= 20%, Er= 2%) was mixed together in a 50 ml-three necked round bottom flask containing (6 mL) OA and (15 mL) ODE. The temperature of the mixture was increased to 160°C while argon was flowing throughout the mixture for 30 min to obtain a clear solution. The mixture was then cooled down to 50°C, and (5 mL) methanol solution of NH$_4$F (4 mmol) and NaOH (2.5 mmol) was added, followed by 30 min stirring at 50°C. The solution was heated to 80°C under argon flow for 20 min to remove the methanol. Then the temperature of the solution was increased to 300°C while stirring for another 90 min. Finally, the reaction solution was cooled down to room temperature, and the products were precipitated by ethanol followed by centrifugation at 7600 g for 5 min. The final LnNPs were washed 3 times by cyclohexane and OA as well as ethanol and methanol followed by 7600 g for 5 min. **Figure 3.1** shows the synthetic procedure of NaYF$_4$: Yb, Er nanoparticles.
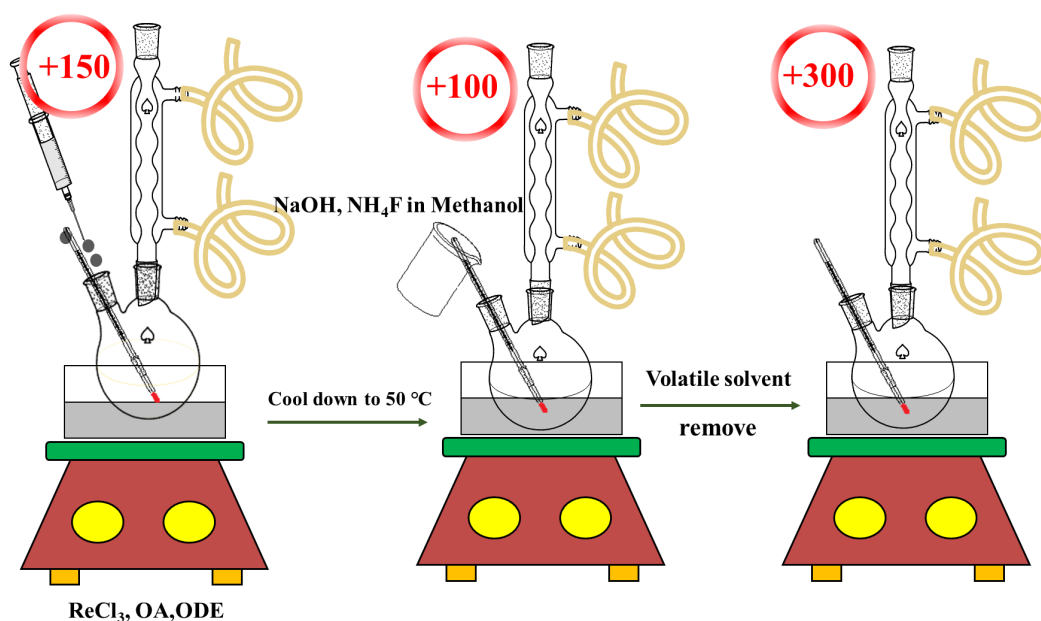
Figure 3.1 Schematic of synthetic procedure of NaYF$_4$: Yb, Er nanoparticles.

3.5.2 Synthesis of RAFT agent

The RAFT agent used in our experiment was 2-(n-butyltrithiocarbonate)-propionic acid (BTPA) synthesised according to the published procedure (**Figure 3.2**).[36] The two solutions including 50 % NaOH and 400 mmol of butanethiol in 60 mL water were mixed, a clear solution was formed after adding acetone (20 mL) with constant stirring for 30 min. After completing the reaction, the system was cooled to room temperature. Then, 27 mL of carbon disulfide was added to form a clear orange solution under stirring for 30 min, and then the internal temperature of the solution was decreased to <10 °C by placing in an ice bath. Then, 2-Bromopropanoic acid (62.73 g, 410 mmol) and 50 % NaOH (32.80 g) respectively were added dropwise to keep the temperature below 30 °C. The ice bath was then removed after the temperature of the reaction had stabilised. 60 mL water was added and the reaction was stirred for 24 h. Then, the reaction mixture was diluted by Mili-Q water (100 mL) while stirring at below 10 °C which could be achieved by adding 10 M HCl (60 mL) in an ice bath. The reaction was allowed to stir for one day at room temperature, 100 mL of distilled water was added dropwise under mild stirring, and 60 mL of hydrochloric acid was added while it was placed in an ice bath to keep the temperature below 10 °C. After adding 60 mL of hydrochloric acid, yellow oil has emerged, then, the reaction stirred at low temperature, to get solidified oil. The solid was collected by suction filtration, pressed and washed with cold water, and dried under reduced pressure to a state of semi-dryness. Then, the semi-dryness precipitate was washed in cold water and refiltered. After the filtration process, the solid sediment was washed with cold water and dried at room temperature to get a powdery yellow solid, 84.98 g, followed by recrystallisation in 180 mL of C_6H_{14} to have bright yellow microcrystals (76.99 g, 81 %) with melting point 53.5-54.5 °C (**Figure 3.3**).
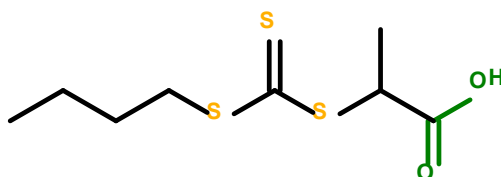
Figure 3.2. Chemical structure of RAFT agent, 2-(n-butyltrithiocarbonate)-propionic acid (BTPA)
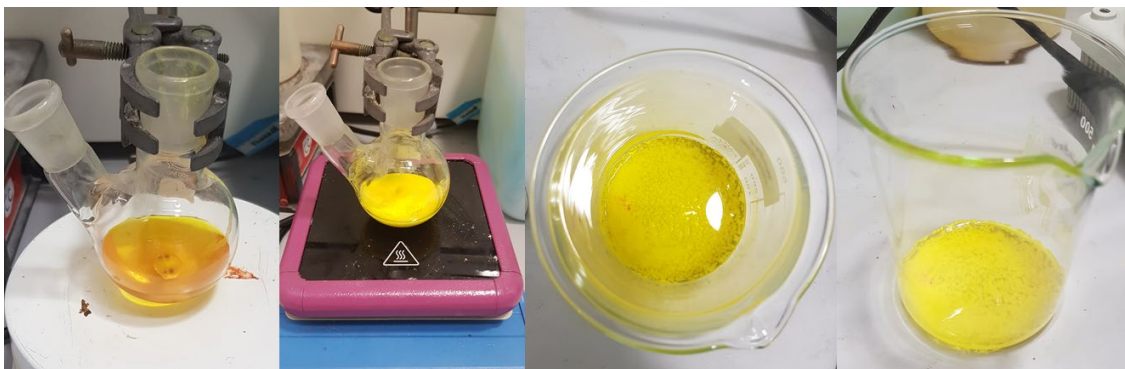
Figure 3.3. Images of RAFT agent during the preparation

3.5.3 Synthesis of POEGMEA macro RAFT agent with different OEGMEA-block chain lengths

Synthesis of POEGMEA was according to our previously published paper.[37] In brief, (5 g) of OEGMEA, (113 mg) RAFT agent, and (7.77 mg) recrystallised AIBN were mixed in a round bottom flask containing (20 mL) toluene. The flask was equipped with a magnetic stirrer bar and sealed under argon flow for 30 min. The reaction solution was then placed in a preheated oil bath at 70°C to decompose the AIBN reagent. To prepare the POEGMEA macroRAFT with 6 OEGMEA units, the polymerisation was terminated after three hours by placing the reaction solution into an ice bath for 5 min. The concentration of initial reagents for the synthesis of POEGMEA with different lengths of OEGMEA-block chains is described in detail in **Table 3.1**. The synthesised POEGMEA with different OEGMEA-block chain lengths was purified three times with n-hexane followed by centrifugation at 7600 g for 5 min. The final samples were stored at 4°C for further chain extension to provide diblock copolymers. The conversion of the monomer for all samples was less than 70% and the synthesised polymers faced narrow molecular weight distribution with a dispersity index (Đ) of 1.06. The percentage of monomer conversion, as well as the molecular weights of the different size polymers, were measured by ^{1}HNMR. The calculations are shown in detail below.

Table 3.1. The concentration of RAFT agent, OEGMEA monomer, and AIBN in different POEGMEA chain lengths, reaction time, and the percentage of monomer conversion.

OEGMEA unit	conc of RAFT agent (M)	conc of OEGMEA (M)	conc ofAIBN (M)	Touene (mL)	α OEGMEA (%)
6	2.36×10^-2	0.52	2.36×10^-3	20	30
13	2.36×10^-2	0.52	2.36×10^-3	20	60
35	2.36×10^-2	1.18	2.36×10^-3	20	70
55	2.36×10^-2	2.36	2.36×10^-3	20	55

$$\alpha^{POEGMEA} = [\int_{4.1} / \int_{4.1} + \int_{4.2}]$$

$$M_{n,NMR}^{POEGMEA} = \alpha^{OEGMEA} \times ([OEGMEA]/[RAFT]) \times M_w^{OEGMEA} + M_w^{RAFT}$$

In the above equation, $\int 4.2$ ppm and $\int 4.1$ ppm represent the integral of the signal of polymer and monomer at 4.1 and 4.2 ppm, respectively.

3.5.4 Synthesis of POEGMEA-*b*-PMEAP

POEGMEA with different numbers of repeating OEGMEA units were used as POEGMEA macro-RAFT agent for further extension of the polymer to produce diblock copolymers for surface modification of LnNPs. According to our previous paper,[37] monoacryloxyethyl phosphate monomer was chosen because of the high affinity of phosphate ligand towards the positively charged lanthanide ions in comparison with the carboxylic group. In detail, (1.4 M) of POEGMEA (6, 13, 35, 55 OEGMEA units), (0.4×10^{-2} M) of AIBN, and (1.43×10^{-1} M) of MAEP were dissolved in (5 mL) acetonitrile in a one-necked round bottom flask equipped with a magnetic stirrer. The reaction solution was sealed by a rubber septum and purged with argon gas for 30 min. The mixture was then placed into the preheated oil bath at 70°C for 17 hours. The polymerisation was quenched by ice-bath after 70 % MAEP monomer conversion. The final 6 and 13 OEGMEA unit polymers were dialysed (3 kDa cut-off) against methanol for 48 hrs, while dialysis of the 35 and 55 OEGMEA unit polymers used a 14 kDa cut-off dialysis membrane. The presence of seven repeat units of the MAEP (second block)

was confirmed by ^{1}HNMR, as detailed below. The narrow molecular weight distribution of the final polymers was confirmed by gel permeation chromatography (GPC). Monomer conversion of the second block was also measured by ^{1}HNMR spectra of the reaction mixture before and after polymerisation by comparing the integral ratio of the vinyl protons of monomer and the unchanged methylene protons of the POEGMEA adjacent to the ester bond at 4.1 ppm. For instance, MEAP conversion was calculated using the following equation:

$$\alpha^{PMAEP} = [\textstyle\int_{6.2 \,(0)\,h} - \int_{6.2\,(t)\,h} / \int_{6.2\,(0)\,h}]$$

The integrals at 4.1 ppm were set at the same value before and after polymerisation. The experimental molecular weight of final diblock copolymer can be calculated by the following equation:

$$M_{n,\,NMR}^{POEGMEA\,-b\text{-}PMAEP} = \alpha^{PMAEP} \times ([POEGMEA] / [RAFT]) \times M_w^{POEGMEA} + M_w^{RAFT}$$

3.5.5 Ligand exchange of LnNPs with POEGMEA-*b*-PMEAP

To use LnNPs in the bioanalytical application, they have to be transferred from an oil phase to an aqueous phase. To achieve this, we used a ligand exchange method. Ligand exchange is a versatile strategy in which the high affinity of the new ligand for the surface of LnNPs drives the reaction (**Figure3.4**).[29] The polymers with 6, 13, 35, and 55 repeating OEGMEA units dissolved in (1 mL) (10 mg/mL) THF, were mixed with LnNPs suspended in (1 mL) (5 mg/mL) THF with the ratio of 2:1 in mass. The reaction solutions were placed on a gentle shaker for 17 hours at room temperature. The polymer-coated nanoparticles were then centrifuged at 20240 g for 30 min, the supernatant removed and the nanoparticles washed by resuspension in (1 mL) of 3:1 THF: MilliQ water. The wash was repeated 3 times with decreasing concentrations of THF in MilliQ water, with the last wash in 100% water. The aqueous well-dispersed LnNPs were then resuspended in MilliQ-water and aliquots were prepared to investigate colloidal stability and subsequent biofunctionalisation by adding 2 Good's buffers (MES, HEPES) to produce 2 different pH conditions. Polymer-coated LnNPs with POEGMEA containing 6, 13, 35, or 55 repeating OEGMEA units will henceforth be abbreviated as 6 PEG, 13 PEG, 35 PEG, or 55 PEG LnNPs, respectively.
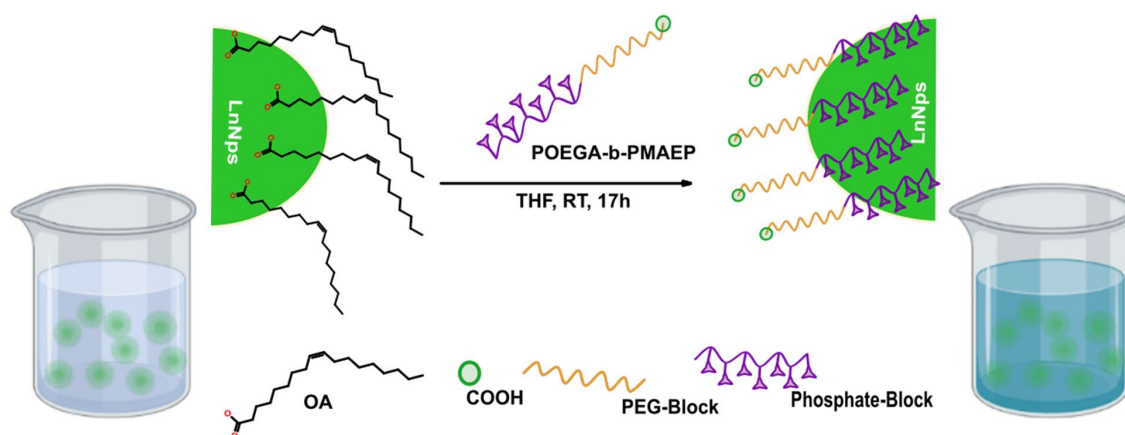
Figure 3.4. Schematic illustration of ligand exchange of OA-capped LnNPs with POEGMEA-*b*-PMAEP polymers.

3.5.6 Bioconjugation of polymer-coated LnNPs coated with an anti-B220 mAb

For bioconjugation, we chose the rat IgG monoclonal antibody RA3-6B2 specific for mouse and human B220 (M_w=180 kDa). Two-step EDC/Sulfo-NHS chemistry was chosen to couple modified LnNPs with anti-B220 mAb. The carboxylic functional end-group of polymers on the surface of LnNPs was activated by EDC, stabilised by Sulfo-NHS, and then reacted with the primary amine groups of lysine within the antibody to create a strong amide bond. In detail, (10 pmol,120 µg) of 13, 35, and 55 PEG LnNPs (M_w=12 MDa)[38] were dispersed into (100 µL, 20 mM, pH=5.5) MES buffer followed by the addition of (1 mg) EDC and (2 mg) Sulfo-NHS. After incubating for 45 min, EDC and excess Sulfo-NHS were removed by centrifugation of the nanoparticles at 20240 g for 10 min, followed by 3 washes comprising resuspension in MES buffer followed by centrifugation at 20240 g for 30 min. After the final centrifugation, the activated LnNPs were resuspended in (50 µL HEPES buffer, 20 mM, pH=7.1) and (300 pmol, 54 µg) of anti-B220 mAb was added to each nanoparticle sample and incubated for 5 hours. The final coupled LnNP/Ab were centrifuged at 20240 g for 10 min, washed twice in HEPES buffer, and then resuspended in 90 µL HEPES buffer. (10 µL BSA, 0.5%) was added before storage at 4°C. DLS, Zeta Potential, and A280 were measured to confirm the successful coupling of LnNPs and mAb, and flow cytometry was conducted to evaluate the preservation of a functional B220 antigen-binding site within the coupled mAb.

3.5.7 Mouse spleen cell staining with LnNPs/anti-B220 mAb

To measure the degree to which the B220 binding site was preserved after EDC/Sulfo-NHS conjugation of RA3-6B2 mAb to LnNPs, dilutions of the 13 PEG and 35 PEG LNPs were added to individual wells of 96-well round-bottom plates (Greiner) containing (1×10^6) mouse spleen cells in (50 μL, pH=7.1) HFS buffer at (150 mM NaCl, 1 mM NaF, 15 mM HEPES, 5% fetal calf serum). Pure RA3-6B2 mAb and no antibody served as positive and negative controls, respectively. After incubation for 45 min, plates were centrifuged at 500 g for 3 min and resuspended in (150 μL) HFS buffer. This washing procedure was repeated 3 times. The cells were then incubated with (50 μL) of a 1:100 dilution of PE-conjugated goat anti-rat IgG secondary antibody (source) for 45 min. Following a further 2 washes in (150 μL) HFS buffer, the cells were resuspended in (200 μL) HFS and analysed using an LSR Fortesss X-20 flow cytometer (Becton Dickinson) and Helios CyTOF system._ Data were analysed using FlowJo software (Becton Dickinson). For CyTOF sample preparation, cells were incubated with DNA intercalator ^{191,193}Ir to recognize the cell in CyTOF, incubated with cis-platinum to gate the Live/Dead cells. The data were collected in FCS files and can be analysed in a manner very similar to standard flow cytometry data by FlowJo software (Becton Dickinson).

3.5.8 Coupling the as-synthesised polymers to adipic acid dihydrazide (ADH)

To evaluate the reactivity of the carboxylic groups on the polymers with different POEGMEA chain lengths, they were coupled to adipic acid dihydrazide (ADH). In detail, (1 μmol) of as-synthesised polymers with 13, 35, or 55 OEGMEA unit chains in (1 mL) HEPES buffer (pH=7.1) was mixed with (10 μmol) EDC and (10 μmol) ADH in a (1.5 mL) eppendorf tube. After gently shaking for 5 hours, the modified polymers were dialysed against MilliQ-water for 24 hours using 3 kDa cut-off (for 13 OEGMEA unit polymer) and 14 kDa cut-off (for 35 and 55 OEGMEA unit polymers) dialysis membranes. The final products were freeze-dried. The functionalised polymers were characterised by ^{1}HNMR and FTIR.

3.6 RESULTS AND DISCUSSION

Previously,[37] we found the phosphate moiety was superior to carboxylic and sulphonic moieties as an anchoring ligand to replace oleic acids on the surface of LnNPs. The work described in this chapter focuses on the effect of RAFT polymer length on LnNP colloidal

stability and efficiency of antibody conjugation to functionalised LnNPs. The LnNPs in my project were synthesised by the coprecipitation method.[35]

3.6.1 Lanthanide nanoparticles preparation

TEM and DLS analysis of NaYF$_4$: Yb, Er suspended in cyclohexane are shown in **Figure 3.5**. The diameter of the nearly spherical nanoparticles by TEM imaging was 23 ± 0.5 nm (**Figure 3.5a**) and the Z-averaged dynamic diameter in cyclohexane solution was 44 nm with a PDI of 0.187 (**Figure 3.5b**). These data indicate that the as-synthesised nanoparticles were uniform (CV< 5%) and suitable for further surface modification and stability testing. ART-FTIR spectra of OA-LnNPs indicate that oleic acid was successfully coordinated to the Ln^{+3} ions on the surface LnNPs and based on **Figure 3.6** all the absorptions of OA-LnNPs were identified.
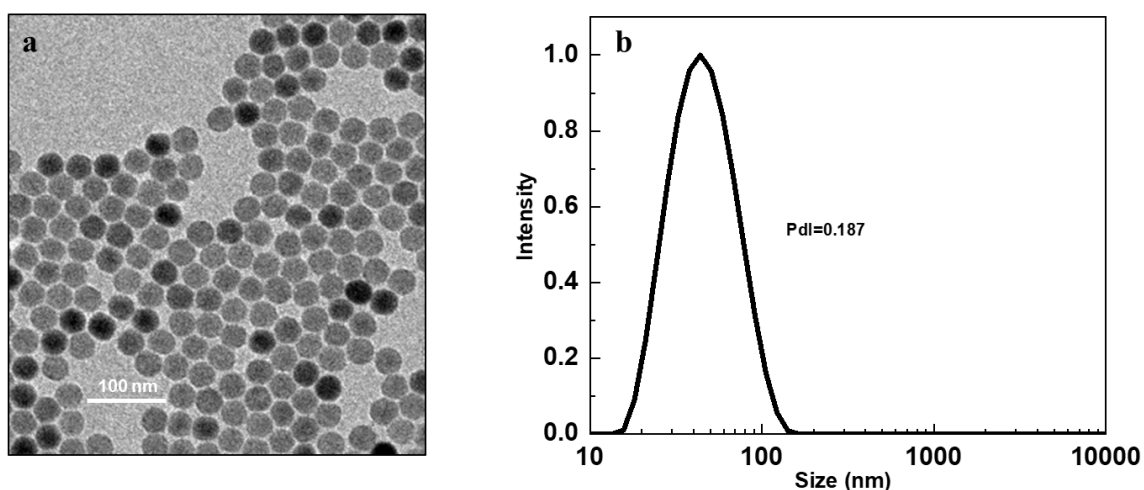
Figure 3.5. TEM image of OA- LnNPs (a), DLS CONTIN plots of OA- LnNPs dispersed in cyclohexane (1.0 mg/mL) (b).
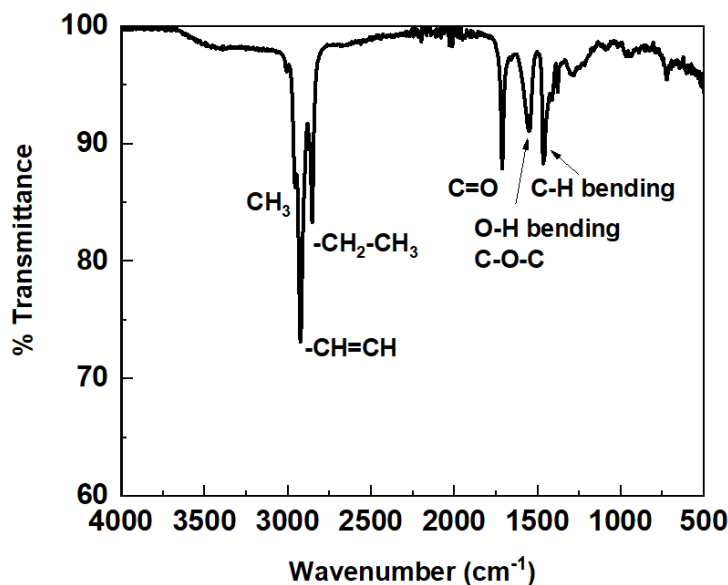
Figure 3.6. FT-IR spectra of OA-capped LnNPs. Functional groups of the OA are shown in the FTIR spectrum.

3.6.2 RAFT agent preparation

ATR-FTIR analysis was taken to characterise to confirm the presence of certain organic groups in RAFT agent,[36] as shown in **Figure 3.7**, the characterisation peaks related to the RAFT agent are as follow: 2952, 2925, 2865, 2710, 2596, 1699, 1462, 1417, 1305, 1204, 1105, 1086, 1064, 1040, 911, 823, 648 cm^{-1}. All the absorptions of RAFT agent were clearly identified. **Figure 3.8a** shows the ^{1}H NMR spectrum of RAFT agent. The peak of solvent (CDCl$_3$, 7.24 ppm) was used as the reference peak. All characterisation peaks related to the ^{1}HNMR spectrum of RAFT agent are as follow: ^{1}H NMR: δ (ppm) 4.87 (q, J = 7.4 Hz, 1H, SCH), 3.37 (t, J = 7.4Hz, 2H, CH$_2$S), 1.69 (quint, J =7.5 Hz, 2H, CH$_2$CH$_2$S), 1.63 (d, J) 7.4 Hz, 3H, SCHCH$_3$), 1.44 (sext, J = 7.5 Hz, 2H, CH$_3$CH$_2$CH$_2$), 0.94 (t, J = 7.4 Hz, 3H, CH$_3$CH$_2$).The ^{13}C NMR instrument setup details as follows: the spectral window of 250 ppm, 0.7 second acquisition time; 2-second relaxation delay. **Figure 3.8b** displays the ^{13}C NMR spectrum of the RAFT agent.
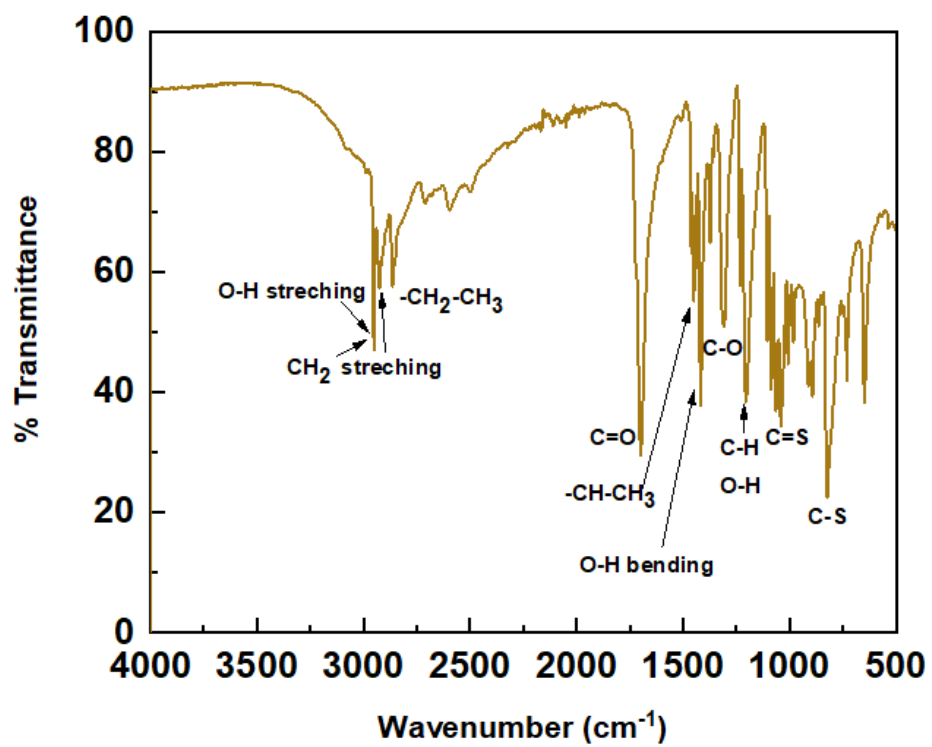
Figure 3.7 ATR-FT-IR analysis of RAFT agent. Functional groups of the RAFT agent are shown in the FTIR spectrum
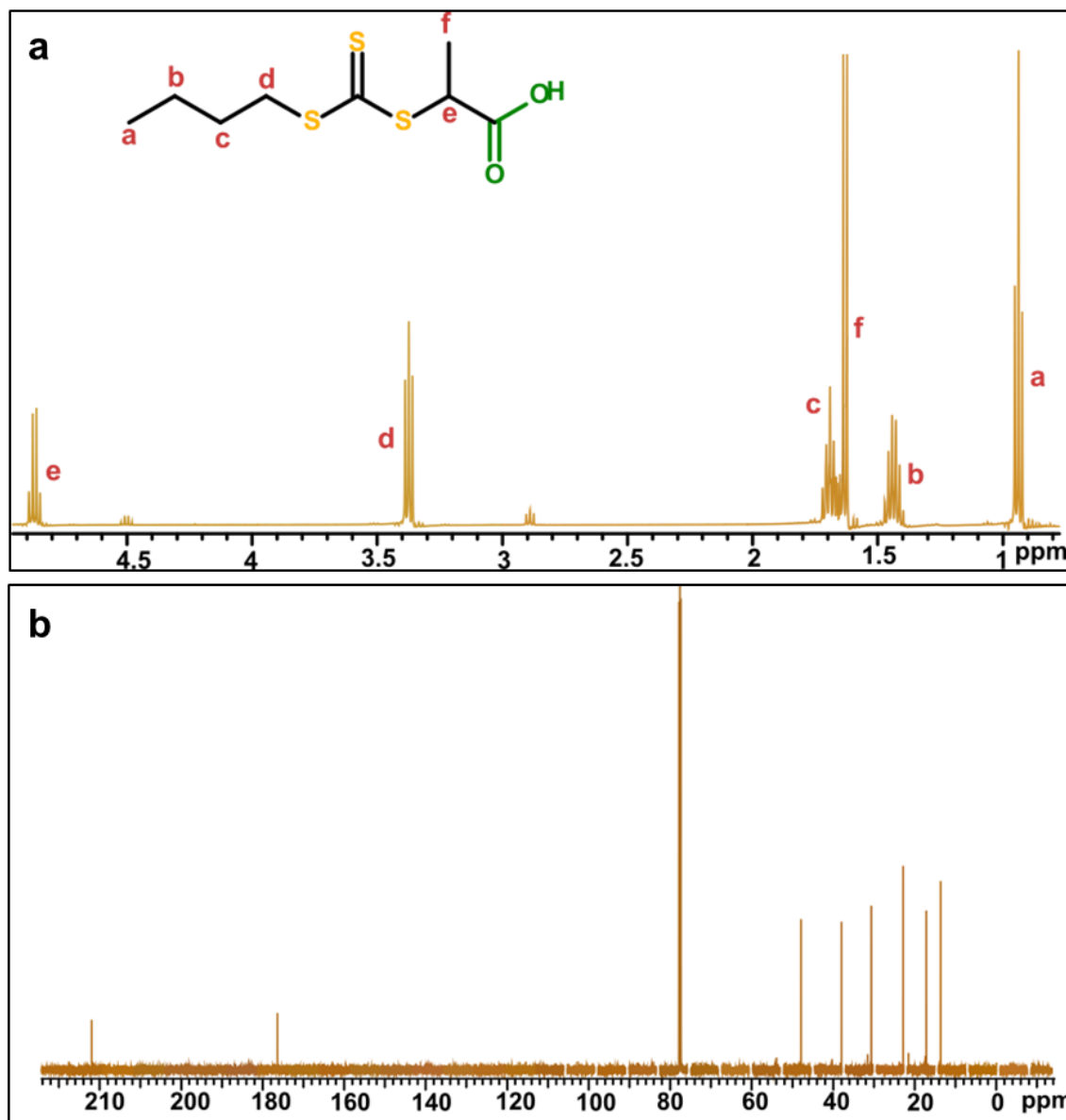
Figure 3.8. ¹H NMR spectrum of RAFT agent (a). ¹³C NMR spectrum of RAFT agent (b).

3.6.3   POEGMEA-*b*-PMEAP (6, 13, 35, and 55 OEGMEA units)

As we mentioned before, the polymers were synthesised through RAFT polymerisation. The two-step synthesis procedure of the diblock copolymer is illustrated in **Figure 3.9**. Oligo(ethylene glycol) methyl ether acrylate (**OEGMEA**) was used as a monomer to produce different chain lengths of the PEG-based **POEGMEA** block that serves as the outer shell of the coated LnNPs. Monoacryloxy ethyl phosphate (MAEP) was used as the second monomer in the chain extension process to form diblock copolymers.
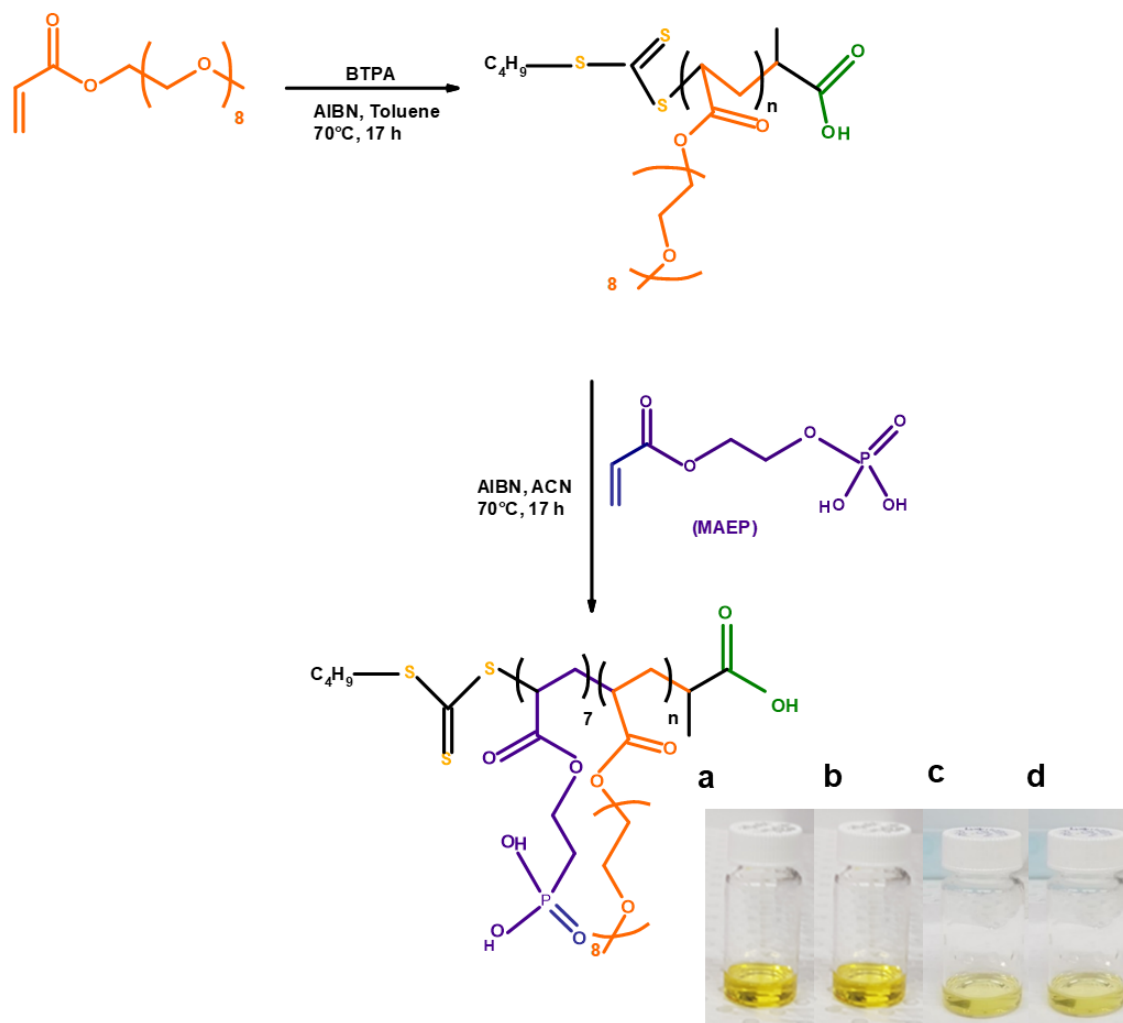
Figure 3.9. Schematic illustration of the two-step synthesis procedure of the diblock copolymer. The photo of the synethesised polymers in different length, 6 PEG (a), 13 PEG (b), 35 PEG (c), 55 PEG (d).

The high-affinity interaction between the phosphate functional group and Ln^{3+} ions was used to drive the replacement of oleic acids by a polymer. Monomer conversion of the different POEGMEA polymers was determined through ^{1}HNMR spectroscopy (detailed in **Table 3.1**). Polymerisation was quenched at less than 70% of monomer conversion during the polymerisation to the formation of polymers with narrow molecular weight distribution. As shown in **Figure 3.10a**, ^{1}HNMR spectrum analysis confirmed the presence of methylene, ester, and the methylene group adjacent to the phosphate groups of the 6 POEGMEA polymer (abbreviated forthwith as 6 PEG). It should be noted that the 13, 35, and 55 PEG polymers had similar ^{1}HNMR spectra (**Figure 3.10b). Figure 3.10 c** is ^{31}P NMR of diblock copolymers bearing phosphate group. The peak at 0 ppm indicates the presence of phosphate in the final polymers.

Chapter 3

a

b

δ (ppm)
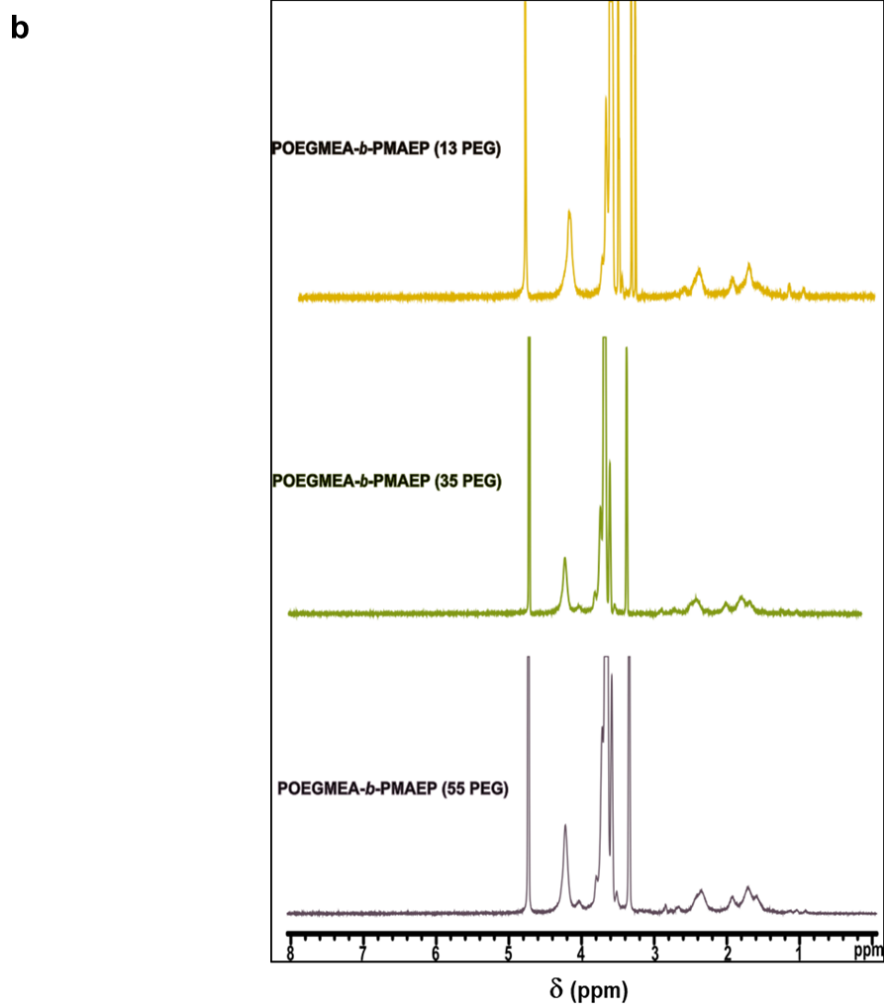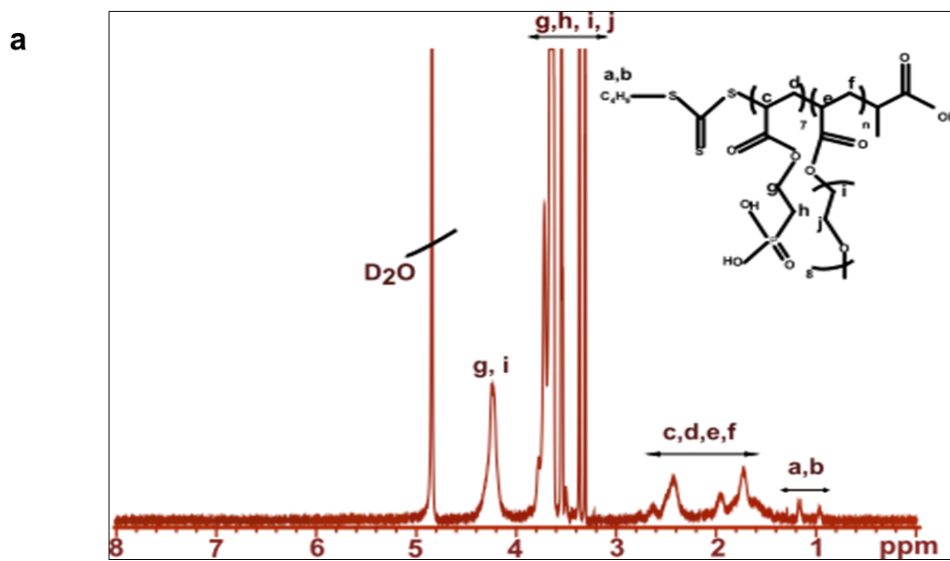
c
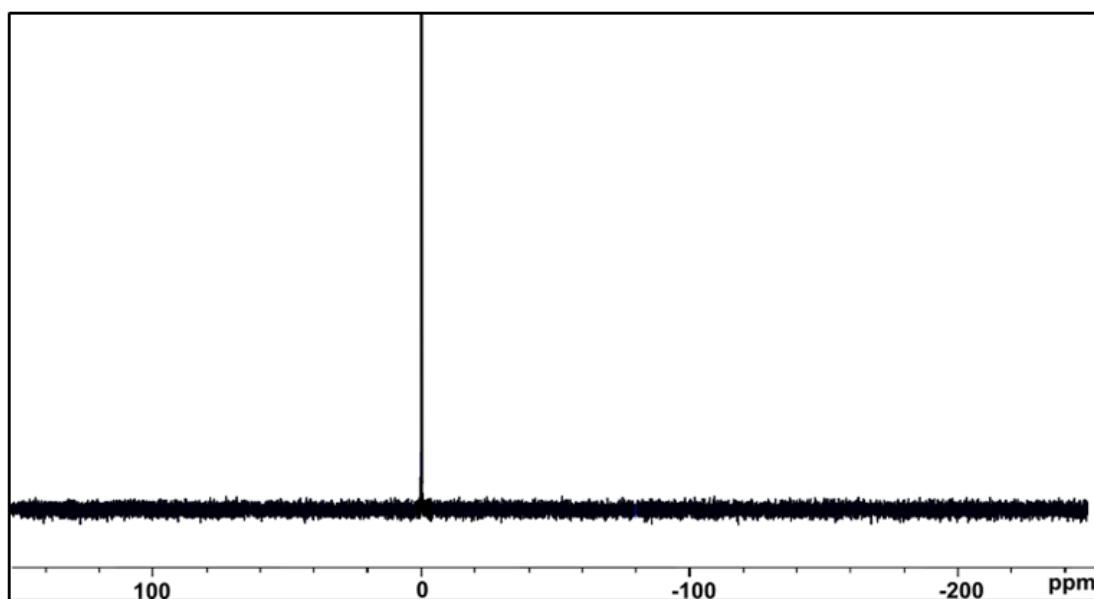
Figure 3.10. ^{1}H NMR spectra of the as-synthesised polymers with different lengths of POEGMEA chain 6 (a) and (13, 35, and 55) (b) in d_6-DMSO. Peak assignments are shown on the structure included in the ^{1}HNMR spectrum. ^{31}P NMR spectrum of as synthesised polymer (c).

Fourier transform infrared spectroscopy (ART-FTIR) was used to further confirm the structure of the 6 PEG polymer, as shown in **Figure 3.11a**. The peaks at 850 and 949 cm$^-$^{1} correspond to P-O from the phosphate block of the polymer and C=S from the RAFT agent. The peak at 1730 cm^{-1} is attributed to C=O of the ester present in the polymer. The C-H stretching and P=O stretching are located at 1094 cm^{-1}, which confirmed the presence of both the POEGMEA block and the phosphate block of the formed polymer. The FTIR spectra of the 13, 35, and 55 PEG polymers were similar to that of the 6 PEG polymer, as displayed in **Figure 3.11b.**

Chapter 3
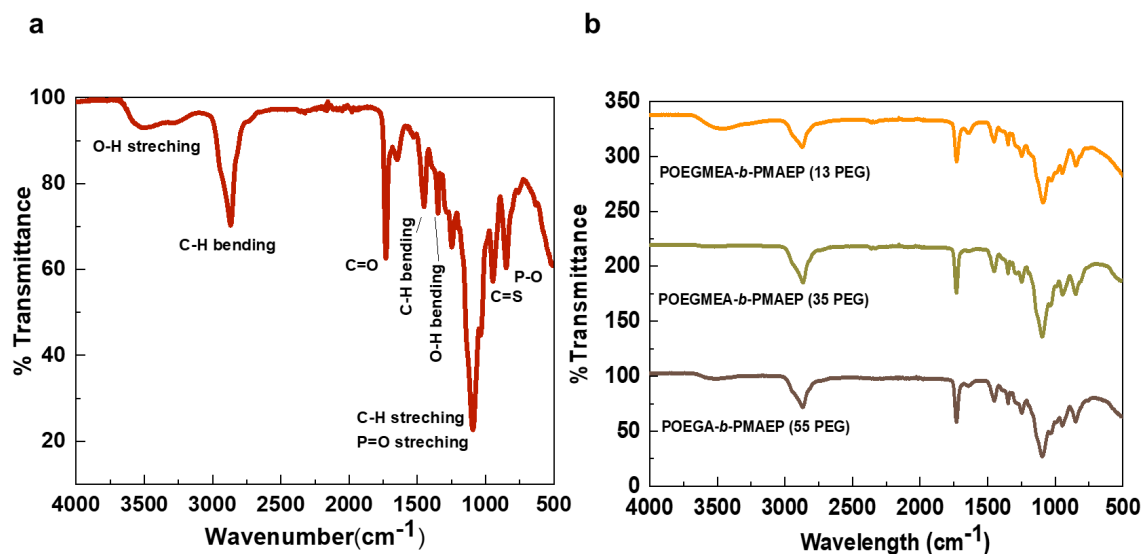
Figure 3.11. FTIR spectra of the as-synthesised polymers with different lengths of POEGMEA chain (6) (a) and (13, 35, and 55) (b). Functional groups of the polymer are shown in the FTIR spectrum.

Gel permeation chromatography (GPC) analysis was further used to determine the relative molecular weight of the formed polymers as well as their molecular weight distribution. As shown in **Figure 3.12**, the molecular weights of the PEG polymers with 6, 13, 35, and 55 POEGMEA repeating units and around 7 PMAEP were 3500 g/mol, 6500 g/mol, 17000 g/mol, and 27000 g/mol, respectively, with narrow molecular weight distribution (Đ= M_w/M_n= 1.06). This confirms the successful polymerisation and best controlled chain extension with the designed molecular weight and chain length of the POEGMEA-*b*-PMAEP.
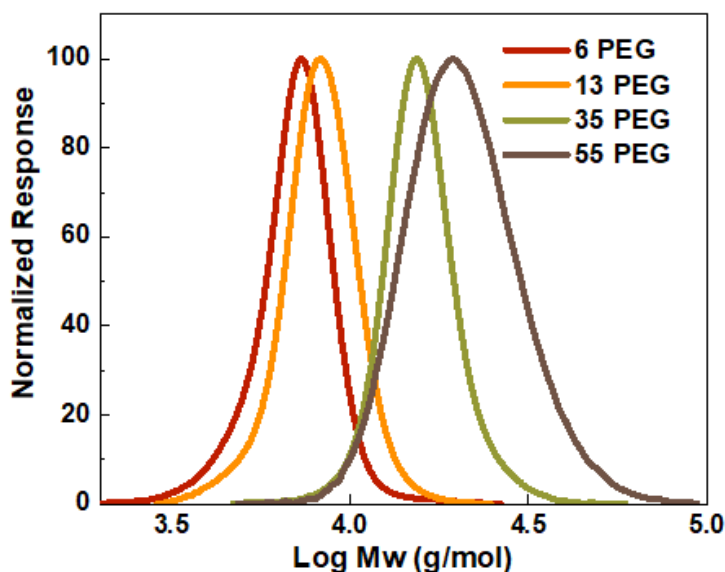
Figure 3.12 GPC curves of POEGMEA-*b*-PMAEP with different units of POEGMEA (6, 13, 35, and 55).

3.6.4 Surface coating of different sizes POEGMEA-*b*-PMAEP copolymers onto LnNPs.

Next, we used the formed polymers with the different POEGMEA chain lengths for surface modification of the as-synthesised LnNPs. Ligand exchange was carried out to replace oleic acid on the surface of LnNPs. Tetrahydrofuran (THF), was used as the solvent for the mixture of OA-capped LnNPs and POEGMEA-polymers. The samples were centrifuged at 20240 g for 30 min to remove excess OA ligand and POEGMEA-polymers, and then washed 4 times in decreasing concentrations (from 75% to 0%) of THF in MilliQ-water. The modified nanoparticles were dispersed in MilliQ-water to generate a clear suspension for further investigation using multiple techniques including TEM, DSL, Zeta potential, and TGA.

We used TEM to measure nanoparticle size, distribution, and morphology after coating with different POEGMEA chain length polymers. As shown in **Figure 3.13a**, the as-synthesised LnNPs were highly monodispersed before the modification, while LnNPs modified with the 6 PEG polymer were significantly aggregated. When a longer POEGMEA chain was used, the polymer-coated LnNPs were monodispersed similarly to as-synthesised OA-capped nanoparticles. These results indicate that the 6 PEG polymer was too small to prevent aggregation in an aqueous solution, possibly due to the formation of only a very small hydrophilic polymer shell that cannot provide enough steric repulsion

among the nanoparticles. To further study the performance of the polymer-coated LnNPs with different length POEGMEA chains, hydrodynamic diameter and surface charge were measured by Zetasizer. As shown in **Figure 3.13b**, after ligand exchange, the Z-averages of nanoparticles coated with 6, 13, 35 and 55 PEG polymers were 60 ± 3.5 nm (PDI=0.45), 44 ±1.2 nm (PDI=0.17), 71 ±1.2 nm (PDI=0.17), and 80 ±1.2 nm (PDI= 0.17), respectively. The DLS CONTIN plot showed that the 6 PEG polymer caused LnNPs to flocculate, which indicates that the POEGMEA chain in the polymer is too short to create sufficient hindrance to separate the nanoparticles. The hydrodynamic diameter (d_h) of 13 PEG LnNPs did not change after ligand exchange (**Figure 3.13b).** The Z-average size of the LnNPs after modification with longer polymers increased from 44 nm to 71 and 80 nm, respectively, for the 35 and 55 PEG polymers. It should be noted that nanoparticles coated with 13, 35, and 55 PEG polymers did not show any sign of aggregation, which confirmed that these polymers kept single nanoparticles monodispersed with a narrow size distribution in an aqueous solution. Since the POEGMEA-*b*-PMAEP polymer contained a carboxylic acid end-functional group that can be ionized in aqueous solutions, zeta potential measurement was used to analyse the surface charge of the nanoparticles. As shown in **Figure 3.13c**, the surface charges of 6, 13, 35, and 55 PEG LnNPs were -9 ±2 mV, -21 ±1 mV, -16 ±1 mV and -11 ±1 mV, respectively. The low negative charge of 6 PEG nanoparticles is explained by the aggregation of the nanoparticles in aqueous media (**Figure 3.13c**). The 13 PEG LnNPs had the highest surface charge, which indicates that most of the deprotonated COO^- were accessible outside of the nanoparticles, without any interaction with adjacent LnNPs. The surface charge of 35 and 55 PEG LnNPs decreased in comparison with 13 PEG LnNPs, possibly due to the enhanced interaction of COO^- of the longer, more mobile, polymers with the surface of adjacent LnNPs.
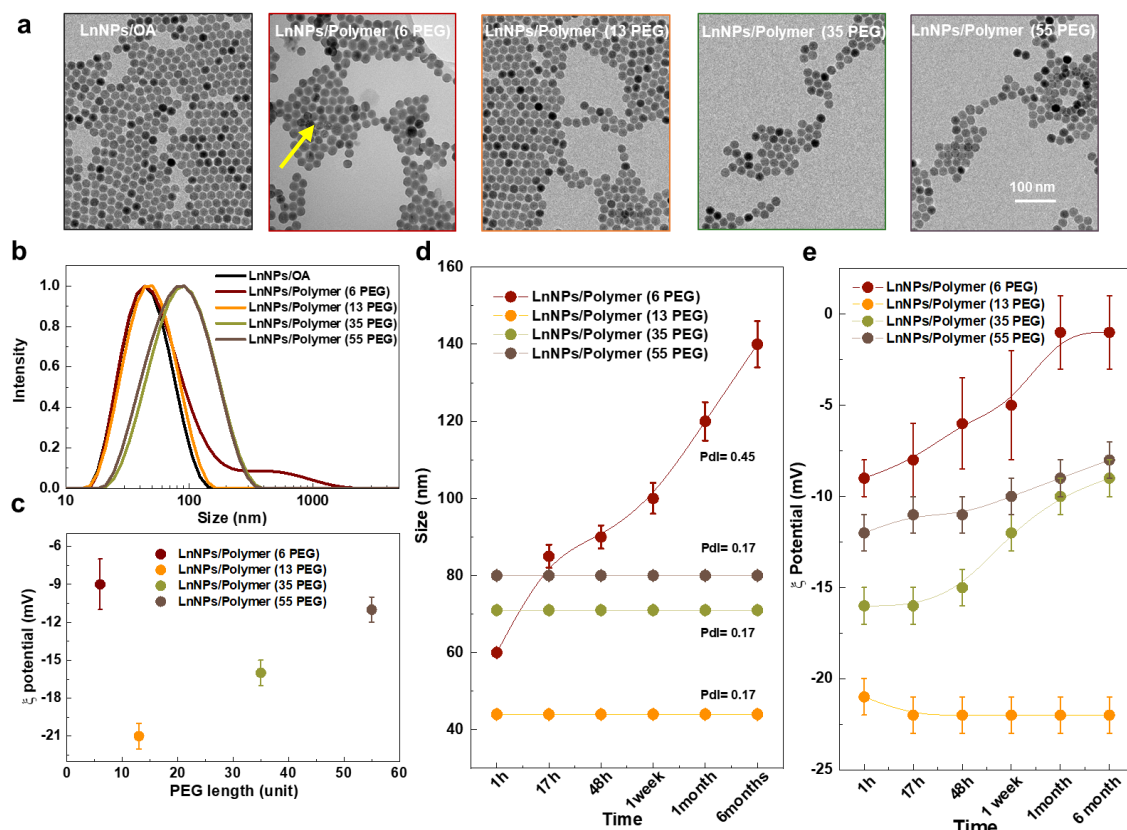
Figure 3.13. TEM images of OA-capped LnNPs and polymer-coated LnNPs with different numbers of POEGMEA units (a). DLS CONTIN plot of LnNPs before and after ligand exchange (b). Zeta potential analysis of polymer-coated LnNPs in MilliQ-water (c). Long-term colloidal stability (hydrodynamic diameter (d_h)) of modified LnNPs from 1 hour to 6 months after polymer modification (d). Long-term surface charge stability of LnNPs with different length polymers (e).

Next, we measured the long-term stability in an aqueous solution of the LnNPs with different length polymers. We systematically tested the DLS size and surface charge of the nanoparticles at times from 1 hour to 6 months after polymer modification (**Figure 3.13d, 3.13e**). As shown in **Figure 3.13d**, DLS measurements over a period of 6 months indicated no change in size or PDI for the nanoparticles modified by polymers with the longer POEGMEA chains (13, 35, and 55). However, the DLS Z-average size of the 6 PEG LnNPs increased over six months from 60 nm to 140 nm, with a relatively larger PDI of 0.45. DLS CONTIN plots are shown in **Figure 3.14**. **Figure 3.13e** shows that the negative surface charge of the 6 PEG nanoparticles decreased over the six months, resulting in the flocculation of the nanoparticles in an aqueous solution. In contrast, the surface charge of the 13 PEG nanoparticles was unchanged over 6 months. For the 35 and 55 PEG nanoparticles, surface charge also decreased, likely due to the interaction between

carboxylate groups and the surface of adjacent LnNPs. These results indicate that LnNPs modified with polymers with long POEGMEA chains are stable for extended periods of time, which meets one of the most important requirements in biomedical applications. Also, we tested colloidal stability of LnNPs coated by polymer with 13 POEGMEA units in MES and HEPES buffer during 1 hour to 1 week. DLS CONTIN Plot are shown in **Figure 3.14e,f**. which indicated narrow size distribution of nanoparticles in physiological buffers.
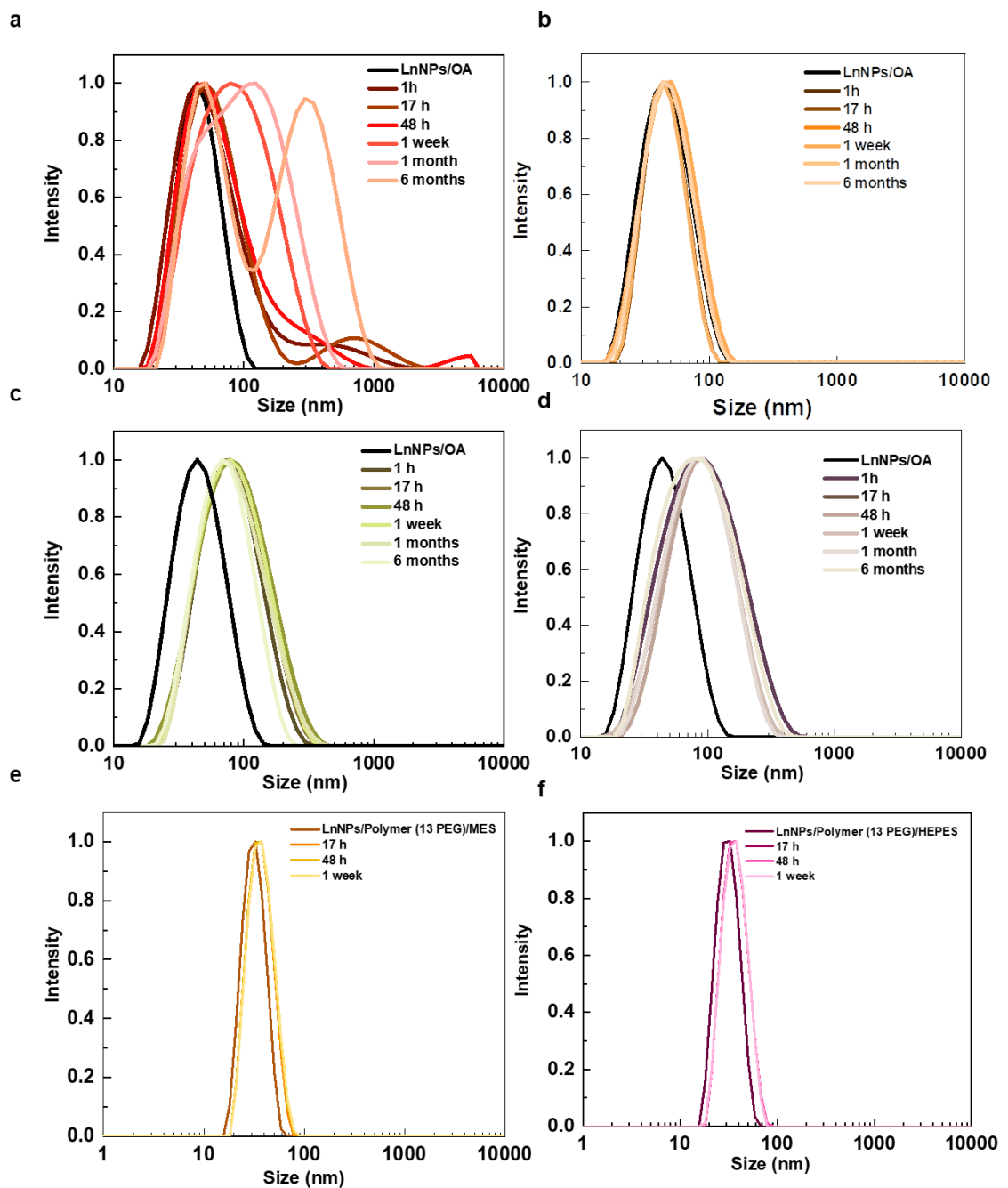
Figure 3.14. CONTIN plots from DLS measurements of LnNPs before and after surface modification with Polymer (6 POEGMEA units) (a), Polymer (13 POEGMEA units) (b), Polymer (35 POEGMEA units) (c), and Polymer (55 POEGMEA units) (d) with different time points from 1 hour to 6 months.Colloidal stability of polymer coated LnNPs (13 POEGMEA units) in MES (20 mM, pH= 4.5) and HEPES (20 mM, pH=7.2) (e,f).

Next, aliquots of polymer-coated LnNPs were lyophilised and examined by thermal gravimetric analysis (TGA) in an N_2 atmosphere to confirm that they had been modified successfully by the different POEGMEA-length polymers (**Figure 3.15**). This measurement confirmed that the lack of colloidal stability of 6 PEG LnNPs was not due to a failure to exchange with the oleic acid ligand. The TGA analysis was also used to estimate the grafting density of different length polymers on the surface of LnNPs. The calculation of grafting density in molecules per nm^2 is described below. We assumed that LnNPs are spherical with a diameter of 23 nm as measured by TEM and $NaYF_4$ bulk density of 4.2 $g.cm^{-3}$.[40] As expected, treatment with higher molecular weight polymers led to lower grafting density due to hindrance between polymers. In other words, more small polymers can fit on the surface of a nanoparticle of a given size. The weight contribution and grafting density of the 4 polymers are shown in **Table 3.2**.
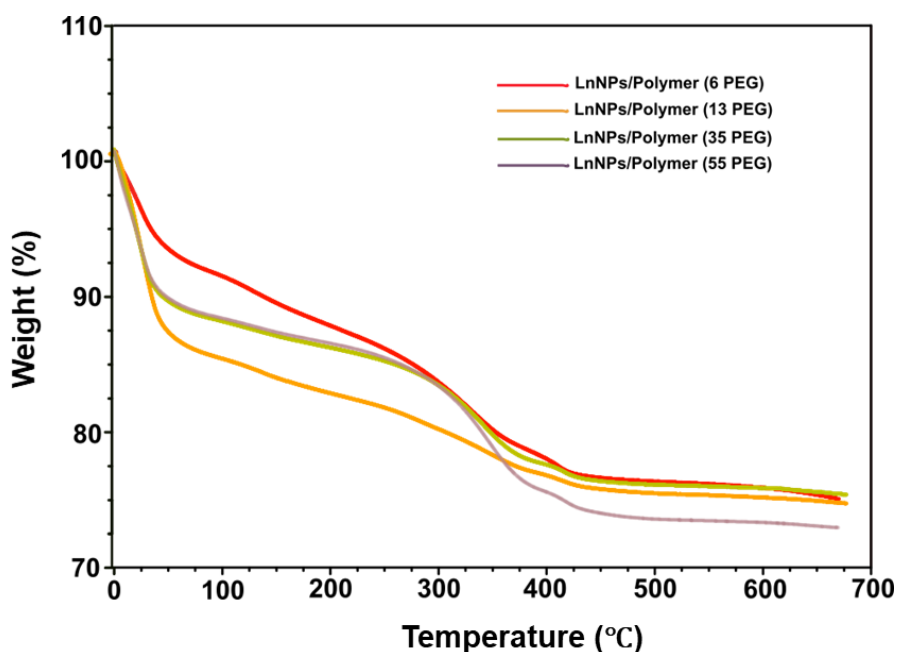
Figure 3.15. TGA curves of LnNPs modified by polymers in different POEGMEA lengths.

By assuming that the LnNPs is spherical, the grafting density of polymers in a different size on the surface of nanoparticles (in molecules/ nm^2) was calculated from weight loss according to the equation below:

$$\text{Grafting Density} = \frac{\text{Number of ligands}}{\text{Surface area of LnNPs}}$$

$$\text{Grafting Density} = \frac{(\text{Weight loss}/M_{n\ \text{Polymer}}) \times N_A}{m_{NPs} \times S_{NP}}$$

In this equation, Mn *polymer* corresponds to the molecular weight of polymer grafted. *NA* is Avogadro's number and *mNP* is the mass of LnNPs used for the TGA analysis (e.g. mass of nanoparticles = initial mass before TGA analysis – loss of weight). Specific Surface Area (SNP) of the synthesised LnNps was calculated, assuming the shape to be spherical and D*NP* is the average diameter of the nanoparticles measured by TEM to be 23 nm. The density of NaYF$_4$ nanocrystal was determined to be ρ = 4.2 g/cm^3 by X-ray energy dispersive spectroscopy (XEDS) analysis.[40] Based on the equation *DNP by TEM* = 6/ ($\rho \times SNP$), the Specific Surface Area of the prepared LnNPs was calculated to be 62.11 m^2/g.

Table 3.2. TGA results and grafting density of LnNPs with the polymer of different POEGMEA lengths

LnNP/POEGMEA	Initial weight LnNPs/Polymer (mg)	Residue weight (LnNPs (mg))	Weight loss of Polymer (%)	Mw of Polymer (g/mol)	Grafting Density (molecules/nm^2)
6	1.52	1.14	17.21	3500	0.632
13	2.095	1.42	16.94	6500	0.368
35	1.94	1.316	19.11	17000	0.16
55	2.54	1.83	17.61	27000	0.088

3.6.5 Stability of polymer-coated LnNPs in different buffer solutions and after freeze-drying

To examine the influence of pH on the colloidal stability of LnNPs, two Good's buffers (MES and HEPES) were chosen to evaluate particle size during buffer exchange. 20 mM MES buffer at pH=5.5 and 20 mM HEPES buffer at pH=7.4 were applied to disperse functionalised LnNPs with the various POEGMEA unit polymers. The hydrodynamic size of the nanoparticles modified with 13, 35, and 55 PEG polymers remained unchanged

over a pH range of 5.5 to 7.4. In contrast, the size of the 6 PEG LnNPs changed significantly at different pHs (**Figure 3.16a**).

The zeta potential measurements of the 4 different polymer-modified LnNPs were reduced, as expected, in MES buffer (pH=5.5) compared with higher pH, due to less ionization of the carboxylic end-functional group. However, the surface charge of the nanoparticles in HEPES buffer at pH=7.4 was very similar to that in MilliQ water at pH=6.8, indicating that HEPES buffer at pH=7.4 would be an appropriate buffer for LnNPs in bioconjugation applications (**Figure 3.16b**).
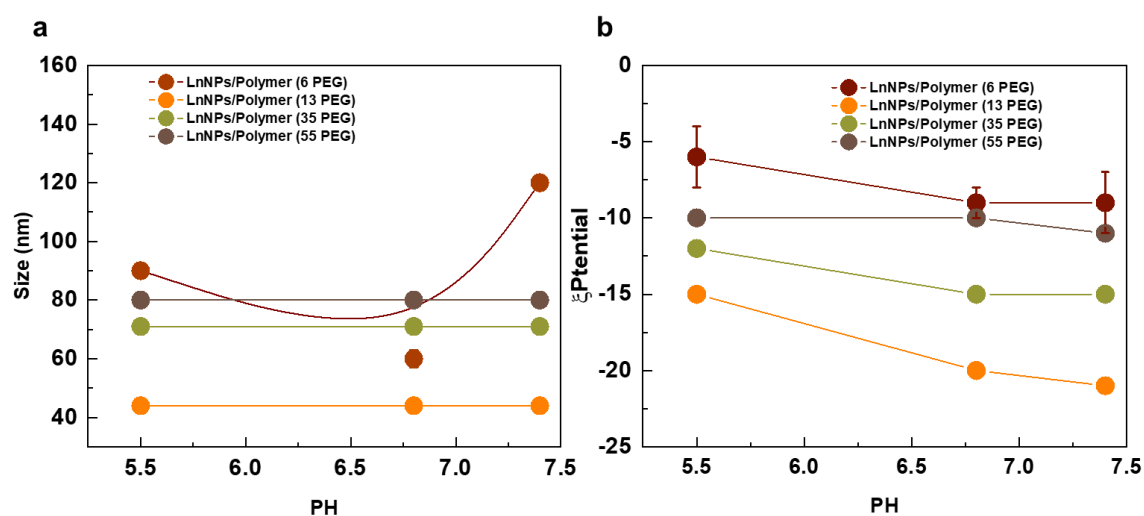
Figure 3.16. DLS (a) and Zeta Potential (b) of LnNPs/Polymers (6, 13, 35, and 55 PEG) in different solvents (aqueous media) with different pH.

Dried nanoparticles are more suited to long-term storage and shipping compared with nanoparticles in solution. The long-term stability of polymer-modified nanoparticles in aqueous media inspired us to further test the stability of the samples after freeze-drying. As seen in the DLS CONTIN plot (**Figure 3.17b-d**), LnNPs coated with polymers ranging from 13 to 55 POEGMEA units withstood the freeze-drying process without any sign of aggregation. TEM analysis (**Figure 3.17f-h**) confirmed the structural integrity of freeze-dried 13, 35, and 55 PEG LnNPs. These results indicate that the polymers can keep nanoparticles apart from each other even in the absence of aqueous media, enhancing their potential shelf life for biomedical applications.
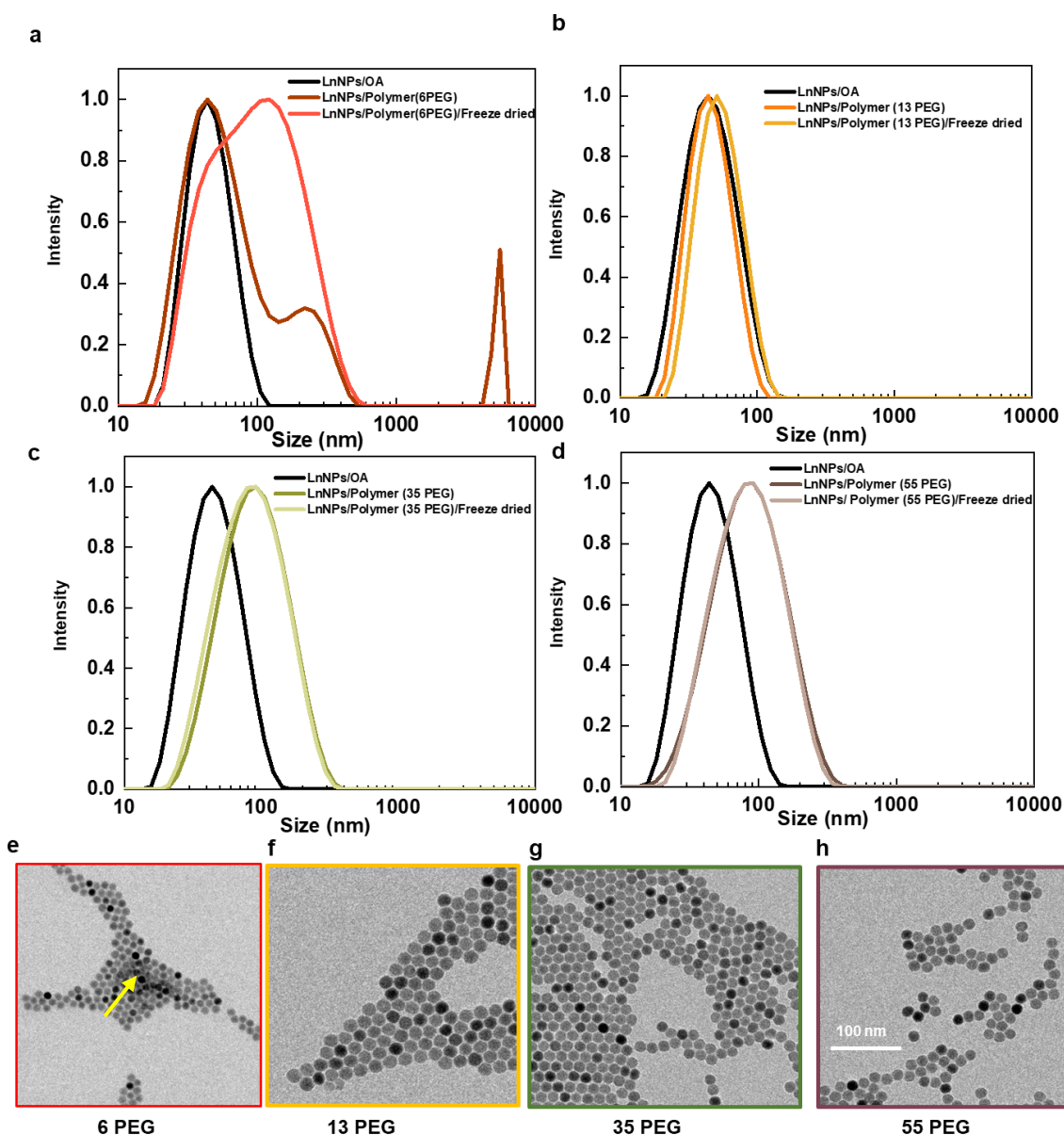
Figure 3.17. CONTIN plots from DLS measurements of LnNPs/OA, LnNPs/Polymer before and after freeze drying, polymer with 6 PEG (a), 13 PEG (b), 35 PEG (c), and 55 PEG (d). TEM image of freeze dried LnNPs/Polymer (6 PEG) (e), LnNPs/Polymer (13 PEG) (f), LnNPs /Polymer (35 PEG) (g), LnNPs /Polymer (55 PEG) (h).

3.6.6. Coupling polymer-capped LnNPs with anti-B220 mAb

We conjugated purified anti-B220 mAb with 13, 35, and 55 PEG LnNPs to evaluate the influence of polymer length on the efficiency of bio-labelling, as illustrated in **Figure 3.18a**. The EDC-dependent activation of carboxylate groups on the surface of the nanoparticles will lead to changes in LnNP surface charge, which can be used to monitor the degree of mAb coupling at the completion of the coupling reaction.

Chapter 3
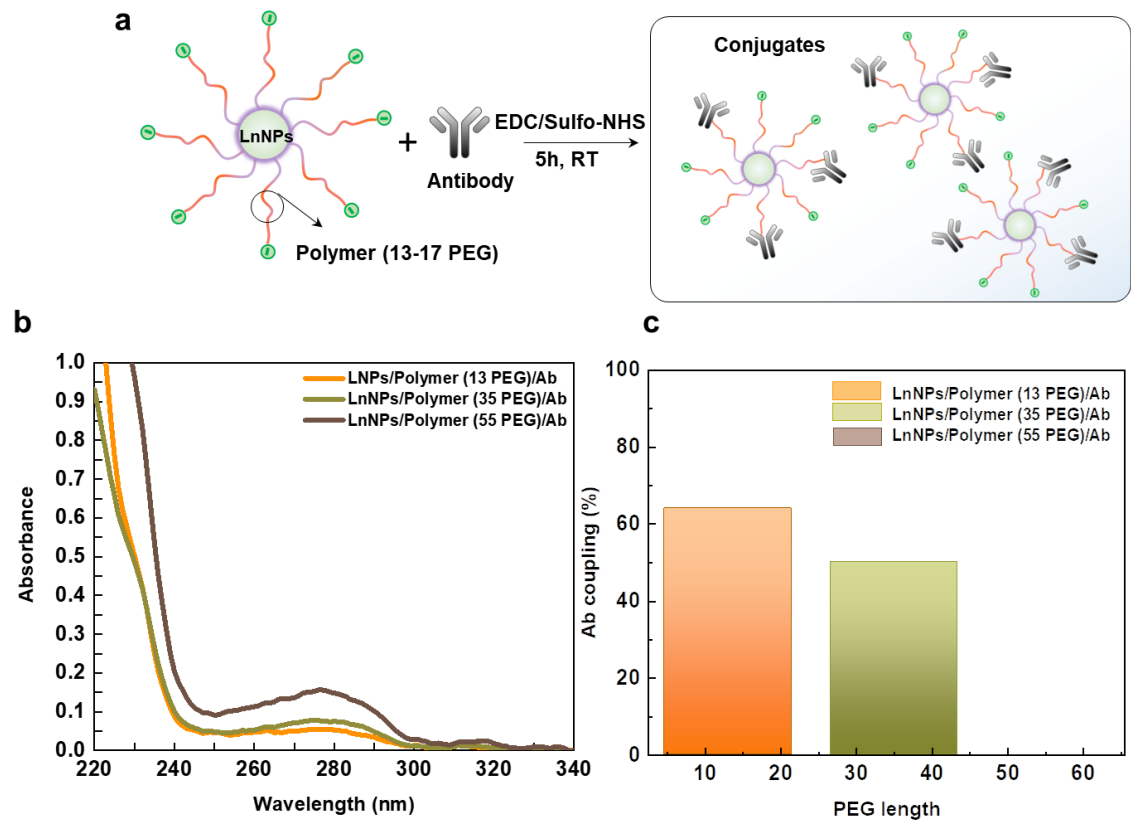
Figure 3.18. Schematic of antibody conjugation with LnNP coated polymer (13-55 PEG) (a). Absorbance spectra of the supernatants after bioconjugation and centrifugation of anti-B220 with different LnNPs/Polymer (b), the percentage of the antibody conjugated to 13 PEG, 35 PEG, and 55 PEG LnNPs calculated from the amount of antibody remaining in the supernatant at the end of the reaction, as measured by UV-absorbance at 280 nm (A280) (c).

As shown in **Figure 3.19**, the surface charge of the 13 PEG LnNPs after antibody conjugation was reduced from -21 ± 0.5 mV to -11 ± 2 mV, while only a slight decrease in surface charge was observed for the 35 PEG LnNPs (-15 ± 0.5 mV to -10 ± 2 mV), and there was no change for the 55 PEG LnNPs. This indicates that the coupling efficiency of 13 PEG LnNPs was higher than that of the 35 and 55 PEG LnNPs.
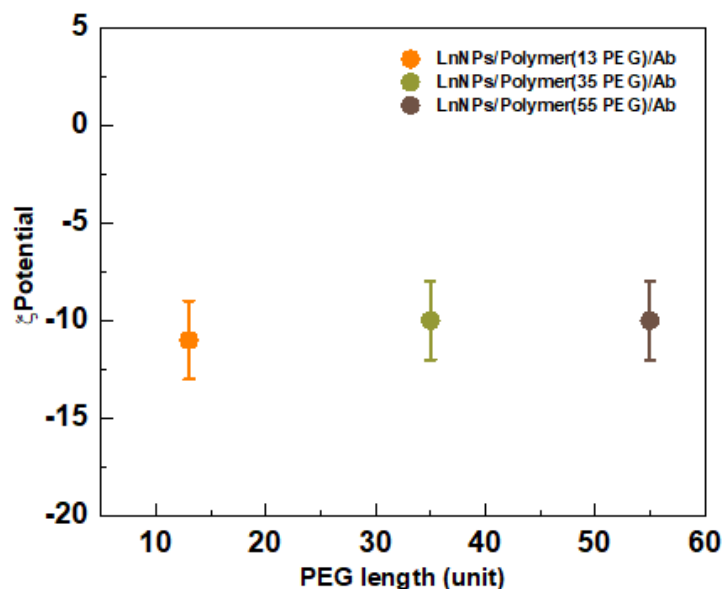
Figure 3.19. Zeta potential of the LnNPs/Polymer after functionalisation with mAb (RA3-6B2 (B220) IgG).

In addition, to measure the amount of coupled Ab, we used UV 280 nm (A280) absorbance to estimate the protein concentration remaining in the supernatants of the 3 coupling reactions after bioconjugation and centrifugation. As shown in **Figure 3.18b**, the A280 measurements of the supernatants from the 13, 35, and 55 PEG LnNP reactions were 0.053, 0.075, and 0.148, respectively. These results indicate that 64% of the Ab was coupled to the 13 PEG LnNPs, while 50% and 0% of Abs were bound to the 35 and 55 PEG LnNPs, respectively (**Figure 3.18c**). Based on these results, we calculated that each nanoparticle in the 13, 35, and 55 PEG preparations was conjugated with approximately 20, 15, and 0 Ab molecules, respectively. These calculations are detailed below. These results indicate that longer polymers on the surface of the nanoparticles are not efficiently functionalised by antibodies (**Figure 3.20**).

Experimental calculation of mole ration Ab/ single LnNPs:

Conc Ab $_{\text{in sample}}$= Initial Conc Ab – S/N

% Ab = $\dfrac{\textbf{Conc Ab}_{\text{in sample}}}{\text{Initial Conc Ab}} \times 100$

Final molar ratio Ab/LnNPs = % Ab × 30
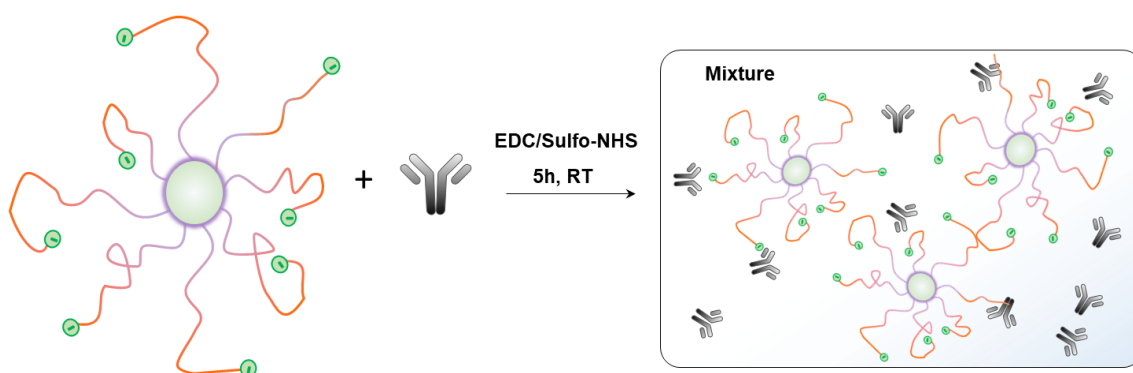
Figure 3.20. Schematic explanation of wrapping up the carboxylic end-functional group towards the inside of the coiled structure of large polymers.

We measured the hydrodynamic size of the nanoparticles after functionalising with mAbs. As seen in **Figure 3.21**, the size of the 13 PEG LnNPs increased from 44 nm to 59 nm, while the sizes of the 35 and 55 PEG LnNPs changed very little.
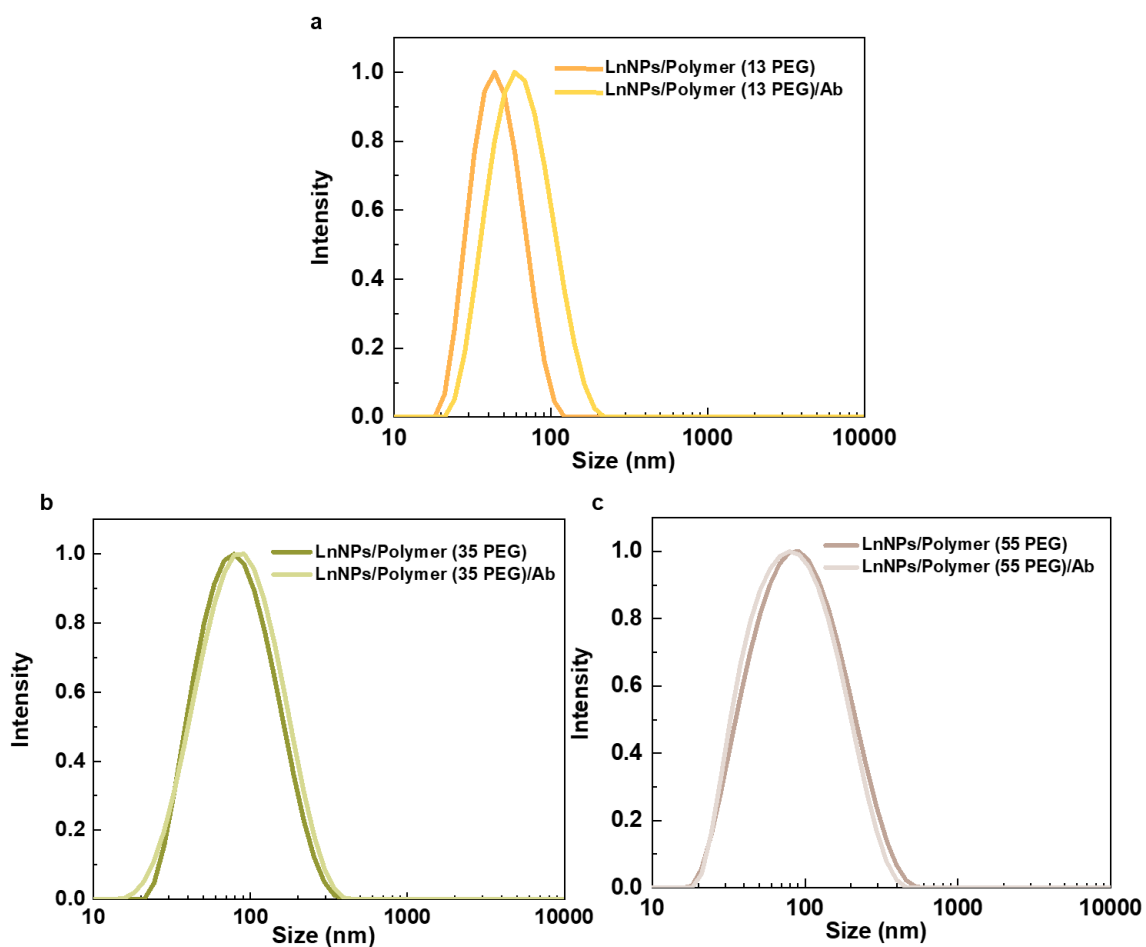
Figure 3.21. DLS CONTIN plot of polymer capped-LnNPs before and after functionalisation with mAb (RA3-6B2 (B220) IgG). LnNPs /Polymer (13 PEG) (a), LnNPs /Polymer (35 PEG) (b), LnNPs /Polymer (55 PEG) (c).

3.6.7 Reactivity of the carboxylic end-functional group of the polymer in different length POEGMEA chains

We hypothesised that POEGMEA chain length-dependent loss of Ab coupling activity could be due to inaccessibility of the carboxylate functional end-group. The reason might be that longer polymers have a stronger tendency to the coil as the length of the polymer exceeds the Kuhn length (**Figure 3.20**). This is driven by the potential interaction of the carboxyl group with the surface of LnNPs, but also other interactions with the polymer backbone such as hydrogen bonding might drive the process. To test this hypothesis, we examined the accessibility of the carboxylic end-functional group of polymers with different lengths of POEGMEA chain from 13 to 55 units, in the absence of LnNPs and antibodies. We coupled the adipic acid dihydrazide (ADH) to the carboxylic end-functional group of the polymers through an carbodiimide chemistry reaction (**Figure 3.22**).
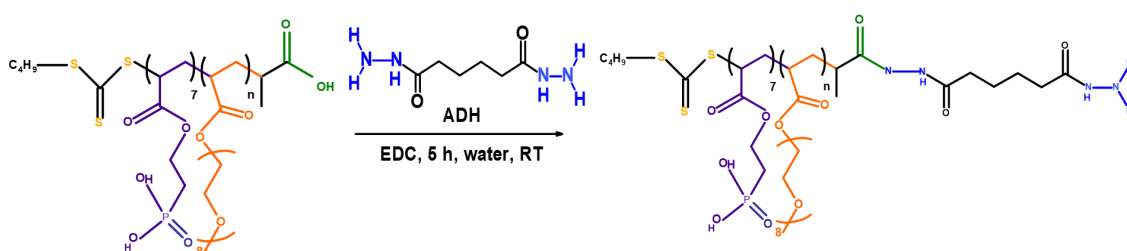
Figure 3.22. Scheme of modifying polymer by ADH

The modified polymers were further analysed by FTIR spectroscopy. As shown in **Figure 3.23**, in the FTIR spectrum of Polymer-ADH with 13 POEGMEA units, the absorption bands at 1537 cm^{-1} and 3311 cm^{-1} are associated with N-H bending and stretching vibration, at 1628 cm^{-1} is attributed to C=O amide, at 1250 cm^{-1} attributed to C-N and C-O stretching vibration, at 2865 cm^{-1} associated with C-H stretching vibration, at 1732 cm^{-1} C=O ester which indicated the presence of ADH bound polymer. However, the FTIR spectra of polymers with 35 and 55 POEGMEA units showed no changes after modification with ADH.
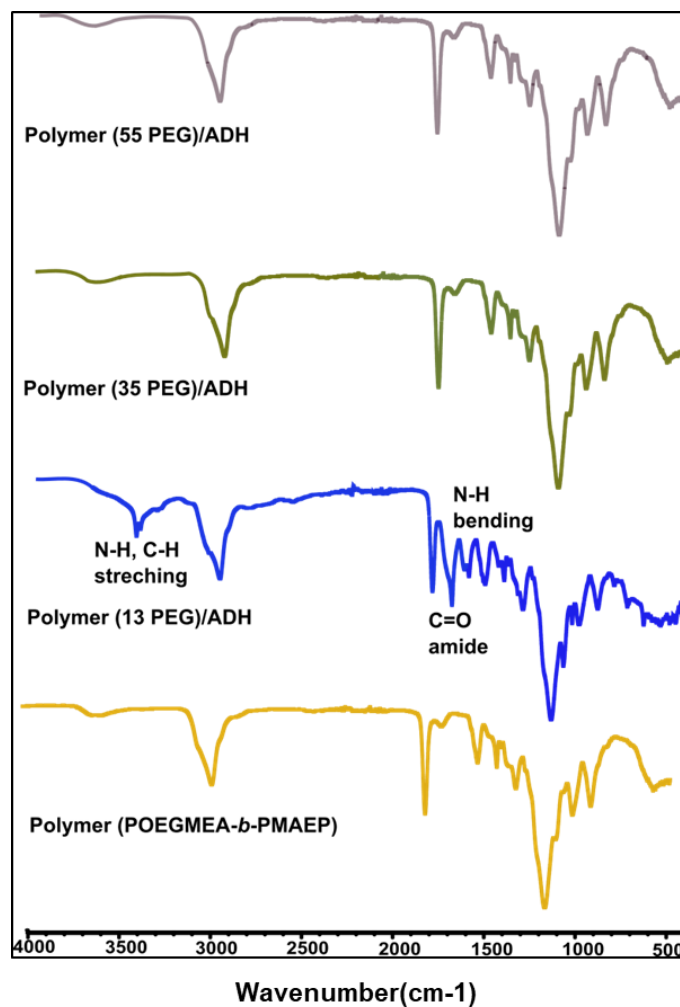
Figure 3.23. FTIR spectra of POEGMEA-*b*-PMAEP (varying in POEGMEA length) before and after functionalisation by ADH.

From ^{1}HNMR spectra (**Figure 3.24**), we also showed that ADH was successfully coupled to the polymer with 13 POEGMEA units while poorly coupled to the polymers with longer POEGMEA units (35 and 55). These data provided support for our hypothesis that longer POEGMEA units might wrap the carboxylic end-functional group inside of the coiled structure of large polymers, and thus the functional end group would have only very limited reactivity for bioconjugation.
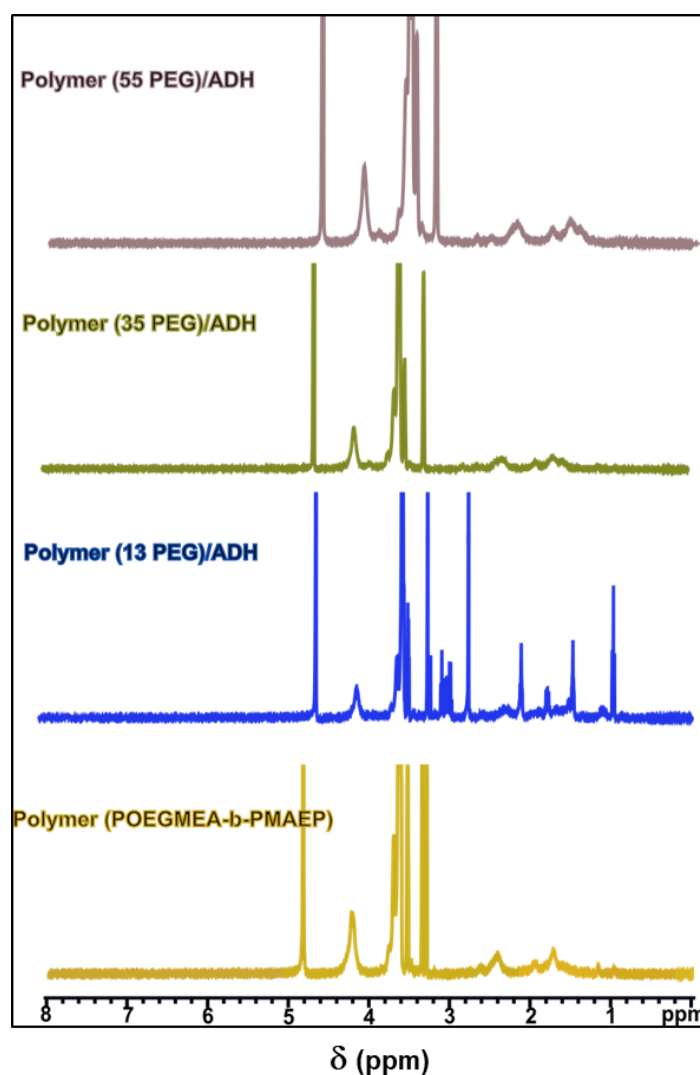
Figure 3.24. ^{1}HNMR spectra of POEGMEA-*b*-PMAEP (varying in POEGMEA length) before and after functionalisation by ADH. δ: 0.9 (4 H, t, C=OCH$_2$), δ: 1.8 (4H, P, C=OCH$_2$CH$_2$), δ: 3.1 (1 H, t, C=ONH), δ: 3.05 (2H, d, C=ONHNH$_2$), δ: 3 (2 H, d, C=ONH-NH-C=O).

3.6.8 Retention of a functional ligand-binding site by LnNP-coupled antibody.

The successful application of LnNPs to antibody-based applications, such as flow cytometry and mass cytometry, requires that the LnNP-coupled antibody retains its sensitivity and specificity as a ligand-specific probe. The A280 measurements of reaction supernatants indicated that rat RA3-6B2 mAb was coupled to the 13 and 35 PEG LnNPs after the conjugation reaction (**Figure 3.18**). To investigate the extent to which the coupled mAb retained a functional binding site for the B220 molecule, we reacted the anti-B220-LnNPs with live murine spleen cells, of which ~50-60% are B cells expressing

high amounts of the B220 molecule on their surface. To detect mouse B cell bound antibody using flow cytometry, a second anti-rat polyclonal antibody, purified from goat and conjugated to phycoerythrin (PE) was used (**Figure 3.25a**). Geometric mean fluorescent intensity (MFI) of the PE-positive cells in each sample was calculated and compared with that of a positive control treated with purified, unconjugated RA3-6B2 plus anti-rat-PE and negative control that was treated with the anti-rat-PE antibody but no anti-B220 (**Figure 3.25b-d**). For the 35 PEG LnNPs (**Figure 3.25b**), the binding activity of a 1:10 dilution was lower than that of purified anti-B220 at a concentration of 1 µg/mL. For the 13 PEG LnNPs (**Figure 3.25c**), the binding activity of a 1:10 dilution was higher than for the 35 PEG LnNPs but lower than the positive control (600 ng/mL at the 1:10 dilution). Calculation of geometric mean fluorescence for the titration of purified anti-B220 and the 13 PEG LnNP-anti-B220 preparation (**Figure 3.25d**) indicated that the binding activity of 13 PEG LnNP-anti-B220 was ~2-fold lower than the positive control (6 µg/mL). Taken together with the data in **Figure 3.18**, this indicates that although over 60% of the starting antibody was conjugated to the 13 PEG LnNPs, only~ 0.5% of the coupled antibody (0.55 of starting antibody) retained its ability to bind to B220 after conjugation. EDC-based conjugation of Abs targets lysine sidechains that are present in both the antigen-binding and constant portions of the Ab. For relatively small molecules such as inorganic fluorescent dyes, this does not usually compromise antigen-binding ability, but it is likely that random orientation of Abs on the surface of a relatively large polymer-coated LnNP would constrain the antibody's ability to bind to a cell surface. For this reason, conjugation techniques that orient antibodies such that the ligand-binding site faces out from the LnNP are likely to yield conjugates that preserve a higher proportion of the original antigen-recognition capacity of the antibody. This experiment is particularly encouraging, as the many unique properties of LnNPs will offer a new library of molecular probes for flow cytometry and mass cytometry applications. The LnNPs can upconvert multiple low-energy near-infrared (NIR) photons into high-energy visible and ultraviolet (UV) light,[11,12] and the unique anti-Stokes emission of LnNPs provides opportunities for background-free detection of cells in rapid flow cytometry, though additional engineering of the flow cytometry instruments is needed. Compared with the dendrimer lanthanide complex being used in mass spectroscopy applications, the high concentration of lanthanide ions in LnNPs can significantly amplify the signal strength for future developments of more sensitive and multiplexed mass flow cytometry and mass imaging applications.[24-28] Moreover, LnNPs generally exhibit negligible cytotoxicity for

Chapter 3

their respective bioapplications in different cell lines.[41] Recently, we have also shown that PPEGMEMA-*b*-PEGMP$_3$ polymer-modified LnNPs have good biocompatibility for three different cell lines (MCF-7, MDA-MB-231, and RAW 264.7) even when their concentration is as high as 0.5 mg/mL,[42] which shows great promise for polymer-modified LnNPs in bioapplications.
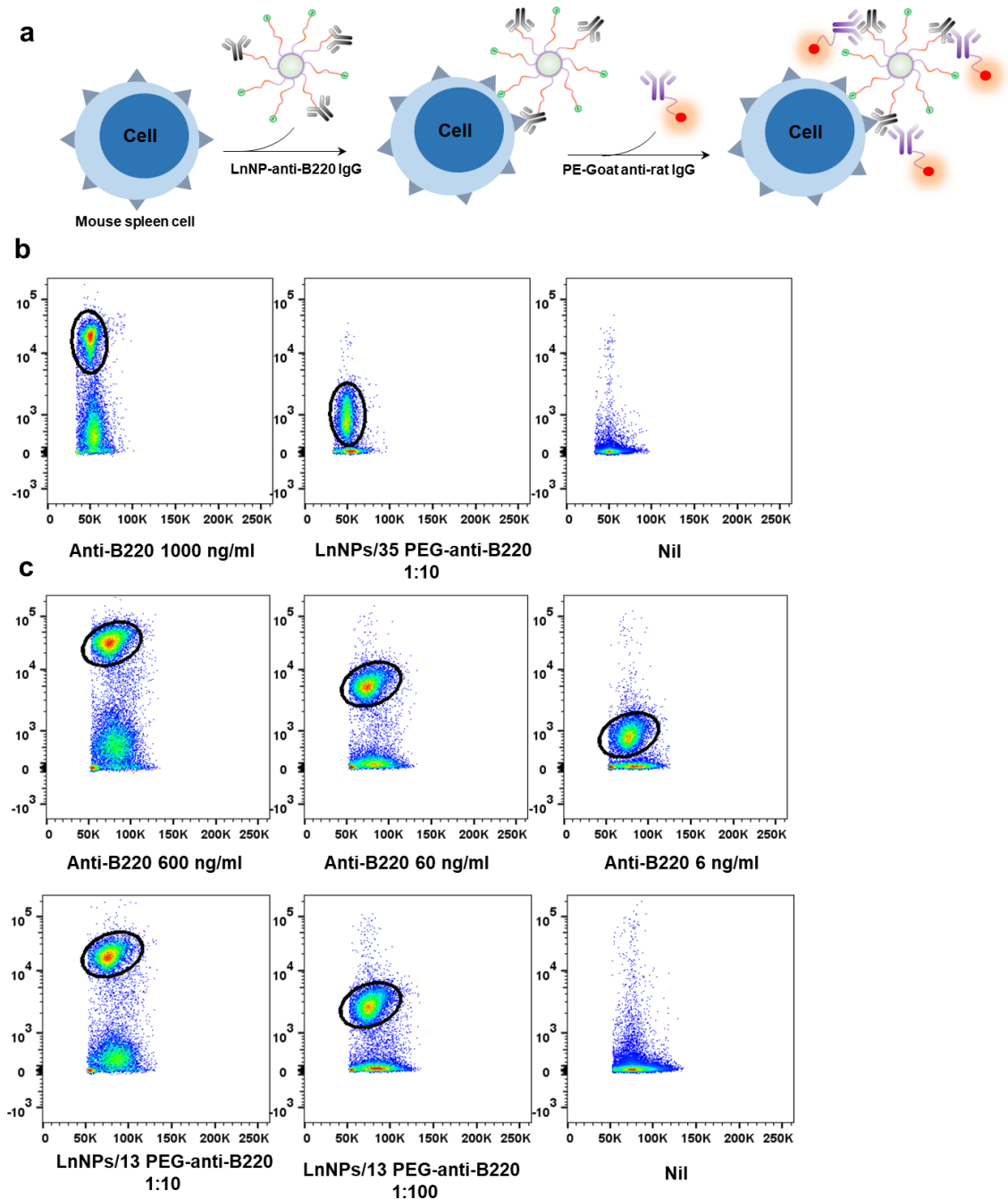
Figure 3.25. Binding of LnNP-anti-B220 to B220 on the surface of live murine splenic B cells, detected using a PE-conjugated goat anti-rat as the secondary reagent (a). Dot plots showing forward scatter vs PE fluorescence for the positive control (purified anti-B220 1 µg/mL), 35 PEG LnNP-anti-B220 conjugate at a 1:10 dilution, and negative control (no anti-B220). The B cell population identified by PE fluorescence is indicated by the black ring. (b). Dot plots showing forward scatter vs PE fluorescence for positive control (purified anti-B220 6 µg/mL at 1:10, 1:100 and 1:1000 dilutions), 13 PEG LnNP-anti-B220 conjugate at 1:10 and 1:100 dilutions and negative control (no anti-B220). The B cell population identified by PE fluorescence is indicated by the black ring (c).

Next, after understanding that the 13 PEG polymer is the best size for the conjugation of LnNPs to antibodies, we conducted a new experiment to optimise the anti-B220 antibody concentration during bioconjugation to reduce antibody wastage. Six new batches of LnNPs and anti-B220 antibody at the molar ratios of 1/5, 1/10, 1/15, 1/20, 1/30, and 1/50 were prepared through EDC/Sulfo-NHS chemistry. The protocol of bioconjugation of LnNPs and Abs was described in previous sections. As shown in **Figure 3.26b**, the binding activity of a 1:10 dilution was enhanced by increasing of molar ratio between nanoparticles and antibodies which can be explained by randomly oriented antibodies towards lanthanide nanoparticles through carbodiimide chemistry.
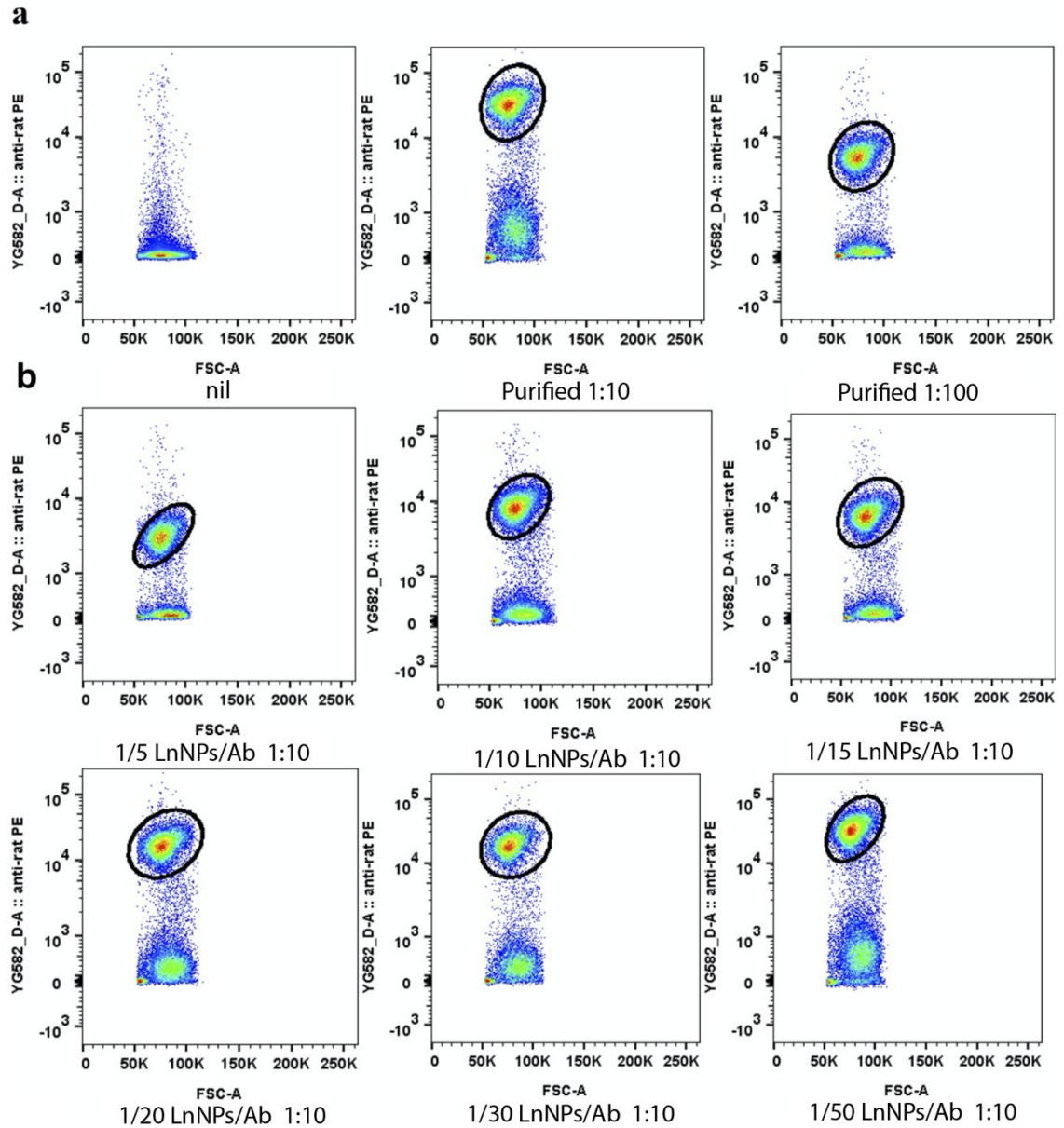
Figure 3.26. Binding of LnNP-anti-B220 to B220 on the surface of live murine splenic B cells, detected using a PE-conjugated goat anti-rat as the secondary reagent. Dot plots showing forward scatter vs PE fluorescence for the negative control (no anti-B220) and positive control (purified anti-B220 6 µg/mL) at 1:10 and 1:100 dilutions (a); 1: 10 dilutions of LnNP-anti-B220 conjugates at molar ratios of 1/5 to 1/50 (b). The B cell population identified by PE fluorescence is indicated by the black ring.

Calculation of the concentration of LnNP/Ab conjugate B220 binding activity as assessed by flow cytometry was performed as detailed in **Figure 3.27a-b**.

Chapter 3
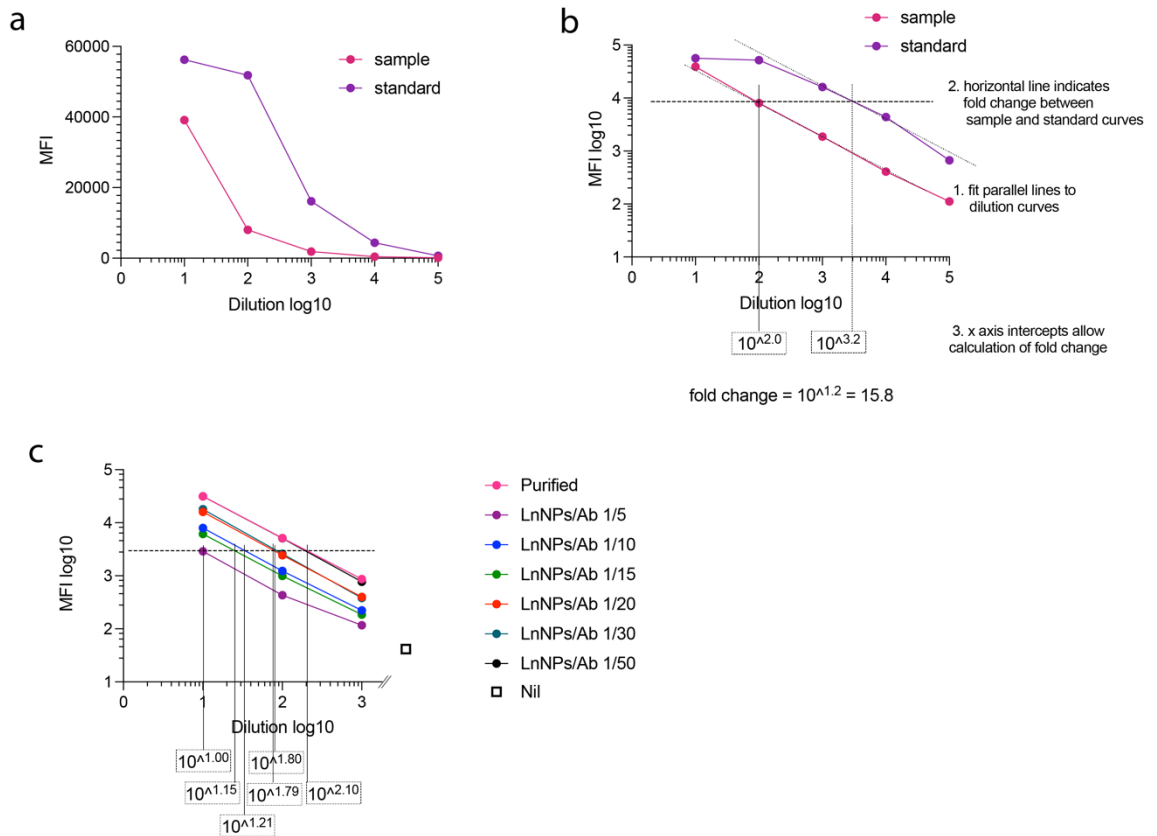
Figure 3.27 Estimation of LnNPs/Ab and supernatant Ab concentrations that retain the ability to bind B220 on the surface of live cells. Dose-response curves for dilution versus MFI are sigmoidal (a), but the central portion is very close to linear when graphed as log dilution versus log MFI (b). To obtain an estimate of the concentration of reactive Ab in each sample, the assumption of linearity allows a simple comparison between the dose-response curves for different preparations. To estimate the concentration of samples by comparison to a control of known concentration, parallel lines are fitted to the dose-response curves for each sample, and the fold difference in starting concentration is estimated by the distance between the lines (b). Dose-response curves for the experiment illustrated in **Figure 3.26** are shown together with their x-intercept estimates (c).

Chapter 3

Table 3.3 Estimation of reactive Ab concentrations from the experiment shown in **Figure 3.25.**

sample	start conc (µg/mL)	X intercept sample	NP/Ab reactive conc (µg/mL)	% efficiency
Purified	6	2.10		
1/5	90	1.00	0.48	0.53
1/10	180	1.21	0.77	0.43
1/15	270	1.15	0.67	0.25
1/20	360	1.78	2.87	0.80
1/30	540	1.80	3.01	0.56
1/50	900	2.10	6.00	0.67

To compare the LnNP-anti-B220 conjugates with a MaxPar®-labelled anti-B220 using mass cytometry, an aliquot of live murine spleen cells was stained with ^{159}Tb anti-B220 or with a 1:10 dilution of the 1/30 LnNPs/anti-B220 conjugate. Samples were incubated with cis-platinum to exclude dead cells, then fixed with paraformaldehyde and incubated with ^{191,193}Ir, a DNA intercalator, to label cell nuclei. ^{159}Tb signal intensity indicated ^{159}Tb anti-B220 binding and ^{89}Y signal indicated binding of LnNPs. **Figure 3.28** shows the comparison between the MaxPar® technique (^{159}Tb, **Figure 3.28a**) and the lanthanide nanoparticles technique (^{89}Y, **Figure 3.28b**). The LnNPs gave very high background staining with no apparent signal.

Comparison of the flow cytometry (**Figure 3.26b**) and mass cytometry (**Figure 3.28b**) results for the 1:10 dilution of the 1/30 LnNPs/anti-B220 conjugate, we concluded that EDC/Sulfo-NHS strategy is not adequate for mass cytometry due to the very high background combined with lack of specific signal.
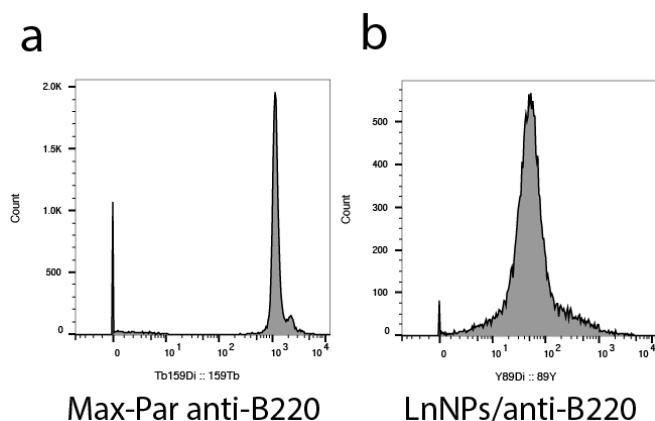
Figure 3.28 Comparison of binding of LnNPs- and Maxpar-labelled anti-B220. Histogram of the signal obtained using Maxpar ^{159}Tb/anti-B220 on mouse spleen cells (a). Histogram of the signal obtained using LnNPs/anti-B220 on mouse spleen cells (b).

3.7   Conclusion:

We synthesised diblock copolymers with a fine-tuneable number of POEGMEA blocks to render OA-capped LnNPs stable in aqueous media. By systematically synthesising polymers with between 6 and 55 POEGMEA units, we could determine how the length of the POEGMEA block affected the long-term stability and efficient bioconjugation of LnNPs. We discovered that when the length of the POEGMEA block segment was too short, it failed to stabilise the nanoparticles in an aqueous solution, resulting in significant aggregation. The POEGMEA-*b*-PMAEP polymer with 13 POEGMEA units produced robust and excellent results, not only for colloidal stability in various physiological buffers at pH=5.5-7.4 but also for bio-conjugation with the antibodies. Although the longer POEGMEA blocks (35-55 units) of the polymer also offered long-term stability to these LnNPs, they failed in exposing active carboxylate functional end-groups outside for the bioconjugation, because of both interaction of polymer end with surrounding LnNPs surface and wrapping towards the inside of branch structure of the large polymer. Moreover, the bio-conjugation of polymer coated LnNPs with anti-B220 through EDC/Sulfo-NHS strategy offered some drawbacks including,

1) Random orientation of anti-B220 antibodies on the surface of LnNPs, as the Carboxylate end functional group coated LnNPs can target lysine (-NH$_2$) of antibodies side chains that are present in both antigen-binding site (Fab) and constant site (Fc), resulting in low conjugation efficiency (**Figure 3.29**).
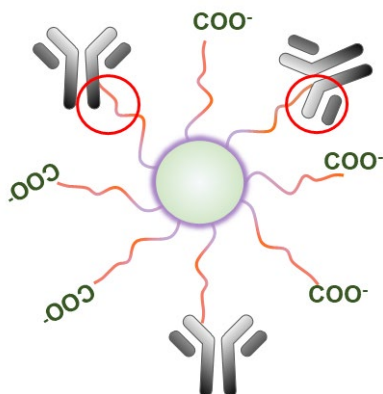
Figure 3.29. Schematic illustration of random coupling polymer-LnNPs to IgG antibodies through EDC/Sulfo-NHS chemistry.

2) Failure to be blocked by blocking reagents, as the unoccupied carboxylates end functional group of polymer-LnNPs can be hydrolysed during the washing steps, resulting in generating a high level of background in CyTOF assays (**Figure 3.30**).
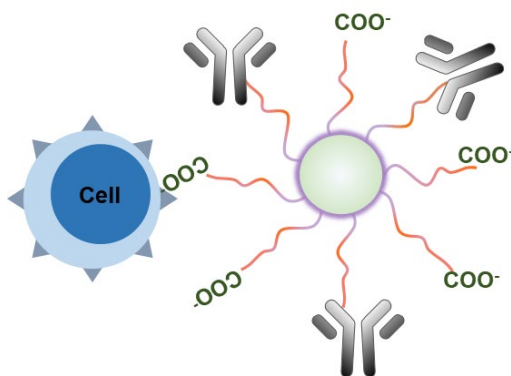
Figure 3.30. Schematic illustration of non-specific binding of unoccupied carboxylate on the surface of LnNPs/antibodies with cells

3) Failure to exclude free nanoparticles from the conjugated ones, resulted in generating a high level of background in CyTOF assays (**Figure 3.31**)
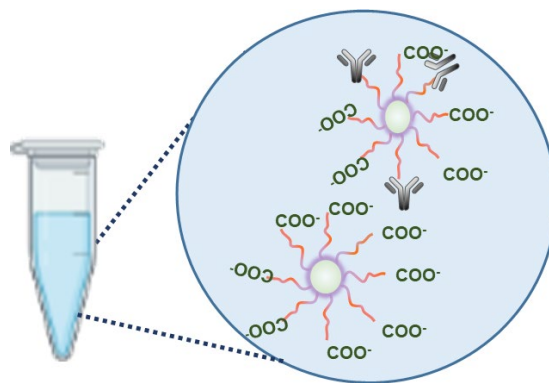
Figure 3.31. Schematic illustration of the prepared conjugated sample comprises both free LnNPs and coupled ones with IgG antibodies.

Therefore, we decided to change the conjugation methodology to achieve a high level of conjugation efficiency. Fortunately, there was a unique and conserved place in Fc region of antibodies which was N-galactosylation and could be oxidised by oxidising reagent to produce aldehyde functional groups, so that by further modification of LnNPs with hydrazide moieties, the oxidised antibodies can be conjugated to LnNPs which faced out of antigen-binding sites.

References

1.	Yang, Y. S.; Atukorale, P. U.; Moynihan, K. D.; Bekdemir, A.; Rakhra, K.; Tang, L.; Stellacci, F.; Irvine, D. J., High-throughput quantitation of inorganic nanoparticle biodistribution at the single-cell level using mass cytometry. *Nat Commun* **2017,** *8,* 14069.

2.	Corot, C.; Robert, P.; Idée, J.-M.; Port, M., Recent advances in iron oxide nanocrystal technology for medical imaging. *Advanced Drug Delivery Reviews* **2006,** *58* (14), 1471-1504.

3.	Chou, S.-W.; Shau, Y.-H.; Wu, P.-C.; Yang, Y.-S.; Shieh, D.-B.; Chen, C.-C., In Vitro and in Vivo Studies of FePt Nanoparticles for Dual Modal CT/MRI Molecular Imaging. *Journal of the American Chemical Society* **2010,** *132* (38), 13270-13278.

4.	Rabin, O.; Manuel Perez, J.; Grimm, J.; Wojtkiewicz, G.; Weissleder, R., An X-ray computed tomography imaging agent based on long-circulating bismuth sulphide nanoparticles. *Nature Materials* **2006,** *5* (2), 118-122.

5.	Le Duc, G.; Miladi, I.; Alric, C.; Mowat, P.; Bräuer-Krisch, E.; Bouchet, A.; Khalil, E.; Billotey, C.; Janier, M.; Lux, F.; Epicier, T.; Perriat, P.; Roux, S.; Tillement, O., Toward an Image-Guided Microbeam Radiation Therapy Using Gadolinium-Based Nanoparticles. *ACS Nano* **2011,** *5* (12), 9566-9574.

6.	Mahato, K.; Nagpal, S.; Shah, M. A.; Srivastava, A.; Maurya, P. K.; Roy, S.; Jaiswal, A.; Singh, R.; Chandra, P., Gold nanoparticle surface engineering strategies and their applications in biomedicine and diagnostics. *3 Biotech* **2019,** *9* (2), 57.

7.	Rana, S.; Bajaj, A.; Mout, R.; Rotello, V. M., Monolayer coated gold nanoparticles for delivery applications. *Advanced drug delivery reviews* **2012,** *64* (2), 200-216.

8.	Dumas, A.; Couvreur, P., Palladium: a future key player in the nanomedical field? *Chemical Science* **2015,** *6* (4), 2153-2157.

9.	Yao, J.; Li, P.; Li, L.; Yang, M., Biochemistry and biomedicine of quantum dots: from biodetection to bioimaging, drug discovery, diagnostics, and therapy. *Acta Biomaterialia* **2018,** *74*, 36-55.

10.	Souza, S. O.; Lira, R. B.; Cunha, C. R. A.; Santos, B. S.; Fontes, A.; Pereira, G., Methods for Intracellular Delivery of Quantum Dots. *Topics in Current Chemistry* **2021,** *379* (1), 1.

11.	Chen, G.; Qiu, H.; Prasad, P. N.; Chen, X., Upconversion nanoparticles: design, nanochemistry, and applications in theranostics. *Chem Rev* **2014,** *114* (10), 5161-214.

12.	Wen, S.; Zhou, J.; Zheng, K.; Bednarkiewicz, A.; Liu, X.; Jin, D., Advances in highly doped upconversion nanoparticles. *Nature Communications* **2018,** *9* (1), 2415.

13.	He, H.; Liu, B.; Wen, S.; Liao, J.; Lin, G.; Zhou, J.; Jin, D., Quantitative Lateral Flow Strip Sensor Using Highly Doped Upconversion Nanoparticles. *Analytical Chemistry* **2018,** *90* (21), 12356-12360.

14.	Bednarkiewicz, A.; Chan, E. M.; Kotulska, A.; Marciniak, L.; Prorok, K., Photon avalanche in lanthanide doped nanoparticles for biomedical applications: super-resolution imaging. *Nanoscale Horizons* **2019,** *4* (4), 881-889.

15.	Wang, F.; Wen, S.; He, H.; Wang, B.; Zhou, Z.; Shimoni, O.; Jin, D., Microscopic inspection and tracking of single upconversion nanoparticles in living cells. *Light: Science & Applications* **2018,** *7* (4), 18007-18007.

16.	Du, Z.; Gupta, A.; Clarke, C.; Cappadona, M.; Clases, D.; Liu, D.; Yang, Z.; Karan, S.; Price, W. S.; Xu, X., Porous Upconversion Nanostructures as Bimodal Biomedical Imaging Contrast Agents. *The Journal of Physical Chemistry C* **2020,** *124* (22), 12168-12174.

17.	Li, M.; Fang, H.; Liu, Q.; Gai, Y.; Yuan, L.; Wang, S.; Li, H.; Hou, Y.; Gao, M.; Lan, X., Red blood cell membrane-coated upconversion nanoparticles for pretargeted multimodality imaging of triple-negative breast cancer. *Biomaterials Science* **2020,** *8* (7), 1802-1814.

18.	Xu, J.; Xu, L.; Wang, C.; Yang, R.; Zhuang, Q.; Han, X.; Dong, Z.; Zhu, W.; Peng, R.; Liu, Z., Near-Infrared-Triggered Photodynamic Therapy with Multitasking Upconversion

Nanoparticles in Combination with Checkpoint Blockade for Immunotherapy of Colorectal Cancer. *ACS Nano* **2017,** *11* (5), 4463-4474.

19. Zhang, Y.; Huang, P.; Wang, D.; Chen, J.; Liu, W.; Hu, P.; Huang, M.; Chen, X.; Chen, Z., Near-infrared-triggered antibacterial and antifungal photodynamic therapy based on lanthanide-doped upconversion nanoparticles. *Nanoscale* **2018,** *10* (33), 15485-15495.

20. Yang, B.; Chen, H.; Zheng, Z.; Li, G., Application of upconversion rare earth fluorescent nanoparticles in biomedical drug delivery system. *Journal of Luminescence* **2020,** *223*, 117226.

21. Zhang, Z.; Jayakumar, M. K. G.; Shikha, S.; Zhang, Y.; Zheng, X.; Zhang, Y., Modularly Assembled Upconversion Nanoparticles for Orthogonally Controlled Cell Imaging and Drug Delivery. *ACS Applied Materials & Interfaces* **2020,** *12* (11), 12549-12556.

22. I, Y. L.; Jiang, M.; Xue, Z.; Zeng, S., 808 nm light triggered lanthanide nanoprobes with enhanced down-shifting emission beyond 1500 nm for imaging-guided resection surgery of tumor and vascular visualization. *Theranostics* **2020,** *10* (15), 6875-6885.

23. Zhong, Y.; Dai, H., A mini-review on rare-earth down-conversion nanoparticles for NIR-II imaging of biological systems. *Nano Research* **2020,** *13* (5), 1281-1294.

24. Lin, W.; Hou, Y.; Lu, Y.; Abdelrahman, A. I.; Cao, P.; Zhao, G.; Tong, L.; Qian, J.; Baranov, V.; Nitz, M.; Winnik, M. A., A high-sensitivity lanthanide nanoparticle reporter for mass cytometry: tests on microgels as a proxy for cells. *Langmuir* **2014,** *30* (11), 3142-53.

25. Pichaandi, J.; Tong, L.; Bouzekri, A.; Yu, Q.; Ornatsky, O.; Baranov, V.; Winnik, M. A., Liposome-Encapsulated NaLnF4 Nanoparticles for Mass Cytometry: Evaluating Nonspecific Binding to Cells. *Chemistry of Materials* **2017,** *29* (11), 4980-4990.

26. Pichaandi, J.; Zhao, G.; Bouzekri, A.; Lu, E.; Ornatsky, O.; Baranov, V.; Nitz, M.; Winnik, M. A., Lanthanide nanoparticles for high sensitivity multiparameter single cell analysis. *Chem Sci* **2019,** *10* (10), 2965-2974.

27. Ornatsky, O.; Bandura, D.; Baranov, V.; Nitz, M.; Winnik, M. A.; Tanner, S., Highly multiparametric analysis by mass cytometry. *J Immunol Methods* **2010,** *361* (1-2), 1-20.

28. Tong, L.; Lu, E.; Pichaandi, J.; Zhao, G.; Winnik, M. A., Synthesis of Uniform NaLnF4 (Ln: Sm to Ho) Nanoparticles for Mass Cytometry. *The Journal of Physical Chemistry C* **2016,** *120* (11), 6269-6280.

29. Muhr, V.; Wilhelm, S.; Hirsch, T.; Wolfbeis, O. S., Upconversion nanoparticles: from hydrophobic to hydrophilic surfaces. *Acc Chem Res* **2014,** *47* (12), 3481-93.

30. Jiang, G.; Pichaandi, J.; Johnson, N. J.; Burke, R. D.; van Veggel, F. C., An effective polymer cross-linking strategy to obtain stable dispersions of upconverting NaYF4 nanoparticles in buffers and biological growth media for biolabeling applications. *Langmuir* **2012,** *28* (6), 3239-47.

31. Sedlmeier, A.; Gorris, H. H., Surface modification and characterization of photon-upconverting nanoparticles for bioanalytical applications. *Chem Soc Rev* **2015,** *44* (6), 1526-60.

32. Chattopadhyay, P. K.; Price, D. A.; Harper, T. F.; Betts, M. R.; Yu, J.; Gostick, E.; Perfetto, S. P.; Goepfert, P.; Koup, R. A.; De Rosa, S. C.; Bruchez, M. P.; Roederer, M., Quantum dot semiconductor nanocrystals for immunophenotyping by polychromatic flow cytometry. *Nat Med* **2006,** *12* (8), 972-7.

33. Cao, P.; Tong, L.; Hou, Y.; Zhao, G.; Guerin, G.; Winnik, M. A.; Nitz, M., Improving lanthanide nanocrystal colloidal stability in competitive aqueous buffer solutions using multivalent PEG-phosphonate ligands. *Langmuir* **2012,** *28* (35), 12861-70.

34. Knop, K.; Hoogenboom, R.; Fischer, D.; Schubert, U. S., Poly(ethylene glycol) in drug delivery: pros and cons as well as potential alternatives. *Angew Chem Int Ed Engl* **2010,** *49* (36), 6288-308.

35. Liu, D.; Xu, X.; Du, Y.; Qin, X.; Zhang, Y.; Ma, C.; Wen, S.; Ren, W.; Goldys, E. M.; Piper, J. A.; Dou, S.; Liu, X.; Jin, D., Three-dimensional controlled growth of monodisperse sub-50 nm heterogeneous nanocrystals. *Nature Communications* **2016,** *7* (1), 10254.

References

36.   Ferguson, C. J.; Hughes, R. J.; Nguyen, D.; Pham, B. T. T.; Gilbert, R. G.; Serelis, A. K.; Such, C. H.; Hawkett, B. S., Ab Initio Emulsion Polymerization by RAFT-Controlled Self-Assembly. *Macromolecules* **2005,** *38* (6), 2191-2204.

37.   Duong, H. T. T.; Chen, Y.; Tawfik, S. A.; Wen, S.; Parviz, M.; Shimoni, O.; Jin, D., Systematic investigation of functional ligands for colloidal stable upconversion nanoparticles. *RSC Advances* **2018,** *8* (9), 4842-4849.

38.   Mackenzie, L. E.; Goode, J. A.; Vakurov, A.; Nampi, P. P.; Saha, S.; Jose, G.; Millner, P. A., The theoretical molecular weight of NaYF 4 :RE upconversion nanoparticles. *Sci Rep* **2018,** *8* (1), 1106.

40.   Liu, H.; Xu, C. T.; Dumlupinar, G.; Jensen, O. B.; Andersen, P. E.; Andersson-Engels, S., Deep tissue optical imaging of upconverting nanoparticles enabled by exploiting higher intrinsic quantum yield through use of millisecond single pulse excitation with high peak power. *Nanoscale* **2013,** *5* (20), 10034-40.

41.   Dong, H.; Du, S.-R.; Zheng, X.-Y.; Lyu, G.-M.; Sun, L.-D.; Li, L.-D.; Zhang, P.-Z.; Zhang, C.; Yan, C.-H., Lanthanide Nanoparticles: From Design toward Bioimaging and Therapy. *Chem Rev* **2015,** *115* (19), 10725-10815.

42.   Zhang, L.; Chen, C.; Tay, S. S.; Wen, S.; Cao, C.; Biro, M.; Jin, D.; Stenzel, M. H., Optimizing the Polymer Cloak for Upconverting Nanoparticles: An Evaluation of Bioactivity and Optical Performance. *ACS Applied Materials & Interfaces* **2021,** *13* (14), 16142-16154.

Chapter 4: Direct Conjugation of LnNPs via the Fc Glycosylation Site of IgG Antibodies (Schiff-base reaction)

Mahnaz Maddahfar, Barbara Fazekas de St Groth*, Seyed Mostafa Hosseinpour Mashkani, Shihui Wen, Helen McGuire, Nima Sayyadi, Martina Stenzel, Dayong Jin*. Cytometry part A (in preparation).

4.1   The aim of the chapter

The successful fabrication of LnNP-based mass tags for enhancing mass cytometry signals requires a high level of antibody conjugation efficiency and substantially reduced non-specific binding of LnNPs to cells and other biomolecules. In this chapter, we are going to develop a unique bioconjugation strategy that offers control over antibody orientation during covalent binding to LnNPs, reduction in the amount of antibody required and a significant decrease in nonspecific binding compared to Carbodiimide Chemistry.

4.2   Abstract

Lanthanide nanoparticles (LnNPs) have the potential to be used as high-sensitivity mass tag reporters in mass cytometry immunoassays. Antibody (Ab) conjugation efficiency plays essential role in fabricating LnNP-based mass tag reporters. Carbodiimide chemistry conjugation has several downsides, including random orientation coupling of the Ab on the surface of LnNPs, lack of a method to block unoccupied carboxylate that produces nonspecific binding, and inability to exclude free LnNPs which can generate a high level of background in mass cytometry. Here we addressed these shortcomings by introducing directional conjugation of Ab to the LnNPs surface. With this method (Schiff-base chemistry), the average number of bound Ab molecule on each LnNP was five, and low molar coupling ratios between LnNP and Ab were sufficient to saturate the LnNPs. Flow cytometry single cell analysis showed that the 13% of the coupled antibody retained its activity to recognise B220 biomarkers on the B cells, which is significantly higher than was achieved using Carbodiimide chemistry. Mass cytometry demonstrated a significant drop in non-specific binding with the addition of blocker to the LnNPs/Ab and confirmed that the aggregated LnNPs (pellet) after centrifugation of blocked LnNPs/Ab had no specific Ab reactivity.

Chapter 4

Keywords: Site specific Ab conjugation, Schiff-base chemistry, Hydrazide-LnNPs, LnNPs-based reporters, Homofunctional linker, Oxidised antibody

4.3 Graphical abstract
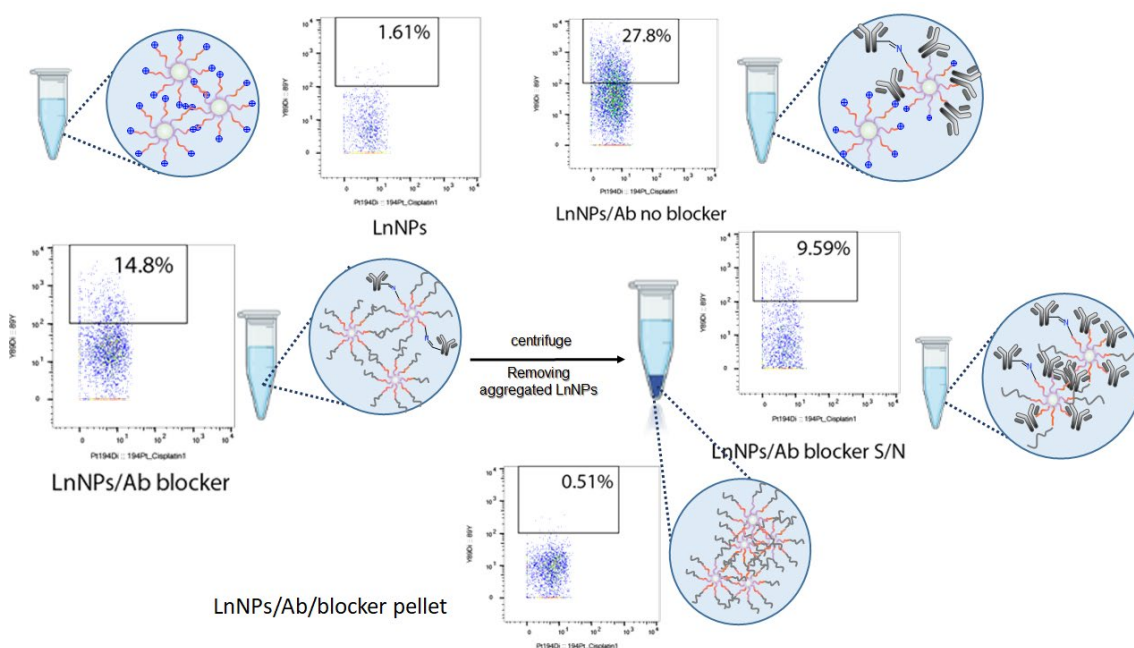
4.4   Introduction

The enormous demand for highly sensitive, multiplexed detection of biomarkers in individual cells exists as it will impact on cell research,[1] drug discovery,[2] disease diagnosis, and treatment.[3] Immunologists, oncologists, haematologists, and biologists are looking for high throughput single cell analysis to efficiently extract as much information as possible from clinical samples of limited mass, such as biopsies and blood samples.[4-6] Flow cytometry is an advanced single-cell analysis technology that is well-established and widely used for multiplex cellular measurements in limited volume samples.[1,7] In flow cytometry, bioaffinity agents are labelled with fluorescent dyes[1] or quantum dots (QDs)[8] to allow rapid cell-by-cell analysis of multiple biomarkers. However, overlapping emission spectra of the fluorescent tags restricts standard flow cytometry when it comes to highly multiplexed assays.[9] Mass cytometry is a state-of-art technology designed to address the challenges of polychromatic flow cytometry by replacing fluorophores with

Chapter 4

stable heavy metal isotopes as Ab tags, which results in no background signal. This unique technique enables researchers to seamlessly multiplex up to 40 independent measurements on single cell.[10] Mass cytometry uses antibodies conjugated to heavy metal isotopes to label the cells in a way similar to what is done for flow cytometry.[11] Labelled cells are then individually injected into the mass cytometer where the cells and mass tags are vaporized, atomized, and ionized. The resulting ions are filtered, and the remaining heavy metal isotopes are detected with single mass resolution by inductively coupled plasma time-of-flight mass spectrometry.[12] Currently, commercially available mass cytometry tags are mainly based on lanthanide isotopes that are chelated to a metal chelating polymer (MCP), which is a branched polymer with multiple metal chelating sites. Antibodies labelled with these polymers typically carry 100-250 metal atoms per antibody.[13-15] Since mass cytometry can detect fewer than ~1 out of 10^5 ions generated in the plasma, 10^4-10^7 antigens per cell must bind to the metal-tagged antibodies in order to elicit a detectable signal above background.[15] Thus to detect low abundance biomarkers, mass tags that can carry more metal ions are required. One approach to increase the number of metal atoms per tag is to conjugate Abs to semiconducting polymer-micelle dots carrying chelators for lanthanide ions or to polystyrene nanoparticles, both of which contain ~2000 lanthanide ions, or to polystyrene microparticles that contain up to 10^6 lanthanide ions. However, with these reagents, researchers observed a signal enhancement of only 4 to 6 fold over the commercial MCP reagent, depending on the marker studied.[16-18] Another potential approach is to conjugate Abs to lanthanide nanoparticles that, depending on their size, can carry more than 10^4 lanthanide ions,[19] potentially enhancing the sensitivity of mass cytometry by up to 100 fold. One of the most popular methods to prepare LnNPs is coprecipitation synthesis, which requires high boiling point organic solvents that produce nanoparticles with bioincompatible hydrophobic capping ligands such as oleic acid.[20] Therefore, subsequent surface coating is a prerequisite to generate a hydrophilic layer that results in well-dispersed nanoparticles in aqueous media. For lanthanide nanoparticles used as mass tags in mass cytometry assays, the coating must provide long term stability in physiological buffers, uniform size with Cv less than 5%, minimal nonspecific binding to cells and other biomolecules, and functional groups with which to attach bioreagents such as antibodies.[21] Pichaandi et al used liposome encapsulated NaYF$_4$:Yb,Er nanoparticles to evaluate nonspecific binding of nanoparticles to cells for mass cytometry.[21] Although the liposomes had minimal interaction with cells, they caused nanoparticles to aggregate after

3 days. In another publication, they used silica coating to produce a LnNPs-based mass barcode.[22] However, more than one LnNP could be encapsulated into each individual silica shell, resulted in a heterogeneous nanoparticle preparation. Also, some of LnNPs, namely NaTbF$_4$ and NaEuF$_4$ NPs, were precipitated when they were coated by silica. Cao and et al synthesised a series of mono-, di-, and tetraphosphonate PEG ligands to produce non-aggregated colloidal stable suspensions of the nanoparticles in phosphate buffers.[23,24] Although the tetraphosphonate ligand produced more stability at high pH and in phosphate buffers, it did not contain any reactive functional group for Ab conjugation in mass cytometry applications.

Thus despite substantial progress in recent years in generating functionalised LnNPs as potential high sensitivity mass tags, there is, to the best of our knowledge, no report that describes the design and fabrication of surface coated LnNPs that satisfy all the essential criteria. Therefore, we designed and synthesised diblock copolymer as a hydrophilic ligand of LnNPs to generate LnNP-based mass tags for high-sensitivity multiparameter single-cell analysis. The results in Chapter 3 indicated that LnNPs functionalised with the POEGMEA-*b*-PMAEP with a 13 OEGMEA chain performed best in terms of long-term colloidal stability and Ab conjugation efficiency. However, the random orientation of Abs on the surface of a relatively large polymer-coated LnNP is likely to constrain the Ab's ability to bind to the antigens on the cell surface.[25] For this reason, conjugation techniques that orient the Ab molecules with the ligand-binding site facing away from the LnNP are likely to generate Ab-conjugated LnNPs in which a higher proportion of the Abs retain the ability to bind to cell surface antigen. Site-specific Ab conjugation techniques such as click chemistry can ensure that Ab orientation is well controlled, but require genetic modification of each individual Ab. For mass cytometry applications where a large number of different Abs must be conjugated to LnNPs containing different lanthanide isotopes, the unique conserved N-linked oligosaccharide moiety within the Fc constant domain of the IgG Ab is a site that can be specifically and covalently linked to LnNPs without hindering the Fab antigen-binding domain.[26,27] This provides a potentially simple and effective method for site-specific and self-oriented immobilisation of Abs on LnNPs. In addition, it requires a significantly reduced amount of antibodies during conjugation as compared to Carbodiimide chemistry. The design of the experiments described in this chapter was to use Schiff-base reaction formation between hydrazide-functionalised LnNPs and reactive di-aldehydes generated via oxidation of the N-linked

oligosaccharides on the two heavy chains of the Fc region of IgG Abs. To achieve this, sodium periodate (NaIO$_4$) was used as a gentle oxidation agent. The oxidised antibody (IgG-CHO) was then reacted with hydrazide functionalised LnNPs through reductive amination.[28] As shown in **Figure 4.1**, adipic acid dihydrazide (ADH, a small hydrazide linker) was first conjugated via one hydrazide to the carboxylate moieties of the polymer-coated LnNPs through carbodiimide chemistry, and then the other hydrazide was covalently coupled to the oxidised polysaccharide residues on the Fc region of the anti-B220 IgG through Schiff-base interaction. Subsequently, any unbound hydrazide groups remaining on the surface of coupled nanoparticles were blocked using a blocking agent containing PEG-CHO 2′000, with the aim of reducing non-specific binding to cells.
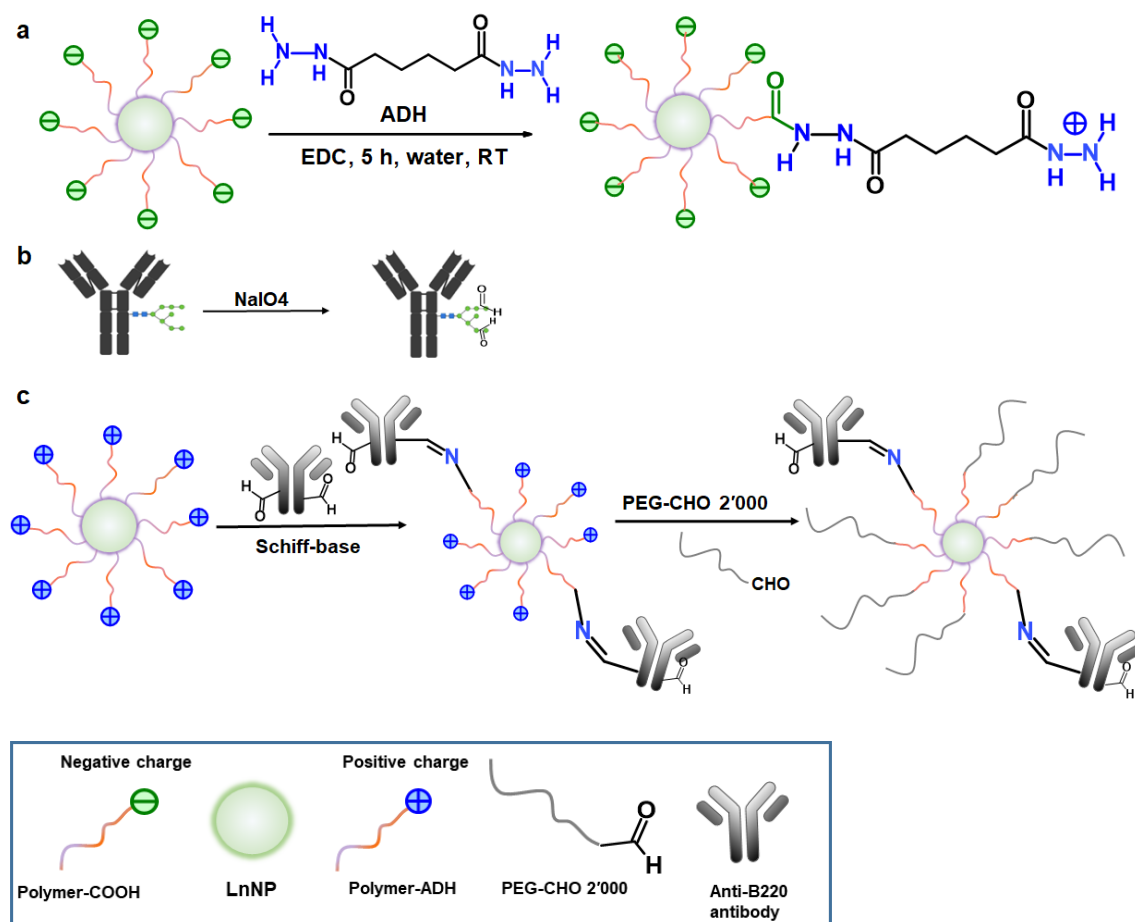
Figure 4.1 Schematic illustration of site-specific conjugation of Abs to LnNPs. Conjugation of ADH to polymer coated LnNPs through carbodiimide reaction (a). Oxidation of polysaccharide residues on the Fc region of the antibody by sodium periodate (NaIO$_4$) (b). Bioconjugation of oxidised Ab (IgG-CHO) with hydrazide-LnNPs through Schiff-base reaction, followed by blocking reaction (c).

4.5   Experimental

Oxidation of polysaccharide residues in glycoproteins with sodium periodate provides an efficient way of generating reactive aldehyde groups for subsequent conjugation with amine- or hydrazide-containing molecules via Schiff-base reaction.[29] The conserved N-linked polysaccharide in the Fc portion of IgG is sufficiently removed from the antigen-binding site to allow conjugation through the polysaccharide chains without compromising antigen-binding activity. Periodate cleaves the carbon-carbon bond connecting adjacent hydroxyl groups in sugar residues to create highly reactive aldehyde moieties. The level of oxidant addition can be adjusted to selectively cleave certain sugars in the polysaccharide structure. For example, at a concentration of 1 mM, sodium periodate at 0-4°C typically oxidises sialic acid residues to aldehydes, leaving all the other monosaccharides untouched. Increasing the concentration to 10 mM at room temperature, however, will cause the oxidation of other sugars in the carbohydrate, including galactose and mannose residues in glycans.[30]

In our study, the functionalised polymer-coated LnNPs were first modified with the small linker ADH to generate hydrazide functional groups on the surface of LnNPs. This enabled their spontaneous reaction with aldehydes from mannose residues in the Fc region to form hydrazone linkages.[31]

This chapter describes experiments to optimise the reaction conditions between anti-B220 Ab and LnNPs with the aim of increasing the conjugation efficiency while preserving the binding activity of the Ab. Single-cell assays, including flow cytometry and mass cytometry, were used to quantify background signal and specific binding to B220 on the surface of live cells.

4.5.1   Functionalisation of polymer capped LnNPs with ADH

A Carbodiimide strategy was applied to conjugate the polymer-coated LnNPs with ADH, in order to convert the carboxylate functional groups into hydrazide groups. 8 mg EDC was added to 5 mg/mL polymer-LnNPs in MilliQ water to activate the carboxylate end moieties of the RAFT polymer linker on the surface of LnNPs. After 30 min gentle shaking, 16 mg ADH was added to the sample. The sample was shaken in a rotary shaker with time and temperature as specified in section 4.6. The ADH modified LnNPs were washed 3 times with MilliQ water using centrifugation at 20240 g for 30 min. The well-dispersed ADH-coated LnNPs were resuspended in MilliQ water and centrifuged at 6000

g for 15 min to separate monodispersed nanoparticles in the supernatant from any aggregates. The colloidal stability of the supernatants in HEPES buffer (pH=7.2, 20 mM) was then tested in preparation for subsequent biofunctionalisation in HEPES buffer (pH=7.2, 20 mM).

4.5.2 Oxidation of anti-B220 mAb

For the oxidation of the oligosaccharides on the heavy chain of the IgG anti-B220 Ab, 500 µL of 20 mM NaIO$_4$ in MilliQ water was mixed with 500 µL of Ab solution (20 mM HEPES buffer, 150 mM NaCl, pH=7.2) at a concentration of 600 µg/mL. The sample was gently mixed at room temperature in the absence of light for times ranging from 15 to 60 min as specified in section 4.6. The oxidation reaction was then quenched by addition of 10 µL glycerol. The oxidised IgG (hereafter abbreviated as IgG-CHO) was purified via overnight (17 hrs) dialysis (14 kDa MWCO) against buffer (20 mM HEPES, 150 mM NaCl, pH= 7.2) at room temperature. The final IgG-CHO was stored at 4°C until bioconjugation. To verify the successful oxidation of the carbohydrate, 20 µL of the antibody solution was mixed with 60 µL of freshly prepared Purpald solution.[32]

4.5.3 Bioconjugation of ADH-coated LnNPs with an anti-B220 mAb

For bioconjugation, we used the same rat IgG mAb employed for the studies described in Chapter 3 (RA3-6B2 specific for mouse and human B220 (Mw=180 kDa)). The ADH-functionalised LnNPs were coupled with the IgG-CHO by means of Schiff-base chemistry in which the hydrazide moiety of polymers on the surface of LnNPs directly react with the aldehyde groups of carbohydrate in the Fc region of the Ab to create an imine bond (C=N). Reactions containing (10 pmol, 120 µg) of ADH-LnNPs (Mw=12 MDa)[33] and a range of Ab concentrations, as specified in section 4.6, were made up to a final volume of 300 µL (20 mM HEPES buffer, pH=7) in Eppendorf tubes. The samples were shaken gently in a rotary shaker overnight (17 hrs) at room temperature or in later experiments for 6 hrs at 35^{oC}. The coupled LnNPs/Abs were then centrifuged at 20240 g for 15 min. The supernatant was removed for further investigation and the samples were washed twice with HEPES buffer with centrifugation at 20240 g before resuspension in 100 µL HEPES buffer.

4.5.4 Blocking unbound hydrazide moieties on LnNPs by PEG-CHO 2′000

The unbound hydrazide moieties on LnNPs/Abs and free ADH-LnNPs were blocked by the addition of PEG-CHO 2′000. This served two purposes: to remove free nanoparticles,

which aggregate and can be separated through centrifugation at 6000 g rather than 20240 g, and to reduce non-specific binding[34] during mouse spleen cell staining for fluorescence flow cytometry and mass cytometry single-cell assays. After each experiment, the final coupled LnNPs/Ab preparation was mixed with 3 mg PEG-CHO 2′000 at room temperature for various times as specified in section 4.6, and then the excess blocking agent was washed off with HEPES buffer (20 mM, pH=7.1) followed by centrifugation at 20240 for 15 min. The final samples were centrifuged at 6000 g to remove the flocculated nanoparticles. The supernatant was kept in the fridge at 4°C until cell staining.

4.5.5 Reduction hydrazone-mediated conjugation

Sodium cyanoborohydride ($NaCNBH_3$) is used as a mild reducing agent to convert imine bonds to amines.[35] In other words, adding $NaCNBH_3$ will result in a reduction of the Schiff-base intermediate and covalent bond formation, creating a secondary amine linkage between the two molecules. It is especially favoured for reductive aminations, wherein aldehydes or ketones are treated with an amine in the presence of this reagent. Thus the addition of a reductant should be helpful for stabilisation of the Schiff-bases formed between hydrazide-containing LnNPs and the aldehydes on the Abs. Different volumes (µL) of 5 M sodium cyanoborohydride in 1 N NaOH (Aldrich) per mL of the conjugation were added to the prepared samples as specified in section 4.6. Since the compound is toxic, all experiments were performed under the fume hood, and care was taken to avoid skin contact.

4.5.6 Mouse spleen cell staining with LnNPs/anti-B220 mAb

The protocol can be found in chapter 3.

4.6 Results and discussion

4.6.1 Surface modification of polymer-coated LnNPs with ADH

Carbodiimide chemistry was used to couple the carboxyl moieties of the 13 PEG polymer-coated LnNPs to ADH to generate hydrazide-ended moieties on the surface of LnNPs. The modified nanoparticles were suspended in MilliQ-water or HEPES buffer (20 mM, pH=7.1) for further characterisation using TEM, DSL, and Zeta Potential. First, we measured hydrodynamic diameter (d_h) and surface charge of the ADH-coated LnNPs using Zetasizer. The DLS CONTIN plot shown in **Figure 4.2a-b** indicates that the hydrodynamic diameter (d_h) of LnNPs in water and in HEPES buffer did not change significantly after ADH functionalisation. The Z-average sizes of the polymer and ADH

coated LnNPs suspended in MilliQ-water were 38 ±1 nm (PDI=0.145) and 44 ±1 nm (PDI=0.145), respectively (**Figure 4.2a**). As shown in **Figure 4.2b**, the hydrodynamic diameter (d_h) of the ADH coated LnNPs did not change significantly after being transferred into HEPES buffer, with the Z-average size measured as 45 ±1 nm (PDI=0.2), which confirmed the high monodispersity of ADH functionalised LnNPs.

Since ADH contains a hydrazide moiety that can be protonated in aqueous solutions, zeta potential measurement was used to monitor the surface charge of LnNPs to confirm successful functionalisation by ADH. As shown in **Figure 4.2c**, the surface charge changed from -21 ±1 mV to +25 ±1 mV, which confirmed the success of ADH functionalisation. We further performed TEM to measure nanoparticle size, distribution, and morphology after coating with polymer and subsequently after ADH functionalisation. As shown in **Figure 4.2d-f**, the LnNPs were highly monodispersed before and after ADH modification, even in HEPES buffer.
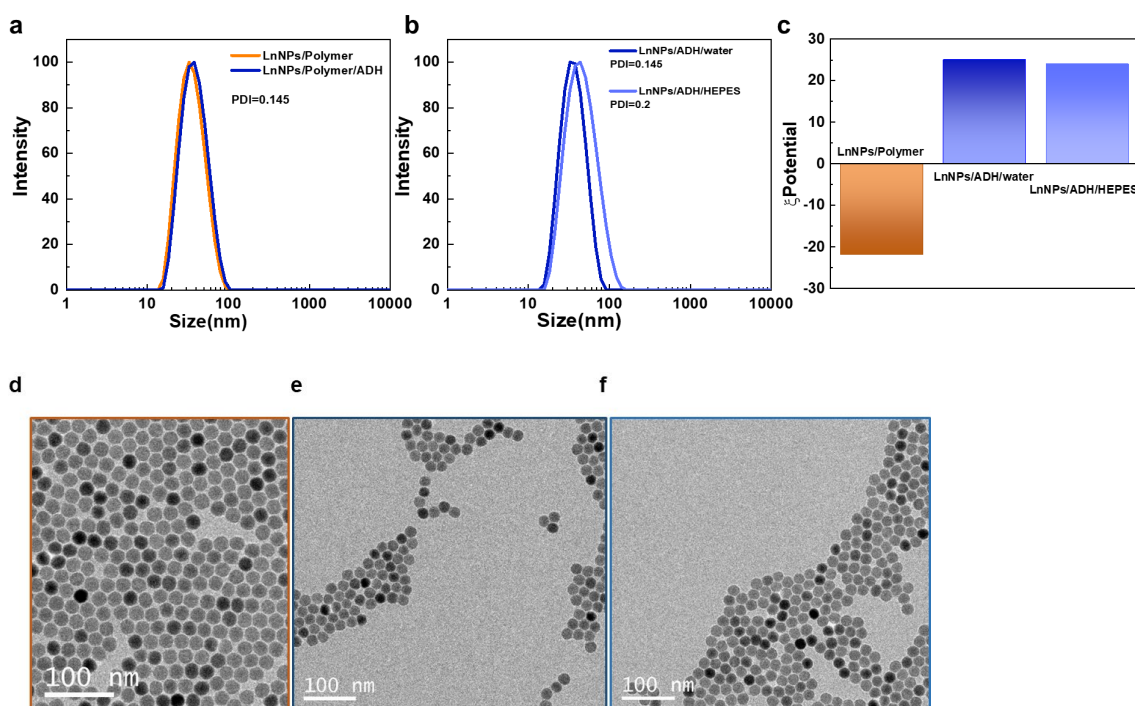
Figure 4.2 DLS CONTIN plot of LnNPs before and after ADH modification in MilliQ-water (a) and in HEPES buffer (b). Zeta potential analysis of functionalised LnNPs with polymer and ADH in MilliQ-water (c). TEM images of polymer (13 PEG) coated LnNPs (d), ADH-coated LnNPs in MilliQ-water (e), and ADH-coated LnNPs in HEPES buffer (f).

4.6.2 Long term stability of ADH-coated LnNPs

We assessed the long-term stability of the ADH functionalised LnNPs in aqueous solution by measuring DLS size and surface charge of ADH-coated LnNPs at times 1 hour, 1 week, and 1 month after modification (**Figure 4.3**). As shown in **Figure 4.3a**, some flocculation was detected in solutions of ADH functionalised nanoparticles after 1 week and 1 month, consistent with a tendency of electron pairs from the primary amines of hydrazide groups to bind with positively charged ions on the surface of adjacent nanoparticles. **Figure 4.3b** shows that the surface charge of the ADH-coated nanoparticles decreased, as expected from the aggregation of the nanoparticles. It is worth mentioning that centrifugation at 6000 g for 15 min can be used to remove the aggregates before their use in bioconjugation protocols.
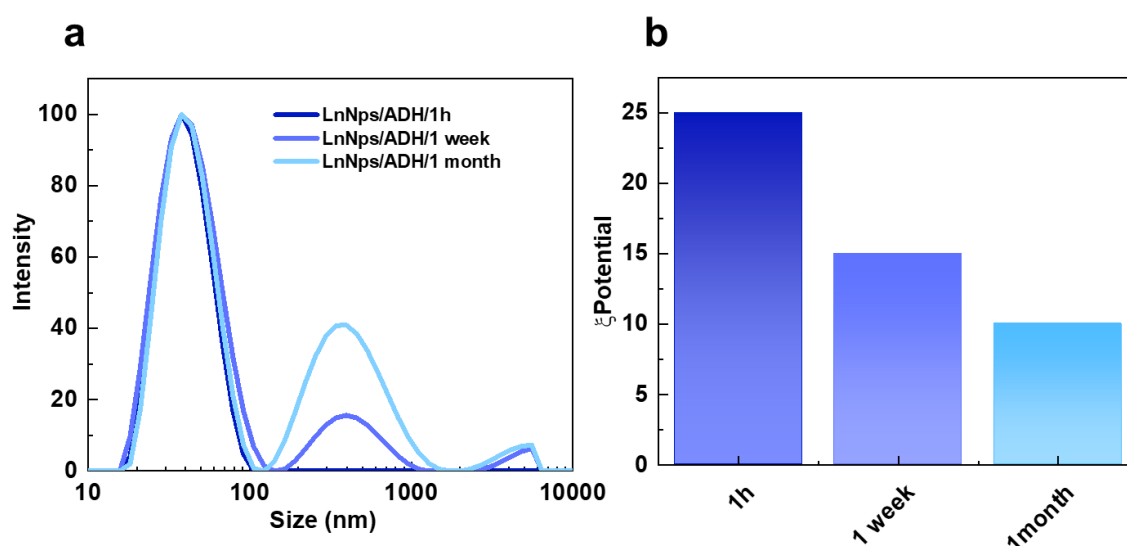
Figure 4.3 Assessment of long term colloidal stability of ADH functionalised LnNPs. Hydrodynamic diameter (d_h) of the ADH functionalised LnNPs after 1 hour, 1 week, and 1 month in aqueous media (a). Surface charge of ADH coated LnNPs after 1 hour, 1 week, and 1 month in aqueous media (b).

4.6.3 Anti-B220 antibody carbohydrate oxidation

The N-linked oligosaccharides at asparagine position 297 (Asn-297) in the CH_2 domain of the Fc region of anti-B220 Ab were oxidised by sodium periodate ($NaIO_4$) to generate active aldehyde groups, as described in 4.5.2. Successful oxidation of the carbohydrate was demonstrated by the addition of Purpald, as shown in **Figure 4.4**.
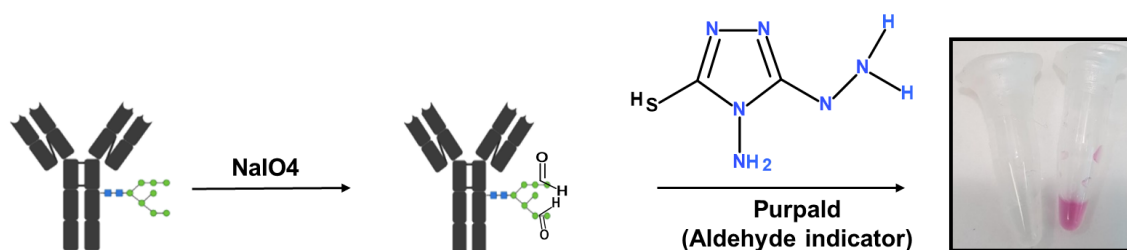
Figure 4.4 Quality control of generated aldehyde in Fc portion of anti-B220 Ab using purpald reagent.

4.6.4 Bio-labelling of anti-B220 antibody by ADH coated LnNPs

Bioconjugation of LnNPs with oxidised anti-B220 Ab (IgG-CHO) was performed using a Schiff-base reaction. To test the efficiency of conjugation over a range of molar ratios of LnNPs to Abs, 10 pmol of LnNPs (120 µg) was mixed with IgG-CHO in amounts ranging from 100 to 500 pmol (18 to 90 µg) to generate 5 preparations at molar ratios of 1/10, 1/20, 1/30, 1/40, and 1/50 in a final volume of 300 µL. After overnight incubation (17 hrs), the samples were precipitated by centrifugation at 20240 g for 15 min and the supernatants removed. The degree of coupling between LnNPs and Ab was calculated by subtracting the concentration of Ab remaining in the supernatant after centrifugation of the reaction mixture, as measured by UV 280 nm (A280) absorbance, from the initial Ab concentration (**Table 4.1**). A280 measurements were converted to Ab concentrations using the known A280 of 1.4 for Ab at 1 mg/mL. The concentrations of Abs in the 5 preparations before and after conjugation with LnNPs are shown in **Table 4.1**. The amount and percentage of coupled Ab was estimated by subtracting the amount of Ab remaining in the supernatant from the starting amount. Based on these calculations, each nanoparticle in the 1/10, 1/20, 1/30, 1/40, and 1/50 LnNPs/Ab preparations was conjugated with approximately 5, 5, 6, 8, and 13 Ab molecules, respectively (see **Figure 4.5**). These calculations are detailed below:

Experimental calculation of molar ratio Ab/ single LnNP:

Conc Ab $_{in\ sample}$= Initial Ab Conc – S/N Conc

$$\% \textbf{ Ab} = \frac{\textbf{Conc of Ab}_{in\ sample}}{\text{Initial Ab Conc}} \times 100$$

Average number of Ab per LnNP = % Ab × initial molar ratio Ab

These results indicated that all conjugations were successful. Increasing the Ab concentration by five-fold increased the average number of Abs on the surface of LnNPs less than three-fold, suggesting that space on the surface of LnNPs was limited.

Table 4.1 A280 results and estimated concentration of Abs in each conjugated sample.

sample	initial Ab (µg)	initial conc (µg/mL)	S/N OD A280	S/N conc = 1000 x A280 / 1.4 (µg/mL)	calc NP/Ab conc = initial - S/N (µg/mL)	% coupled	Ab amount coupled (µg)	ratio coupled Ab/LnNP
1/10	18	60	0.042	30	30	50	9	5
1/20	36	120	0.127	91	29	24	9	5
1/30	54	180	0.198	141	39	21	12	6
1/40	72	240	0.266	190	50	21	15	8
1/50	90	300	0.312	223	77	26	23	13
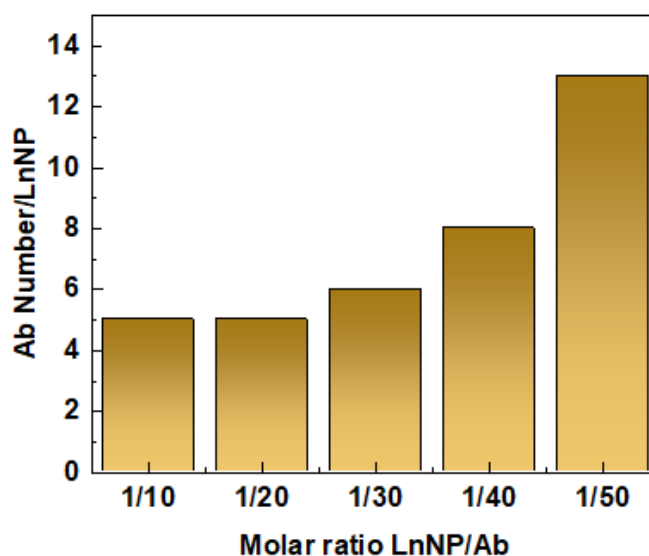
Figure 4.5. The average number of antibody molecules conjugated to a single LnNP for the five titration samples at different molar ratios of LnNP/Ab.

4.6.5 Fluorescence and mass cytometry measurement of LnNPs/Ab concentrations

To evaluate how much of the IgG-CHO coupled to LnNPs had retained its ability to specifically bind to cell surface B220 molecules, we reacted the LnNPs/Ab with live murine spleen cells, of which ~50-60% are B cells expressing a high concentration of B220 molecules on their surface. Ten-fold dilution series of each sample, including

Chapter 4

purified Ab and IgG-CHO at known concentrations, were prepared to ensure that one or more dilutions from each preparation was within the linear detection range of the flow cytometer. As in chapter 3, a secondary PE-labelled Ab was used to detect anti-B220 bound to mouse B cells using flow cytometry (**Figure 4.6**).
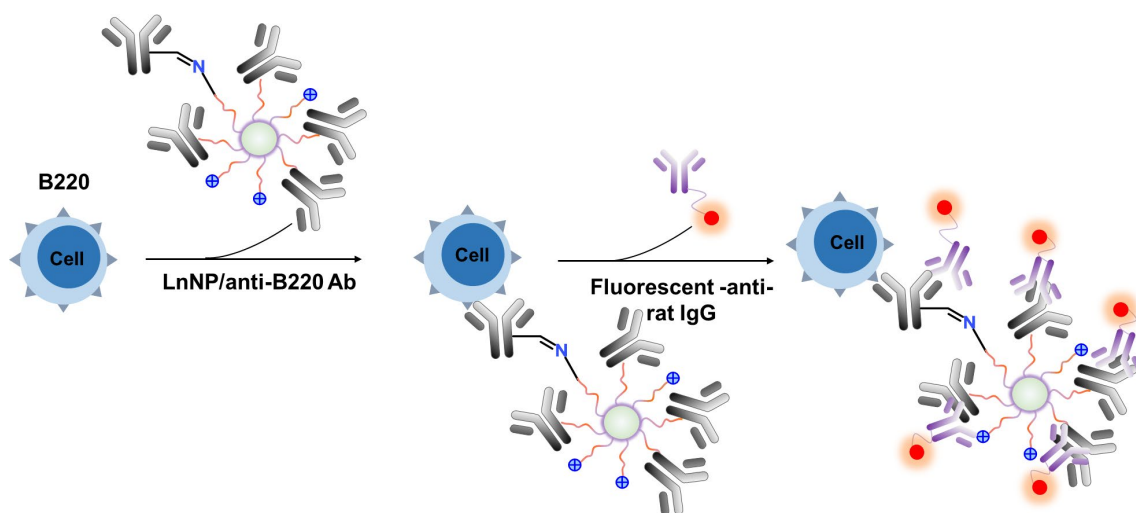
Figure 4.6 Schematic illustration of labelling live murine splenic B cells using LnNPs/Ab to recognize B220 antigens on the surface of cells. Detection of binding was achieved by adding a fluorochrome-conjugated goat anti-rat Ab as the secondary reagent.

a

b

c

Purified 600 ng/mL

IgG-CHO 2000 ng/mL

Nil

d

1/10 LnNPs/Ab 1:10

1/20 LnNPs/Ab 1:10

1/30 LnNPs/Ab 1:10

1/40 LnNPs/Ab 1:10

1/50 LnNPs/Ab 1:10

e

1/10 S/N 1:100

1/20 S/N 1:100

1/30 S/N 1:100

1/40 S/N 1:100

1/50 S/N 1:100
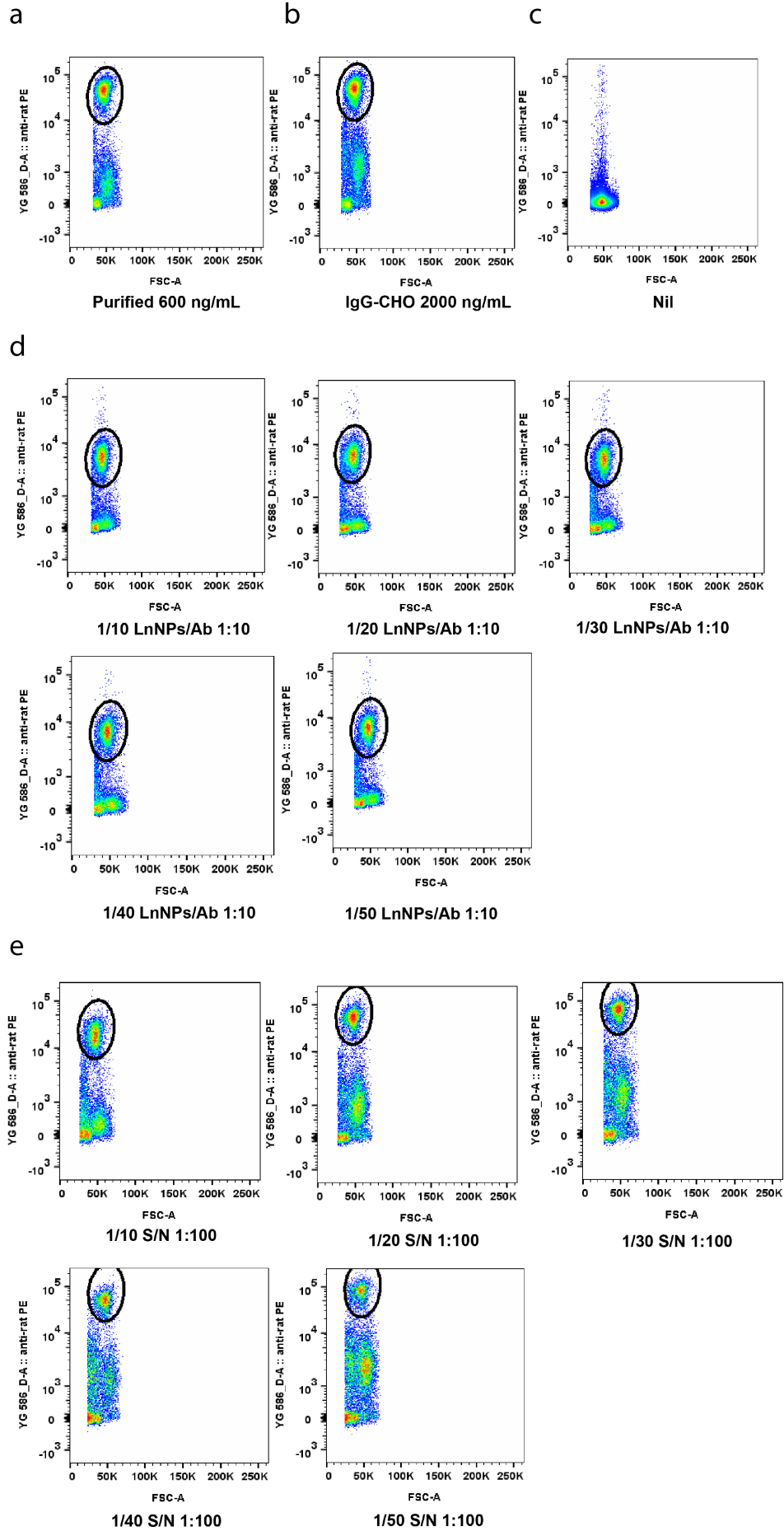
Figure 4.7 Dot plots of flow cytometry forward scatter vs PE fluorescence, with the fluorescent B cell population circled in black. Positive control (purified anti-B220 6 µg/mL) at 1:10 dilution (a); IgG-CHO (200 µg/mL) at 1:100 dilution (b); negative control (no anti-B220) (c); LnNPs/Ab conjugates at molar ratios of 1/10, 1/20, 1/30, 1/40, and 1/50, respectively, at 1:10 dilutions (d); supernatants from LnNPs/Ab conjugation reactions at 1:100 dilutions (e).

Geometric mean fluorescent intensity (MFI) of the PE-labelled cells in each sample was calculated and dose-response curves of dilution versus MFI were used to estimate the amount of reactive anti-B220 Ab in each sample, as detailed in chapter 3 (**Figure 3.27**). **Figure 4.8a** shows that the $NaIO_4$-oxidised IgG-CHO retained most of its activity. Fold change between purified and oxidised Ab, as estimated from the MFI data was $10^{1.3}$ = 20 fold. Known starting concentrations were 6 and 200 µg/mL respectively ie 33 fold different. **Figure 4.8b** shows the dose-response curves for the 5 LnNPs/Ab conjugates and the 5 conjugation reaction supernatants. The linear segments of the curves were not all parallel due to an unappreciated level of carry-over while using the same micropipette tips to perform the 10-fold dilutions (an error that was corrected in subsequent experiments), so the estimates are inaccurate, but the graph clearly indicates that the binding activity of the 5 LnNPs/Ab preparations was very similar, and the concentration of reactive Ab remaining in the supernatants increased as the molar ratio increased. While the disparities in these estimates indicate that the flow-based technique can be imprecise, the calculations in **Table 4.2** show that the ability of LnNPs/Ab to bind to B220 on the cell surface is at least 50-fold lower than expected from A280 estimates of unconjugated Ab in the reaction supernatants. The reasons for this disparity are explored below.
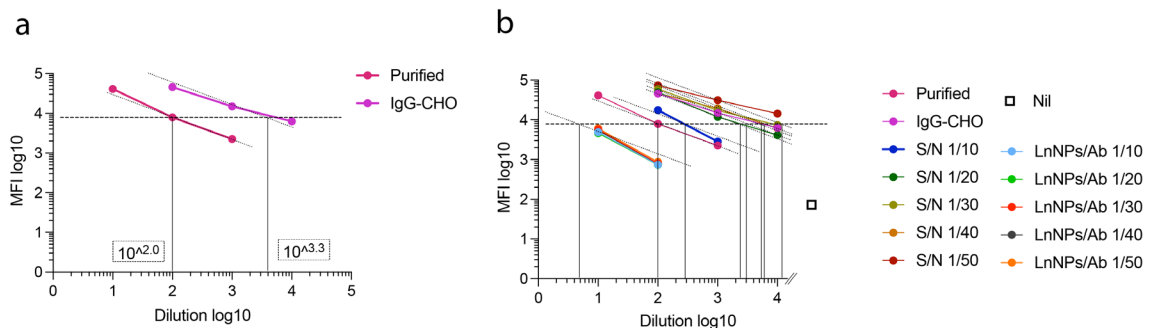
Figure 4.8 Graph of dilution vs MFI for murine B cells. Control purified 6 µg/mL and IgG-CHO 200 µg/mL (a); conjugated LnNPs and supernatants from the 5 reactions at different molar ratios (b).

Chapter 4

Table 4.2 Concentration of Abs in each sample (coupled and non-coupled Abs) measured by A280 and flow cytometry.

sample	initial conc (µg/mL)	S/N OD A280	S/N conc = 1000xA280 /1.4 (µg/mL)	calc NP/Ab conc = initial - S/N (µg/mL)	X intercept samples	X intercept S/N	NP/Ab reactive conc (µg/mL)	S/N reactive conc (µg/mL)
Purified	6				2.00			
IgG-CHO	200				3.20			95
1/10	60	0.042	30	30	0.40	2.19	0.15	9
1/20	120	0.127	91	29	0.40	3.13	0.15	81
1/30	180	0.198	141	39	0.40	3.42	0.15	158
1/40	240	0.266	190	50	0.40	3.50	0.15	190
1/50	300	0.312	223	77	0.40	4.01	0.15	614

To further evaluate the performance of the prepared LnNPs/Ab conjugates for mass cytometry assays, the stained samples from the 1/10 molar LnNPs/Ab preparation were incubated with cis-platinum to exclude dead cells, then fixed with paraformaldehyde and incubated with ^{191,193}Ir DNA intercalator to label cell nuclei. The stained cells were analysed by MC, yielding a signal intensity histogram. **Figure 4.9** shows a comparison of the histograms derived from the fluorescence flow and mass cytometry analysis (of ^{89}Y channel) of the 1/10 LnNPs/Ab at a 1:10 dilution. The mass cytometry analysis shows that although the background was high, a positive signal very similar to that in the fluorescence flow was detected.
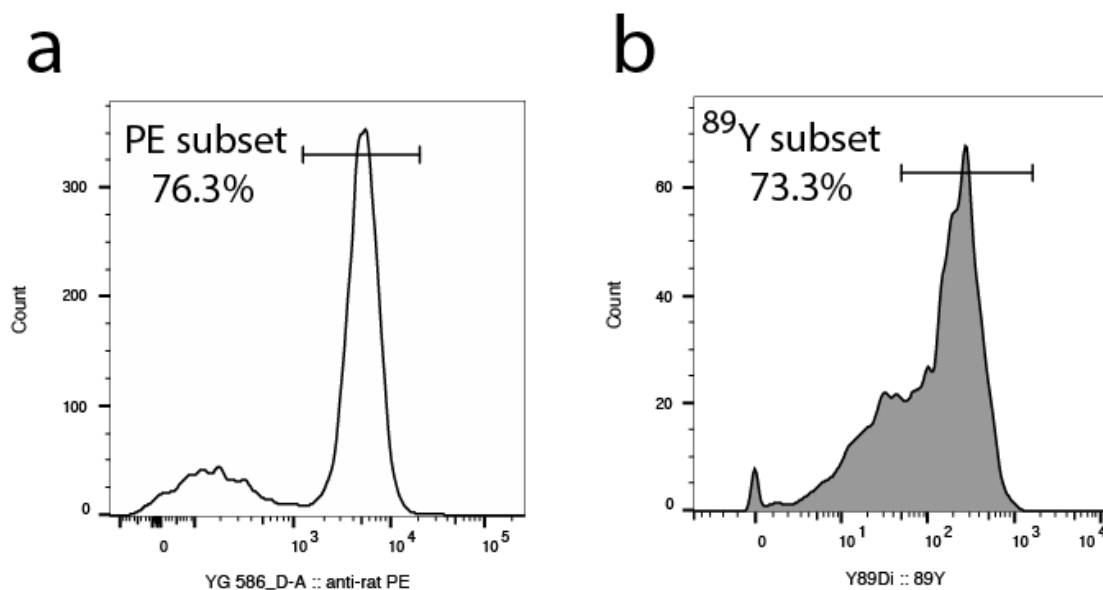
Figure 4.9 Comparison LnNPs/Ab signals derived from fluorescence flow versus mass cytometry of the same sample. Histogram of signal at 1:10 dilution of 1/10 LnNPs/Ab detected by PE-anti-rat Ab (a) and ^{89}Y channel (b).

The above results indicated that Schiff-base reactions could be used to couple LnNPs and mAbs, although the antigen-binding capacity of the resulting LnNPs/Ab complexes was considerably lower than the amount of conjugated Ab, calculated from the A280 estimates of Ab concentration of the reaction supernatants. Further experiments were therefore conducted to optimise the reaction conditions, with reference to coupling reaction time, ratio between LnNPs and Ab, use of a blocking reagent to reduce non-specific binding and allow removal of unconjugated LnNPs, and use of reducing agent to make the reaction irreversible. These experiments are described in the following sections.

4.6.6 Optimization and evaluation of coupling reaction parameters

To improve the efficiency of conjugation between LnNPs and anti-B220 antibody, reaction parameters were optimised.

4.6.6.1 Stability testing of oxidised anti-B220 antibody

To test the stability of oxidised anti-B220 Ab in HEPES buffer, IgG-CHO was stored in the fridge at 4°C for 20 days before conjugation. In the same experiment, the molar ratios of LnNPs to Ab were adjusted on the basis of the previous results. The similarity in the amount of anti-B220 bound to LnNPs at the different molar ratios, as estimated both from the A280 measurements in **Table 4.1** and the MFIs of the flow cytometry samples (**Table 4.2**) indicated that even at a 1/10 molar ratio, the amount of antibody was close to saturating. Molar ratios lower than 1/10 were therefore tested.

Seven conjugates were prepared using ADH-LnNPs at the same concentration as in the previous experiment (10 pmole, 120 µg) combined with increasing amounts of IgG-CHO, from 10 pmol to 200 pmol, in a final volume at 300 µL HEPES buffer (20 mM, pH=7). After overnight incubation (17 hrs), the samples were precipitated by centrifugation at 20240 g for 15 min and the supernatants were reserved for A280 measurement and flow cytometry. The LnNPs/Ab conjugates were then washed twice in HEPES buffer using centrifugation at 20240 g for 15 min. The seven samples were then resuspended in 100 µL HEPES buffer and kept at 4°C until flow cytometric analysis.

Flow cytometric analysis of mouse spleen cells was conducted using the method described in the previous section. Ten-fold dilution series of the coupled samples,

Chapter 4

supernatants, IgG-CHO and purified antibody, and negative control (without any antibody) were incubated with spleen cells. Cell binding was detected with PE-labelled anti-rat Ab and the MFIs of B cell populations were calculated. The IgG-CHO preparation used as control was prepared 2 days before the flow cytometric analysis, allowing the activity of preparations made 2 versus 20 days before analysis to be compared.

As shown in **Figure 4.10**, the LnNPs/Ab conjugates showed virtually no binding activity, and the amount detected in the supernatants was far lower than expected. For example, the dose-response curve for the 1/20 supernatant lay to the left of the purified Ab, whereas in the previous experiment, it was positioned at least 10-fold to the right. In contrast, the A280 values for the 1/10 and 1/20 supernatants were within the range of the previous experiment (**Table 4.3**).
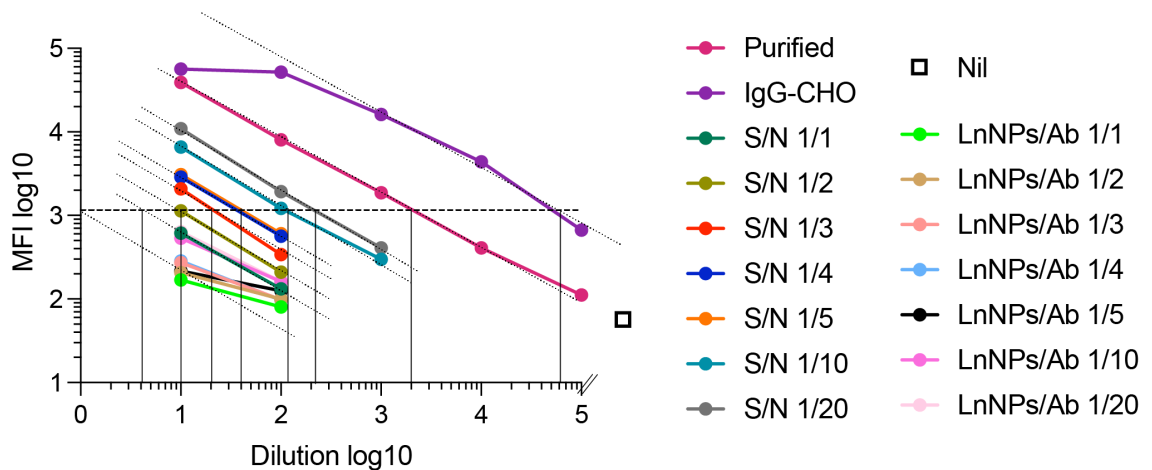
Figure 4.10 Graph of dilution vs MFI of coupled and non-coupled Abs indicated only low reactivity to cell surface B220. The freshly made control IgG-CHO retained the expected level of reactivity.

Table 4.3. Measured concentration of Abs for each sample (coupled and non-coupled Abs) by A280 and flow cytometry.

Chapter 4

sample	initial conc (µg/mL)	S/N OD A280	S/N conc = 1000 x A280 / 1.4 (µg/mL)	calc NP/Ab conc = initial - S/N (µg/mL)	X intercept samples	X intercept S/N	NP/Ab reactive conc (µg/mL)	S/N reactive conc (µg/mL)
Purified	6				3.10			
IgG-CHO	200				4.50			150
1/1	6	0.000	0.0	6.0	0.00	0.40	0.00	0.01
1/2	12	0.000	0.0	12.0	0.00	0.90	0.00	0.04
1/3	18	0.004	2.9	15.1	0.00	1.10	0.00	0.06
1/4	24	0.010	7.1	16.9	0.00	1.10	0.00	0.06
1/5	30	0.008	5.7	24.3	0.00	1.28	0.00	0.09
1/10	60	0.040	28.6	31.4	0.40	2.01	0.01	0.49
1/20	120	0.063	45.0	75.0	0.40	2.11	0.01	0.61

These results indicated that storage of oxidised Ab resulted in the loss of the ability to detect it in the flow cytometry assay, while the A280 signal was relatively unaffected. Loss of antibody binding to B220 on the cell surface, and/or loss of the sites recognised by the PE-labelled anti-rat Ab, could account for this. The underlying mechanism may have been cross-linking between aldehydes generated by the oxidation reaction and lysines present in the Abs, leading either to aggregation or interference with the antigen-binding site. Irrespective of the underlying cause, this experiment indicated that the oxidised antibody should be prepared and used freshly for nanoparticle conjugation and cell staining experiments.

In a further experiment, the Ab oxidation time was increased from 30 min to 1 hr (**Figure 4.11**). This reduced the antigen recognition capacity of the IgG-CHO control, the conjugation reaction supernatants, and the LnNPs/Ab conjugates by over 90%, indicating that extended oxidation disrupted the ability of the Ab to bind to its specific antigen. Calculation of the antigen-recognition capacity of the IgG-CHO indicates that it represented less than 4% of that expected on the basis of the A280 result (**Table 4.4**).
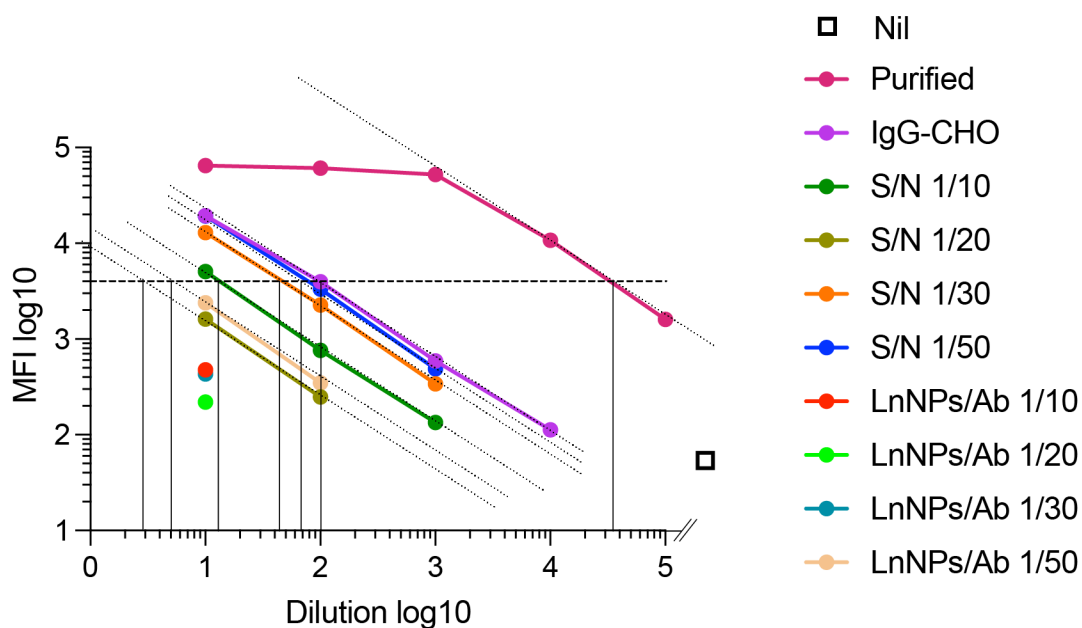
Figure 4.11. Graph of dilution vs MFI of coupled and non-coupled Ab indicated that oxidation for 1hr greatly reduced the ability of the IgG-CHO to recognise cell surface antigen.

Table 4.4. Measured concentration of Abs for each sample (coupled and non-coupled Abs) by A280 and flow cytometry.

samples	start conc (ug/ml)	S/N OD	S/N Conc (ug/ml)	estimated NP/Ab Conc (ug/ml)	X intercept samples	X intercept S/N	samples reactive Conc (ug/ml)	S/N reactive conc	samples reactive Conc (ug/ml)	S/N reactive conc
							rel to pur	rel to pur	rel to IgG-CHO	rel to IgG-CHO
Purified	1000				4.24					
IgG-CHO	160				2.00		5.75			
1/10	30	0.018	13	17		1.02		0.60		17
1/20	60	0.053	38	22		0.18		0.09		2
1/30	90	0.075	54	36		1.31		1.17		33
1/50	150	0.148	106	44	0.40	1.69	0.14	2.82	4.02	78

4.6.6.2 Effect of reaction conditions for ADH modification of LnNPs on Ab coupling efficiency

In this experiment, ADH modification of LnNPs was carried out overnight at room temperature, as previously, or for 5 hrs at 35°C. Conjugation with IgG-CHO was then performed at molar ratios of 1/2 to 1/20. Analysis of reaction supernatants and LnNPs/Ab conjugates by absorbance and flow cytometry was performed as above. There was no detectable difference in coupling performance between ADH-LnNPs prepared under the

two conditions. The shorter and more convenient 5h/35°C protocol was therefore used for all subsequent experiments.
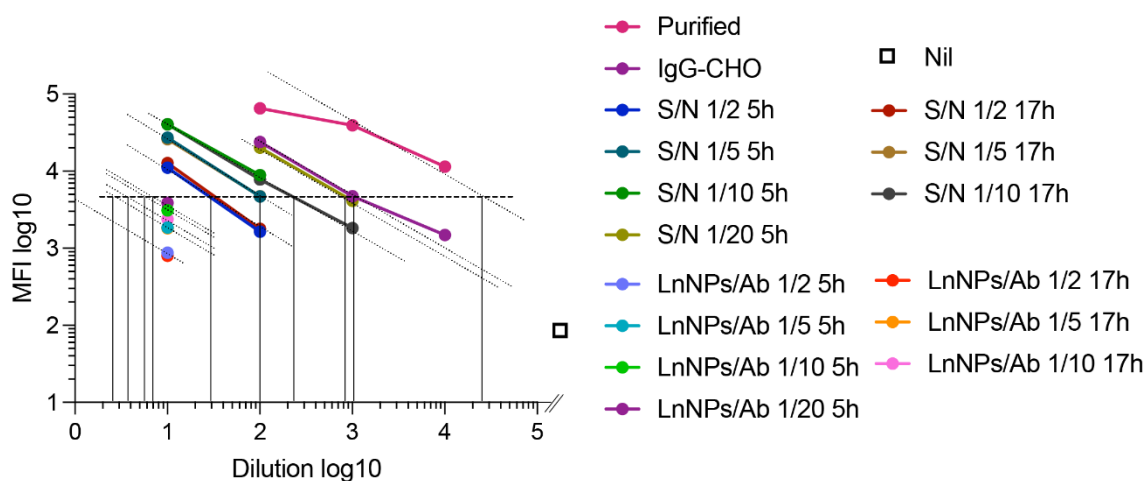
Figure 4.12 Graph of dilution vs MFI of coupled and non-coupled Abs in conjugation reactions using LnNPs modified by ADH for 5h or 17h.

Table 4.5. Measured concentration of Abs for each sample (coupled and non-coupled Abs) by A280 and flow cytometry.

samples	start conc (μg/mL)	S/N OD	S/N conc (μg/mL)	estimated NP/Ab conc (μg/mL)	X intercept samples	X intercept S/N	samples reactive conc (μg/mL)	S/N reactive conc (μg/mL)	samples reactive conc (μg/mL)	S/N reactive conc (μg/mL)
							rel to pur	rel to pur	rel to IgG-CHO	rel to IgG-CHO
Purified	400				4.14					
POX	145				3.00		29.0000			
1_2 5h	12	0.005	4	8		1.20		0.46		2.30
1_5 5h	30	0.021	15	15	0.15	2.00	0.04	2.90	0.20	14.50
1_10 5h	60	0.035	25	35	0.46	2.11	0.08	3.73	0.42	18.68
1_20 5h	120	0.105	75	45	0.60	2.12	0.12	3.82	0.58	19.11
1_2 17h	12	0	0	12		1.20		0.46	0.15	2.30
1_5 17h	30	0.025	18	12	0.15	2.00	0.04	2.90	0.20	14.50
1_10 17h	60	0.055	39	21	0.27	2.11	0.05	3.73	0.27	18.68

4.6.6.3 Using appropriate blocking reagent (PEG-aldehyde 2′000)

We tested whether blocking the unoccupied hydrazide functional groups on the surface of the antibody conjugated LnNPs would reduce the non-specific binding apparent from the mass cytometry analysis in **Figure 4.9**. PEG-CHO 2′000 was chosen as a blocking

agent, not only due to its ability to block the free hydrazide-LnNPs through Schiff-base reaction (**Figure 4.13**), but because PEG molecules can inhibit non-specific binding to cells.
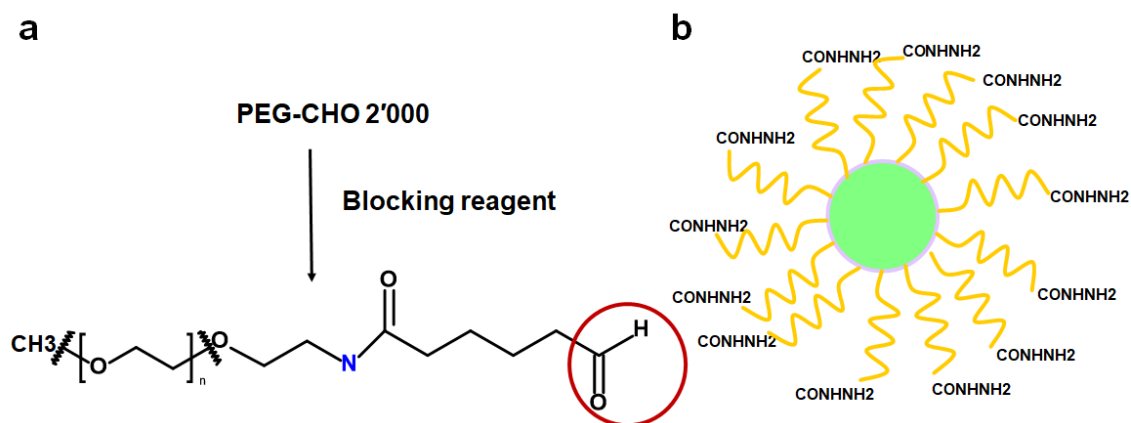
Figure 4.13 Schematic illustration of O-2-(6-Oxocaproylamino) ethyl-O′-methylpolyethylene glycol 2′000 as a blocking reagent (a). ADH coated LnNPs (b).

In an initial experiment, the ability of the blocking reagent to reduce the surface charge of ADH-LnNPs was tested. Briefly, 1 mg ADH-LnNPs was mixed with 15 mg PEG-CHO 2′000 in 1 mL MilliQ-water and incubated for 48 hrs. The sample was centrifuged at 20240 g for 30 min to precipitate the LnNPs, which were then washed twice more with MilliQ-water using centrifugation at 20240 g for 30 min. As expected, the nanoparticles showed some aggregation, with PDI=0.5 after modification with blocking reagent (**Figure 4.14a**). After centrifugation at low speed (6000 g) for 15 min to remove the aggregates, the supernatant contained ADH-LnNPs with a hydrodynamic size about $d_{(h)}$ 40±1 nm with PDI=0.13. The presence of residual monodispersed LnNPs in the original LnNPs-blocker preparation indicated that not all the surface hydrazide groups had been blocked. Zeta potential measurements were consistent with the DLS result, as the surface charge of LnNPs decreased from +25±1mV before addition of the blocker (**Figure 4.3b**) to +8 mV (**Figure 4.14b**). After centrifugation at low speed to remove the aggregates, the zeta potential was +19±1 mV, indicating that the majority of hydrazide groups in the supernatant had not been blocked.

This experiment also indicated that addition of PEG-CHO 2′000 to block unoccupied hydrazide sites after conjugation of LnNPs with IgG-CHO would lead to aggregation of

unconjugated LnNPs, which could then be removed by low speed centrifugation (**Figure 4.15**). Thus the addition of the blocking reagent would assist in generating an LnNPs/Ab reagent that was not contaminated with unconjugated LnNPs.
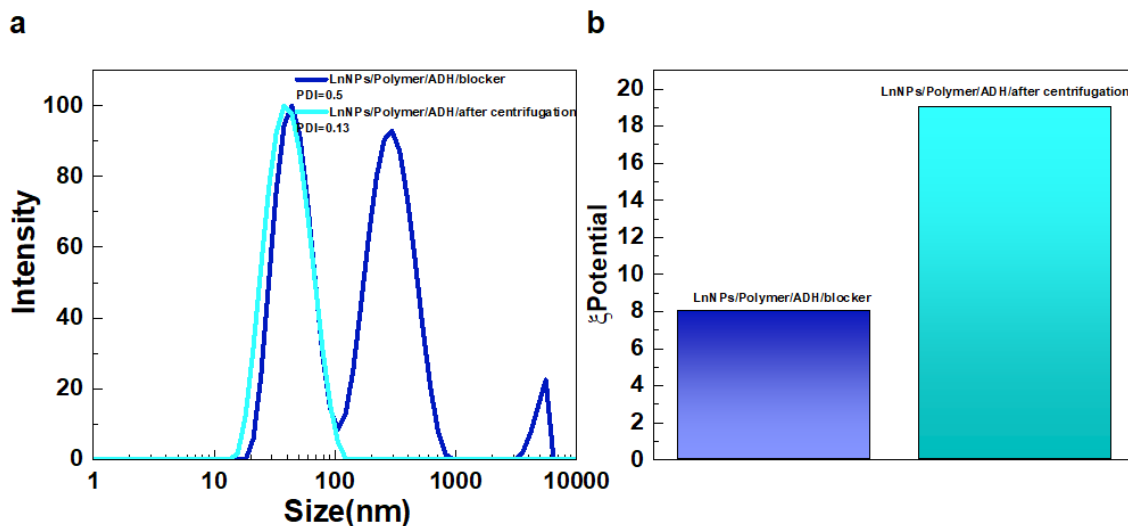
Figure 4.14 DLS CONTIN plot of ADH-LnNPs after modification by blocker followed by centrifugation at 6000 g (a). Zeta potential analysis of ADH-LnNPs in MilliQ-water after modification with PEG-CHO 2′000 (dark blue) and followed by centrifugation at 6000 g to remove aggregates (light blue).
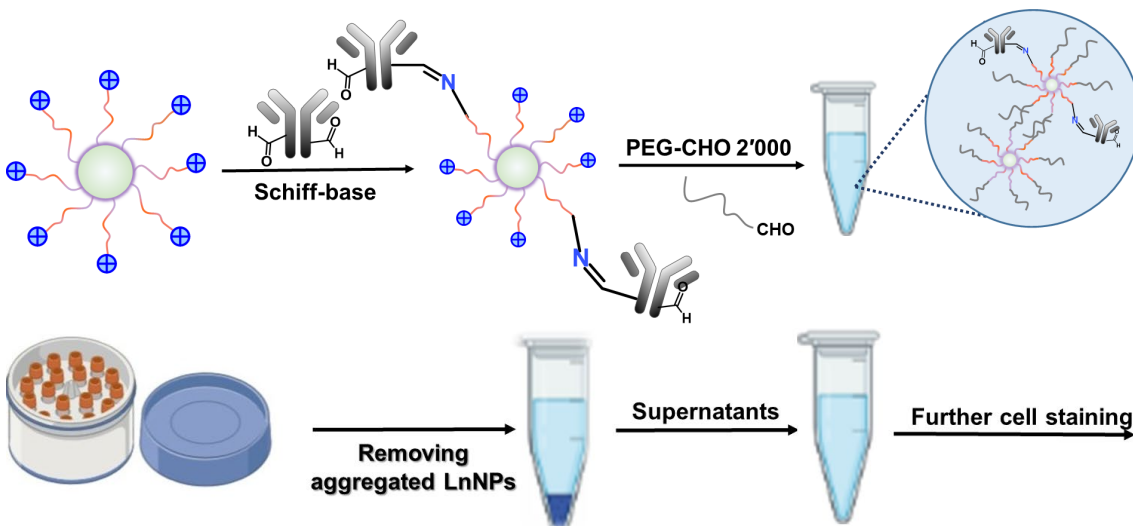
Figure 4.15 Schematic illustration of bioconjugation of LnNPs/Ab along with blocker and centrifugation. Note that Ab will likely be conjugated to LnNPs via only one of the two aldehydes present on optimally oxidised IgG heavy chains, which may allow the other aldehyde to interfere with antigen-binding by reacting with lysines in the variable region of other Abs.

Chapter 4

Next, after confirmation that the blocker had successfully modified the nanoparticles, we prepared four separate batches of LnNPs/Ab at molar ratios of 1/5, 1/10, 1/20, and 1/30, using the coupling protocol described above with addition of blocker as illustrated in **Figure 4.16**.
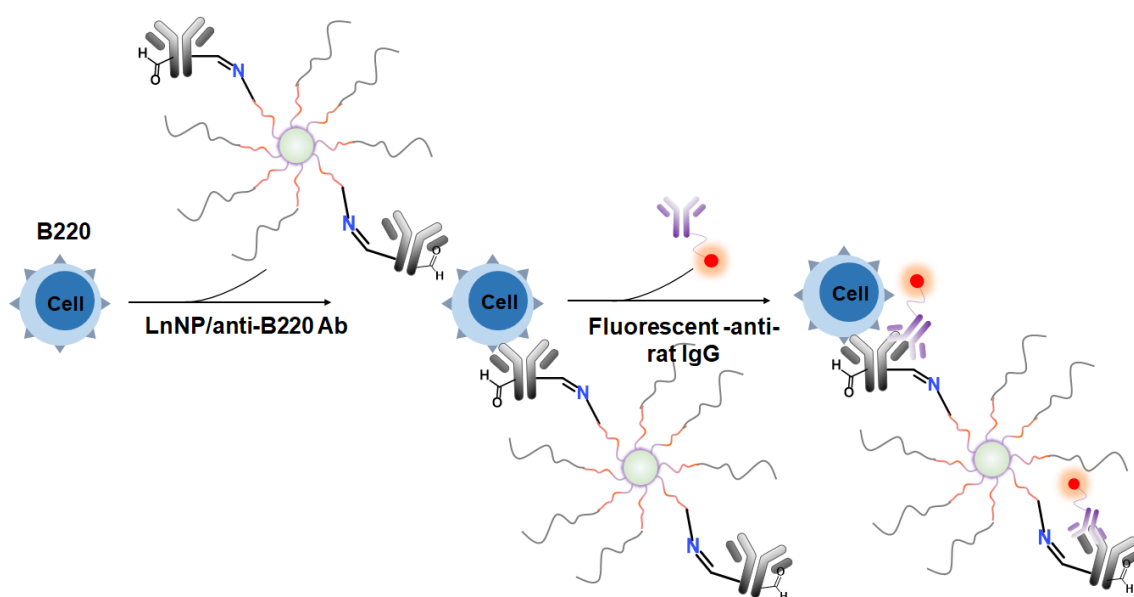
Figure 4.16 Schematic illustration of labelling of PEG-blocked anti-B220 conjugated LnNPs to recognize B220 antigens on the surface of live murine splenic B cells. Successful labelling is confirmed by the detection of fluorescent cells after the addition of a fluorochrome-labelled goat anti-rat Ab as the secondary antibody labelling reagent in fluorescence flow cytometry.

After taking the supernatants and washing the samples with HEPES buffer (20 mM, pH =7.1), 3 mg blocker reagent dissolved in 600 µL HEPES buffer was added to each coupled sample and incubated for 48 hrs. The samples were then washed twice with HEPES buffer with centrifugation at 20240 g for 15 min. Free nanoparticles were spun down at 6000 g for 10 min and supernatants containing mono-dispersed Ab-conjugated LnNPs were set aside for further analysis. The pellets were pooled to provide enough material to measure hydrodynamic size and zeta potential (**Figure 4.17**). As expected the hydrodynamic size increased (**Figure 4.17a**) and the surface charge (**Figure 4.17b**) decreased.
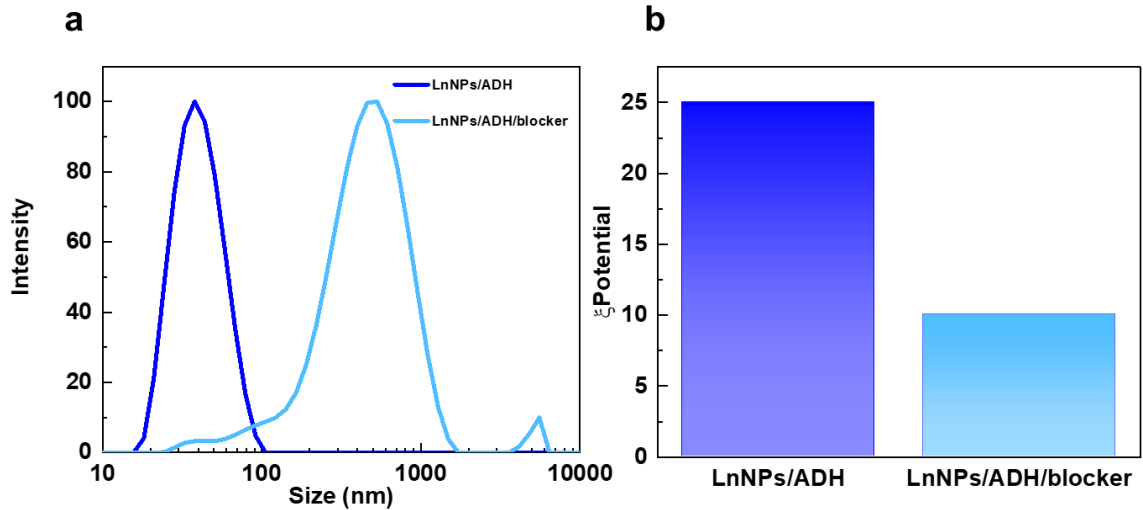
Figure 4.17 DLS CONTIN plot of ADH-LnNPs before and after bioconjugation with Abs followed by modifying with blocker (a). Zeta potential analysis (b).

Flow cytometric analysis of the conjugation reaction supernatants and the blocked LnNPs/Ab conjugates after 6000g centrifugation was then conducted. **Figure 4.18a** shows the dose-response data for the MFIs of the fluorescent mouse B cells. In parallel with this experiment, an EDC conjugation experiment was performed using the protocols outlined in chapter 3 (**Figure 4.18b**).
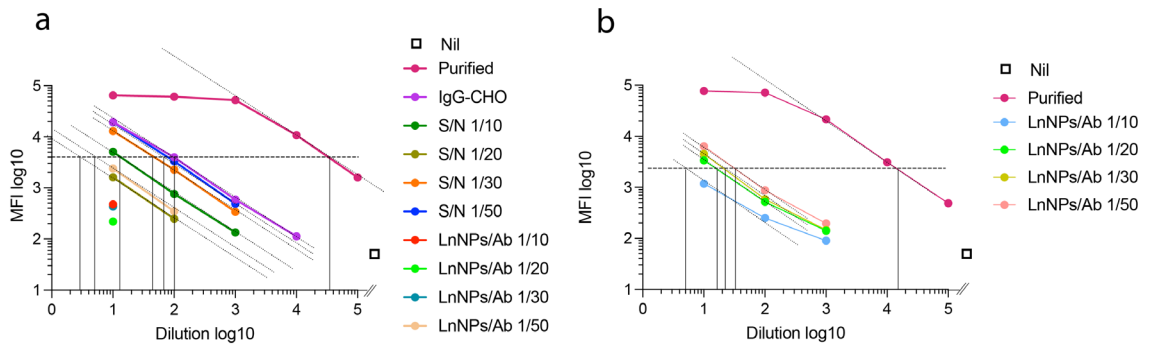
Figure 4.18 Graph of dilution vs geometric mean fluorescence of the B cell populations detected by flow cytometry. Schiff-base with blocker (a); Carbodiimide chemistry (b).

Table 4.6 The measured concentration of antibody-conjugated LnNPs and the relevant supernatants along with purified and oxidised anti-B220 antibodies via A280 and flow cytometry.

samples	start conc (μg/mL)	S/N OD	S/N conc (μg/mL)	estimated NP/Ab conc (μg/mL)	X intercept samples	X intercept S/N	samples reactive conc (μg/mL)	S/N reactive conc (μg/mL)	samples reactive conc (μg/mL)	S/N reactive conc (μg/mL)	% efficiency	% efficiency
							rel to pur	rel to pur	rel to IgG-CHO	rel to IgG-CHO	rel to pur	rel to IgG-CHO
Purified	520				4.05							
IgG-CHO	115				2.65		21					
1/5	15	0.006	4.3	10.7	0.40	1.60	0.12	1.8	0.6	10.2	0.8	4.3
1/10	30	0.015	10.7	19.3	0.60	2.08	0.18	5.6	1.0	31.0	0.6	3.4
1/20	60	0.073	52.1	7.9	1.00	2.40	0.46	11.6	2.6	64.7	0.8	4.3
1/30	90	0.113	80.7	9.3	1.04	2.65	0.51	20.7	2.8	115.0	0.6	3.1
1/10 EDC	60				0.32		0.10				0.16	
1/20 EDC	120				1.05		0.52				0.43	
1/30 EDC	180				1.10		0.58				0.32	
1/50 EDC	300				1.21		0.75				0.25	

For the Schiff-base method, the concentration of reactive oxidised antibodies and the supernatants measured by flow cytometry were not consistent with A280 results (**Table 4.6**). Cell labelling was conducted 6 days after bio-conjugation due to the unavailability of the flow cytometer, and this may have been responsible for the loss of activity of the IgG-CHO and the supernatants (unconjugated Ab). Binding activity for the LnNPs/Ab followed the same pattern, suggesting that IgG-CHO was unstable even after conjugation to LnNPs. Each IgG would be expected to have 2 aldehyde residues (one on each heavy chain), and it is possible that binding of one to an LnNP-ADH amine would position the Ab such that the second was not available to bind. This would result in free aldehydes that could then lead to inactivation of the antigen-binding sites of other Abs.

The overall efficiency of generating antigen-reactive LnNPs/Ab using the Schiff-base is a little bit higher than carbodiimide strategy when calculated with respect to the purified Ab control (**Table 4.6**). When the antigen-reactivity of Schiff-base LnNPs/Ab was recalculated relative to the decreased IgG-CHO antigen-reactivity, the Schiff-base method was ~5-fold more efficient (**Table 4.6**).

4.6.6.4 Reductive amination of Aldehyde with Sodium Cyanoborohydride (NaCNBH₃)

The Schiff-base reaction between IgG-CHO or PEG-CHO 2′000 and ADH-LnNPs generates a reversible hydrazone bond. Under the conditions for addition of PEG-CHO 2′000 to LnNPs/Ab (48 hrs incubation suspended in a high volume of buffer (600 μL)), it is possible that the Ab dissociated from the LnNPs. Therefore we tested the effect of

adding a reducing reagent such as NaCNBH$_3$ to make the reaction irreversible. The addition of sodium cyanoborohydride[36] to a reaction medium containing an aldehyde compound and an amine-containing molecule will result in a reduction of the Schiff-base intermediate and covalent bond formation by production of a secondary amine linkage between the two molecules (**Scheme 4.1**).[37] Hydrazone linkages may be further stabilised by cyanoborohydride reduction. The addition of a reductant during hydrazide/aldehyde reactions has been shown to increase the efficiency and yield of the reaction.[38,39]

Scheme 4.1 Scheme of reductive amination in Schiff base reaction.[37]
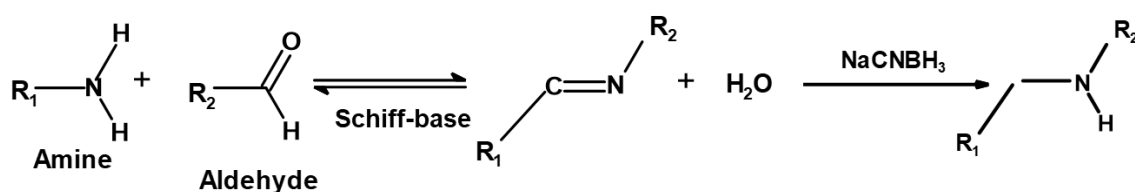
In one experiment, we tested the efficacy of NaCNBH$_3$ (reducing agent) to stabilise Schiff-base reaction, ADH-LnNPs was treated with blocker (PEG-CHO 2′000) (**Scheme 4.2**). Briefly, 1 mg ADH-LnNPs at the concentration of 1 mg/mL was mixed with 3 mg PEG-CHO 2′000 in MilliQ-water. The sample was shaken gently for 2 hrs at room temperature, and then 10 µL of NaCNBH$_3$ (5 M solution in 1 N NaOH) was added. After that, the sample was incubated for a further 30 min. The sample was centrifuged at 20240 g for 30 min and washed twice with MilliQ-water using centrifugation at 20240 for 30 min. Finally the sample was resuspended in 1 mL MilliQ-water and DLS and zeta potential measurements were performed (**Figure 4.19**).

Scheme 4.2 Scheme of reduction of hydrazone linkage in Schiff-base reaction
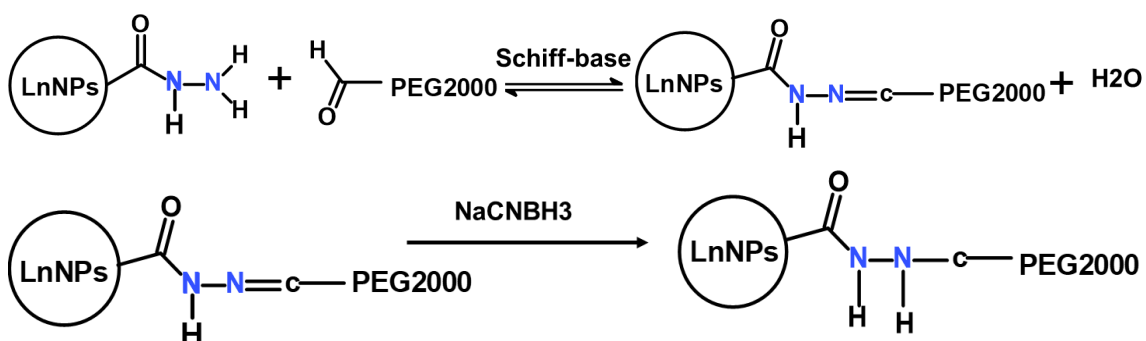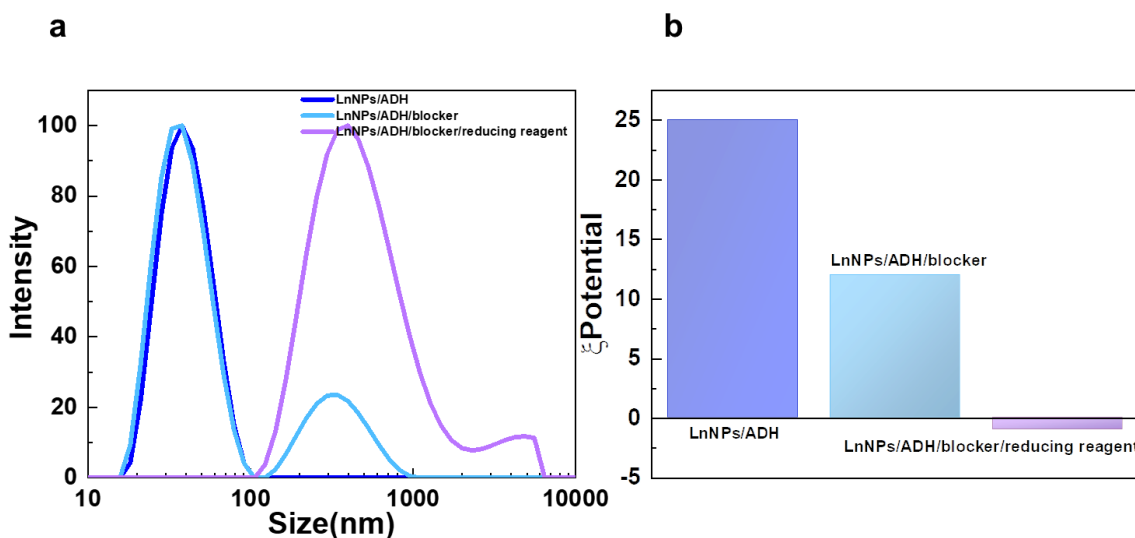
Figure 4.19 Stabilisation of the Schiff-base reaction with NaCNBH$_3$. DLS CONTIN plot of ADH-LnNPs, ADH-LnNPs treated by blocker, and further stabilised by NaCNBH$_3$ (a). Monitoring the surface charges of ADH-LnNPs after treating with PEG-CHO 2′000 and NaCNBH$_3$.

The DLS CONTIN plot shown in **Figure 4.19a** shows that the hydrodynamic diameter (d_h) of ADH-LnNPs increased after modification with PEG-CHO 2′000, consistent with partial aggregation of ADH-LnNPs, and then increased further after stabilisation by NaCNBH$_3$, which caused all the ADH-LnNPs to aggregate. As shown in **Figure 4.19b**, the surface charge of the ADH-LnNPs decreased from +25 ±1 mV to +11±1 mV after the reaction with the blocking reagent and subsequently decreased to -2±1 mV after further reduction by NaCNBH$_3$. This again confirmed the successful stabilisation (irreversibility) of the Schiff-base reaction between ADH-LnNPs and PEG-CHO 2′000. These data also suggested that the reaction time for the Schiff-base interaction between ADH-LnNPs and PEG-CHO 2′000 could be decreased if they were subsequently treated with NaCNBH$_3$ to stabilise the reaction.

Based on the above-mentioned results and conclusion, we decided to conduct a new experiment using NaCNBH$_3$ to increase conjugation efficiency between LnNPs and anti-B220 antibody.

In a pilot experiment, we simultaneously compared the effectiveness of 15 versus 30 min incubation for the oxidation reaction that generated IgG-CHO, performed coupling of the ADH-LnNPs and the two batches of IgG-CHO, added blocker as above, and finally added 1 µL or 3 µL of 5 M NaCNBH$_3$ to the reaction solution for either 15 or 30 min. It is

important to mention that NaCNBH$_3$ is extremely toxic, so all the operations should be done with care in a fume hood and physical contact with the reagent should be carefully avoided, as the 5 M solution is prepared in 1 N NaOH.

The supernatants and LnNPs/Ab were then tested for reactivity to B220 using flow cytometry (**Figure 4.20**). Calculation of the antigen reactivity (**Table 4.7**) indicated that oxidation for 15 mins was superior to 30 min, and that 3 µL of 5 M NaCNBH$_3$ preserved higher binding activity than 1 µL.

Figure 4.20 Graph of dilution vs geometric mean fluorescence of the B cell populations detected by flow cytometry.

Table 4.7 The measured concentration of antibody-conjugated LnNPs and the relevant supernatants along with purified and oxidised anti-B220 antibodies via A280 and flow cytometry.

samples	start conc (µg/mL)	S/N OD	S/N conc (µg/mL)	estimated NP/Ab conc (µg/mL)	X intercept samples	X intercept S/N	samples reactive conc (µg/mL)	S/N reactive conc (µg/mL)	samples reactive conc (µg/mL)	S/N reactive conc (µg/mL)
							rel to pur	rel to pur	rel to IgG-CHO	rel to IgG-CHO
Purified	220				3.10					
IgG-CHO 15min	150				2.62		73			
IgG-CHO 30 min	150				2.35		39			
15 min 1ul	135	0.185	132	2.86	0.20	2.00	0.28	17.5	0.28	17.5
15 min 3ul	135	0.186	133	2.14	0.50	2.12	0.55	23.0	0.55	23.0
30 min 1ul	135	0.183	131	4.29	0.50	1.70	0.55	8.8	0.55	8.8
30 min 3ul	135	0.176	126	9.29	0.50	2.07	0.55	20.5	0.55	20.5

To test whether 3 µL of NaCNBH$_3$ was sufficient to fully stabilise ADH-LnNPs treated with PEG-CHO 2'000, four batches of 1 mg ADH-LnNPs at a concentration of 1 mg/mL in MilliQ-water were prepared and 3 mg blocking reagent was added to each reaction. After 2 hrs incubation, 0, 1, 3, or 10 µL of NaCNBH$_3$ (5 M solution in 1 N NaOH) were added and the samples were incubated for a further 30 min. The samples were centrifuged at 20240 g for 30 min and washed 3 times with MilliQ water using centrifugation at 20240 g for 30 min. Surface charge was then monitored through zeta potential as shown in **Figure 4.21**. Surface charge decreased as the concentration of NaCNBH$_3$ increased, with the sample treated with 10 µL of NaCNBH$_3$ no longer having a positive charge, indicating that all the hydrazone linkages from the Schiff-base interaction between ADH-LnNPs and PEG-CHO 2'000 conjugation were now converted to stable covalent bonds.
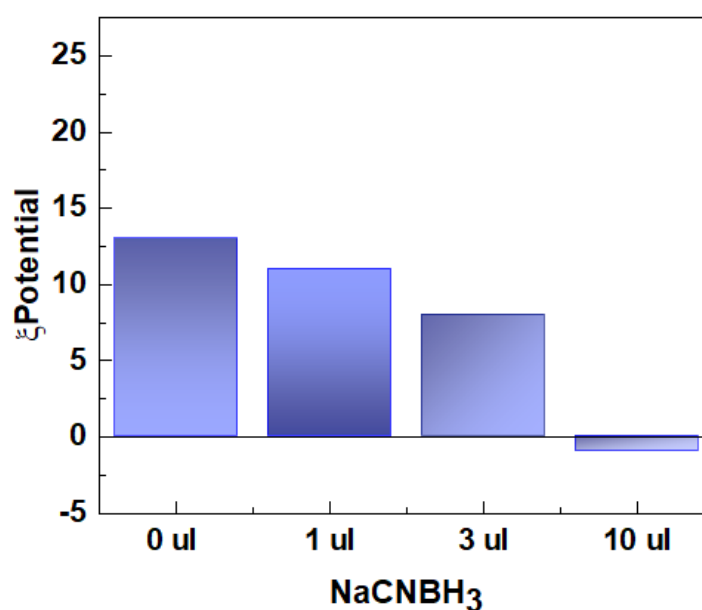
Figure 4.21 Surface charge of blocked ADH-LnNPs when treated with different amounts of reducing reagent (NaCNBH$_3$).

4.6.6.5 Optimizing the ADH-LnNPs/Abs coupling reaction time

To optimize the coupling time between ADH-LnNPs and IgG-CHO, two sets of reactions were set up with molar ratios of 1/5, 1/10, 1/20, 1/30 and 1/40. Briefly, 10 pmole (120 µg, Mw=12 MDa) LnNPs was mixed with 50, 100, 200, 300, and 400 pmole IgG-CHO (Mw = 180 kDa) in a total volume of 900 µL HEPES buffer (20 mM, pH= 7). The incubation times for the two series were 6 hours or overnight (17 hrs), respectively. After incubation, 600 µg PEG-CHO 2'000 was added to each sample and incubated for 2 hours,

Chapter 4

then 10 µL of 5M NaCNBH$_3$ in NaOH was added and incubated for 30 min. The samples were centrifuged at 20240 g for 30 min to remove the supernatants for further investigation and the LnNPs/Ab were washed twice with HEPES buffer using centrifugation at 20240 g for 30 min. Both series of samples were resuspended in 100 µL HEPES buffer and stored at 4°C until flow cytometry single cell measurement.
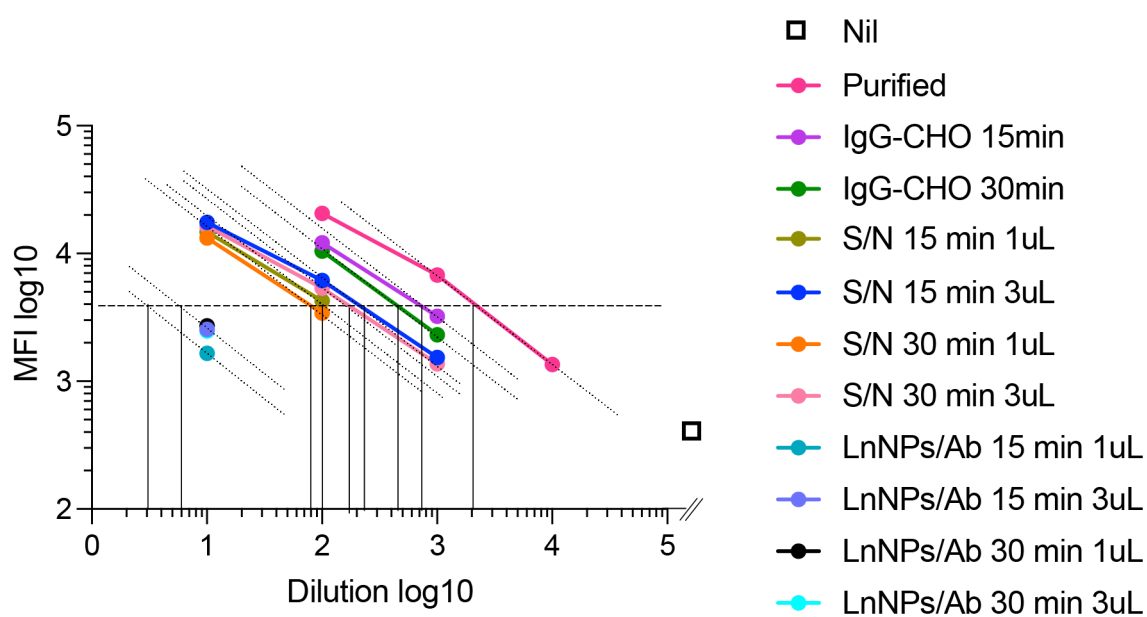
Chapter 4
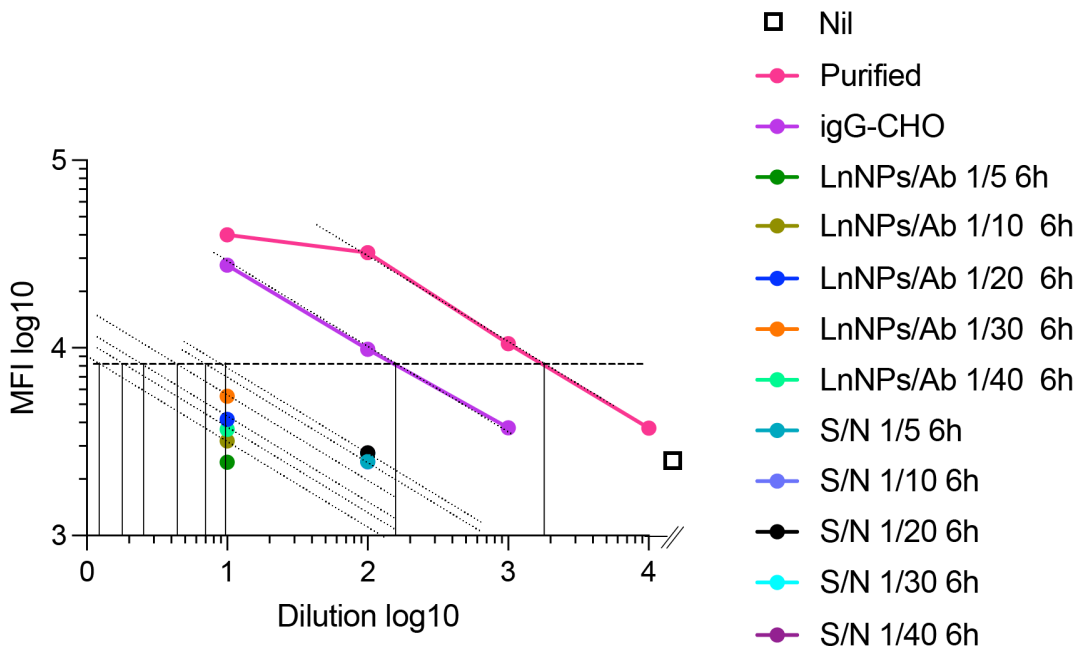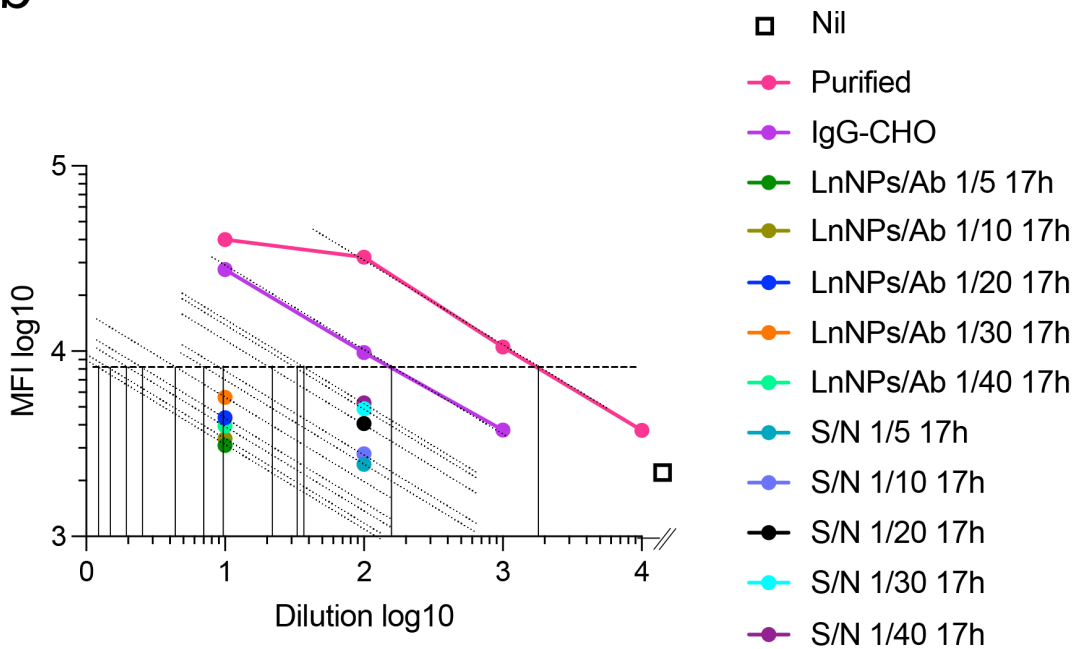
Figure 4.22 Graph of dilution vs geometric mean fluorescence of the B cell populations detected by flow cytometry. 6 hrs coupling reaction for LnNPs/Ab (a); 17 hrs coupling reaction for LnNPs/Ab (b).

Table 4.8 The measured concentration of antibody-conjugated LnNPs and the relevant supernatants along with purified and oxidised anti-B220 antibodies via A280 and flow cytometry.

samples	start conc (µg/mL)	S/N OD	S/N conc (µg/mL)	estimated NP/Ab conc (µg/mL)	X intercept samples	X intercept S/N	samples reactive conc (µg/mL)	S/N reactive conc (µg/mL)	samples reactive conc (µg/mL)	S/N reactive conc (µg/mL)
							rel to pur	rel to pur	rel to IgG-CHO	rel to IgG-CHO
Purified	240				3.09					
IgG-CHO	100					22.92				
1/5 6h	10	0.036	26	-16		0.06		0.22		0.98
1/10 6h	20	0.023	16	4	0.00	0.06	0.20	0.22	0.85	0.98
1/20 6h	40	0.043	31	9	0.01	0.08	0.20	0.23	0.87	1.02
1/30 6h	60	0.046	33	27	0.03	0.08	0.21	0.23	0.91	1.02
1/40 6h	80	0.075	54	26	0.01	0.08	0.20	0.23	0.86	1.02
1/5 17h	10	0.036	13	-3	0.00	0.42	0.20	0.51	0.85	2.24
1/10 17h	20	0.039	14	6	0.00	0.80	0.20	1.23	0.86	5.37
1/20 17h	40	0.063	23	18	0.01	1.11	0.20	2.51	0.88	10.96
1/30 17h	60	0.092	33	27	0.03	1.22	0.21	3.24	0.91	14.13
1/40 17h	80	0.11	39	41	0.01	1.25	0.20	3.47	0.87	15.14

While 17 hrs generated higher MFI signals, the flow cytometry analysis revealed very little reactive Ab in the LnNPs/Ab and supernatant samples. This suggested that although 30 min exposure to 10 µL of 5M NaCNBH$_3$ effectively stabilised the Schiff-base reaction, it also severely compromised the ability of the Ab to bind its ligand.

4.6.6.6 Optimising of NaCNBH$_3$ reaction time in coupling LnNPs/Ab

To test whether a shorter reaction time could reduce the effect of NaCNBH$_3$ on Ab activity while still converting the hydrazone bonds to secondary amines, 4 1/30 molar LnNPs/Ab reactions were set up in a final volume of 80 µL. After 14 hrs incubation, 1 mg blocking reagent was added to each sample followed by 2 hrs incubation. Then 10 µL of NaCNBH$_3$ (5M NaCNBH$_3$ in 1 N NaOH) was added and the samples were incubated for 15, 30, 45, and 60 min, respectively. Tubes were centrifuged at 20240 g for 10 min and the supernatant was taken for further investigation. The LnNPs/Ab samples were washed 3 times with HEPES buffer using centrifugation at 20240 g for 10 min. Finally, the coupled LnNPs were resuspended in HEPES buffer (20 mM, pH=7, 1mM NaF) and kept in the fridge at 4°C until analysis. First, A280 analysis was applied to each supernatant to measure estimated protein concentration and calculate the amount of IgG-

Chapter 4

CHO conjugated to LnNPs. As shown in **Figure 4.23** maximum conjugation was seen in the sample with 45 min reduction time, indicating that reduction of most of the hydrazone bonds between LnNPs, IgG-CHO, and blocking reagents takes 45 min. The calculated percentage coupling of the samples is displayed in **Table 4.9**.
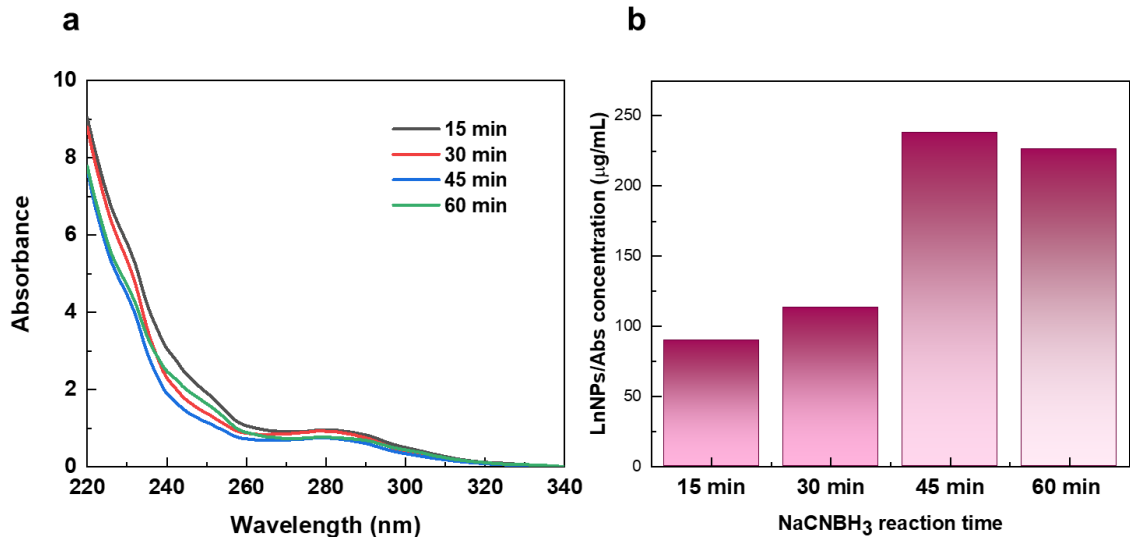
Figure 4.23 Absorbance spectra of the supernatants after bio-conjugation and stabilisation with reducing reagent for different times (a). Estimated Ab concentrations for LnNPs/Ab after stabilizing with $NaCNBH_3$ for different times (b).

Next, we stained mouse spleen cells with the LnNPs/Ab and supernatants from this experiment. The staining protocol was similar to the previous sections. MFI of fluorescent cells in each sample was calculated and compared with positive controls treated with purified Ab or IgG-CHO, and a negative control that received no anti-B220 (**Figure 4.24**).
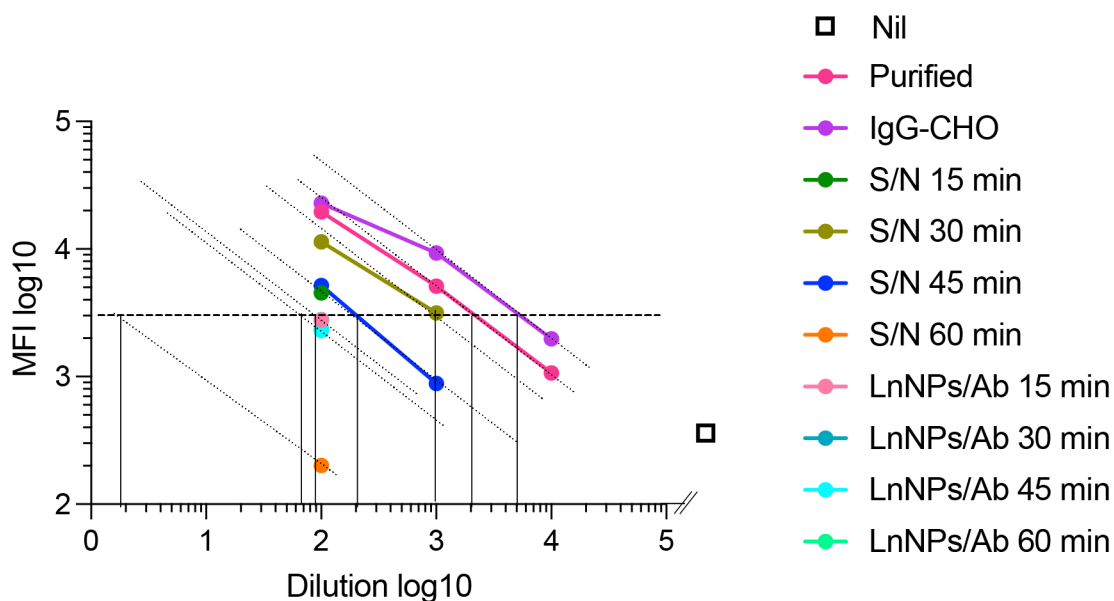
Figure 4.24 Graph of dilution vs geometric mean fluorescence of the B cell populations detected by flow cytometry.

Table 4.9 The measured concentration of antibody-conjugated LnNPs and the relevant supernatants along with purified and oxidised anti-B220 antibodies via A280 and flow cytometry.

samples	start conc (μg/mL)	S/N OD	S/N conc (μg/mL)	estimated NP/Ab conc (μg/mL)	X intercept samples	X intercept S/N	samples reactive conc (μg/mL)	S/N reactive conc (μg/mL)	samples reactive conc (μg/mL)	S/N reactive conc (μg/mL)
							rel to pur	rel to pur	rel to IgG-CHO	rel to IgG-CHO
Purified	220				3.10					
IgG-CHO	600				3.40		439			
15 min	675	0.952	680	-5	1.80	2.10	11.03	22		30
30 min	675	0.920	657	18	1.80	3.00	11.03	175	15.07	239
45 min	675	0.745	532	143	1.60	2.10	6.96	22	9.51	30
60 min	675	0.762	544	131	1.60	0.01	6.96	0	9.51	0

As shown in **Table 4.9**, sample supernatants displayed lower antigen-binding capacity as measured by flow cytometry compared with protein concentration measured by A280, indicating that most of the Ab had lost activity. Only the 30 min supernatant retained some reactivity. The LnNPs/Ab in this experiment also showed little specific binding, considering the high initial IgG-CHO concentration. Together with the previous results, these experiments confirmed that although NaCNBH$_3$ assisted in the conversion of the

hydrazone bond to a secondary amine, it also had a major negative impact on the ability of the anti-B220 Ab to bind to antigen. As an alternative way to decrease the concentration-dependent reversal of the Schiff-base production of imines over time, we instead increased the reactant concentrations. Therefore in the next experiment the reaction volume was reduced as much as practicable.

4.6.6.7 Coupling ADH-LnNPs to an oxidised anti-B220 antibody with concentrated initial materials

As mentioned above, bioconjugation was performed with more concentrated materials. Briefly, 5 pmole ADH-LnNPs (60 µg, 12 µL) at 5 mg/mL in HEPES buffer was added to 150 pmole oxidised anti-B220 (27 µg) to give a molar ratio of 1/30. The final reaction volume was of 60 µL. After 14 hrs incubation at room temperature, the sample was centrifuged at 20240 g for 10 min and the supernatants removed. The LnNPs were washed twice in HEPES buffer with centrifugation at 20240 g for 10 min and resuspended in 70 µL HEPES buffer (20 mM, 1 mM NaF, pH=7). The sample was then divided into two, 500 µg blocker (PEG-CHO 2′000) was added to one aliquot and the samples were incubated at room temperature for 2 hrs. A280 measurement was used to estimate the supernatant Ab concentrations (**Figure 4.25**). The A280 measurements of the initial IgG-CHO and the supernatant were 0.806 and 0.590, respectively. Based on this result, the concentration of antibodies bound to LnNPs was ~62 µg/mL. In other words, 13% of initial Ab was coupled to LnNPs.

Chapter 4
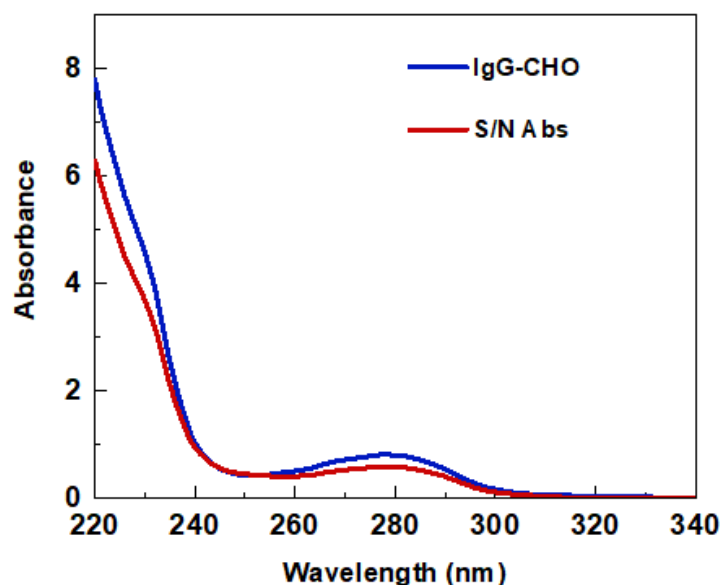
Figure 4.25 Absorbance spectra of IgG-CHO and supernatant of IgG-CHO LnNPs conjugation reaction.

The LnNPs/Ab conjugates were tested for ability to bind to cell surface B220 and MFI of the fluorescent cells in each sample was calculated as described previously (**Figure 4.26**). Specific binding activity of LnNPs/Ab was the same whether or not blocker was present in the reaction. Although the degree of conjugation, as assessed by A280, was only 12.8%, over 11% of the bound Ab retained activity as measured by binding to cell surface B220.
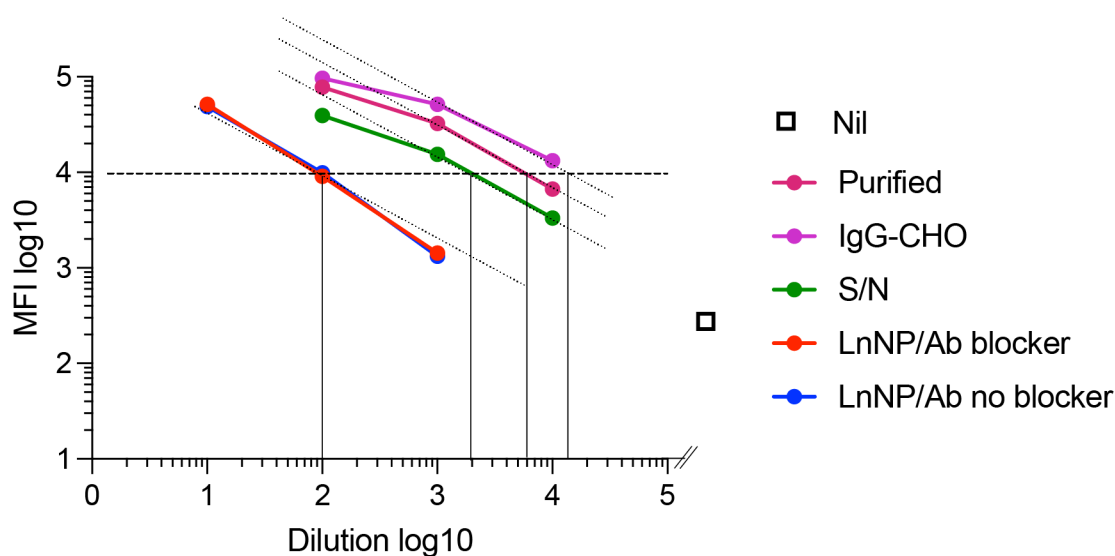
Figure 4.26 Graph of dilution vs geometric mean fluorescence of the B cell populations detected by flow cytometry

Table 4.10 The measured concentration of antibody-conjugated LnNPs and the relevant supernatants along with purified and oxidised anti-B220 antibodies via A280 and flow cytometry.

samples	start conc (µg/mL)	S/N OD	S/N conc (µg/mL)	estimated NP/Ab conc (µg/mL)	% coupled	X intercept samples	X intercept S/N	samples reactive conc (µg/mL)	S/N reactive conc (µg/mL)	% reactive of coupled
Purified	220					3.50				
IgG-CHO	576	0.806	576			4.03		745		
blocker	483	0.590	421	62	12.75	2.00	3.10	6.96	87.58	11.30
no blocker	483	0.590	421	62	12.75	2.00	3.10	6.96	87.58	11.30

Finally, the high concentration samples were tested for their signal in mass cytometry. For this assay, no mouse spleen cells were available, so human peripheral blood mononuclear cells containing ~10% B cells were used. Anti-B220 mAb has a high affinity for human as well as mouse B220. Five samples were prepared using human cells plus LnNPs/Ab with and without blocker, supernatant from LnNPs/Ab with blocker spun at 6000 g to remove aggregated LnNPs, resuspended pellet from LnNPs/Ab with blocker spun at 6000 g (aggregated LnNPs) or an aliquot of pre-conjugation ADH-LnNPs. **Figure 4.27** shows the ^{89}Y channel signals for the 5 samples, indicating the presence of LnNPs.
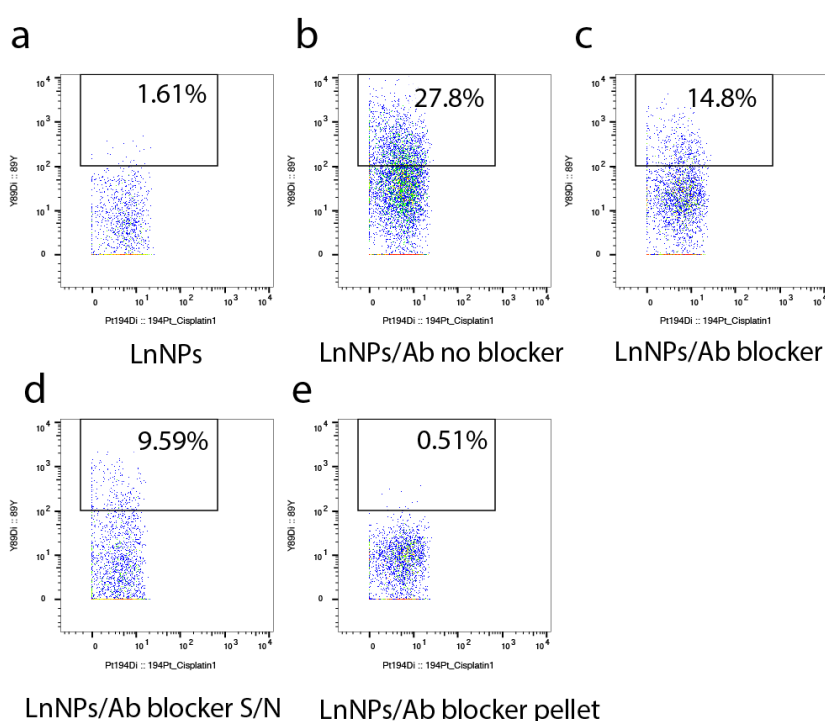
Figure 4.27 Dot plots of ^{194}Pt versus ^{89}Y for MC analysis. The samples were gated to exclude doublets and dead cells (^{194}Pt positive). ^{89}Y positive cells are gated within the black rectangle. Percentage of cells within the gate are shown.

Figure 4.27a shows the background signal from LnNPs. Comparison of **Figures 4.27b** and **4.27c** demonstrates the significant drop in non-specific labelling with the addition of blocker to the LnNPs/Ab, and further comparison of **Figures 4.27c** and **4.27d** shows that the mono-dispersed LnNPs/Ab in the supernatant after centrifugation at 6000 g retain a high signal with lower background. Finally, **Figure 4.27e** confirms that the aggregated LnNPs that pellet after centrifugation of blocked LnNPs/Ab at 6000 g had no specific Ab

reactivity. Thus conjugation with an Ab appears sufficient to prevent LnNP aggregation after blocking with PEG-CHO 2′000.

In future it will be important to include additional Abs such as anti-CD19 to specifically detect B cells in the mass cytometry analysis, in order to test whether the ^{89}Y signal from LnNPs/Ab is restricted to B cells.

Of all the experiments presented in this thesis, the experiment shown in **Figure 4.26** and **Figure 4.27** achieved the highest retention of specific binding activity (11%) by LnNPs/Ab. While promising, it indicates that further optimisation will be required for efficient generation of LnNPs/Ab for use in MC, as the percentage of IgG-CHO coupled was only 13%, so that the overall efficiency of the coupling reaction was 1.4%. A molar coupling ratio of less than 1/10, combined with a high concentration reaction, may lead to a higher percentage of IgG-CHO coupled, with a consequent increase in specific binding activity relative to initial IgG-CHO concentration.

It is possible that although hydrazide functionalised nanoparticles target carbohydrate sidechains that are present in the constant portion of Abs through Schiff-based interactions, low flexibility between LnNPs and Abs constrains the Ab's ability to bind to a cell surface. In other words, LnNPs produce a hindrance effect that does not allow Ab to approach the cell surface. In addition, the three-dimensional structure of IgG Ab may limit their approach to LnNPs, which decreases the bioconjugation efficiency. These limitations may possibly be rectified by substituting a longer hydrazide linker to create more flexibility and distance between LnNPs and the antigen-binding site on the Ab.

4.7 Conclusion

In this chapter, a strategy to orient the antibody molecules on the surface of nanoparticles has been explored, with the aim of increasing the conjugation efficiency between LnNPs and anti-B220 Ab and improving the bioactivity of Ab for mass cytometry applications. By taking advantage of the carbodiimide crosslinker chemistry, polymer functionalised LnNPs prepared in chapter 3 were modified by adipic acid dihydrazide to introduce hydrazide groups on the surface of nanoparticles. Anti-B220 antibodies oxidised by NaIO$_4$ could then be directly coupled to hydrazide functionalised nanoparticles. More importantly, the use of PEG-CHO 2′000 as the blocking agent not only reduced non-specific binding by blocking unoccupied hydrazide groups on Ab-conjugated nanoparticles but also blocked LnNPs without Ab conjugates, leading to their aggregation

and allowing removal by low speed centrifugation. Sodium cyanoborohydride (NaCNBH$_3$) was used as a reducing agent to stabilise Schiff-base reactions. Although it achieved this, it also caused the antigen-binding activity of the Ab to decrease dramatically, so its use was discontinued. Increasing the concentration of the LnNPs and anti-B220 Ab in the conjugation reaction led to a significant improvement in the specific binding activity of LnNPs/Ab, which will serve as the basis for further optimisation in future. The bi-functional hydrazide linker used in these studies was quite small which may have constrained interactions between LnNPs and anti-B220 Ab and between Ab and antigen on the cell surface. For this reason, the overall antibody conjugation efficiency was lower than expected but still higher than carboiimide chemistry strategy achieved in chapter 3 (**Table 4.6**). By applying site-specific conjugation and optimising the concentrations of oxidised Ab, ADH-LnNPs and blocking agent, the promising results in this chapter can serve as the basis for synthesis of biologically active, reliable LnNPs/Ab conjugate probes to improve sensitivity in mass cytometry applications.

The summary of two conjugation strategies is represented here:

EDC/Sulfo-NHS chemistry (Figure 4.28a)

- Overlapping of carboxylic functional group between polymer-LnNPs and Ab: cross-linking and aggregation
- Unsuitablility of blocking reagent due to the hydrolysis of unoccupied carboxylate during washing steps: non-specific binding
- Random orientation coupling the antibodies on the surface of LnNPs: low percentage of Abs can bind to cell surface antigen
- Unable to exclude unconjugated LnNPs from the LnNPs/Ab preparation: high level of background

Schiff-base reaction (Figure 4.28b)

- Single functional group on the surface of LnNPs and antibodies: avoids cross-linking and aggregations
- Able to use aldehyde-PEG as blocking reagent: avoids non-specific binding and background
- Directed orientation of antibodies coupled to the surface of LnNPs: a higher percentage of Abs can bind to cell surface antigen
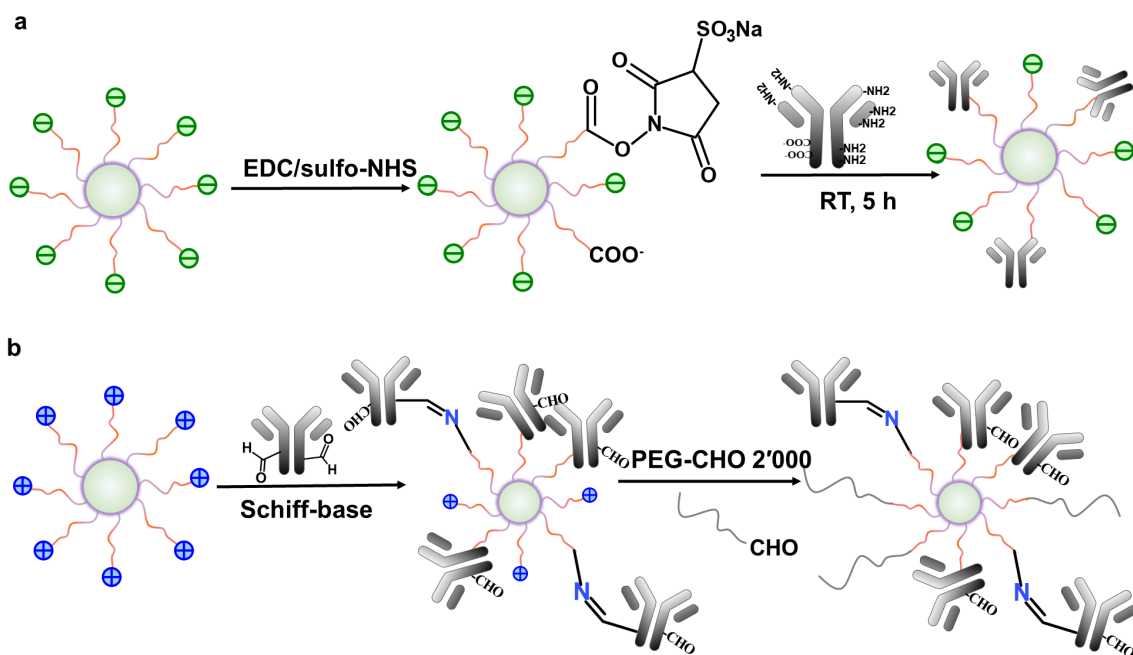
Figure 4.28. Schematic illustration of EDC/Sulfo-NHS (a) and Schiff-base (b) strategies for conjugation of monoclonal antibodies and LnNPs.

References

1.	Bendall, S. C.; Nolan, G. P.; Roederer, M.; Chattopadhyay, P. K., A deep profiler's guide to cytometry. *Trends Immunol* **2012,** *33* (7), 323-32.

2.	Atkuri, K. R.; Stevens, J. C.; Neubert, H., Mass Cytometry: A Highly Multiplexed Single-Cell Technology for Advancing Drug Development. **2015,** *43* (2), 227-233.

3.	Kingsmore, S. F., Multiplexed protein measurement: technologies and applications of protein and antibody arrays. *Nat Rev Drug Discov* **2006,** *5* (4), 310-20.

4.	Newell, E. W.; Davis, M. M., Beyond model antigens: high-dimensional methods for the analysis of antigen-specific T cells. *Nature biotechnology* **2014,** *32* (2), 149-57.

5.	Bodenmiller, B.; Zunder, E. R.; Finck, R.; Chen, T. J.; Savig, E. S.; Bruggner, R. V.; Simonds, E. F.; Bendall, S. C.; Sachs, K.; Krutzik, P. O.; Nolan, G. P., Multiplexed mass cytometry profiling of cellular states perturbed by small-molecule regulators. *Nature biotechnology* **2012,** *30* (9), 858-67.

6.	Angelo, M.; Bendall, S. C.; Finck, R.; Hale, M. B.; Hitzman, C.; Borowsky, A. D.; Levenson, R. M.; Lowe, J. B.; Liu, S. D.; Zhao, S.; Natkunam, Y.; Nolan, G. P., Multiplexed ion beam imaging of human breast tumors. *Nat Med* **2014,** *20* (4), 436-42.

7.	Ivask, A.; Mitchell, A. J.; Malysheva, A.; Voelcker, N. H.; Lombi, E., Methodologies and approaches for the analysis of cell-nanoparticle interactions. *Wiley Interdiscip Rev Nanomed Nanobiotechnol* **2018,** *10* (3), e1486.

8.	Chattopadhyay, P. K.; Perfetto, S. P.; Yu, J.; Roederer, M., The use of quantum dot nanocrystals in multicolor flow cytometry. *Wiley Interdiscip Rev Nanomed Nanobiotechnol* **2010,** *2* (4), 334-48.

9.	Chattopadhyay, P. K.; Price, D. A.; Harper, T. F.; Betts, M. R.; Yu, J.; Gostick, E.; Perfetto, S. P.; Goepfert, P.; Koup, R. A.; De Rosa, S. C.; Bruchez, M. P.; Roederer, M., Quantum dot semiconductor nanocrystals for immunophenotyping by polychromatic flow cytometry. *Nat Med* **2006,** *12* (8), 972-7.

10.	Spitzer, M. H.; Nolan, G. P., Mass Cytometry: Single Cells, Many Features. *Cell* **2016,** *165* (4), 780-91.

11.	Tanner, S. D.; Baranov, V. I.; Ornatsky, O. I.; Bandura, D. R.; George, T. C., An introduction to mass cytometry: fundamentals and applications. *Cancer Immunol Immunother* **2013,** *62* (5), 955-65.

12.	Di Palma, S.; Bodenmiller, B., Unraveling cell populations in tumors by single-cell mass cytometry. *Current opinion in biotechnology* **2015,** *31*, 122-9.

13.	Lou, X.; Zhang, G.; Herrera, I.; Kinach, R.; Ornatsky, O.; Baranov, V.; Nitz, M.; Winnik, M. A., Polymer-Based Elemental Tags for Sensitive Bioassays. *Angewandte Chemie* **2007,** *119* (32), 6223-6226.

14.	Bandura, D. R.; Baranov, V. I.; Ornatsky, O. I.; Antonov, A.; Kinach, R.; Lou, X.; Pavlov, S.; Vorobiev, S.; Dick, J. E.; Tanner, S. D., Mass Cytometry: Technique for Real Time Single Cell Multitarget Immunoassay Based on Inductively Coupled Plasma Time-of-Flight Mass Spectrometry. *Analytical Chemistry* **2009,** *81* (16), 6813-6822.

15.	Illy, N.; Majonis, D.; Herrera, I.; Ornatsky, O.; Winnik, M. A., Metal-chelating polymers by anionic ring-opening polymerization and their use in quantitative mass cytometry. *Biomacromolecules* **2012,** *13* (8), 2359-69.

16.	Vancaeyzeele, C.; Ornatsky, O.; Baranov, V.; Shen, L.; Abdelrahman, A.; Winnik, M. A., Lanthanide-Containing Polymer Nanoparticles for Biological Tagging Applications: Nonspecific Endocytosis and Cell Adhesion. *Journal of the American Chemical Society* **2007,** *129* (44), 13653-13660.

17.	Wu, X.; DeGottardi, Q.; Wu, I. C.; Yu, J.; Wu, L.; Ye, F.; Kuo, C. T.; Kwok, W. W.; Chiu, D. T., Lanthanide-Coordinated Semiconducting Polymer Dots Used for Flow Cytometry and Mass Cytometry. *Angew Chem Int Ed Engl* **2017,** *56* (47), 14908-14912.

18.   Abdelrahman, A. I.; Dai, S.; Thickett, S. C.; Ornatsky, O.; Bandura, D.; Baranov, V.; Winnik, M. A., Lanthanide-Containing Polymer Microspheres by Multiple-Stage Dispersion Polymerization for Highly Multiplexed Bioassays. *Journal of the American Chemical Society* **2009,** *131* (42), 15276-15283.

19.   Tong, L.; Lu, E.; Pichaandi, J.; Zhao, G.; Winnik, M. A., Synthesis of Uniform NaLnF4 (Ln: Sm to Ho) Nanoparticles for Mass Cytometry. *The Journal of Physical Chemistry C* **2016,** *120* (11), 6269-6280.

20.   Kavand, A.; Serra, C. A.; Blanck, C.; Lenertz, M.; Anton, N.; Vandamme, T. F.; Mély, Y.; Przybilla, F.; Chan-Seng, D., Controlled Synthesis of NaYF4:Yb,Er Upconversion Nanocrystals as Potential Probe for Bioimaging: A Focus on Heat Treatment. *ACS Applied Nano Materials* **2021,** *4* (5), 5319-5329.

21.   Pichaandi, J.; Tong, L.; Bouzekri, A.; Yu, Q.; Ornatsky, O.; Baranov, V.; Winnik, M. A., Liposome-Encapsulated NaLnF4 Nanoparticles for Mass Cytometry: Evaluating Nonspecific Binding to Cells. *Chemistry of Materials* **2017,** *29* (11), 4980-4990.

22.   Pichaandi, J.; Zhao, G.; Bouzekri, A.; Lu, E.; Ornatsky, O.; Baranov, V.; Nitz, M.; Winnik, M. A., Lanthanide nanoparticles for high sensitivity multiparameter single cell analysis. *Chem Sci* **2019,** *10* (10), 2965-2974.

23.   Cao, P.; Tong, L.; Hou, Y.; Zhao, G.; Guerin, G.; Winnik, M. A.; Nitz, M., Improving lanthanide nanocrystal colloidal stability in competitive aqueous buffer solutions using multivalent PEG-phosphonate ligands. *Langmuir* **2012,** *28* (35), 12861-70.

24.   Zhao, G.; Tong, L.; Cao, P.; Nitz, M.; Winnik, M. A., Functional PEG-PAMAM-tetraphosphonate capped NaLnF(4) nanoparticles and their colloidal stability in phosphate buffer. *Langmuir* **2014,** *30* (23), 6980-9.

25.   Maddahfar, M.; Wen, S.; Hosseinpour Mashkani, S. M.; Zhang, L.; Shimoni, O.; Stenzel, M.; Zhou, J.; Fazekas de St Groth, B.; Jin, D., Stable and Highly Efficient Antibody-Nanoparticles Conjugation. *Bioconjug Chem* **2021**.

26.   Acchione, M.; Kwon, H.; Jochheim, C. M.; Atkins, W. M., Impact of linker and conjugation chemistry on antigen binding, Fc receptor binding and thermal stability of model antibody-drug conjugates. *MAbs* **2012,** *4* (3), 362-72.

27.   Joshi, P. P.; Yoon, S. J.; Hardin, W. G.; Emelianov, S.; Sokolov, K. V., Conjugation of antibodies to gold nanorods through Fc portion: synthesis and molecular specific imaging. *Bioconjug Chem* **2013,** *24* (6), 878-88.

28.   Xing, Y.; Chaudry, Q.; Shen, C.; Kong, K. Y.; Zhau, H. E.; Chung, L. W.; Petros, J. A.; O'Regan, R. M.; Yezhelyev, M. V.; Simons, J. W.; Wang, M. D.; Nie, S., Bioconjugated quantum dots for multiplexed and quantitative immunohistochemistry. *Nat Protoc* **2007,** *2* (5), 1152-65.

29.   Wendeler, M.; Grinberg, L.; Wang, X.; Dawson, P. E.; Baca, M., Enhanced Catalysis of Oxime-Based Bioconjugations by Substituted Anilines. *Bioconjugate Chemistry* **2014,** *25* (1), 93-101.

30.   Abraham, R.; Moller, D.; Gabel, D.; Senter, P.; Hellström, I.; Hellström, K. E., The influence of periodate oxidation on monoclonal antibody avidity and immunoreactivity. *Journal of Immunological Methods* **1991,** *144* (1), 77-86.

31.   Basu, A.; Shrivastav, T. G.; Kariya, K. P., Preparation of enzyme conjugate through adipic acid dihydrazide as linker and its use in immunoassays. *Clin Chem* **2003,** *49* (8), 1410-2.

32.   Quesenberry, M. S.; Lee, Y. C., A rapid formaldehyde assay using purpald reagent: application under periodation conditions. *Anal Biochem* **1996,** *234* (1), 50-55.

33.   Mackenzie, L. E.; Goode, J. A.; Vakurov, A.; Nampi, P. P.; Saha, S.; Jose, G.; Millner, P. A., The theoretical molecular weight of NaYF 4 :RE upconversion nanoparticles. *Sci Rep* **2018,** *8* (1), 1106.

34.   Buchwalow, I.; Samoilova, V.; Boecker, W.; Tiemann, M., Non-specific binding of antibodies in immunohistochemistry: fallacies and facts. *Sci Rep* **2011,** *1*, 28.

35.   Borch, R. F.; Bernstein, M. D.; Durst, H. D., Cyanohydridoborate anion as a selective reducing agent. *Journal of the American Chemical Society* **1971,** *93* (12), 2897-2904.

References

36.   Bernstein, M. A.; Hall, L. D. J. C. R., A general synthesis of model glycoproteins: coupling of alkenyl glycosides to proteins, using reductive ozonolysis followed by reductive amination with sodium cyanoborohydride. **1980,** *78* (1), C1-C3.

37.   Fleminger, G.; Hadas, E.;   Wolf, T.; Solomon, B., Oriented immobilization of periodateoxidized monoclonal antibodies on amino and hydrazide derivatives of eupergit C. *Applied Biochemistry and Biotechnology* **1990,** *23* (2), 123-137.

38.   Sato, S.; Sakamoto, T.; Miyazawa, E.; Kikugawa, Y., One-pot reductive amination of aldehydes and ketones with α-picoline-borane in methanol, in water, and in neat conditions. *Tetrahedron* **2004,** *60* (36), 7899-7906.

39.   Veeraraghavan Ramachandran, P.; Gagare, P. D.; Sakavuyi, K.; Clark, P., Reductive amination using ammonia borane. *Tetrahedron Letters* **2010,** *51* (24), 3167-3169.

Chapter 5: Conclusions and Future Perspectives

5.1 Conclusions

High-dimensional and multi-parametric single-cell assays of human blood samples are increasingly important in clinical decision-making, particularly with the new generation of monoclonal therapies that regulate the immune system's functions. Adoption of the mass cytometry platform will provide major advantages for the development of these multiplexing assays in high throughput fashion, but currently available mass cytometry reagents use polymer-lanthanide complexes that are not ideal in providing high sensitivity, having only a maximum of 250 lanthanide ions per antibody. To this end, this dissertation mainly focuses on generating antibody conjugated LnNPs to significantly amplify the signal by highly doping the concentration of lanthanide ions into every single nanoparticle, thereby enhancing the sensitivity of mass cytometry. To generate LnNPs suitable for biotechnology and biomedical applications, including mass-tag cellular barcoding, their surface needs to be engineered to meet the specific requirements of cell and molecular biology applications. In particular, they need to be uniform in size, stable long-term in physiological buffers and in the presence of bio-molecular complexes, and engineered to carry functional groups appropriate for conjugation of specific molecules such as antibodies, peptides, and nucleic acid oligomers. The major milestones achieved during my PhD study included:

1) Synthesis of uniform $NaYF_4$:Yb, Er UpConversion Nanoparticles (UCNPs), a type of LnNP that can be visualised under a near-infrared laser. I have learned to use FT-IR, TEM, and DLS to characterise the series of nanoparticles. Based on TEM characterisation, the average diameter was 23 nm with a $C_V < 5$ %.

2) Design and synthesis of diblock copolymers using Addition Fragmentation Chain Transfer RAFT polymerisation in order to transfer LnNPs from the oil phase to the aqueous phase. I systematically evaluated the role of the length of the POEGMEA chain in the colloidal stability and antibody-conjugation efficiency of nanoparticles.

3) Identification of the key to controlling the stability of polymer-coated LnNPs both in buffer solutions and after freeze-drying (for long-term stability in industry settings) and the key to optimising antibody conjugation efficiency. I achieved

this by doing a series of experiments and using multiple characterisation techniques.

4) Application of EDC/Sulfo-NHS chemistry to conjugate anti-B220 antibodies to LnNPs and stain cells with antibody functionalised nanoparticles. Use of LnNPs for flow cytometry and mass cytometry applications requires that the LnNP-coupled antibody retains its activity and specificity as a ligand-specific probe. By analysing the fluorescence intensities of cells using a flow cytometer, I calculated that less than 1% of the coupled antibody retained its ability to bind to B220 antigen on the cell surface. Since EDC-based conjugation of antibodies targets lysine sidechains that are present in both the antigen-binding and constant portions of the antibody, random orientation of antibodies on the surface of polymer-coated LnNPs would constrain the antibody's ability to bind to the antigens on the cell surface. For this reason, conjugation techniques that orient antibodies such that the ligand-binding site faces away from LnNPs are likely to yield conjugates that preserve a higher proportion of antibodies capable of recognizing antigens.

5) Detection of non-specific cell binding by polymer-coated LnNPs during mass cytometric analysis. This sets a crucial hurdle in the development of LnNPs for mass cytometry applications. Since the carboxylate functional group required for the carbodiimide chemistry strategy cannot be blocked, uncoupled nanoparticles unavoidably contributed to the background in mass cytometry. For these reasons, conjugation techniques that can separate free and conjugated nanoparticles are preferred.

6) Design of a site-specific conjugation strategy to orient the binding site of B220 antibody facing outward from the surface of LnNPs. One of the two hydrazide moieties of adipic acid dihydrazide (ADH) was conjugated to the carboxylated-end of the polymer-coated LnNPs, leaving the other hydrazide for covalent binding to the **oxidised** polysaccharide residues on the Fc region of the B220 antibody. PEG-aldehyde was applied to block the non-specific binding sites of antibody-conjugated LnNPs and any unconjugated LnNPs in the reaction mixture. This orientation control maximised the exposure of the B220 epitopes to the antigen on the surface of spleen mouse cells. This method has been investigated to avoid the low-efficiency issue of the Carbodiimide strategy and to improve the bio-activity of the antibody for recognising leucocyte antigens. By analysing the fluorescence intensities of cells using a flow cytometer, I calculated that 13% of

the coupled antibody retained its ability to bind to B220 antigen on the cell surface. The site-specific Ab orientation achieved by Schiff-based strategy offered high LnNP-Ab conjugation efficiency, significantly reduced non-specific binding to the cells and other biomolecules, and reduced the amount of Ab required during covalent binding to LnNPs, compared to carbodiimide strategy.

To put it in a nutshell, these studies conducted during my Ph.D. resulted in an extensive series of data correlating the polymer design and nanoparticle-antibody stoichiometry with retention of antibody ligand binding affinity with minimal nonspecific binding as well as preventing nanoparticle aggregation in physiological buffer and during the cell labelling process.

5.2 Future perspectives

Published studies of nanoparticle staining of cells usually present selective single-cell images, which do not provide information about labelling consistency and quantitative analysis of a large population of cells. The advantage of using flow cytometry to analyse multiple single cells using the antibody-nanoparticle conjugates lies in its high throughput at single-cell sensitivity, therefore providing a large amount of quantitative data to assess the variation of labelling among the cells. My PhD project made advances in developing a new library of lanthanide-doped nanoparticles as fluorescent labelling probes for up-conversion flow cytometry and near-infrared flow cytometry, once the instrument can be further engineered. With the recent introduction of mass cytometry and mass cytometry imaging systems, my work can immediately benefit this emerging field by using lanthanide nanoparticles as the isotope labels to enhance sensitivity in detecting biomarker expression at levels of <10,000 antigen biomarkers per cell. Due to the novelty and potential advantages of using LnNPs as isotope tags, the development of nanoparticle reagents for mass cytometry and imaging systems will require further investigation and optimisation.

5.2.1 Surface chemistry and polymers

The polymer designed and used in this thesis met all the essential criteria to produce biospecific nanoparticles for biomedical application including mass cytometry. There is, however, still some room for improvement. A major challenge that we encountered was that the polymer did not generate stability in harsh environments such as PBS and alkaline buffers. This is probably due to the replacement of phosphate salt in PBS buffer and OH

Chapter 5

ions in alkaline conditions, due to residual OA ligand that had not been replaced completely by phosphate containing polymer. This may cause the release of OA in physiological buffers resulting in aggregation of LnNPs. Also, the phosphate in PBS buffer could compete with with polymer itself on the surface of nanoparticles. In order to synthesise new polymer with better performance in competitive conditions, a shorter OEGMEA monomer such as diethylene glycol ethyl ether acrylate with average Mn= 188 could be used to generate a more linear diblock copolymer rather than the bulk branched one. With this polymer, more OA molecules could be replaced during the ligand exchange process.

To introduce some flexibility in the link between nanoparticles and antibodies in order to increase the antibody bioconjugation efficiency and the ability of conjugated antibodies to bind to cell surface ligands, a longer linker with a hydrazide bifunctional group, such as hydrazide-PEG-hydrazide (2000, 5000 Da), can be applied (**Scheme 5.1**). A longer hydrazide linker on the surface of LnNPs would not only allow antibodies to approach nanoparticles more easily but should also prevent binding interference between antibody and cell surface antigen. An alternative approach would be to coat the LnNPs with a mixture of polymers with different POEGMEA chain lengths, with the aim of preferentially conjugating antibody to the longer, more flexible chains. This could be enhanced by synthesising polymers with different functional end groups, so that only the longer polymer could undergo conjugation to antibody.

Moreover, computational studies such as molecular dynamic simulation can further advance our knowledge of the linker, antibody, and the flexibility of the antigen-binding site on the antibody. For example, on the basis of our published experimental data presented in chapter 3, Walsh and et al proposed a mathematical model to predict the relation between polymer sizes and three key properties: surface charge, maximum loading, and maximum thickness of the coatings.[1] The molecular simulation can be applicable to determine quantitative relationships for a range of properties, enabling optimisation prior to experiment.

Scheme 5.1. Scheme of hydrazide-PEG-Hydrazide (2000, 5000 Da)
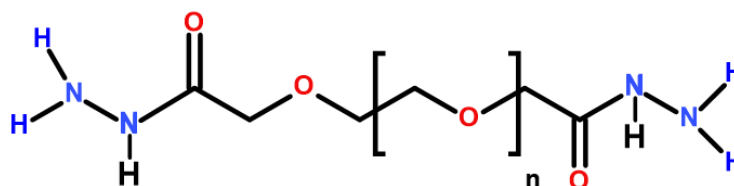
5.2.2 Conjugation methodology

Schiff-base chemistry generates a reversible conjugation reaction that should ideally be converted to a stable covalent bond in nanoparticle reagents manufactured for use in biological applications. The studies described in this thesis showed that $NaCNBH_3$ was not suitable for this purpose, as it drastically reduced the ability of the antibody to recognise antigen. Alternative reducing agents such as 2-methylpyridine borane complex (2-picoline borane complex)[3], which does not contain the cyanide group, could be substituted for $NaCNBH_3$. A second strategy to further optimise the Schiff-base method would be to further decrease the buffer volume for the conjugation reaction, effectively increasing the likelihood of interaction between nanoparticles and antibodies. Given that the optimal signal to noise ratio in mass cytometry would be for each antibody binding to specific antigen on the cell to carry a single nanoparticle, a highly concentrated reaction at a molar ratio of 1/10 or less may result in more efficient coupling. A third strategy to improve the stability of antibody after coupling to nanoparticles would be to inactivate any remaining aldehyde groups on the conjugated antibody, since both the oxidised antibody and the antibody nanoparticle conjugates were shown to be unstable, likely due to aldehyde-dependent cross-linking.

Another site-specific conjugation strategy, the maleimide-thiol reaction, can be used to orient the binding site of B220 antibody outward from the surface of LnNPs. This method is currently being applied for the Fluidigm conjugates (MCP, CyTOF reagent)[4] and for many therapeutic antibody-drug conjugates, confirming the widespread use of this chemistry for antibody conjugation. As shown in **Figure 5.1**, to conjugate LnNPs to anti-B220 antibodies, the maleimide functional group can be introduced on the surface of LnNPs by synthesising a new polymer containing a maleimide end functional group. In this method, TCEP (tris(2-carboxyethyl)phosphine)[5] is currently used as a reducing agent

to break the hinge disulfide bonds between the two antibody chains of IgG, allowing their conjugation to maleimide functionalised LnNPs.

The maleimide-thiol method, while appropriate for most monoclonal antibodies, results in the inactivation of some particular antibody specificities.[6] In its current form, it brings the maleimide residue bearing structure very close to the antibody and its antigen recognition site. Adaptation for nanoparticle conjugation would likely require the use of a highly flexible linker,[7] as described above in 5.2.2.
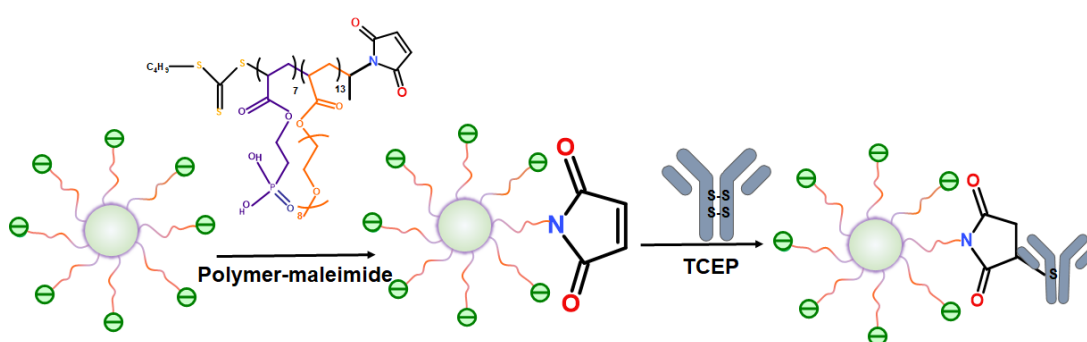

Figure 5.1. Proposed schematic design of polymer and steps for antibody-nanoparticle conjugation using TCEP chemistry.

In summary, the key major challenge in our study is to obtain a high percentage of active and specific antibody-LnNPs conjugates. Through the experiments presented in my thesis, this will become possible by tuning surface conditions of nanoparticles using the design of polymer linkers and antibody-specific conjugation strategy. With both sufficient colloidal stability in physiological buffers and antibody conjugation efficiency achieved in this work, and once high yield LnNPs-antibody conjugates are in hand, nanoparticle based isotope tags can be integrated into an immune signature panel to improve the sensitivity and specificity of detection of low-expression biomarkers at the single-cell level.

References

1.   Maddahfar, M.; Wen, S.; Hosseinpour Mashkani, S. M.; Zhang, L.; Shimoni, O.; Stenzel, M.; Zhou, J.; Fazekas de St Groth, B.; Jin, D., Stable and Highly Efficient Antibody-Nanoparticles Conjugation. *Bioconjug Chem* **2021**.

2.   Pham, L. N.; Walsh, T. R., Design Traits for Diblock Copolymer Coating Properties on NaGdF4 Upconversion Nanoparticles. *ACS Applied Polymer Materials* **2022**.

3.   Ruhaak, L. R.; Steenvoorden, E.; Koeleman, C. A. M.; Deelder, A. M.; Wuhrer, M., 2-Picoline-borane: A non-toxic reducing agent for oligosaccharide labeling by reductive amination. **2010,** *10* (12), 2330-2336.

4.   Illy, N.; Majonis, D.; Herrera, I.; Ornatsky, O.; Winnik, M. A., Metal-chelating polymers by anionic ring-opening polymerization and their use in quantitative mass cytometry. *Biomacromolecules* **2012,** *13* (8), 2359-69.

5.   Ravasco, J.; Faustino, H.; Trindade, A.; Gois, P. M. P., Bioconjugation with Maleimides: A Useful Tool for Chemical Biology. *Chemistry (Weinheim an der Bergstrasse, Germany)* **2019,** *25* (1), 43-59.

6.   Renault, K.; Fredy, J. W.; Renard, P.-Y.; Sabot, C., Covalent Modification of Biomolecules through Maleimide-Based Labeling Strategies. *Bioconjugate Chemistry* **2018,** *29* (8), 2497-2513.

7.   Niwayama, S.; Abdullatif, S.; Zhao, T.; Sutton, R.; Altenberg, G., A Pyrene Maleimide with a Flexible Linker for Sampling of Longer Inter-Thiol Distances by Excimer Formation. *PloS one* **2011,** *6*, e26691.

References